

**IRSN**

INSTITUT  
DE RADIOPROTECTION  
ET DE SÛRETÉ NUCLÉAIRE

TECHNICAL REPORT SEMCA-2006-183

**A STATE-OF-THE-ART REVIEW  
OF PAST PROGRAMS DEVOTED TO  
FUEL BEHAVIOR UNDER LOCA CONDITIONS**

**Part Two.  
Impact of clad swelling  
upon assembly cooling**

**Author: Claude GRANDJEAN**

**DIRECTION DE LA PRÉVENTION DES ACCIDENTS MAJEURS**

Service d'études et de modélisation du combustible en situations accidentelles

**DIRECTION DE LA PRÉVENTION DES ACCIDENTS MAJEURS**

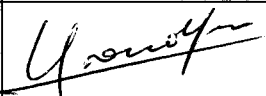
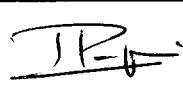
Service d'études et de modélisation du combustible en situations accidentelles

BP 3 13115 Saint-Paul-lez-Durance Cedex France tél. (33) 4 42 19 95 46 fax (33) 4 42 19 91 65

**A State-Of-The-Art Review of Past Programs Devoted  
to Fuel Behavior Under LOCA Conditions.****Part Two****Impact of clad swelling upon assembly cooling**

DPAM/SEMCA

Technical Report SEMCA-2006-183 - June 2006

	Auteur	Vérificateur	Approbateur
Nom	Claude GRANDJEAN	Georges REPETTO	Joëlle PAPIN
Date	23/06/2006	4 Juillet 2006	11/07/2006
Visa			

*La diffusion des informations contenues dans ce document auprès d'un tiers extérieur à l'IRSN est soumise à l'accord de l'unité émettrice.*

*This document, which contains proprietary or other confidential or privileged information, and any reproduction in whole or in part, shall not be disseminated outside the organization of the recipient without prior approval of the IRSN*

**DIRECTION DE LA PRÉVENTION DES ACCIDENTS MAJEURS**

Service d'études et de modélisation du combustible en situations accidentelles

BP 3 13115 Saint-Paul-lez-Durance Cedex France tél. (33) 4 42 19 95 46 fax (33) 4 42 19 91 65

**A State-Of-The-Art Review of Past Programs Devoted to Fuel Behavior Under LOCA Conditions. Part Two: Impact of clad swelling upon assembly cooling.**

Claude GRANDJEAN

Technical report SEMCA-2006-183 - June 2006

**Abstract:**

*This technical report provides a state of the art review of the main LOCA programs carried out in the 80s and focusing on the coolability of an assembly containing a partial blockage in a group of ballooned fuel rods under accidental LOCA conditions.*

*The experimental characteristics and main results of the FEBA, SEFLEX, THETIS, CEGB and FLECHT SEASET programs, as well as several analytical developments performed in association with these experimental programs, are reviewed in detail in this document.*

*The comparison and combination of conclusions drawn from these results and studies were used to improve our understanding of the physical phenomena governing the behavior of a partially blocked rod array during a LOCA reflood scenario. It has also been possible to determine the limits of blockage coolability under the most severe geometric (blockage length) and thermohydraulic conditions. Therefore, even a severe blockage ratio (90%) of a moderate length (<10 cm) does not cause any particular problems in terms of coolability during two-phase reflood. A severe blockage with considerable axial extension (> 15 cm) and a high blockage ratio (> 80%) can lead - with low reflood rate conditions - to a significant increase in blockage surface temperatures, hindering the final coolability of this blockage.*

*It is important to stress the fact that these results were obtained in out-of-pile tests performed on simulator assemblies containing electrically heated rods, making it impossible to simulate the possible fuel accumulation occurring in cladding balloons (fuel relocation), as was observed during in-pile tests with irradiated fuel rods. The impact of fuel relocation upon blockage coolability remains to be investigated. It must also be underlined that reflood conditions - representative of a large break LOCA scenario - were the main thermohydraulic conditions studied in these experimental programs. Blockage coolability during an intermediate break scenario has not been investigated in tests performed under representative thermohydraulic conditions and therefore will not be discussed in this paper.*

**Key-words: LOCA, Ballooning, Flow blockage, Coolability.**

# TABLE OF CONTENTS

<b>1</b>	<b>INTRODUCTION</b> .....	<b>5</b>
<b>2</b>	<b>FEBA AND SEFLEX PROGRAMS</b> .....	<b>7</b>
2.1	FEBA PROGRAM .....	7
2.1.1	<i>Objectives</i> .....	7
2.1.2	<i>Experimental characteristics of tests performed on 5x5 rod bundles</i> .....	8
2.1.3	<i>Results</i> .....	11
2.1.3.1	90% blockage (Series III) .....	11
2.1.3.2	62% blockage (Series IV) .....	14
2.1.3.3	Combined effects of several consecutive blockages and spacer grids.....	17
2.1.3.4	By-pass effects .....	19
2.1.4	<i>FEBA program conclusions</i> .....	20
2.2	SEFLEX PROGRAM .....	20
2.2.1	<i>Objectives</i> .....	20
2.2.2	<i>Experimental characteristics</i> .....	21
2.2.3	<i>Test matrix</i> .....	23
2.2.4	<i>Results</i> .....	24
2.2.4.1	Blockage-free tests .....	24
2.2.4.2	90% blockage tests.....	27
2.3	SEFLEX PROGRAM CONCLUSIONS AND COMMENTS .....	29
2.4	ANALYTICAL SIMULATION OF FEBA AND SEFLEX TESTS.....	30
2.4.1	<i>COBRA-TF computer code</i> .....	30
2.4.2	<i>Simulation of FEBA and SEFLEX tests using the COBRA-TF code</i> .....	31
<b>3</b>	<b>THETIS PROGRAM</b> .....	<b>35</b>
3.1	EXPERIMENTAL CHARACTERISTICS .....	35
3.2	TESTS WITH A 90% BLOCKAGE RATIO .....	39
3.2.1	<i>Reference test</i> .....	39
3.2.2	<i>Effect of pressure</i> .....	42
3.2.3	<i>Effect of input temperature</i> .....	43
3.2.4	<i>Effect of reflood rate</i> .....	45
3.2.5	<i>Variable power tests</i> .....	46
3.2.6	<i>Tests with variable power and reflood rate</i> .....	49
3.3	TESTS WITH AN 80% BLOCKAGE RATIO .....	52
3.4	DISCUSSION: QUALITATIVE ANALYSIS OF PHENOMENA .....	58
3.5	GRAVITY REFLOOD TESTS WITH AN 80% BLOCKAGE RATIO .....	61
3.5.1	<i>Hydraulic behavior</i> .....	62
3.5.2	<i>Thermal behavior</i> .....	65
3.5.3	<i>Impact of flow and level oscillations</i> .....	69
3.5.4	<i>Conclusions</i> .....	71
3.6	COOLABILITY OF THETIS BLOCKAGES .....	71
3.7	INTERPRETATION OF THETIS RESULTS.....	72
<b>4</b>	<b>ACHILLES PROGRAM</b> .....	<b>75</b>
4.1	EXPERIMENTAL CHARACTERISTICS .....	75
4.2	EXPERIMENTAL PROGRAM .....	76
4.3	MAIN RESULTS .....	77
4.3.1	<i>Results of the base case test (Run A2R038)</i> .....	77
4.3.2	<i>Results of variations about the base case at constant reflood rate</i> .....	80
4.3.2.1	Repeatability .....	80
4.3.2.2	Effect of pressure .....	81
4.3.2.3	Effect of inlet subcooling.....	81
4.3.2.4	Effect of rod power .....	81

4.3.2.5	Effect of unpowered rods.....	81
4.3.2.6	Effect of imposed flow oscillations .....	81
4.3.3	<i>Results of experiments with varying reflood rates</i> .....	81
4.3.3.1	Reference case (A2R037) .....	82
4.3.3.2	Effects of rod power and initial rod temperature .....	82
4.4	DISCUSSION .....	83
4.5	CONCLUSIONS .....	83
<b>5</b>	<b>CEGB PROGRAM .....</b>	<b>85</b>
5.1	EXPERIMENTAL CHARACTERISTICS .....	85
5.2	REFLOOD TESTS .....	87
5.2.1	<i>Tests performed on Blockage 2</i> .....	88
5.2.2	<i>Tests performed on Blockage 3</i> .....	90
5.2.2.1	Steady power tests .....	90
5.2.2.2	+1 kW power tests .....	92
5.3	COMPARISON OF CEGB RESULTS WITH THETIS AND FEBA/SEFLEX RESULTS .....	94
5.4	CEGB ANALYTICAL MODEL.....	95
5.4.1	<i>Model description</i> .....	95
5.4.2	<i>Comparison of model predictions with experimental results</i> .....	98
5.4.3	<i>Parametric calculations under PWR reflood conditions</i> .....	98
<b>6</b>	<b>FLECHT SEASET PROGRAM.....</b>	<b>100</b>
6.1	TESTS PERFORMED ON A 21 FUEL ROD ARRAY .....	101
6.1.1	<i>Experimental characteristics</i> .....	101
6.1.2	<i>Test matrix</i> .....	104
6.1.3	<i>Results</i> .....	105
6.1.3.1	Coplanar blockage .....	105
6.1.3.2	Non-coplanar blockage.....	106
6.2	TESTS PERFORMED ON A 163 FUEL ROD ARRAY .....	110
6.2.1	<i>Experimental characteristics</i> .....	110
6.2.2	<i>Results</i> .....	111
6.3	ANALYSIS OF RESULTS USING THE COBRA-TF CODE .....	113
6.3.1	<i>Comparison with 21 rod array test results</i> .....	114
6.3.2	<i>Comparison with 163 rod array test results</i> .....	116
6.4	FLECHT SEASET FLOW BLOCKAGE PROGRAM CONCLUSIONS .....	117
<b>7</b>	<b>CONCLUSION .....</b>	<b>118</b>
7.1	DATA OBTAINED FROM EXPERIMENTAL PROGRAMS.....	118
7.1.1	<i>Blockage representativity</i> .....	118
7.1.2	<i>Effect of blockage ratio</i> .....	119
7.1.3	<i>Effect of the blockage length</i> .....	119
7.1.4	<i>Effect of blockage configurations: coplanar or non-coplanar</i> .....	120
7.1.5	<i>By-pass effects</i> .....	120
7.1.6	<i>Effect of reflood characteristics: forced or gravity</i> .....	120
7.2	ANALYTICAL DEVELOPMENTS .....	121
7.3	PENDING QUESTIONS.....	121
	<b>REFERENCES.....</b>	<b>123</b>
	<b>ABBREVIATIONS .....</b>	<b>124</b>

# 1 INTRODUCTION

Many experimental programs have been devoted to the study of rod cladding deformations produced during a LOCA transient and the resulting local blockages that may occur in the assembly. Part One of this State-of-the-Art-Review<sup>[1]</sup> specifically examines the most important of these programs and the main conclusions drawn from results.

A major question associated with the study of clad ballooning and resulting partial sub-channel blockage is that of the coolability of partially blocked regions in a PWR fuel assembly undergoing a LOCA.

The problem of cooling blockage regions varies according to the LOCA type (corresponding to break size) and in relation to coolant flow characteristics in the blockage region.

For a small-break LOCA scenario, blockage resulting from rod cladding swelling appears during uncovering and dry-out of the upper part of the core. During this time, blockage regions are cooled by steam produced by water boiling in the lower part of the core. Under such conditions, steam flow redistribution occurs near blockages, which slows down the steam flow rate in and downstream from these blockages. Steam flow redistribution can lead to a significant decrease in heat transfers between the cladding and coolant in the vicinity of the blockages.

For a large-break LOCA scenario, blockages resulting from clad swelling mainly occur during adiabatic and reflood phases. These blockages are therefore cooled down by a flow of "mist" during the greater part of the thermal transient preceding rod quench. Cooling conditions near a blockage can therefore be defined as the combination of the following complex - favourable or adverse - thermohydraulic conditions:

- flow redistribution around the blockage, which leads to a flow decrease within and downstream from the blockage, thereby evacuating less heat,
- an increase in liquid quality at the blockage entrance due to droplet inertia, which enhances heat transfers with blockage walls,
- intensification of turbulence within the blockage, caused by droplet impacts on cladding and droplet fragmentation which desuperheats steam and favours cooldown.

The consequence of these effects - positive or negative - greatly depends on the blockage characteristics (blockage ratio<sup>a</sup> and axial extension) and coolant conditions (flow, system pressure, inlet temperature). The combination of the different effects can either degrade or, on the contrary, improve cladding-coolant exchanges in the vicinity of the blockage under large-break LOCA conditions.

Faced with this uncertainty, the 10CRF50 Appendix K - which sets forth the required and acceptable features of the Evaluation Models in accordance with which the ECCS cooling performance should be calculated under LOCA situations - issued the following restrictive requirement:

*...(I.D.5.b): "During refill and during reflood when reflood rates are less than one inch per second, heat transfer calculations shall be based on the assumption that cooling is only by steam, and shall take into account any flow blockage calculated to occur as a result of cladding swelling or rupture, as such blockage might affect both local steam flow and heat transfer"*

A number of experimental programs were launched with the aim of providing information on this specific question, and for which a review of their main experimental characteristics and conclusions will be provided hereafter.

These programs were all performed out-of-reactor and were based on thermohydraulic tests on rod simulator assemblies containing a blockage. For obvious practical reasons, deformed geometries were pre-shaped and did not change during tests. The representativity of an artificial blockage simulation in comparison with a blockage resulting from real fuel rods swelling is a fundamental aspect in evaluating the validity of this type of test. It is important to underline that this type of simulation is unable to represent the possible accumulation of fuel in balloons (relocation), such as what was observed in in-pile tests with irradiated fuel rods, i.e.: FR2 and PBF-LOC tests (cf. [1]).

---

<sup>a</sup> The blockage ratio within a group of deformed fuel rods is defined by:  $\tau = 1 - S_d/S_{nd}$ ; with  $S_d$  representing the flow area in the group of deformed fuel rods and  $S_{nd}$  representing the flow area in the same group of non-deformed fuel rods.

It must also be pointed out that the thermohydraulic conditions of tests in all programs were mainly reflood conditions, which are typically found in large-break LOCA scenarios, these being considered as bounding case for deformations and flow area restriction in relation to safety evaluation results of the different LOCA scenarios. The coolability of a blockage under thermohydraulic conditions representative of intermediate-break LOCA scenarios will therefore not be directly discussed in this SOA review.

## 2 FEBA and SEFLEX Programs

These two complementary programs were successively performed in the same KfK facility and by the same team of experimentalists. In relation to the FEBA program, the SEFLEX program mainly consisted in a sensitivity analysis on fuel rod and blockage simulation technologies. This program was based on a limited number of tests under conditions identical to those of some selected FEBA tests, thus enabling the immediate comparison of results.

### 2.1 FEBA Program

#### 2.1.1 Objectives

The FEBA (Flooding Experiments with Blocked Arrays)<sup>[2]</sup> program involved performing separate effects tests under different reflood conditions (coolant pressure, temperature and flooding rate) with the specific aim of quantifying the effects of:

- the presence of spacer grids,
- a partial blockage in a group of fuel rods, with or without a by-pass (non-deformed fuel rods at the blockage periphery),

upon cladding-coolant heat transfers in the vicinity of the blockage.

Two sets of tests were carried out in the same facility, using a 1x5 row of rods and a 5x5 rod array respectively.

The 1x5 rod row tests, whose results will not be reported here, were performed to investigate the influence of blockage geometry. From the literature available at the time (< 1975) only the results of plate blockage tests were known for two-phase flow conditions. These tests were characterised by an abrupt reduction, then expansion, of the flow path. FEBA tests on 1x5 rods were used to compare tests results using plate and sleeve blockage (cf. Figure 1).

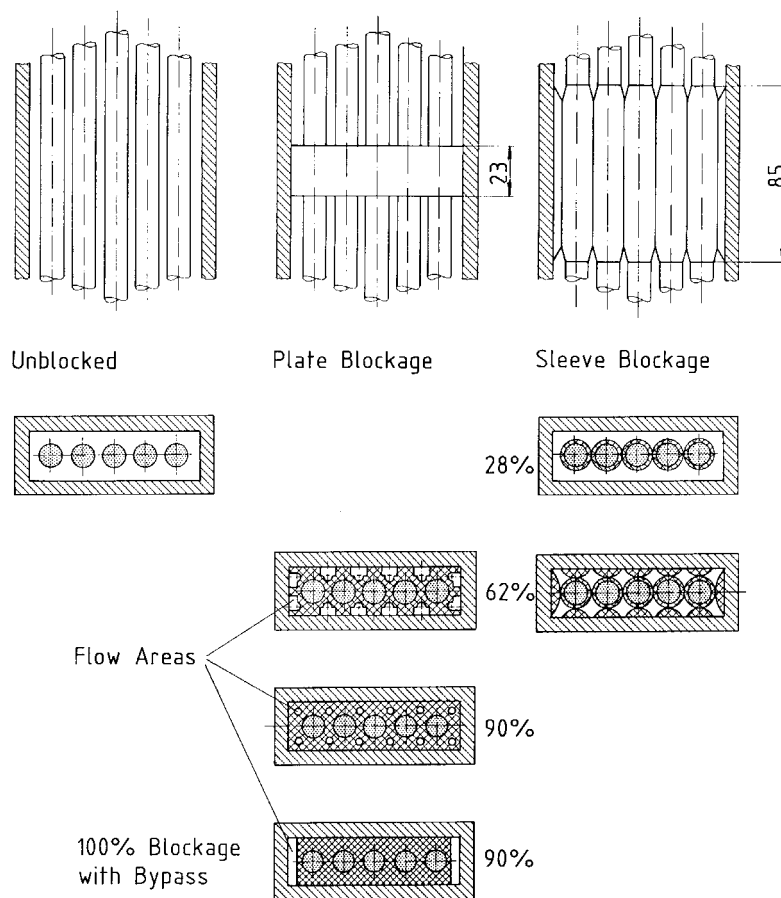


Figure 1: FEBA 5 rods row tests - Plate and sleeve blockages.

These results revealed a cooling effect downstream from the blockage that was significantly more pronounced for the plate than for the sleeve blockage, with occurrence of a secondary quench front at low reflood rates. This effect is obviously due to the greater turbulence induced by the crossing of the plate. It was concluded that a correct evaluation of the effect of clad ballooning upon thermohydraulics during the reflood phase in a LOCA scenario requires a geometrically realistic simulation of the blockage resulting from ballooning, which could be achieved by using tapered sleeves on heater rods, as was done in the tests on 5x5 rod bundles performed afterwards.

The 5x5 rod bundle tests were divided into 8 series - each corresponding to a different grid and blockage combination - as illustrated in Figure 2.

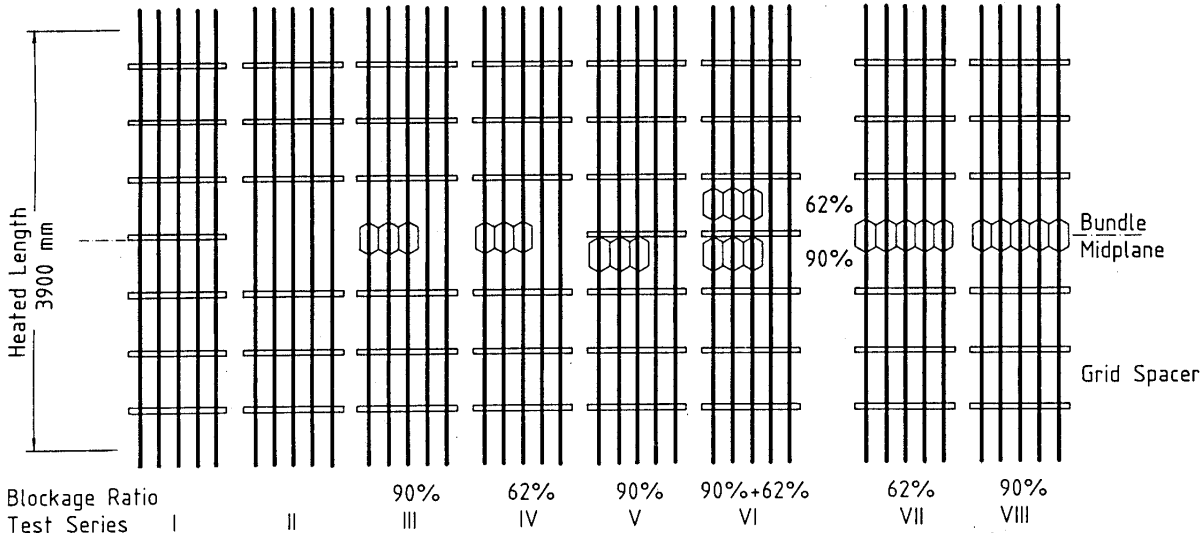


Figure 2: FEBA 5x5 rod bundle - Bundle geometries of test series I to VIII.

2.1.2 Experimental characteristics of tests performed on 5x5 rod bundles

The heater rods used in 5x5 bundle tests were “solid type” fuel rod simulators, each composed of an electrically heated spiral element embedded in a magnesium oxide insulator, itself tightly encased in 1mm thick stainless steel cladding (cf. Figure 3). These fuel rods were 3.9 m long and held by 7 spacer grids. The axial power cosine profile was approximated by 7 power steps (cf. Figure 4).

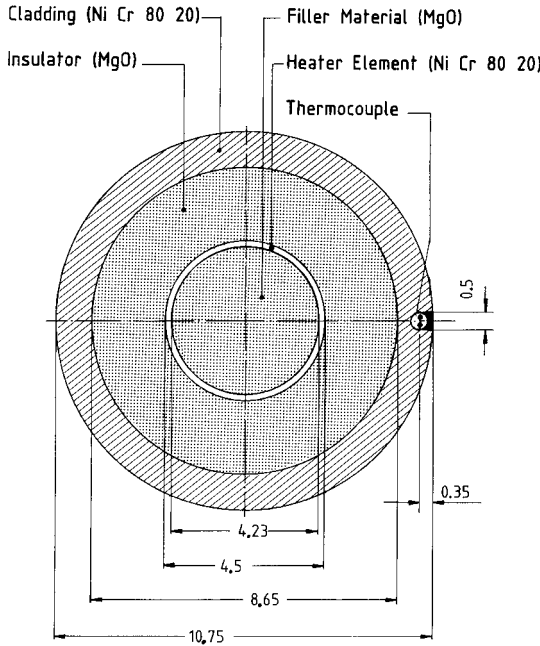


Figure 3: Cross section of the FEBA heater rod.

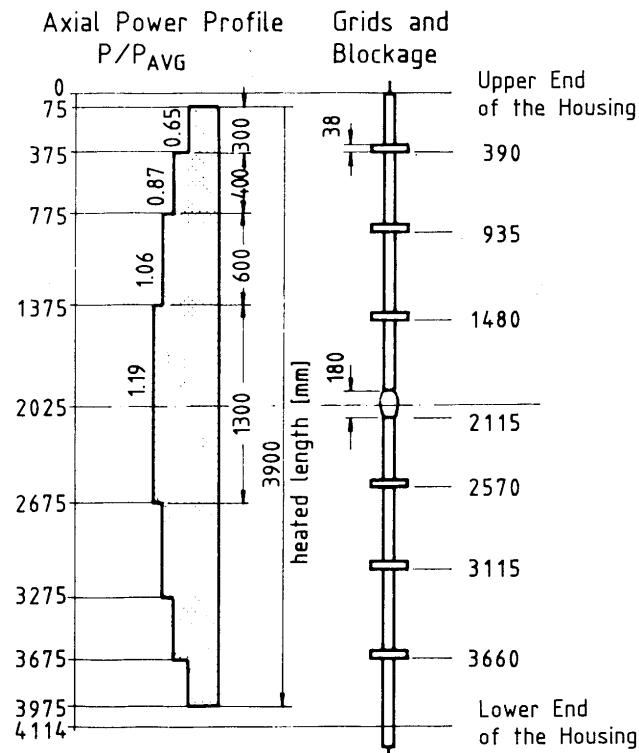


Figure 4: Layout of the FEBA heater rod.

The 5x5 bundle was housed in a 6.5 mm thick stainless steel shroud whose large calorific capacity was used to partially simulate the thermal environment of surrounding rods in a real fuel assembly prior to the start of the reflood transient. The shroud dimensions were chosen so that the hydraulic diameter in the 5x5 rod bundle was equal to that in an infinite bundle array. The shroud was heated by radiation from the heater rods for about 2 hours in order to reach initial conditions.

Series I tests were performed on a blockage-free geometry containing all spacer grids; these tests served as a reference for comparison with the subsequent series. Series II tests were also performed on a blockage-free array with the mid-plane spacer grid having been removed.

Blockages were simulated by superimposing hollow sleeves onto a 3x3 group (or the whole 5x5) rods in a coplanar manner. Two blockage ratios were chosen: 62% and 90%, which are illustrated in Figures 5 and 6 with corresponding sleeve geometries. The overall length of these stainless steel sleeves was 180 mm, with maximum blockage lengths of 125 mm (62%) and 65 mm (90%) respectively, capped with conical tapers. These sleeves were particularly thick: 1 mm in uniform thickness for the 62% blockage and 1 to 2.35 mm thick for the 90% blockage. A gap of 0.8 mm separated the sleeves from the heater rod cladding in the maximum blocked region.

In test series III to VI, blockage was simulated at the bundle mid-plane in a 3x3 rod section located in a corner of the 5x5 array, with a by-pass region around the 16 remaining rods. This configuration was designed to simulate a quarter of a 10x10 array with a central blockage on a 6x6 rod cluster.

90% and 62% blockages at bundle mid-plane were chosen in test series III and IV respectively, with the mid-plane grid removed.

The combined effects of spacer grids and blockage were examined in the test series V with a 90% blockage located immediately upstream from the mid-plane grid.

The combined effects of two successive blockages - 90% and 62% respectively - in the same rod cluster, located upstream and downstream from the mid-plane grid, were examined in the test series VI.

In test series VII and VIII, ballooning was simulated at the bundle mid-plane on all 25 rods - thereby eliminating the by-pass region - with blockage ratios of 62% and 90% respectively of the bundle flow section. Results from test series III (and IV) were compared with test series VIII (and VII) results to assess the effect of a by-pass for a given blockage ratio.

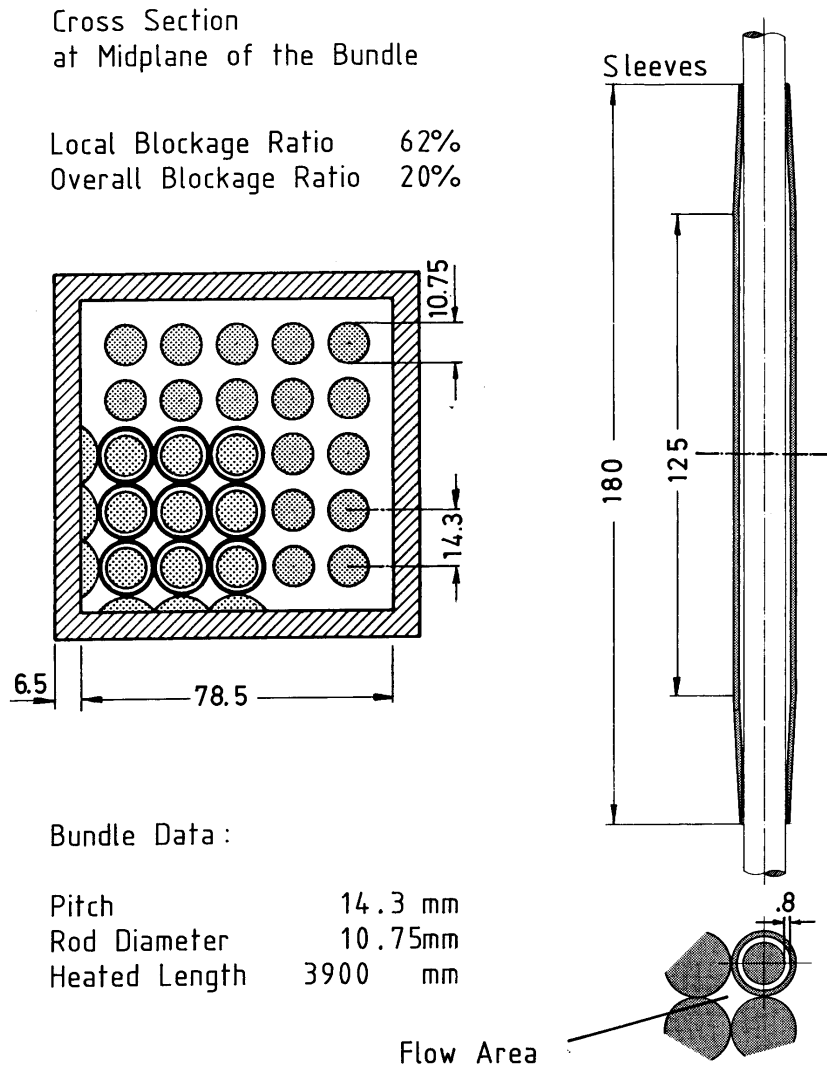


Figure 5: FEBA 5x5 rod bundle with 62% partial blockage.

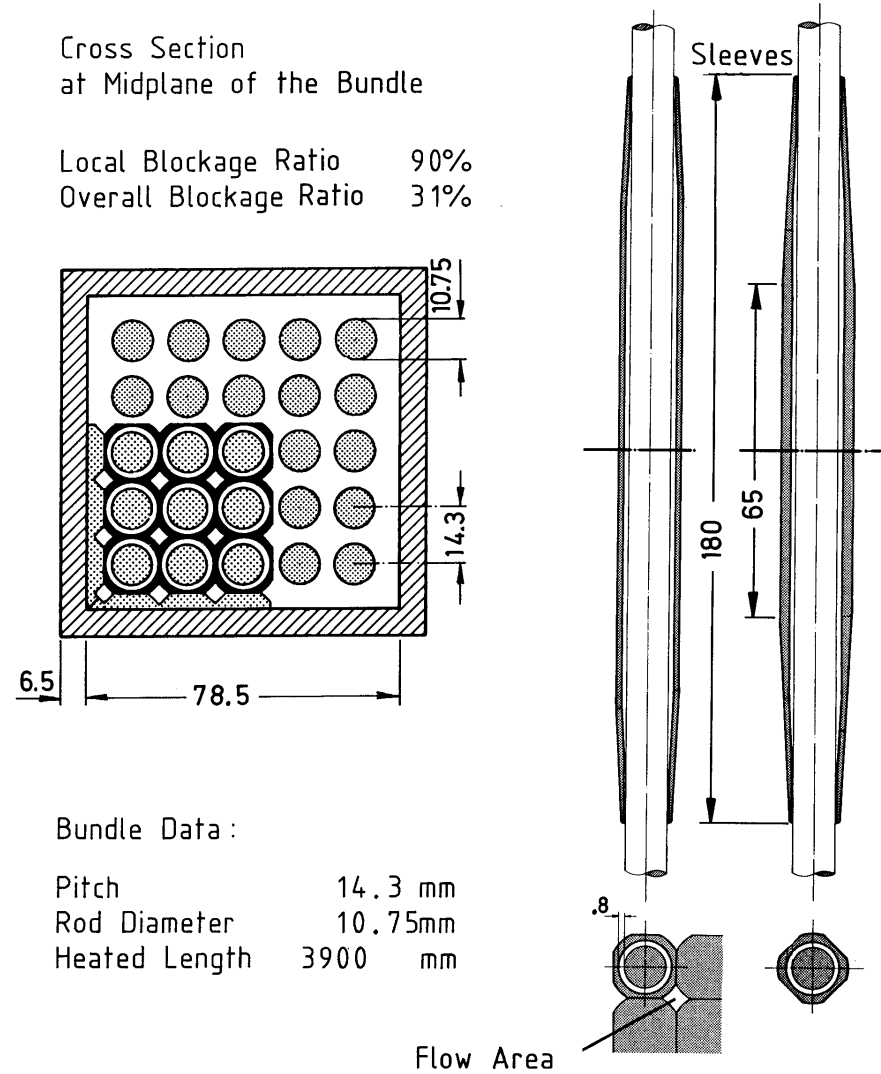


Figure 6: FEBA 5x5 rod bundle with 90% partial blockage.

For test series with blockages, side plate elements were fitted between the shroud and the sleeves of the outer fuel rods in order to obtain the target blockage ratio in the corresponding sub-channels; these elements may have favoured radial thermal leaks towards the shroud, which was slightly cooler than the bundle rods.

Tests were performed using the same experimental procedure:

- Reaching initial steady-state operating conditions in stagnant steam with the required power to obtain the desired temperature at the bundle mid-plane between 600 and 800 °C.
- Establishing reflood at a constant forced rate with a power history defined according to the decay heat ANS71 +20%, 40 seconds after reactor shutdown for most of the tests. Within the same series, the test parameters included: reflood rate, coolant temperature at the bottom of the bundle and system outlet pressure. A pressure of 4 bar and a reflood rate of 3.8 cm/s were chosen as reference conditions.

### 2.1.3 Results

#### 2.1.3.1 *90% blockage (Series III)*

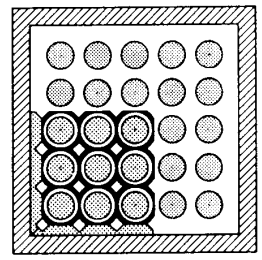
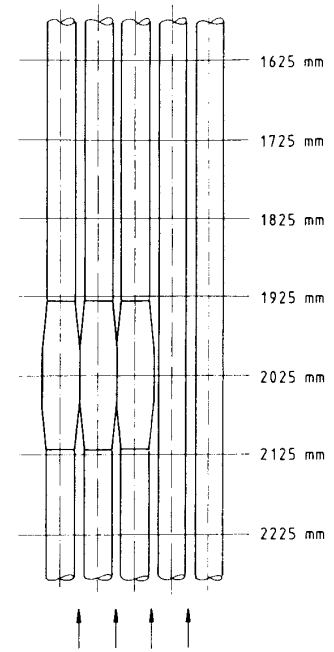
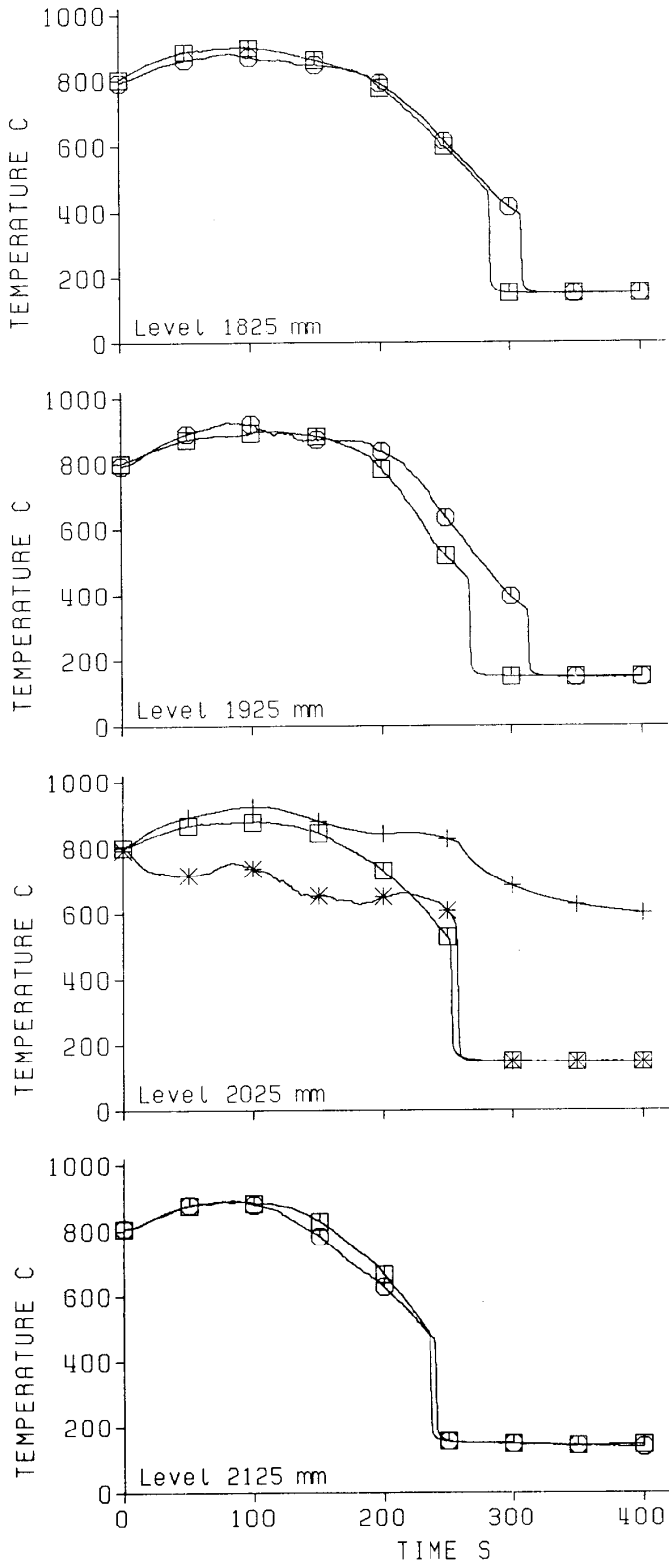
For a representative test of this series ( $P= 4$  bar;  $V_{\text{reflood}} = 3.8$  cm/s), Figure 7 illustrates the temperature variations for a) the sleeves in the blockage and b) the cladding in the by-pass, at different levels in the region of the blockage. Figure 8 superposes the temperature variations in Figure 7 with the cladding temperature variations of a test from series II (blockage-free) performed under identical conditions.

Upstream from the blockage (level 2125 mm), cladding temperatures in the blockage are close to those in the by-pass at same level. This is particularly true at the beginning of the reflood and until turnaround is reached, then even slightly lower, probably due to the cooling effect resulting from liquid droplets breaking up at the leading edge of the blockage.

At the mid-plane of the blockage (2025 mm), the sleeve temperature in the blockage is noticeably lower than the cladding temperature in the by-pass, except during the first 30 seconds preceding the quench, which occurs a little later for this sleeve. Figure 8 shows that temperature variations in the by-pass are similar to those recorded in the corresponding blockage-free test.

Downstream from the blockage (1925 mm), cladding temperatures in the blockage seem to be slightly higher than those recorded in the by-pass. There is a difference of  $\sim 40^\circ\text{C}$  at turnaround increasing up to about  $100^\circ\text{C}$  during cooling that precedes rewetting, which affects the blocked cluster 45 seconds after it does in the by-pass (cf. Figure 7). In comparison to a blockage-free test under the same conditions (cf. Figure 8), the maximum temperature at turnaround is no higher in the test with blockage, however rewetting does occur 50 seconds later. According to the FEBA experimentalists, this rewetting delay immediately downstream from the blockage would be caused by axial thermal conduction on the rod cladding from the hot region located under the sleeve, which may have prevented the propagation of the main quench front. During this cooling period, the cladding temperature should fall below that of rods at the same level in the by-pass (by approximately  $-100^\circ\text{C}$  in Figure 7) in order to initiate a second quench front. This quench front propagates at a slightly faster velocity than the quench front in the by-pass, before the two quench fronts meet further downstream. Such behavior is therefore related to the particularity of simulating cladding balloons using thick sleeves superimposed on the claddings, which most likely leads to conservative results concerning quenching delays downstream of the blockage.

The test series III did not include tests with a reflood rate below 3.8 cm/s. Therefore, it was not possible to evaluate the impact of a low reflood rate - for a blockage ratio of 90% - upon the differences in temperature and quench times as shown for the test illustrated in Figure 7.



Test No. 239  
 6 Grid Spacers  
 Blocked Bundle (3x3 Rods)  
 Blockage at Level 2025 mm  
 Blockage Ratio 90%

Flooding Rate 3.8 cm/s  
 Pressure 4.1 bar

□ Bypass Region  
 ○ Blocked Region  
 \* Sleeve  
 + Underneath Sleeve

Figure 7: FEBA - Test series III cladding temperatures.

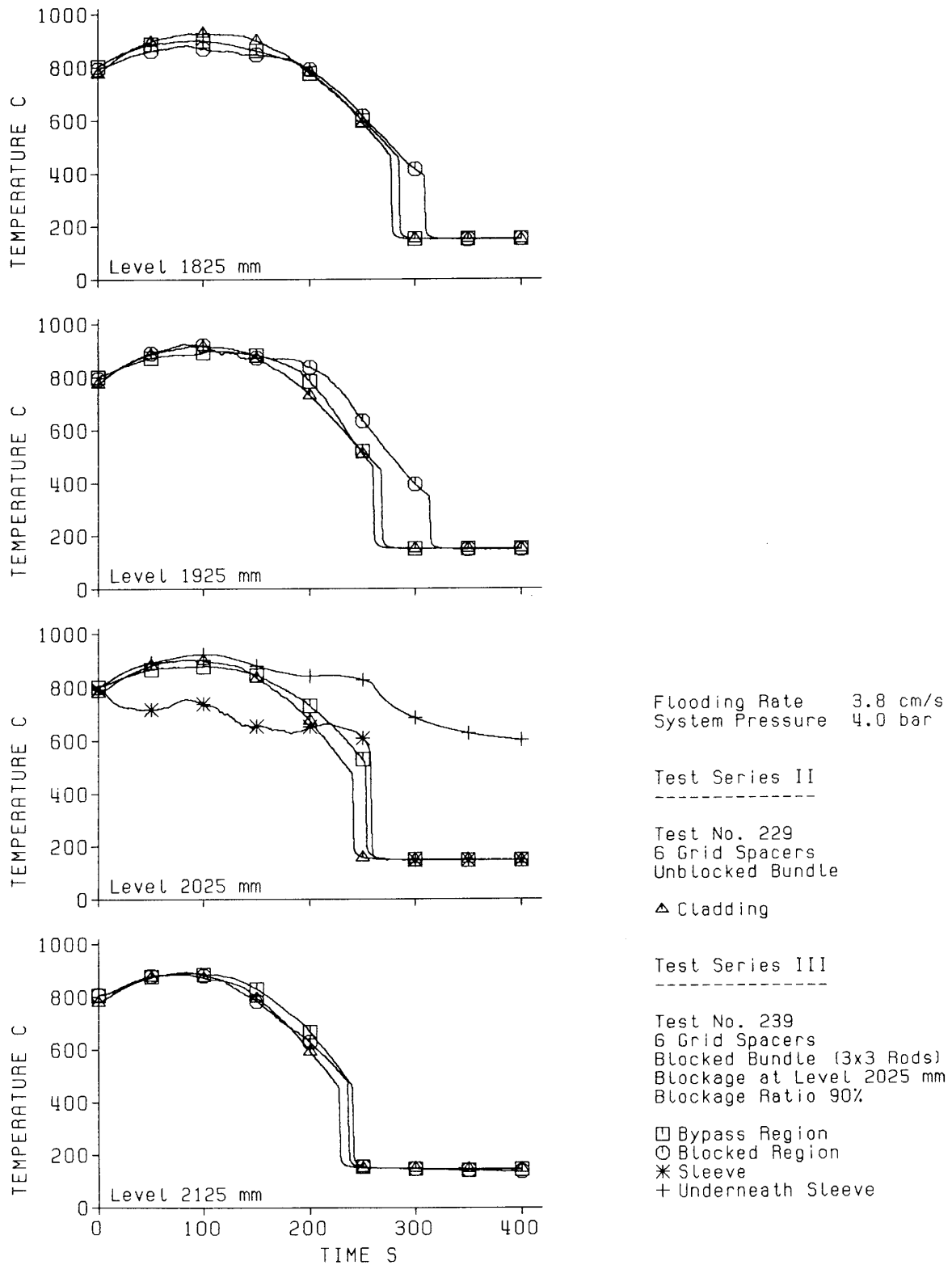


Figure 8: FEBA - Test series II and III cladding temperatures.

### 2.1.3.2 62% blockage (Series IV)

Figure 9 illustrates temperature variations recorded at different levels for a test in this series, under identical conditions ( $P = 4$  bar,  $V_{\text{reflood}} = 3.8$  cm/s) to those of test illustrated in Figure 7. On the whole, these variations are similar to those obtained in the 90% blockage case, with however, two significant differences: rewetting of the sleeves within the blockage and of the cladding just downstream from the blockage occurs earlier than in the by-pass at the same levels. Downstream from the blockage (1925 mm), a second quench front therefore occurs before the main quench front reaches the same level in the by-pass, with these two quench fronts meeting up 100 mm further downstream.

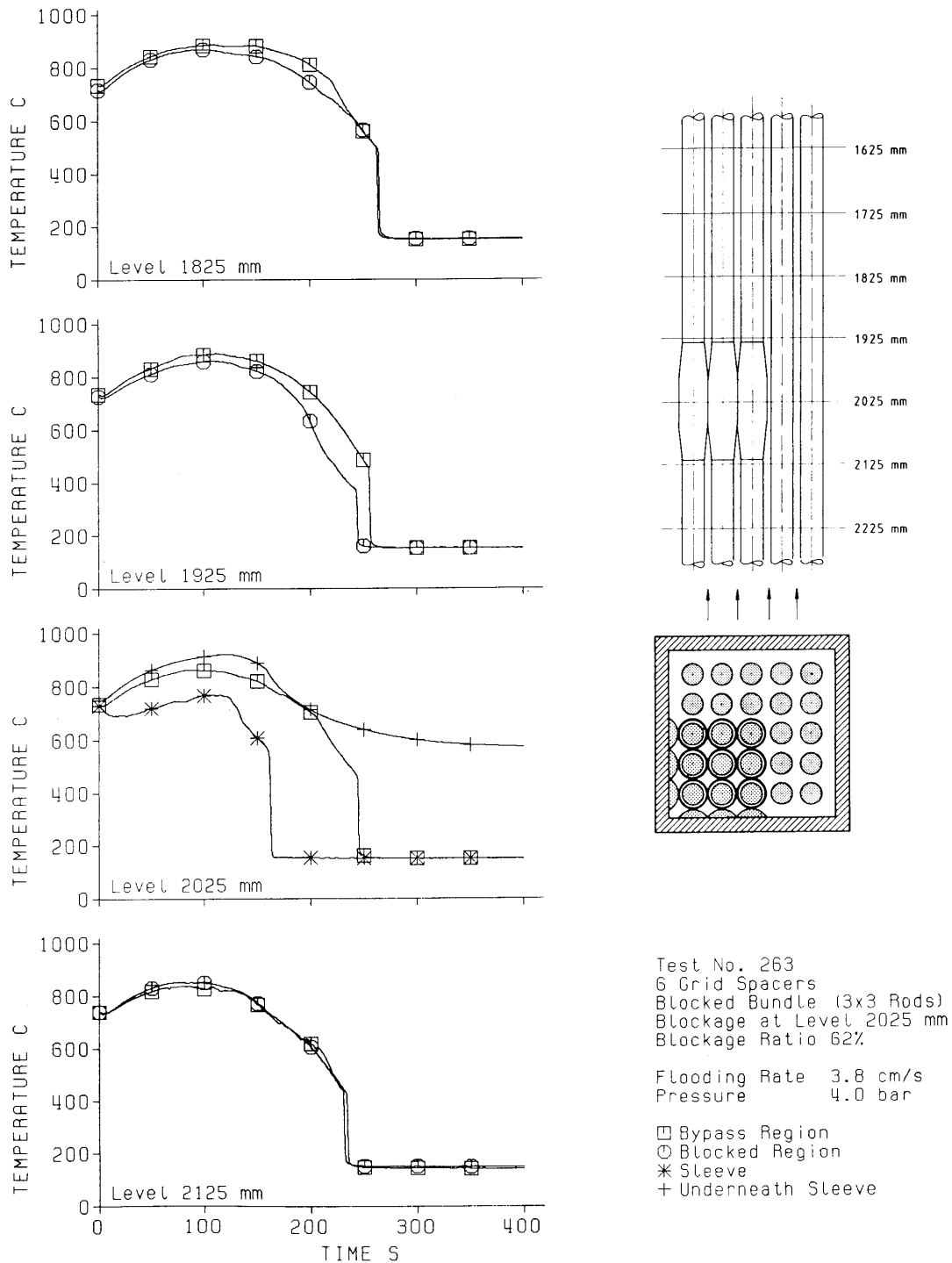


Figure 9: FEBA - Test series IV cladding temperatures.





### 2.1.3.3 Combined effects of several consecutive blockages and spacer grids

Test series V and VI were designed to investigate the combined effects of one or several blockages near a spacer grid.

For the test series V with a 90% blockage located just upstream from the mid-plane spacer grid, results show very similar temperature variations to those observed in corresponding tests of series III without a mid-plane grid. The presence of this spacer grid does not reduce the slight superheating of the cladding downstream from the blockage in comparison to the cladding in the by-pass, but does lead to a slightly earlier quenching than the quenching occurring in the by-pass.

For test series VI with two blockages of 90% and 62% located upstream and downstream from the mid-plane grid respectively, test results under "standard" conditions revealed (cf. Figure 12):

- at levels of the upstream 90% blockage (2225 - 2025 mm), behavior similar to that observed in the series III test with only one blockage (cf. Figure 7);
- at levels of the downstream 62% blockage (1925 - 1725 mm), a marked reduction in cladding temperatures just at the blockage outlet, in comparison to cladding temperatures in the by-pass at the same level, but a reverse of this tendency further downstream where cladding temperatures of the blocked cluster rise above those recorded in the by-pass 200 mm downstream from the second blockage.

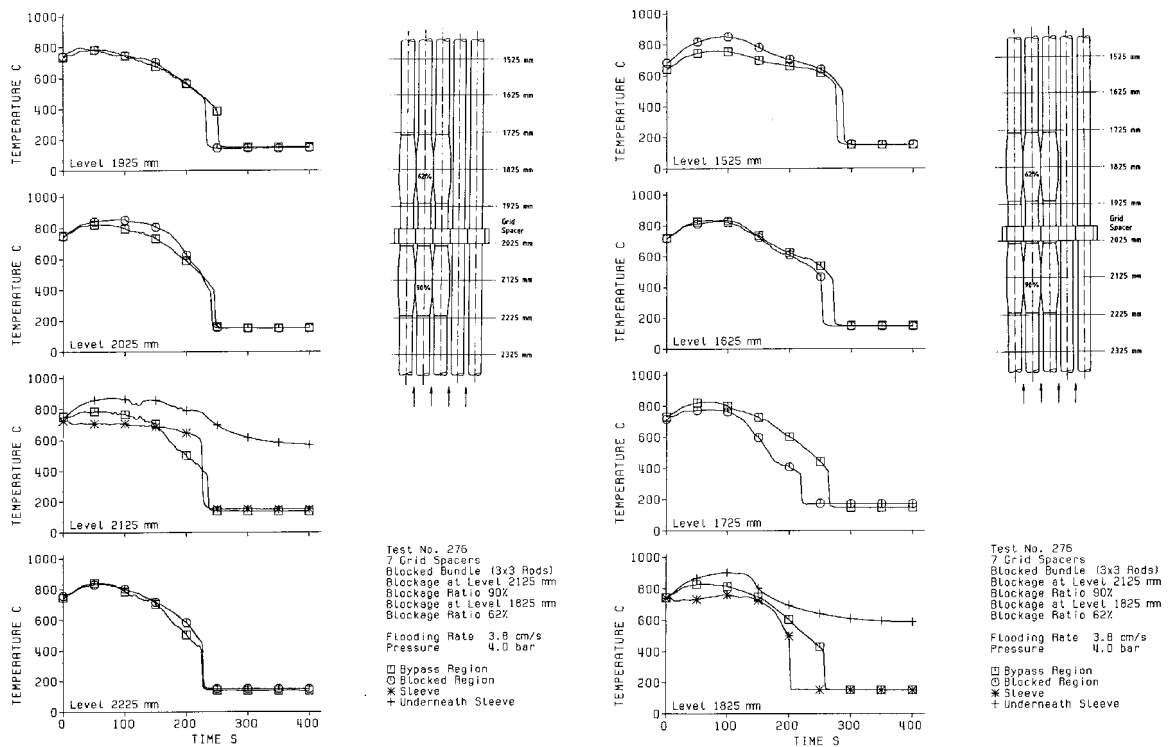
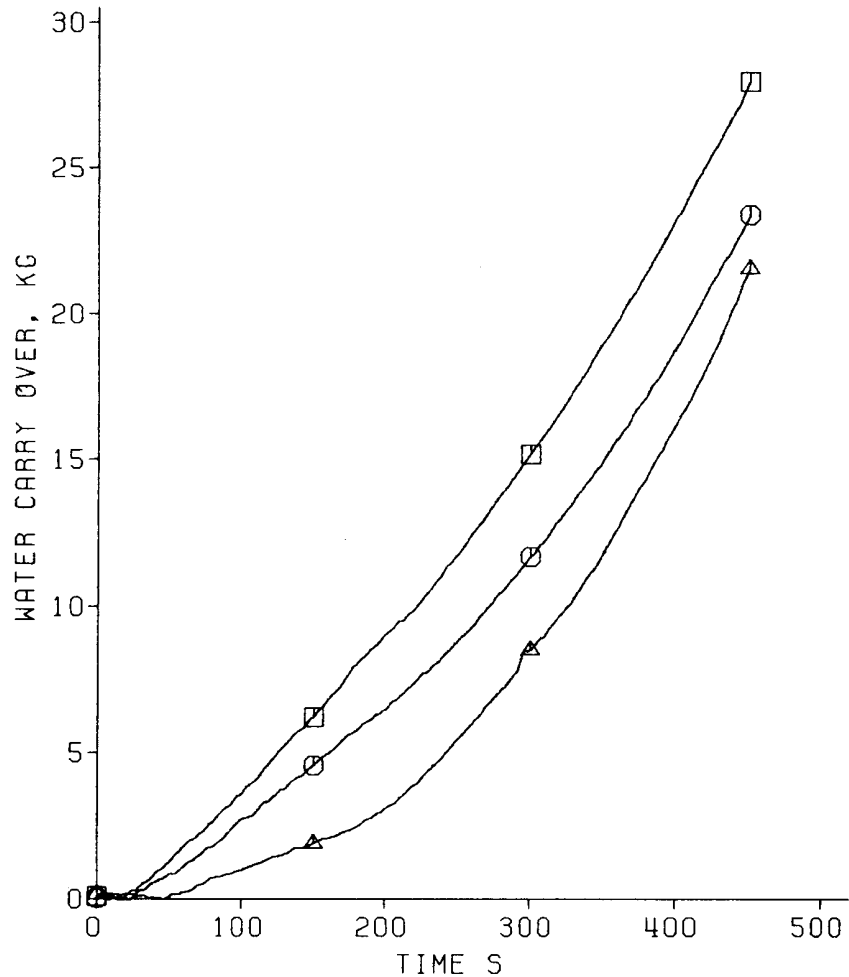


Figure 12: FEBA - Test series VI cladding temperatures.

The behavior observed downstream from the second blockage can be explained by the decrease in the liquid content of the coolant flow after having passed through successive obstacles due to the impact of the droplets on the balloons and the spacer grid. This tends to fragment these droplets into smaller droplets and accentuate the evaporation process.

Figure 13 illustrates the variations in water carry over at the bundle exit for 3 tests performed under the same conditions taken from 3 series with differing configurations: series IV (62% blockage without mid-plane grid), series V (62% blockage with mid-plane grid) and series VI (90% blockage + mid-plane grid + 62% blockage). This Figure shows that towards 250 s - corresponding to the quenching of the 62% blockage outlet in each series - the water carry over for the series VI test is less than half of the water carry over recorded for the series IV test. Thus, far downstream from the second blockage, the liquid content of the coolant flow is lower, which leads to the clad superheating observed in this region in comparison to the by-pass region.



Flooding Parameters:  $V = 3.8 \text{ cm/s}$ ,  $P = 4.1 \text{ bar}$

- Test Series IV, Test No. 263
- Test Series V, Test No. 282
- △ Test Series VI, Test No. 276

Figure 13: FEBA - Water carry over: influence of flow blockage.

Therefore, the series VI test results indirectly suggest a significant influence of balloon lengths, which will be examined in the THETIS and CEGB tests discussed further on in this document.

### 2.1.3.4 By-pass effects

In the last two series VII and VIII, the blockage - set at 62% and 90% respectively - was extended to all sub-channels, thereby removing the possibility for the coolant to by-pass the blocked region. The mass flux in the blocked sub-channels of these tests was identical to that of tests performed under the same conditions in the blockage-free reference series I. Though non-representative of reactor conditions (where by-passes always exist), the last two series nevertheless made it possible to quantitatively evaluate the effect of the blockage ratio under comparative cooling rate conditions.

Figure 14, which superposes the results of a series III test (90% blockage in a 3x3 rod region) on the results of a series VIII test (90% blockage in a 5x5 rod region) performed under reference conditions ( $P = 4$  bar,  $V_{\text{reflood}} = 3.8$  cm/s), shows a higher cooling of the blockage sleeves with earlier rewetting for a bypass-free test than for a test with by-pass. Cooldown is particularly pronounced downstream from the blockage, occurring almost at the beginning of the transient. This unrealistic variation is certainly due to the significant increase in the mass flux in the blockage sub-channels caused by the absence of a by-pass.

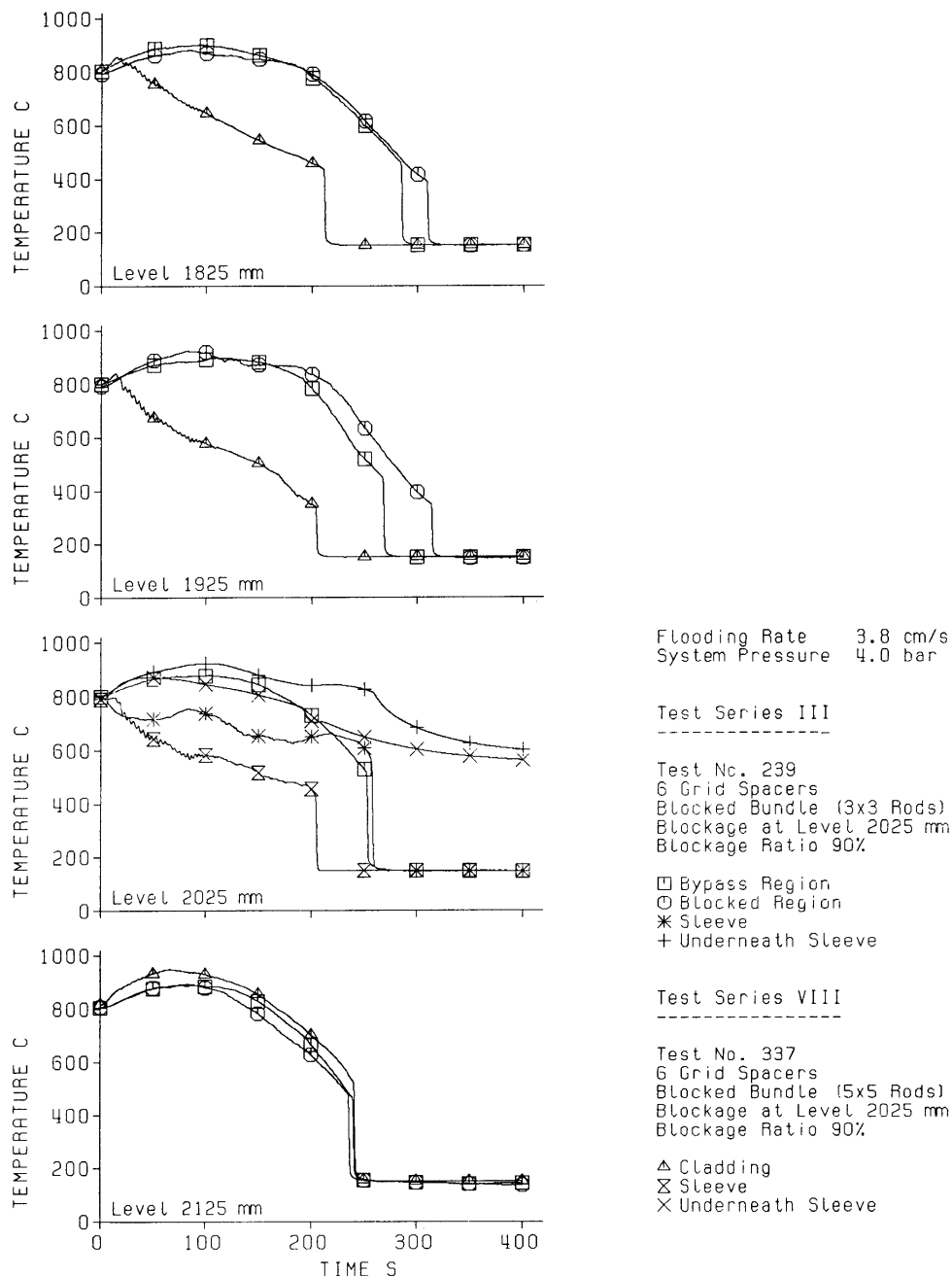


Figure 14: FEBA - Test series III and VIII cladding temperatures: effect of blockage extension.

#### 2.1.4 FEBA program conclusions

Under the blockage conditions simulated in FEBA tests obtained by superimposing a thick sleeve on a "solid type" simulator rod (without gap between the heated core and the cladding), results may be summarised as follows:

- With a blockage ratio of 90%, the temperatures of the blockage sleeves are significantly lower than those of the cladding in the by-pass, except during the 30 seconds preceding rewetting for the test with a reflood rate of 3.8 cm/s, where sleeve rewetting is slightly delayed. Downstream from the blockage, the maximum cladding temperature of the blocked rods appears to be slightly higher (~40 °C) than the maximum temperature of the by-pass rods. This difference in temperature reaches approximately 100°C during cooldown preceding rewetting, which occurs with a delay of 45 s for the blocked rods in comparison to the by-pass rods. However, compared with a blockage-free test under the same conditions, the maximum temperature at turnaround is no higher in the test with blockage, although rewetting does occur 50 s later.
- With a blockage ratio of 62%, the temperatures of the blockage sleeves are always significantly lower than those of the cladding in the by-pass. Rewetting also occurs earlier in the blockage, except for the test with a reflood velocity of 2.2 cm/s where rewetting occurs in the by-pass first. Downstream from the blockage, the maximum cladding temperature in the blocked region always appears lower than the maximum temperature in the by-pass region.
- For a double blockage of 90% and 62%, located respectively upstream and downstream from the mid-plane spacer grid, behavior in the blockages appears to be similar to that recorded in tests with only one blockage. A marked reduction in cladding temperatures is observed at the 62% blockage outlet (in comparison to those recorded in the by-pass at the same level). However, this tendency reverses further downstream where blockage cladding temperatures rise above cladding temperatures in the by-pass. This observation suggests a possible penalising behavior in a blockage configuration with long balloons.
- As expected, coolability significantly increases in the absence of a by-pass, both within and downstream from the blockage in comparison to a test with a by-pass under the same inlet conditions.

Even though FEBA test results do not reveal any alarming behavior impairing the coolability of a blocked fuel assembly under reflood conditions (no detrimental behavior with a 62% blockage ratio and only a 40°C penalty upon the maximum temperature downstream from a 90% blockage), one of the major criticisms of this program concerns the low representativity of tests in comparison to fuel rods subjected to realistic PWR conditions, where cladding ballooning leading to blockage proportionally reduces their thickness, hence thermal inertia. It was also pointed out earlier that superimposing sleeves on heater rods induces a delay in rewetting immediately downstream from the blockage, due to the axial thermal conduction on rod cladding from the hot region located under the sleeve, which hinders the propagation of the main quench front.

It had been admitted from the very beginning that the FEBA results would provide conservative estimates. The SEFLEX tests, which were undertaken to evaluate the margin of these conservative estimates, were performed in the same facility using identical procedures, but with a realistic blockage design and the selection of a set of conditions to enable the immediate comparison with FEBA results.

## 2.2 **SEFLEX Program**

### 2.2.1 Objectives

As the name indicates, the SEFLEX program (Fuel Rod Simulator Effects in Flooding Experiments)<sup>[3]</sup> was designed to evaluate the sensitivity of FEBA-type reflood test results to the simulation techniques of the fuel rods and flow blockage.

As a reminder, the heater rods used in the FEBA tests were "solid-type" simulators composed of a spiral wound heating element embedded in the MgO insulator and then tightly encapsulated in a 1 mm thick NiCr 80 20 cladding (cf. Figure 3).

LOCA-type comparative in-pile tests carried out in the Halden Boiling Water Reactor (HBWR) using both nuclear reactor fuel rods and standard SEMISCALE fuel rod simulators revealed a significant delay in quenching for fuel rod simulators in comparison to nuclear fuel rods (cf. Figure 15). However, similar tests performed on electric fuel rod simulators developed for the REBEKA program revealed the ability of the REBEKA simulators to better reproduce nuclear reactor fuel rod behavior (cf. Figure 16). These results supported qualitative results from other comparative tests, thereby demonstrating the conservative character of reflood tests using solid-type rod simulators.

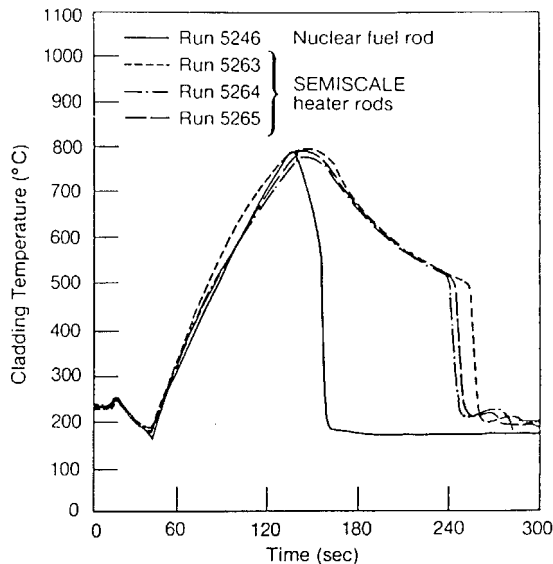


Figure 15: Comparison of nuclear fuel rod and SEMISCALE heater rod responses in the Halden reactor.

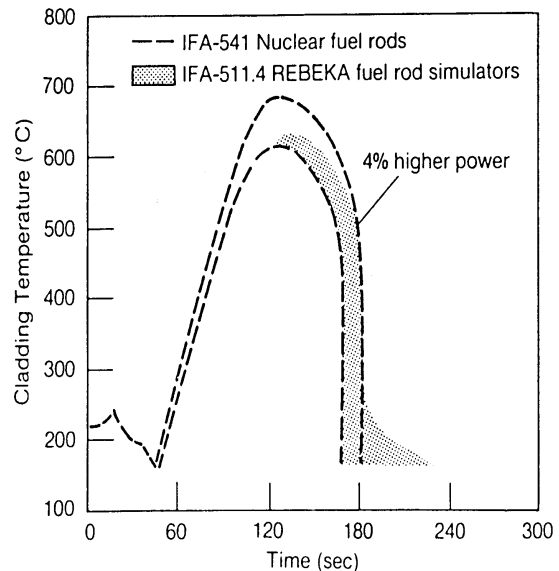


Figure 16: Comparison of nuclear fuel rod and REBEKA heater rod responses in the Halden reactor.

With this in mind, the SEFLEX program was intended to quantify the influence of the design and physical features of fuel rod simulators upon heat transfers and quench front progression during a LOCA reflood scenario in blocked and unblocked rod assemblies. In addition to using a representative electric fuel rod simulator (REBEKA rod), the other major difference between SEFLEX and FEBA tests lies in the blockage design: the blockages in SEFLEX were no longer obtained by superimposing sleeves on the cladding, but by initial pre-forming of the cladding.

### 2.2.2 Experimental characteristics

The fuel rod simulators used in the SEFLEX program are REBEKA-type rods, which were developed to simulate the behavior of German PWR fuel rods in cladding deformation-failure tests for the REBEKA program. From the centre outwards, these simulators consist of (cf. Figure 17):

- a heater rod with a 6.02 mm outer diameter, composed of an Inconel annular heater rod sheath enveloping an MgO insulating core and insulated from an Inconel cladding by a boron nitride sleeve;
- annular alumina pellets simulating fuel pellets;
- a 0.725 mm thick Zircaloy cladding with a 9.3 mm internal diameter, separated from the alumina pellets by a 0.05 mm wide gap filled with helium or argon depending on the test series.

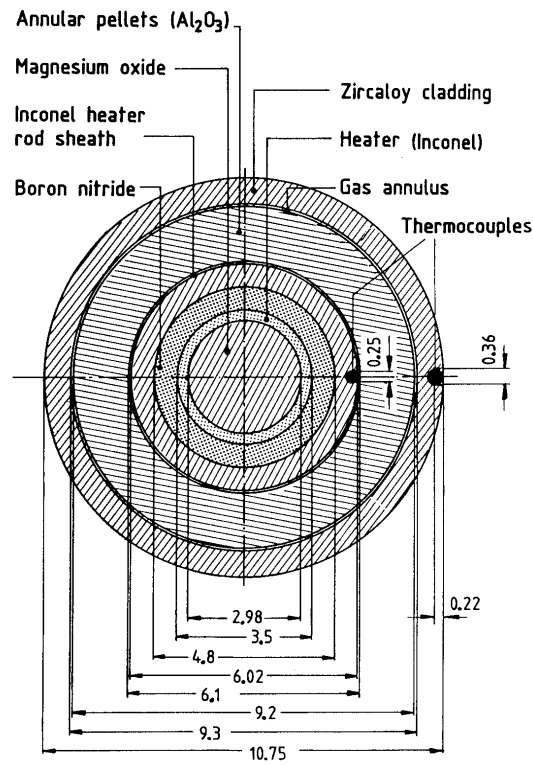


Figure 17: Cross section of a REBEKA fuel rod simulator.

As in the FEBA assembly, the 5x5 SEFLEX rods, 3.9 m long, were held in a set of 7 grids within a stainless steel shroud identical to that used for the FEBA tests (6.5 mm thick, 78.5 mm inside width).

Four series of tests were performed: two blockage-free series and two series with a 90% blockage in a 3x3 group of rods in a corner of the 5x5 rod array.

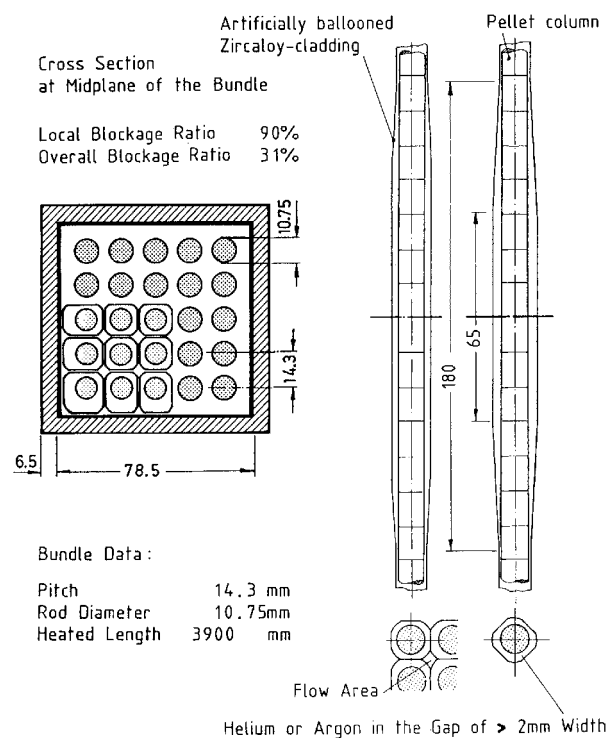


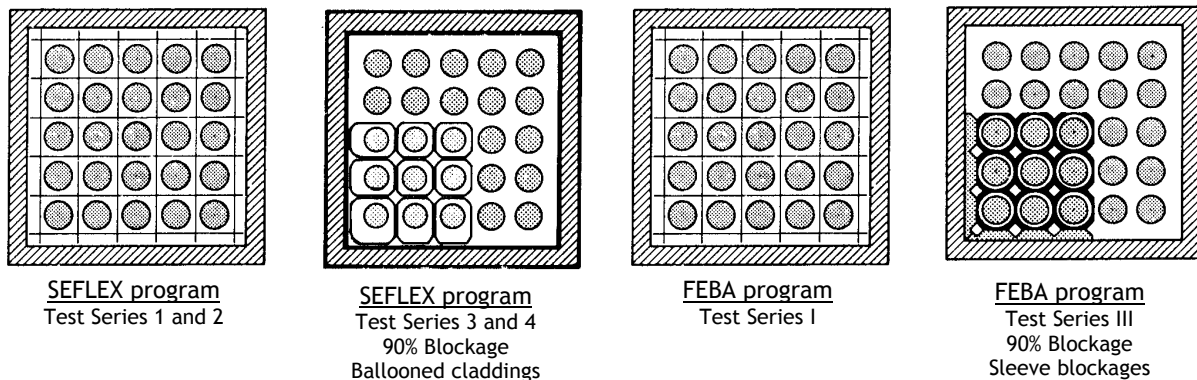
Figure 18: Sectional view of the SEFLEX 90% blockage

As a main difference with the FEBA tests, blockages simulated in the SEFLEX assembly were obtained by heating up and ballooning a pressurized Zircaloy tube inside an appropriately sized mould until the intended geometry was obtained, before slowly cooling it down to avoid deformation or rupture. This procedure leads to a cladding thickness in the deformed part of the tube that is representative of the thickness observed in a nuclear reactor fuel rod having undergone a LOCA swelling phase. The balloons formed in this manner have axial dimensions equivalent to those obtained in the FEBA sleeves: a total deformed length of 180 mm for a deformed length of 65 mm with a blockage ratio of 90% (cf. Figure 18). To avoid using additional pieces for the peripheral sub-channels - as was the case in the FEBA program - specific deformations were simulated in peripheral and corner fuel rods (cf. Figure 18).

### 2.2.3 Test matrix

Table 1 shows the SEFLEX test matrix, indicating the FEBA tests with corresponding conditions. These tests were divided into four series.

- Series 1 was performed on a blockage-free bundle containing 7 spacer grids; rods were pressurised with helium. This series of reference tests is to be compared with FEBA series I.
- Series 2 was a variation of series 1 using argon-pressurised rods.
- Series 3 involved a 90% blockage ratio near the mid-plane elevation in a 3x3 cluster in the corner of the 5x5 array, with the mid-plane spacer grid having been removed. Fuel rods were pressurised with helium. This series is to be compared with series III of the FEBA program.
- Series 4 was a variation of series 3 using argon-pressurised rods.



Program	Test Series	Test-N°	Rod Design	Cladding Material	Gap Gas Filling	Flooding Velocity (cm/s)	System Pressure (bar)	Feedwater Temperature (°C)	Reference Tests	
									FEBA N°	SEFLEX N°
SEFLEX	1	05	REBEKA	Zircaloy	Helium	3.8	2.1	40	223	07
SEFLEX	1	03	REBEKA	Zircaloy	Helium	3.8	4.1	40	216	
SEFLEX	1	06	REBEKA	Zircaloy	Helium	5.8	2.1	40	218	
SEFLEX	1	04	REBEKA	Zircaloy	Helium	5.8	4.1	40	214	
SEFLEX	2	07	REBEKA	Zircaloy	Argon	3.8	2.1	40	223	05
FEBA	I	223	FEBA	SS	gapless	3.8	2.1	40		05 and 07
FEBA	I	216	FEBA	SS	gapless	3.8	4.1	40		03
FEBA	I	218	FEBA	SS	gapless	5.8	2.1	40		06
FEBA	I	214	FEBA	SS	gapless	5.8	4.1	40		04
SEFLEX	3	32	REBEKA	Zircaloy	Helium	3.8	2.1	40	241	
SEFLEX	3	35	REBEKA	Zircaloy	Helium	3.8	4.1	40	239	
SEFLEX	4	33	REBEKA	Zircaloy	Argon	3.8	2.1	40	241	
SEFLEX	4	34	REBEKA	Zircaloy	Argon	3.8	4.1	40	239	
FEBA	III	241	FEBA	SS	gapless	3.8	2.1	40		32 and 33
FEBA	III	239	FEBA	SS	gapless	3.8	4.1	40		34 and 35

Table 1: SEFLEX program test matrix

Rods were pressurised with helium or argon in order to study the influence of the gap thermal conductivity on the reflood behavior. Helium is the filling gas for fresh fuel rods whereas the argon thermal conductivity simulates roughly that of the fission gas mixed with helium found in high burnup fuel rods. The internal gas pressure was set at 1 bar above test pressure conditions.

It is important to point out that the SEFLEX test matrix included a limited number of tests, only with an injection temperature of 40°C and flooding velocities of 3.8 and 5.8 cm/s.

## 2.2.4 Results

### 2.2.4.1 Blockage-free tests

Figure 19 compares the temperature variations at different levels in blockage-free tests under identical reflood conditions of the FEBA and SEFLEX series (with helium or argon pressurised rods).

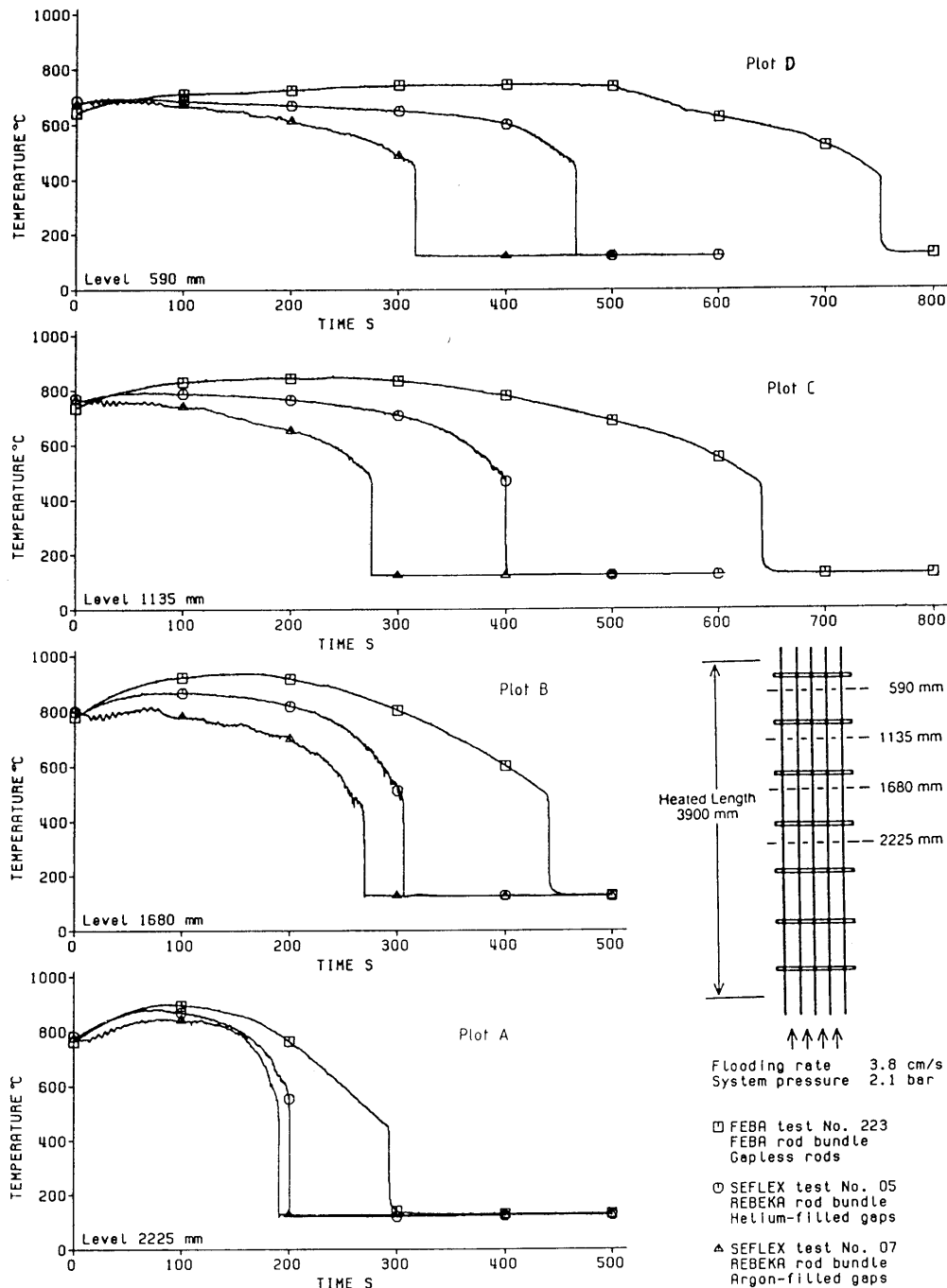


Figure 19: Cladding temperatures measured at 4 different axial levels in FEBA and SEFLEX rod bundles.

These temperature variations clearly show:

- quicker quench front progression for the SEFLEX tests in comparison to the FEBA test;
- lower cladding temperatures for the REBEKA fuel rod simulators than for the gapless FEBA simulators.
- an accentuation of these effects for the filling gas with the lowest conductivity (argon) in the SEFLEX tests.

Such differences in behavior can be explained by the lower heat capacity of the Zircaloy cladding, as well as by the higher thermal decoupling of the cladding from the heat source in the REBEKA rod simulators, in comparison to the thick stainless steel cladding of the solid-type FEBA rods:

- for identical initial temperatures, the stored energy per unit length in a REBEKA rod cladding is 2.7 times lower than that stored in a FEBA rod cladding ( $\rho C_p = 2.15$  for Zircaloy in comparison to 4.17 for stainless steel; REBEKA cladding thickness = 0.725 mm in comparison to 1.05 mm for FEBA cladding);
- the thermal conductance on the inner surface of the cladding for a REBEKA rod is between 5 (He-filling) and 40 (Argon-filling) times lower than for a FEBA rod.

Comparative thermal analysis of these tests was carried out by KfK (now FZK) based on a set of inverse conduction calculations performed with the modified HETRAP computer code (ORNL). These calculations helped reproduce the 1) radial temperature profile in the rod, 2) cladding-coolant heat flux and the heat transfer coefficient and 3) stored heat per unit of length, with input data of the specific rod power and the measured surface & coolant temperatures.

For the period preceding rewetting, these calculations indicated slightly higher cladding-coolant heat fluxes for REBEKA rods than for FEBA rods, which leads to a more rapid release of stored heat (cf. Figure 20). It can be noticed that the heat release is faster for the argon-pressurised REBEKA rod, despite a higher thermal resistance across the gap; this can be explained by the substantially higher surface heat flux of the argon-filled REBEKA rod than that of the helium-filled rod for most part of the reflood period. The increased reflood heat transfer of REBEKA rod bundles compared to that of FEBA rod bundles results from both gap conductance effects and variations in cladding properties and geometry, without it being possible to quantify the respective effect of each parameter using the FEBA and SEFLEX results only.

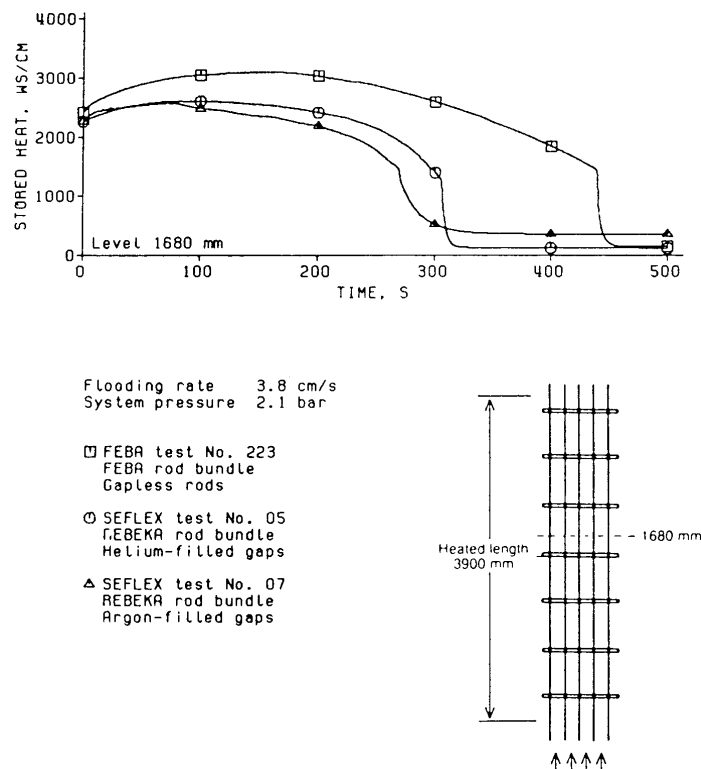


Figure 20: Release of stored heat from FEBA and SEFLEX rods.

Figure 21 compares - for the same 3 tests at level 1680 mm - the calculated radial temperature profiles in the FEBA and SEFLEX rods, at different times before and after rewetting occurs. In the SEFLEX tests (Plot B and C), the arrival of the quench front leads to a rapid fall in cladding temperatures whereas temperature profiles in the rest of the rod remain rather flat, with a slight delay in cooldown, particularly for argon-pressurised rods. As for the FEBA test (Plot A), the rising quench front has to remove more heat stored in the cladding and the filler material in close contact with it: no abrupt variations are observed in the temperature profiles. This causes a slower quench front progression and a globally slower release of stored energy from the rod. Figure 22 illustrates these results, comparing the water carry-over downstream from the FEBA and SEFLEX bundles: for identical reflood injection rates, the mass of water exiting the test section is noticeably lower in the SEFLEX tests, which involves a higher evaporated amount of water when passing through the bundle, therefore more effective heat removal from the rods.

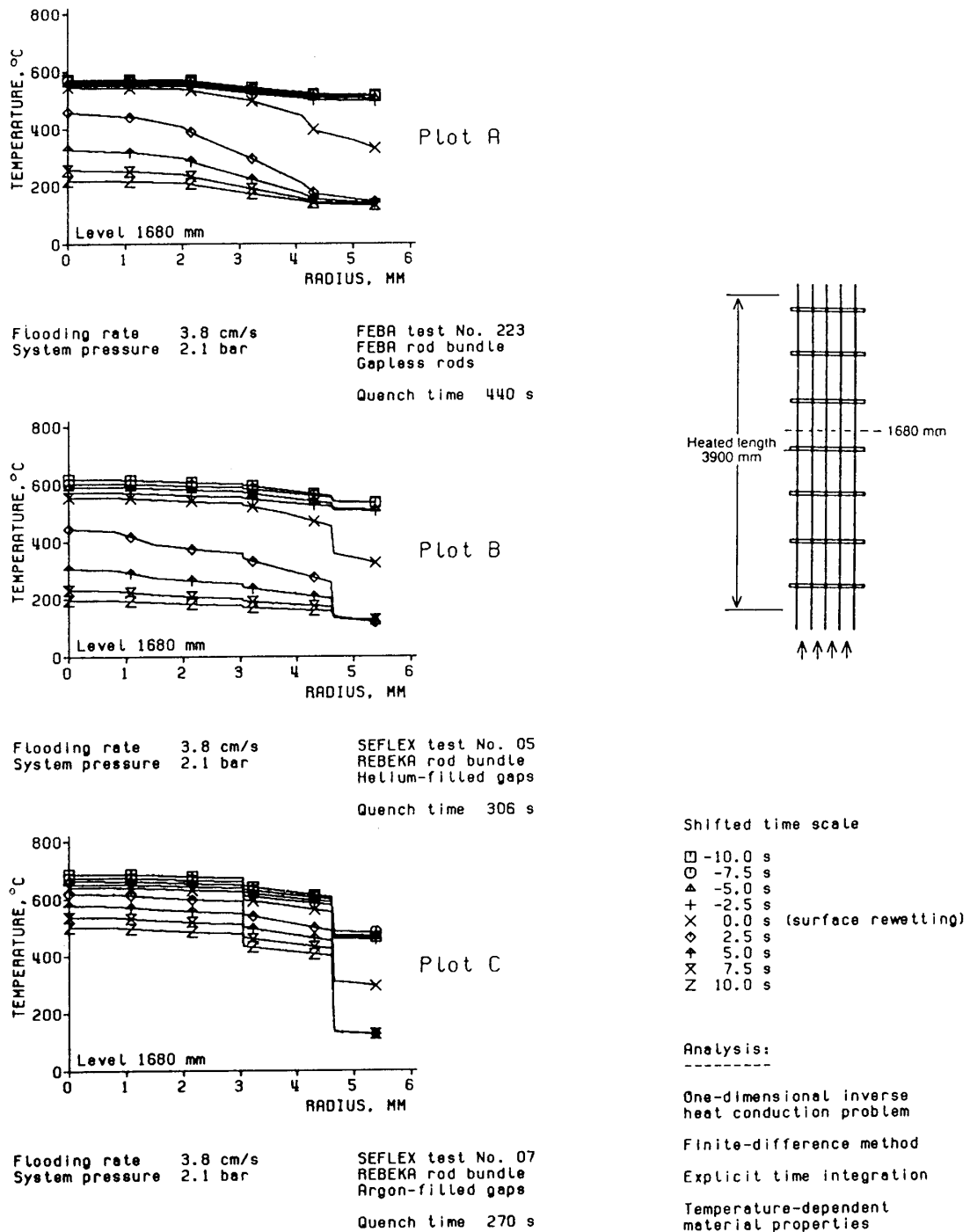


Figure 21: Radial temperature profiles as function of time during quenching of FEBA and SEFLEX rods.

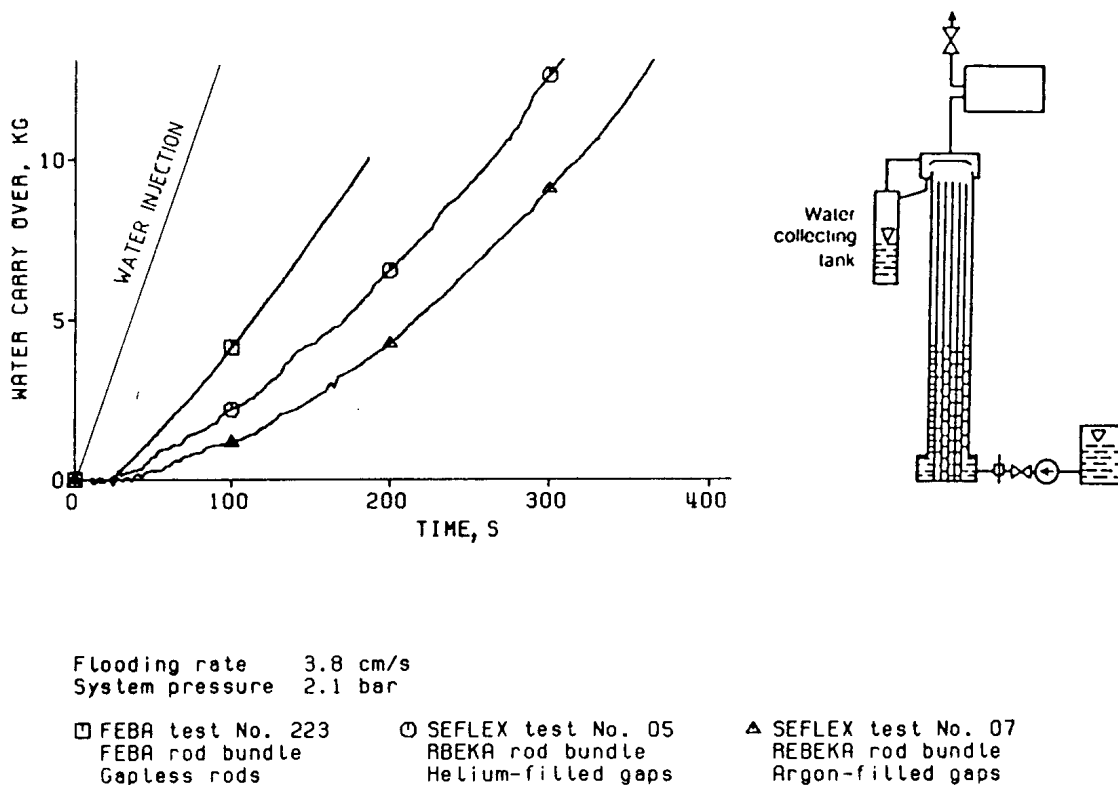


Figure 22: Water carry-over from FEBA and SEFLEX rod bundles.

#### 2.2.4.2 90% blockage tests

Figure 23 compares temperature variations measured at the mid-plane of the 90% blockage for a FEBA test (Plot A) and two SEFLEX tests, with helium-filled (Plot B) and argon-filled (Plot C) gaps. All three tests were performed under the same reflow conditions (3.8 cm/s, 2.1 bar). Concerning the FEBA test, the sleeve temperature is lower than the cladding temperature of a by-pass rod at the same level for a period of 300 s; then the sleeve temperature exceeds the cladding temperature in the by-pass, until quenching which occurs at 385 s, approximately 30 s later than for the by-pass rod. As for the SEFLEX tests, ballooned cladding temperatures are always lower than those of the by-pass rod. Moreover, cladding rewetting occurs at a considerably earlier stage -around 15 s - than it does for a by-pass rod, occurring between 130 to 150 s. This difference in behavior can be explained by the much lower thermal capacity of the SEFLEX balloons in comparison to FEBA sleeves, as well as greater thermal decoupling from the heater rod due to a larger gap. After balloon rewetting, the temperature of the heater sheath underneath the balloon remains high, particularly for the argon-pressurised rod, due to the high thermal resistance in the 2.3 mm wide gap; this had already been observed in the FEBA test rods, with however a narrower steam-filled gap (~ 0.8 mm).

Figure 24 compares the temperature variations immediately downstream from the blockage for the same tests. In the FEBA test, the cladding temperatures of the blocked rod are close to those of the by-pass rod until turnaround is reached, after which they decrease at a slightly slower rate until rewetting occurs, with a delay of 80 s in comparison to rewetting in the by-pass. Concerning the SEFLEX tests, early rewetting that is initiated in the region of maximum blockage leads to the rapid propagation of secondary quench fronts, both upstream and downstream from the blockage. The blockage exit level is rewet at approximately 30 s, whereas rewetting occurs at approximately 170 s in the by-pass. The argon-pressurised rod undergoes rewetting several seconds earlier than the helium-pressurised rod due to lower gap conductance, which provides better insulation for the heater sheath. In comparison with the previous figure, a significantly greater cooldown of the heater rod than at the balloon level is observed, even though the heater sheath temperature remains at a rather high level late after clad rewetting for the argon-pressurised rod.

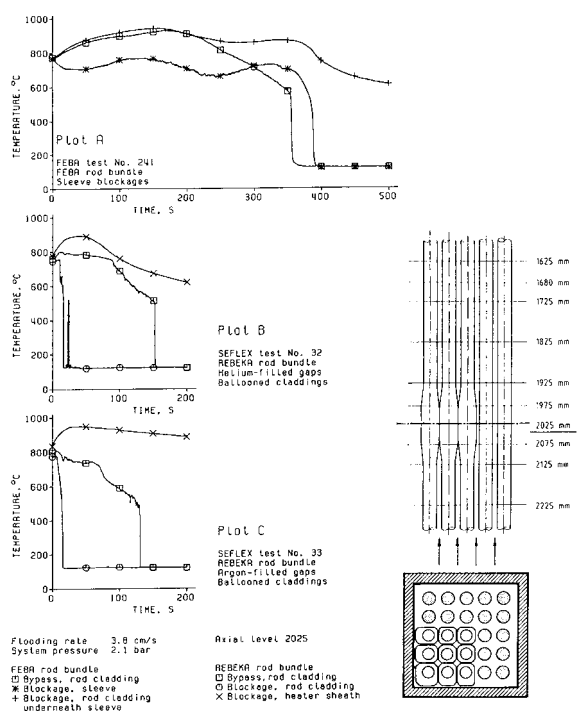


Figure 23: Temperature measured at the mid-plane of a 90% blockage and in the by-pass of FEBA and SEFLEX rod bundles.

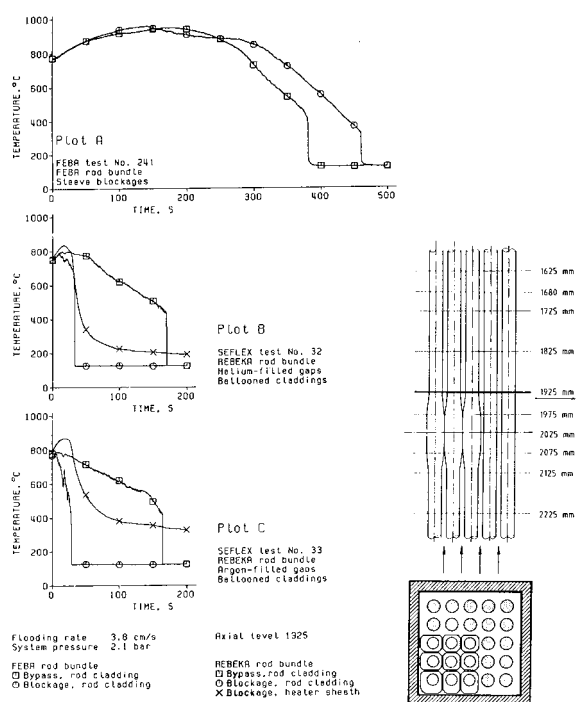


Figure 24: Temperature measured 10 mm downstream from a 90% blockage and in the by-pass of FEBA and SEFLEX rod bundles.

Figure 25 provides temperature variations in the cladding and heater sheath at various levels upstream, within and downstream from the blockage for SEFLEX test No. 32 (helium-filled gap). Upstream from the blockage (level 2225 mm), the heater sheath temperature follows roughly that of the Zircaloy cladding, particularly when cladding rewetting occurs at approximately 140 s. At the axial level 2075 mm, i.e. at the bottom of the 90% ballooned region, the cladding undergoes early rewetting - at about 100 s - and the cladding and heater sheath temperatures are no longer similar. This behavior is even more pronounced at the axial level 2025 mm, at blockage mid-plane, where the cladding undergoes rewetting as early as 16 s. Therefore, as soon as rewetting occurs at this mid-plane level, a secondary quench front progresses upstream to meet the main quench front. At levels 1975 mm and 1925 mm, the propagation of an additional quench front downstream is also observed, which leads to rewetting of the blockage outlet (1925 mm) before it occurs at the upstream non-deformed level (2225 mm). However, temperatures at the blockage outlet (axial level 1925 mm, Plots E and F) indicate a much more efficient cooling of the heater rod after rewetting in comparison to that observed in the blockage where the wide gap insulates the heater rod from the balloon, which can therefore undergo very early rewetting.

Ultimately, reflood behavioral differences between FEBA and SEFLEX tests with their respective simulated blockages of 90% result from an accentuation - in and downstream from the blockage - of the effects resulting from simulator design differences (solid-type or REBEKA-type simulators):

- reduction of cladding and balloon thermal capacities,
- increase in thermal resistance between the heater rod and the cladding or balloon.

These effects induce an early rewetting of the SEFLEX balloons and the rapid propagation of a secondary quench front downstream, leading to early rewetting of the cladding of deformed rods downstream from the blockage.

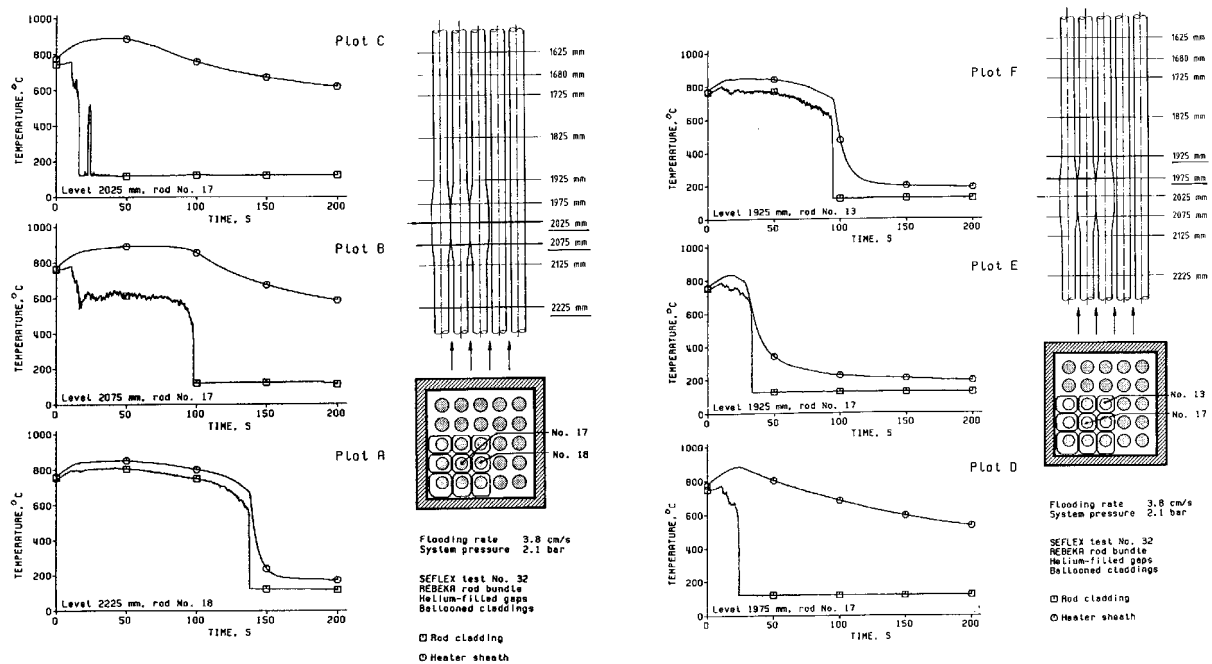


Figure 25: Cladding and heater sheath temperature measured upstream, at and downstream from the bundle mid-plane in the blocked rod cluster of a SEFLEX test rod bundle.

### 2.3 SEFLEX program conclusions and comments

The SEFLEX tests carried out using representative electric fuel rod simulators and a blockage simulated by initially deforming the cladding greatly helped improve the representativity of thermal behavior observed in both blocked and unblocked regions in comparison to behavior observed in the FEBA tests using gapless rod simulators and a blockage simulated by superimposing thick sleeves onto these rods.

Realistic fuel rod simulators with Zircaloy claddings and a gas-filled gap between the cladding and heater (REBEKA type) lead to a noticeably earlier rewetting than "solid-type" fuel rod simulators (FEBA type) tested under identical conditions, particularly when the thermal conductivity of the gas in the gap is low. Early rewetting of the cladding - even though highly decoupled from heater rod cooling - helps remove stored energy at a quicker rate throughout the rod section.

In a severe blockage (90%), simulated in a realistic manner by initial swelling of the cladding, rewetting of the central section of the balloons occurs at a very early stage due to increased turbulence and cooling from liquid droplets. Quenching progresses further via secondary quench fronts upstream and downstream from the blockage, leading to the earlier rewetting of the non-deformed parts of the rods near the balloon in comparison to a non-deformed bundle.

Within the limited range of the selected test conditions, SEFLEX program results therefore illustrate that better cooldown and significantly earlier cladding rewetting occur within and downstream from the blockage in comparison to the by-pass or during a blockage-free test.

However, it would have been desirable that the SEFLEX test matrix include blockage tests performed under severe reflood conditions: 2 cm/s flooding velocity, 2 bar pressure and an inlet temperature of about 100°C. Such tests would have made it possible to evaluate the effect of favourable elements (thermal inertia of the cladding or balloon, low conductance with the heater rod) under the most adverse thermohydraulic conditions, particularly taking into account the trends observed in FEBA and THETIS tests, which partially met these conditions.

Concerning the simulation of a blockage for which the heater elements remain unchanged in the balloon and non-deformed regions, SEFLEX test results tend to highlight the marked conservatism of FEBA test results. In contrast, the marked difference in the results of the comparable program tests seems to indicate that a high coupling between the heat source and the ballooned cladding (such as what can be found in a reactor situation for a balloon filled with relocated fuel fragments) might significantly impair the coolability of a blockage formed by such balloons in comparison to a scenario without fuel relocation. This problem cannot be correctly investigated by extrapolating FEBA or SEFLEX test results and therefore requires performing specific tests.

## **2.4 Analytical simulation of FEBA and SEFLEX tests**

An analysis of a limited number of FEBA and SEFLEX tests was carried out by KfK using the computer code COBRA-TF (Coolant Boiling in Rod Arrays - Two Fluid).

After having briefly described the computer code, a selection of calculated results will be provided in comparison with corresponding experimental data, even if the simulation of the FEBA and SEFLEX tests concerned blockage-free tests only. This will provide a first estimate of the performance of the COBRA-TF code, whose blockage models were adjusted in relation to FLECHT SEASET test data in association with FEBA test data. Comparison of results from FLECHT tests containing blockages and their simulation using the COBRA-TF code will be discussed in detail in Chapter 6 devoted to the FLECHT SEASET program.

### **2.4.1 COBRA-TF computer code**

The COBRA-TF computer code is as a “best-estimate” code which was developed by the Pacific Northwest Laboratory (PNL) to simulate the thermohydraulic behavior of a light water reactor (LWR) assembly during reflood under LOCA conditions.

The COBRA-TF code provides a two-phase fluid, three-field representation of the two-phase flow. The three fields are: continuous liquid, continuous gas and entrained liquid droplets. The gas can be a mixture of noncondensable gas and steam. This description of the two-phase flow results in a system of nine conservation equations:

- 4 continuity equations for the continuous liquid, liquid droplets, steam and noncondensable gas;
- 3 momentum equations for the continuous liquid, liquid droplets and gas mixture;
- 2 energy equations for the liquid phase (continuous liquid + droplets) and gas phase (steam + noncondensable gas); the continuous liquid and entrained droplets fields are assumed to be in thermal equilibrium.

The constitutive relations include models for interfacial mass transfer, wall and interfacial drag forces, wall and interfacial heat transfer, liquid entrainment and de-entrainment and the fluid thermodynamic properties.

The set of surface heat transfer models was composed of the following components:

- ♦ a conduction model designed to handle a fuel rod, an electrically heated rod, a pipe or a wall;
- ♦ a heat transfer package for the selection of the appropriate heat transfer correlation according to the for flow regime;
- ♦ a quench front model using a fine mesh re-zoning technique, taking into account the axial and radial conduction in the fine mesh;
- ♦ a conduction model in the pellet-cladding gap;
- ♦ a sub-channel radiation model calculating rod to rod, rod to steam, and rod to liquid droplets radiative heat transfer.

Furthermore, specific models were implemented in the code to describe in a realistic manner the effects of:

- spacer grids, by taking into account the convective heat transfer enhancement, droplet impact heat transfer, droplet fragmentation, droplet entrainment/de-entrainment, evaporation of fine droplets, and spacer grid rewetting;
- blockages, by taking into account flow redistribution, steam convective heat transfer enhancement, droplet impact heat transfer and droplet fragmentation on blockage walls.

The digital processing of the set of equation relies on a finite-difference discretization scheme according to a staggered Eulerian mesh and a semi-implicit solving method.

## 2.4.2 Simulation of FEBA and SEFLEX tests using the COBRA-TF code

Only blockage-free tests from the FEBA and SEFLEX programs were simulated using the COBRA-TF code.

According to the symmetries, only one eighth of the test section was represented for the simulation. In this section, only 2 sub-channels were modelled and the test rods were divided into 2 groups: rod 1 located in the centre sub-channel and rod 2 located in the peripheral sub-channel, this channel being in contact with the shroud surface (cf. Figure 26).

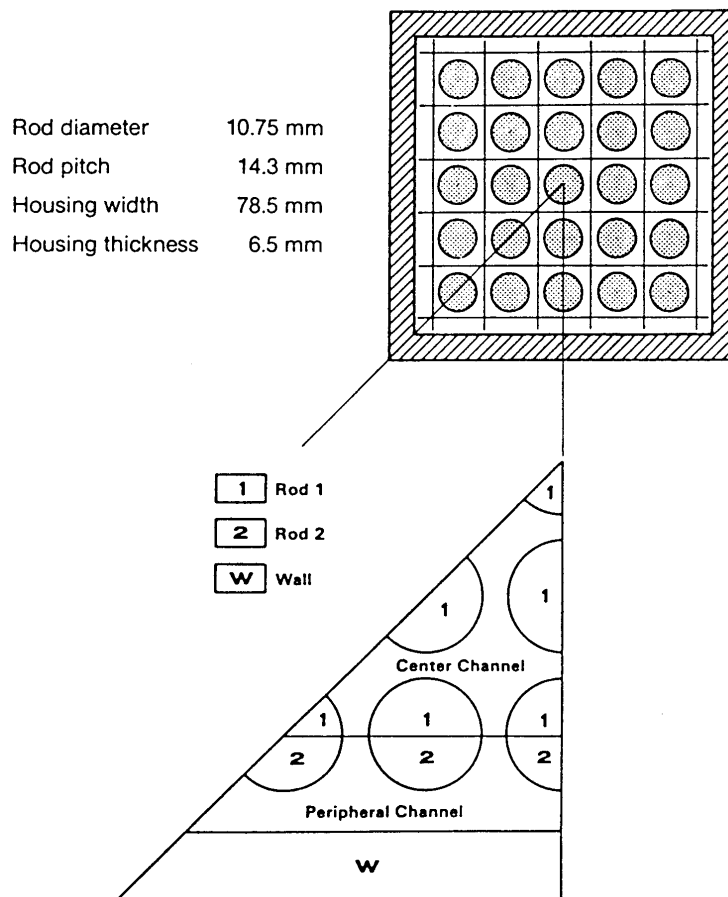


Figure 26: Radial nodding scheme of the FEBA test section for COBRA-TF calculations.

The heated length of the rods was discretized into 18 axial meshes with variable node length. This axial meshing increases or reduces automatically if the temperature difference between two nodes is above (or below) a given value. It is also important to point out that, due to a maximum of 5 different material tables that can be used by the code data input, it was necessary to homogenize the description of the heated element of the REBEKA fuel rods used in the SEFLEX program (cf. Figure 17) by using a pseudo-material. The 7 spacer grids were represented in the simulation.

The main comparison between experimental data and COBRA code predictions concerned the SEFLEX 03 test, with a blockage-free array, helium-pressurised rods and a reflood rate of 3.8 cm/s for a 4.1 bar system pressure.

Figure 27 compares the recorded and calculated temperature variations for the "central" fuel rod (with respect to the COBRA code description) at 3 different levels located approximately 30 cm downstream from spacer grids 3, 4 and 5. The temperature at the beginning of the transient was slightly overestimated in the calculation, particularly for level 2225 mm in the maximum flux region, and then this trend reversed with the temperature being underestimated by 150°C to 180°C just before the quench. Agreement between code calculations and experimental results was generally acceptable and tended to improve in the higher levels. Quench time tended to be slightly underestimated, by 10 to 25 s for each of the 3 represented levels, whereas rewetting temperatures were correctly predicted by the code.

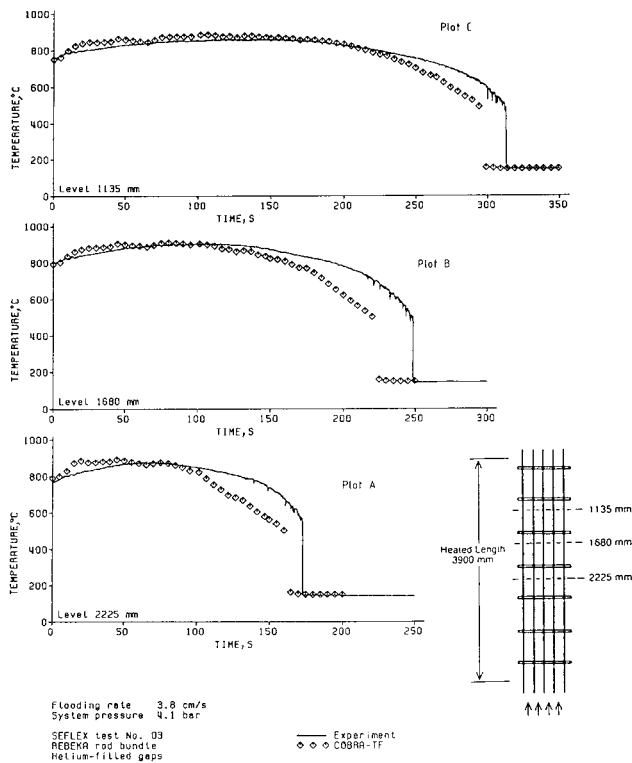


Figure 27: Comparison of measured and calculated centre rod cladding temperatures for SEFLEX test 03.

Figure 28 compares the temperature variations - measured and calculated - on spacer grids 3, 4 and 5, showing excellent agreement between experiment and code prediction on the quench time at the leading edge of the spacer grid.

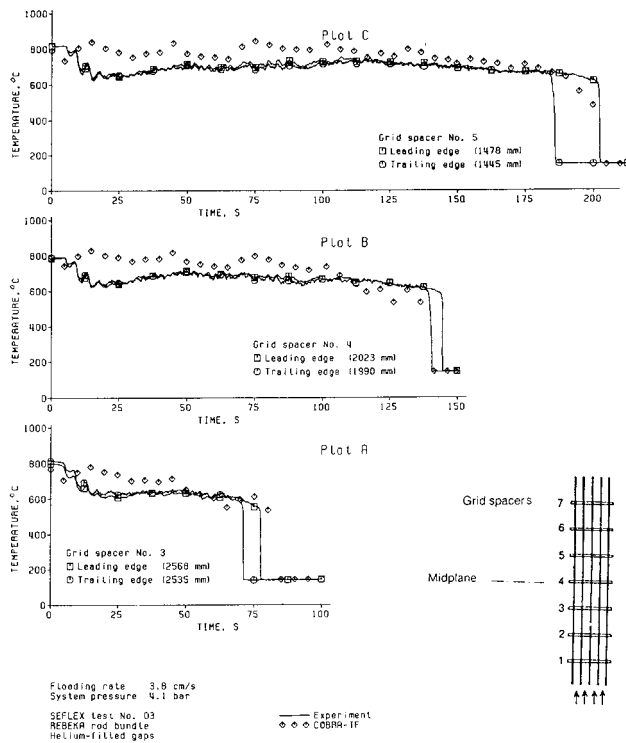


Figure 28: Comparison of measured and calculated grid spacer temperatures for SEFLEX test 03.

Figure 29 compares the measured and COBRA-TF-calculated quench front progression, indicating good agreement of data in the lower half of the bundle and increasing differences as the quench front moves into the upper half of the bundle, where quench times are slightly under-estimated by approximately 10%.

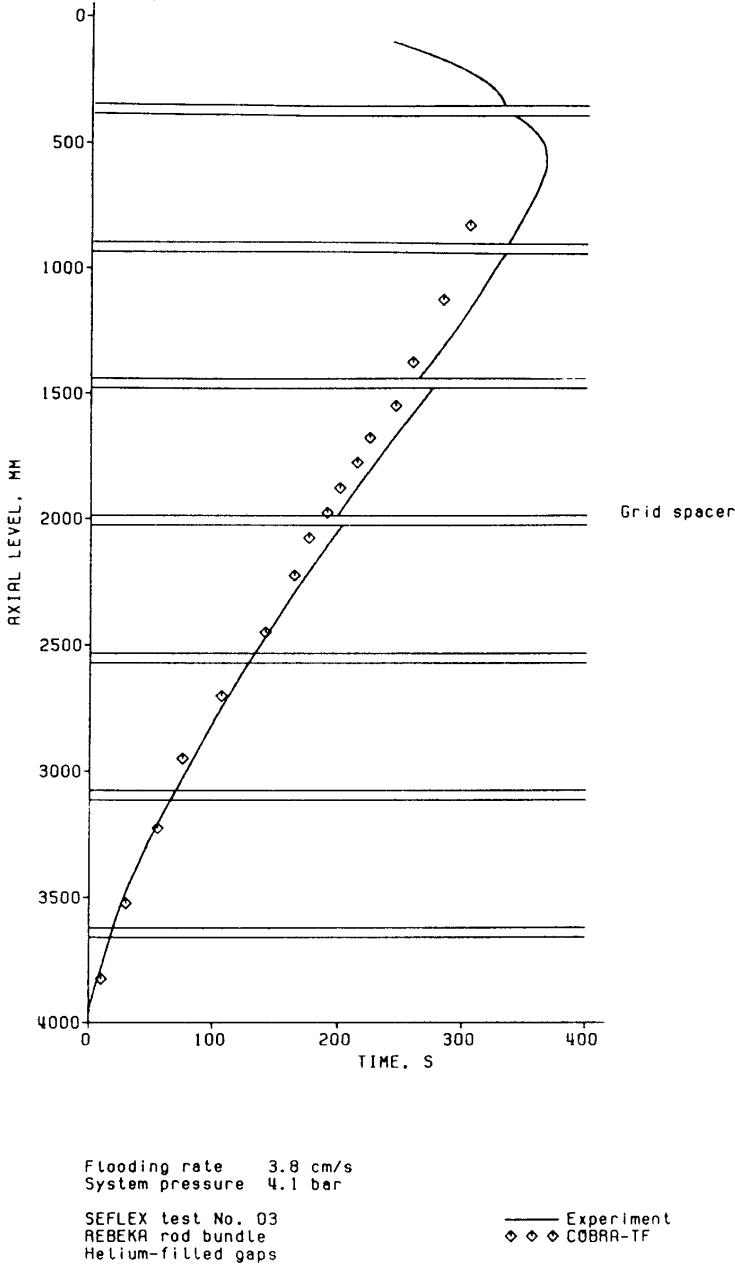
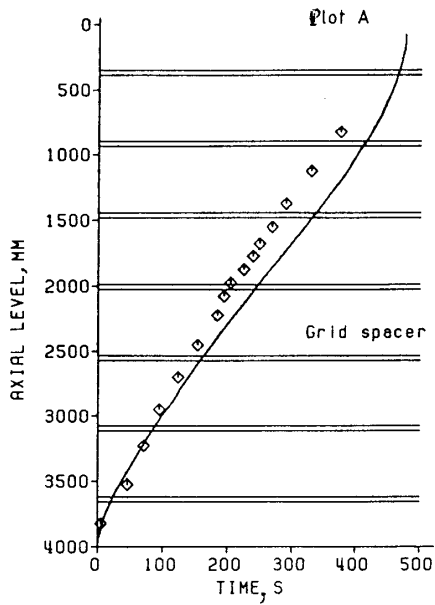
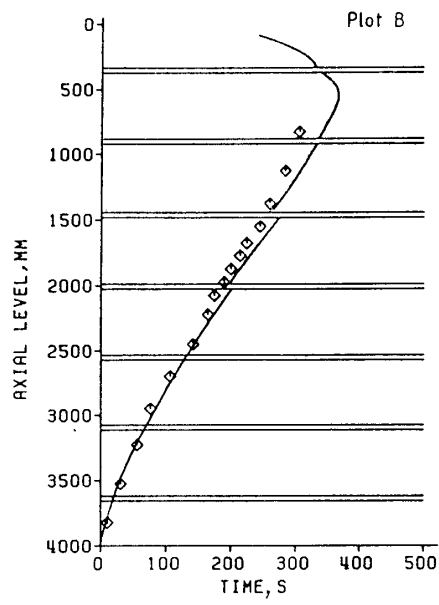


Figure 29: Comparison of the measured and calculated quench front progression for SEFLEX test 03.

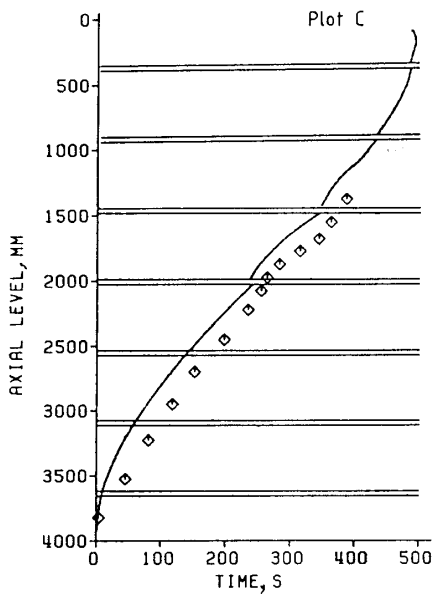
Last of all, Figure 30 compares COBRA-TF code predictions of the quench front progression with the experimental values recorded during the 4 SEFLEX and FEBA tests that were simulated with this computer code. It is important to remember that these tests were blockage-free, with a reflood rate of 3.8 cm/s and system pressures of 4 or 2 bar. For the FEBA test, the quench times are under-estimated as the axial elevation increases. The corresponding SEFLEX test (No. 3) - the test discussed in the previous figures - shows the best agreement between experiment and code prediction. The SEFLEX tests performed at a system pressure of 2.1 bar - with respectively helium- (Plot C) and argon-pressurised (Plot D) rods - show an overestimation of the quench times which, according to the authors of the study, is presumed to be due to an under-prediction of the liquid fraction in the flow and hence, heat transfer at low system pressure.



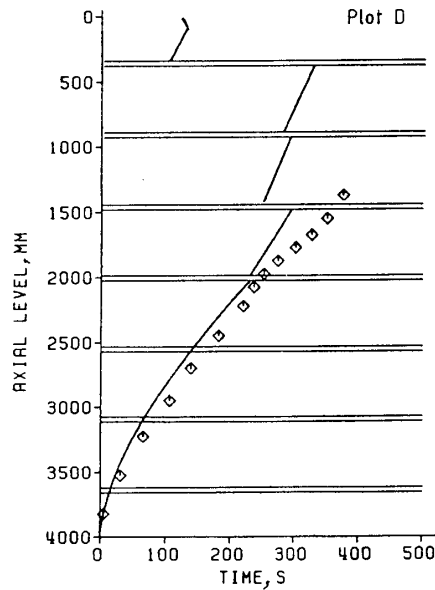
Flooding rate 3.8 cm/s  
 System pressure 4.1 bar  
 FEBA test No. 05  
 FEBA rod bundle  
 Gapless rods  
 — Experiment  
 ◇ ◇ ◇ COBRA-TF



Flooding rate 3.8 cm/s  
 System pressure 4.0 bar  
 SEFLEX test No. 03  
 REBEKA rod bundle  
 Helium-filled gaps  
 — Experiment  
 ◇ ◇ ◇ COBRA-TF



Flooding rate 3.8 cm/s  
 System pressure 2.1 bar  
 SEFLEX test No. 05  
 REBEKA rod bundle  
 Helium-filled gaps  
 — Experiment  
 ◇ ◇ ◇ COBRA-TF



Flooding rate 3.8 cm/s  
 System pressure 2.1 bar  
 SEFLEX test No. 07  
 REBEKA rod bundle  
 Argon-filled gaps  
 — Experiment  
 ◇ ◇ ◇ COBRA-TF

**Figure 30: Comparison of measured and calculated quench front progressions for FEBA test 223, SEFLEX tests 03, 05 and 07.**

The scientists who conducted the study came to the conclusion that the COBRA-TF predictions of the SEFLEX results were very encouraging, considering the code's low level of validation at the time of the study, as well as having used its standard version, without any possibility for adjustment or improvement of the models during the study.

### 3 THETIS Program

The THETIS program was carried out by the United Kingdom Atomic Energy Authority (UKAEA) at the Winfrith Atomic Energy Establishment. This program involved conducting a set of thermohydraulic tests on an assembly containing 49 full-length electrically-heated rods with a severe blockage of 90%<sup>[4]</sup> or 80%<sup>[5, 6]</sup> maximum value over a length of 200 mm.

Four different types of experiments were performed:

- 1) Single-phase (nitrogen) flow heat transfer tests,
- 2) Forced reflood tests,
- 3) Gravity reflood tests,
- 4) Level-swell tests.

Forced reflood test results will mainly be discussed in this chapter, having been the greatest in number and providing analytical information on the cooling of a partially blocked assembly. Selected information will also be provided concerning gravity reflood tests, whose results in terms of blockage coolability are similar to forced test results conducted under comparable inlet conditions, which justifies the choice of forced reflood tests for the study of partially blocked assembly cooling.

#### 3.1 Experimental characteristics

Figure 31 provides a simplified layout of the THETIS rig, composed of 3 main elements connected in parallel: 1) the test section containing the bundle of heater rods, 2) the downcomer used in gravity reflood tests and 3) an adjustable weir vessel for maintaining a constant head for level swell tests.

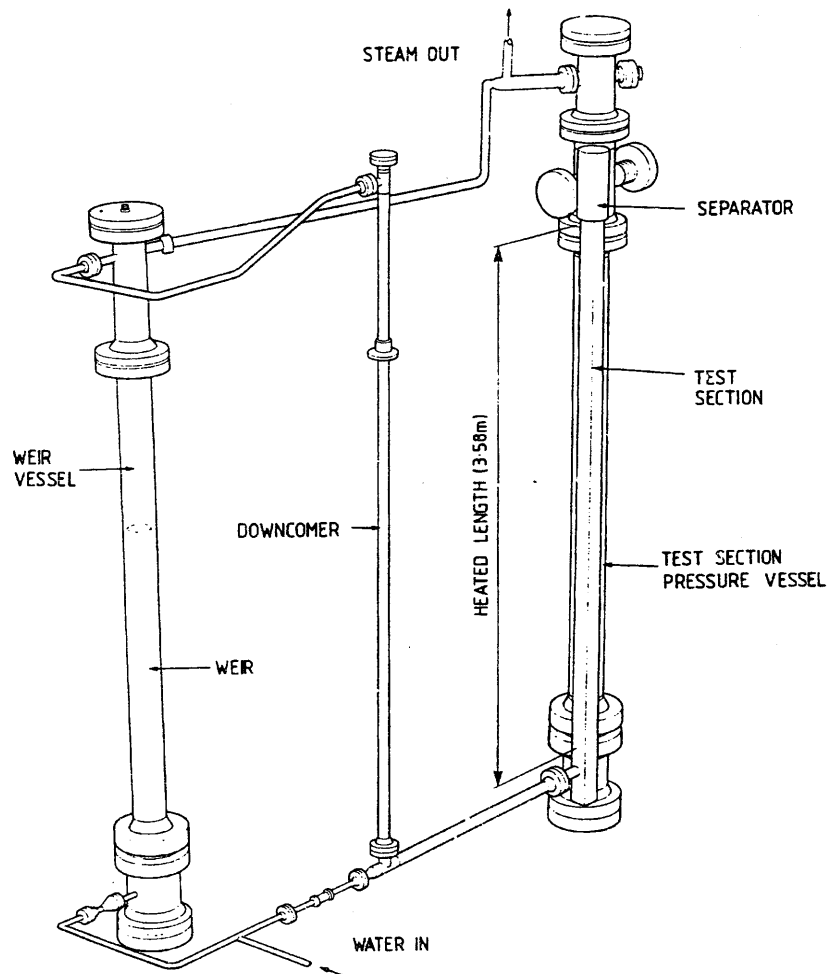
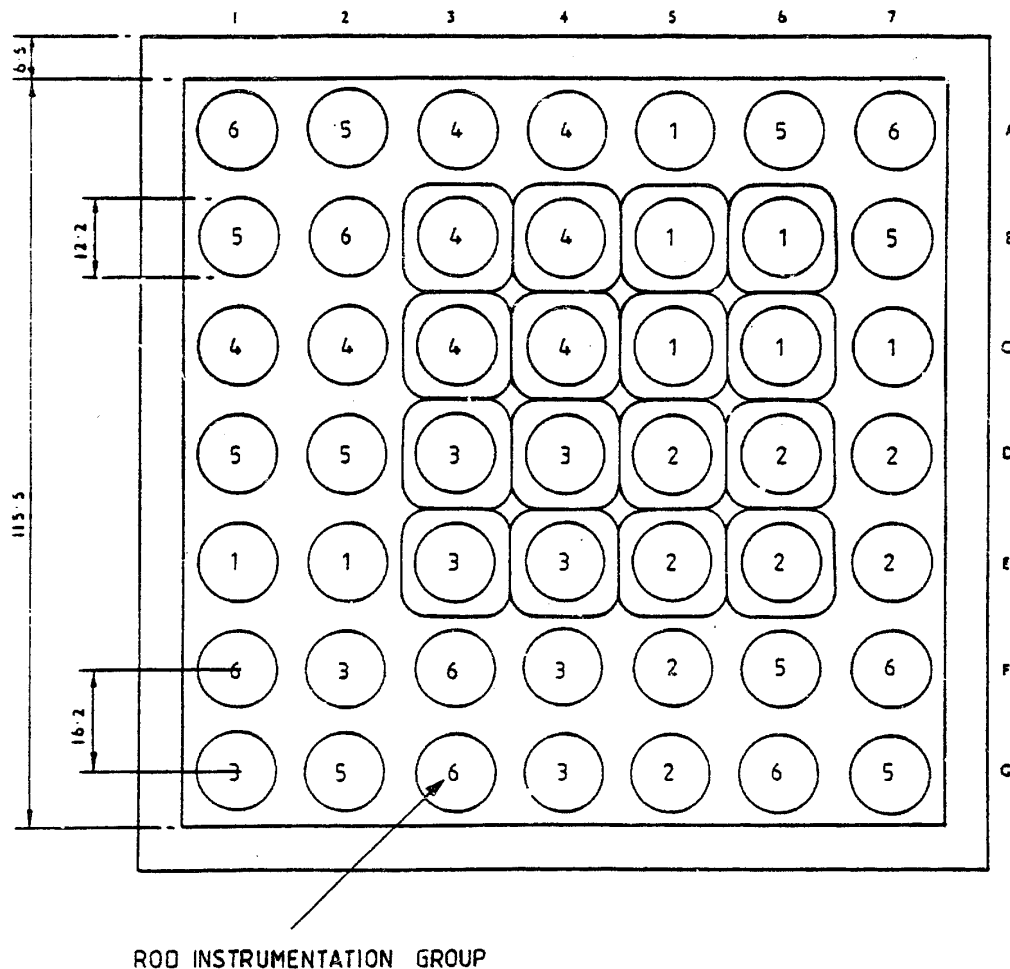


Figure 31: Layout of the THETIS rig.

The THETIS test assembly - schematised in Figure 32 - consisted of a 7x7 rod array with a 4x4 group of rods containing the blockage region. The assembly was enclosed in a square shroud tube having an inner width of 115.5 mm and a thickness of 6.5 mm. This shroud was not directly heated but raised to thermal equilibrium with the rods through radiation exchange before the test transient started.



ROD INSTRUMENTATION GROUP

Figure 32: THETIS 7x7 rod cluster with 4x4 blockage.

The fuel rod simulators used in the THETIS experiments were SGHWR-size pins with a 12.2 mm outer diameter, greater than the standard PWR rod diameter of 9.5 mm. Therefore, a pitch of 16.2 mm was chosen to keep the same pitch-to-rod diameter ratio as that in a PWR assembly. The rods - with a heated length of 3.58 m - were held in a set of 8 spacer grids 38 mm high, distributed according to an axial pitch of 523 mm.

The rods were solid-type electric simulators similar to FEBA rods, composed of an 0.8 mm thick Inconel tube with a central spiral heating element, the pitch of which was varied to obtain a chopped-cosine axial power profile. The heated element was encased in BN + MgO insulation in contact with the Inconel tube. Each rod was instrumented with 12 thermocouples (TC) placed on the inner surface of the tube.

The blockage was simulated in a 4x4 rod array separated from the shroud by one or two rows of non-deformed rods (cf. Figure 32), with the two rows of non-deformed rods delimiting the by-pass region on two sides. The outer row of 24 rods formed a guard ring with the cold shroud. This configuration prevented thermal conduction through the direct contact between the balloons and the shroud, as was the case for blockages located on the edge of the assembly in FEBA and SEFLEX tests.

Ballooning of the rod cladding was simulated by superimposing a pre-shaped Inconel sleeve, whose geometry is described in detail in Figure 33 for the 90% blockage ratio. The maximum blocked region extended over 200 mm, with a 200 mm entry taper and a 50 mm exit taper connecting the regular section of the rod with the square section of the sleeve. The cladding balloons therefore occupied almost a complete grid interval. The sleeve thickness in the maximum deformed region was 0.3 mm, which is comparable to that of a real cladding balloon. The atmosphere within the sleeves - filled with helium or nitrogen - was insulated from the coolant atmosphere but nevertheless maintained in equipressure with the coolant atmosphere. It is important to point out that, downstream from the upper taper, a 14.4 mm diameter sleeve was extended up to the top of the rods to contain the TC wires located on the inner surface of the balloons. This corresponded to a residual blockage of 31.5% in the sub-channels downstream from the balloons, which led to a faster steam flow rate than that in the by-pass sub-channels.

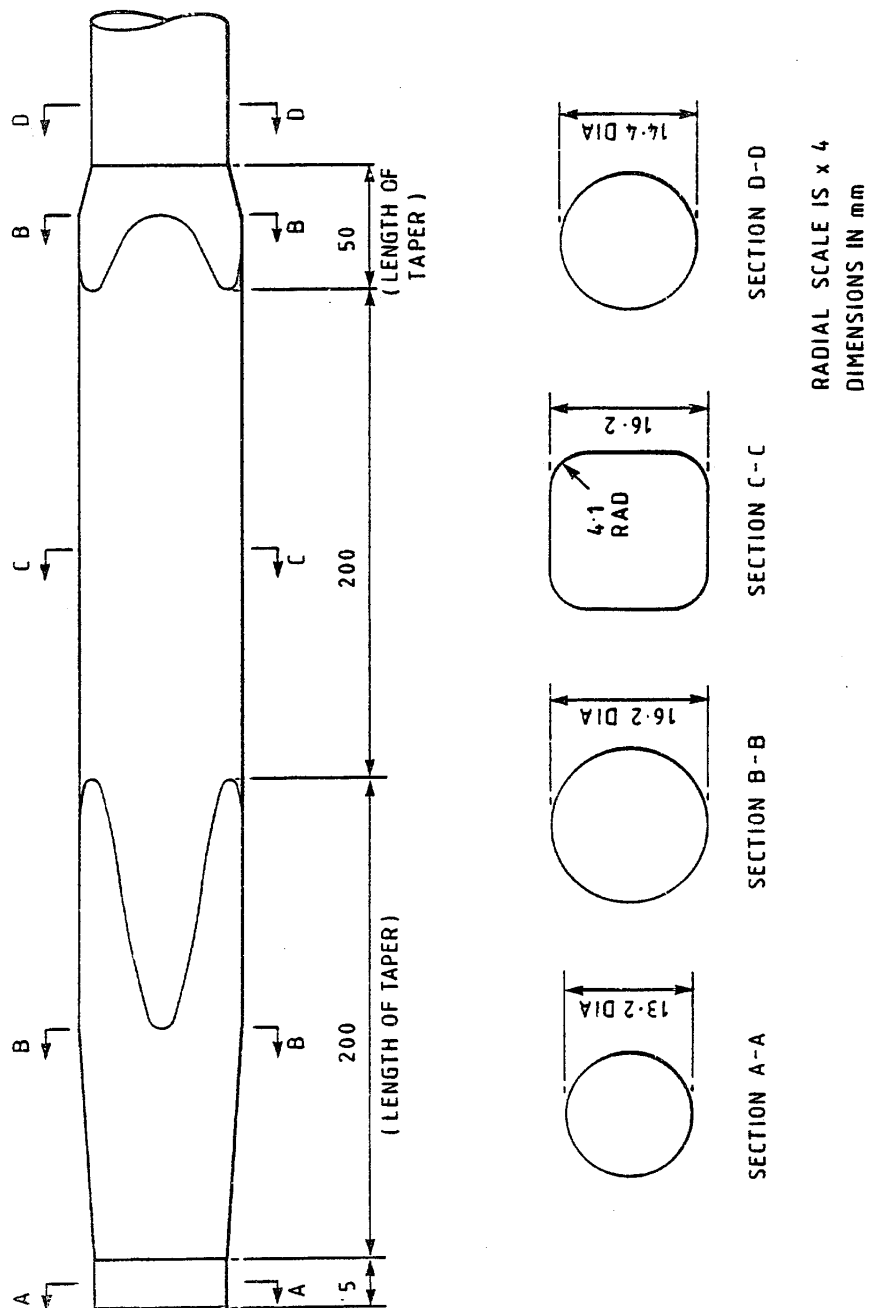


Figure 33: THETIS - Shape the cladding sleeve for the 90% blockage.

Figure 34 illustrates the axial locations of a) the blockage region, b) the spacer grids and c) the TCs in each of the 6 different groups of rods relative to the TC distribution. For a correct understanding of the following figures, it must be remembered that all axial levels were measured downwards from the bottom of the top grid plate.

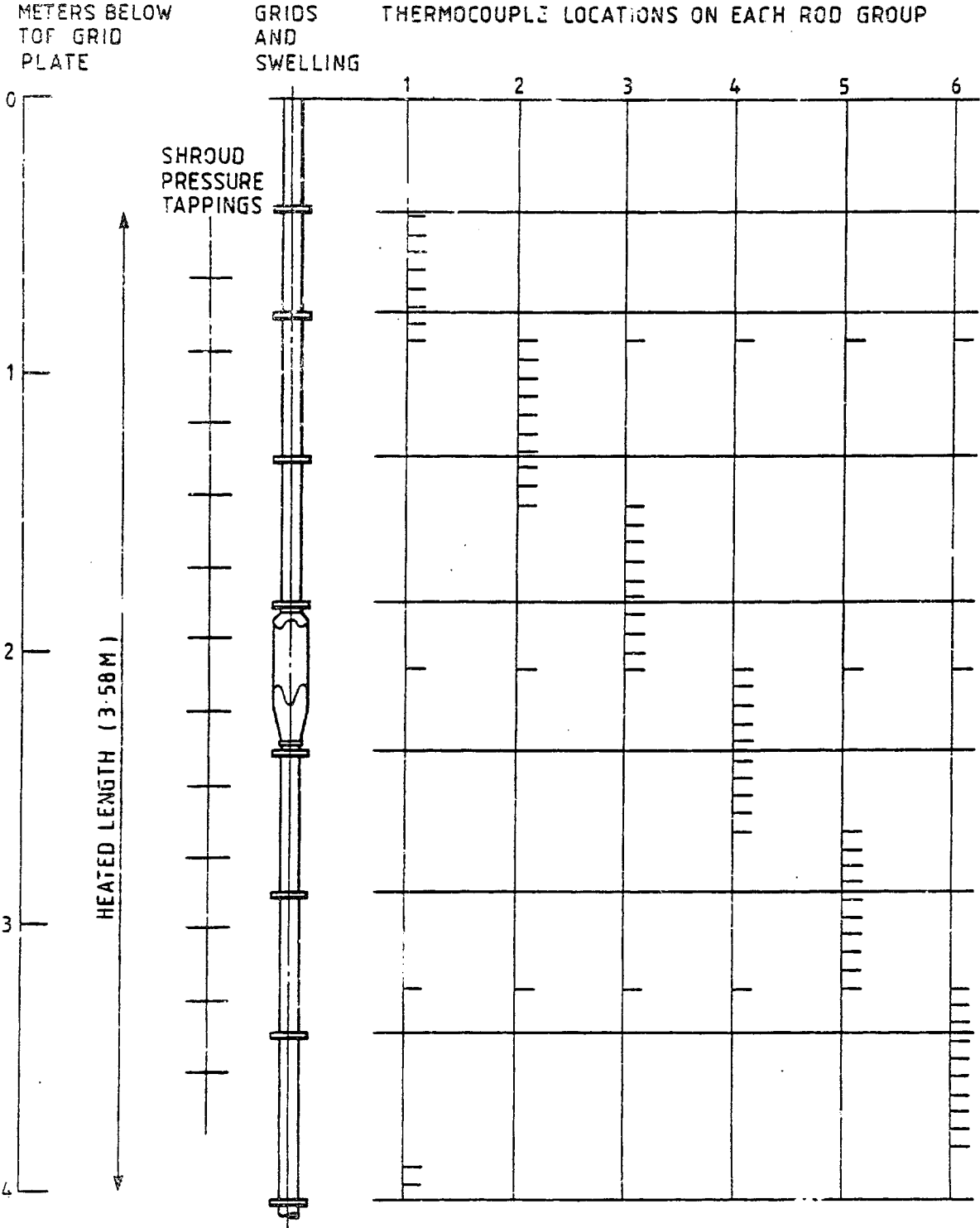


Figure 34: THETIS - Axial locations of swellings, grids and thermocouples.

### 3.2 Tests with a 90% blockage ratio

The nominal conditions of the THETIS 90% blockage forced reflood tests are summarised in Table 2. It should be noted that all of these tests - except one - were conducted with nitrogen-filled balloons, contrary to the original intention to use helium in general. This was due to the development of a small leak in a balloon weld early in the experimental program, which led to the switch from helium filling to nitrogen filling for the remainder of the program.

Run	Pressure (bar)	Reflood rate (cm/s)	Inlet temperature (°C)	Power (kW)	Filling gas
41	2.2	3.9	92	147	Helium
65	2.1	2.0	88	99	Nitrogen
66	2.1	3.8	91	147	"
68	2.1	1.0	86	74	"
70	4.1	2.0	90	98	"
72	1.3	2.0	90	98	"
73	2.1	2.0	48	98	"
75	2.1	5.7	95	200	"
78	2.2	5.8	94	<i>Fig. 44</i>	"
79	2.3	3.7	91	"	"
80	2.2	2.0	86	"	"
82	2.1	2.9	97	"	"
123	2.1	3.0	92	"	"
124	1.9	<i>Note 4</i>	88	"	"

#### Notes

1. Conditions listed are for 100 s after the start of reflood. Pressure and inlet temperature varied slightly during each run.
2. Reflood rate is notionally based on a liquid density of 1000 kg/m<sup>3</sup> and the cluster flow area at inlet of 7.61 10<sup>-3</sup> m<sup>2</sup>.
3. Pressure is at exit from the cluster.
4. In Run 124 reflood rate varied as follows:

0 to 8 s	~ 8 cm/s
8 to 58 s	3.0 cm/s
58 to 500 s	1.9 cm/s

**Table 2: Nominal conditions of the THETIS 90% blockage forced reflood tests.**

#### 3.2.1 Reference test

Test No. 65 performed under the following conditions was chosen as the reference test for the presentation of results:

Pressure	2.1 bar
Reflood rate	2 cm/s
Inlet temperature	88°C
Power	99 kW

A result of the generic character in all reflood tests is the effect of spacer grids. Figure 35 illustrates the temperature variations on a by-pass rod just below and just above a spacer grid: much better cooling downstream from the grid is evident, with drastic improvement at ~90 s when grid rewetting occurs. This cooldown clearly results from the increased desuperheating of steam passing through the grid, essentially due to the convective transfer with the liquid film that develops on the grid surface. Despite such accentuated cooling, the downstream level rewets slightly later, but from a lower rewetting temperature in comparison to the upstream level.

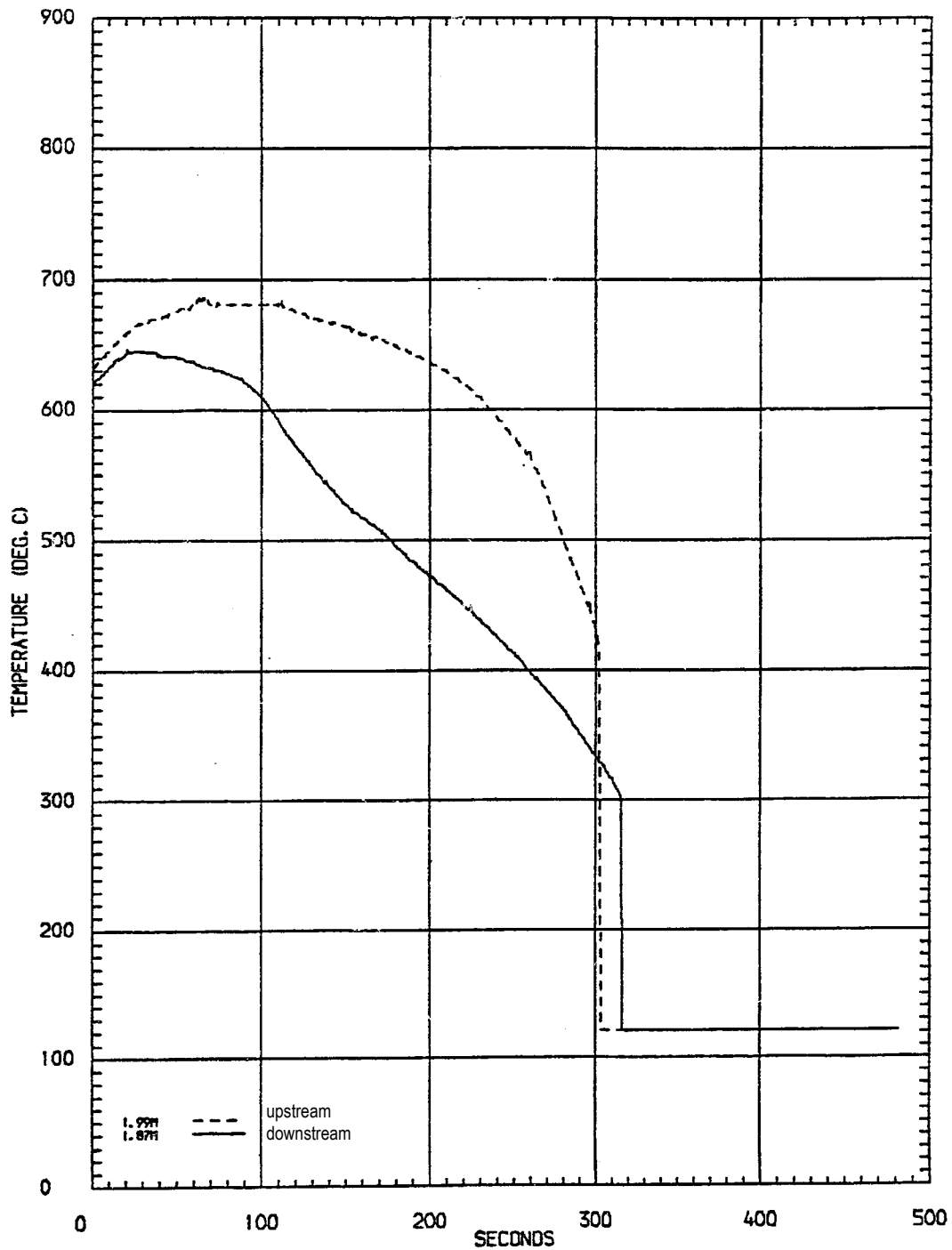


Figure 35: Run T1R065 - Temperature histories upstream and downstream from a grid spacer.

Figure 36 illustrates the comparison in temperatures of the upper part of the blocked region and the by-pass at the same level. The temperature of the rod located in the by-pass rises to 680°C at approximately 100 s before cooling down at an increasing rate until rewetting. The balloon temperature - measured by the internal TC or derived from rod temperatures using an inverse conduction calculation - rises erratically until it reaches a maximum of 720°C and then falls slightly until just before rewetting, which occurs at practically the same time as that for the by-pass rod. The succession of intermediary temperature drops before the maximum temperature is reached can be explained by the effect of the upstream grids which, as reached by the rising quench front, induce temporary increases in liquid evaporation, therefore accelerating the steam and increasing droplet entrainment in the blockage.

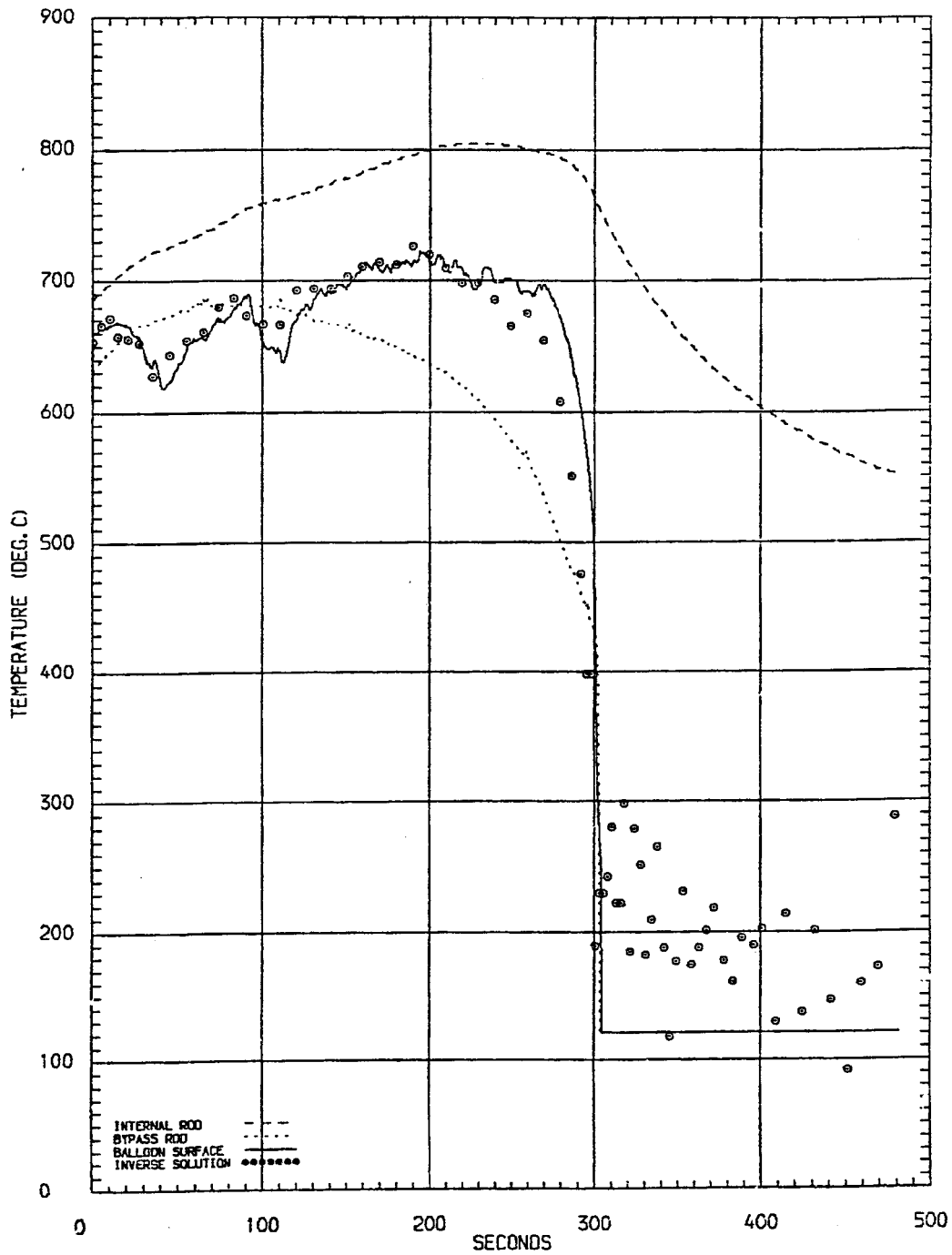


Figure 36: Run T1R065 - Maximum blockage and by-pass temperatures.

Figure 37 shows the temperature variations with time from bottom (marker 1) to top (marker 4) of a balloon delimiting the central blockage sub-channel. Following erratic temperature variations over approximately 150 s, an axial gradient of 140°C is reached at about 200 s along the 200 mm of maximum blockage. Cooling then sets in at the bottom of this region and progresses towards the top, with rewetting occurring at the upper level approximately 40 s after it occurs at the lower level.

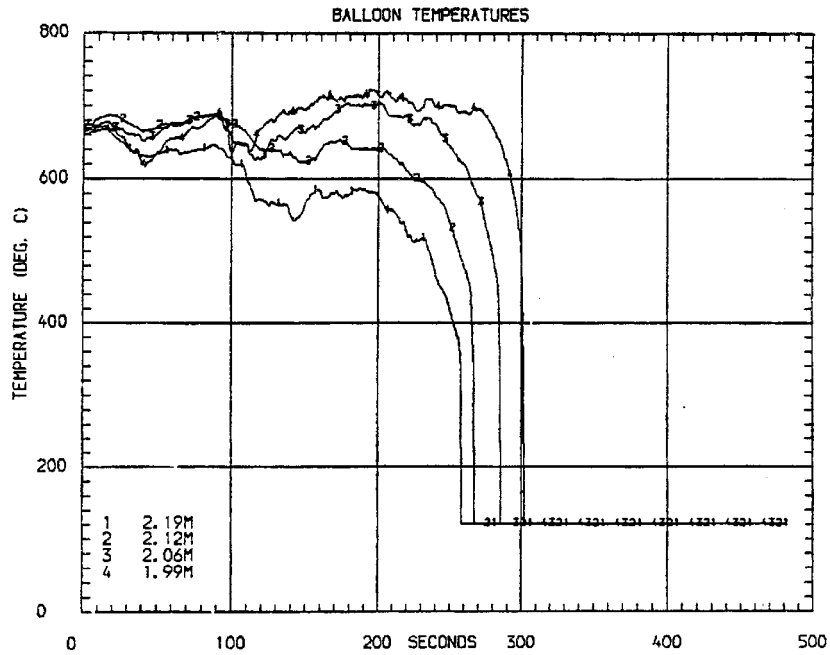


Figure 37: Run T1R065 - Axial distribution of balloon temperatures.

### 3.2.2 Effect of pressure

The effect of pressure upon the quench front progression is illustrated in Figure 38; as the blockage and by-pass regions undergo rewetting at about the same time, only the by-pass is represented here. As expected, the quench front velocity increases with pressure by a factor of 2 between 1.3 and 4.1 bar.

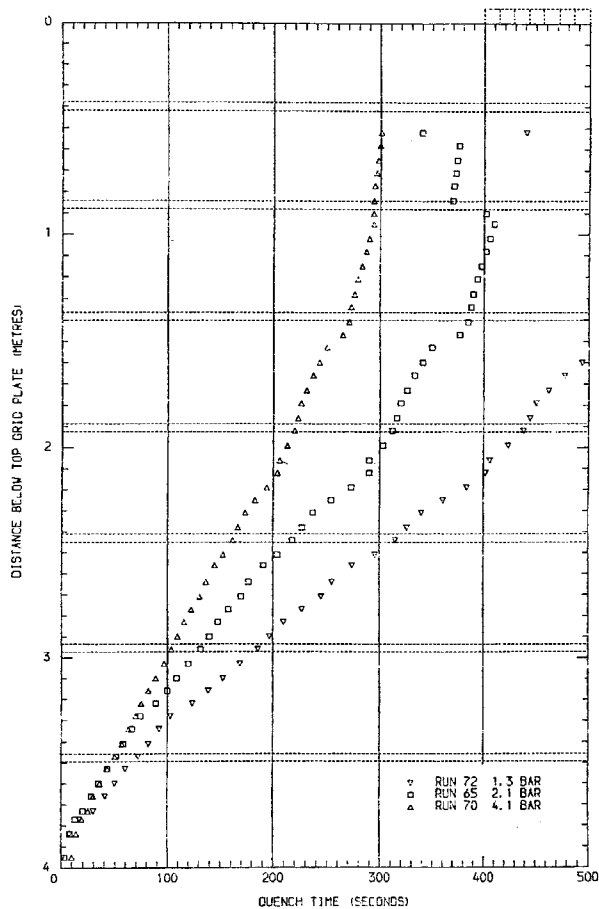


Figure 38: THETIS - Effect of pressure on quench front progression.

The effect of pressure upon maximum temperature variations in the blockage and by-pass is illustrated in Figure 39 for pressures of 1.3 and 4.1 bar, which is to be compared with Figure 36 for a pressure of 2 bar. Besides different rewetting times - 210 s for 4 bar and 410 s for 1.3 bar - variations remain similar with comparable blockage and by-pass temperatures during a first phase lasting 40% to 50% of the time to rewetting, then diverging in a second phase where the by-pass cools down and the blockage heats up to reach a maximum temperature of 740°C before cooling down and quenching. Intermediary drops in the balloon temperature during the first phase are still observed.

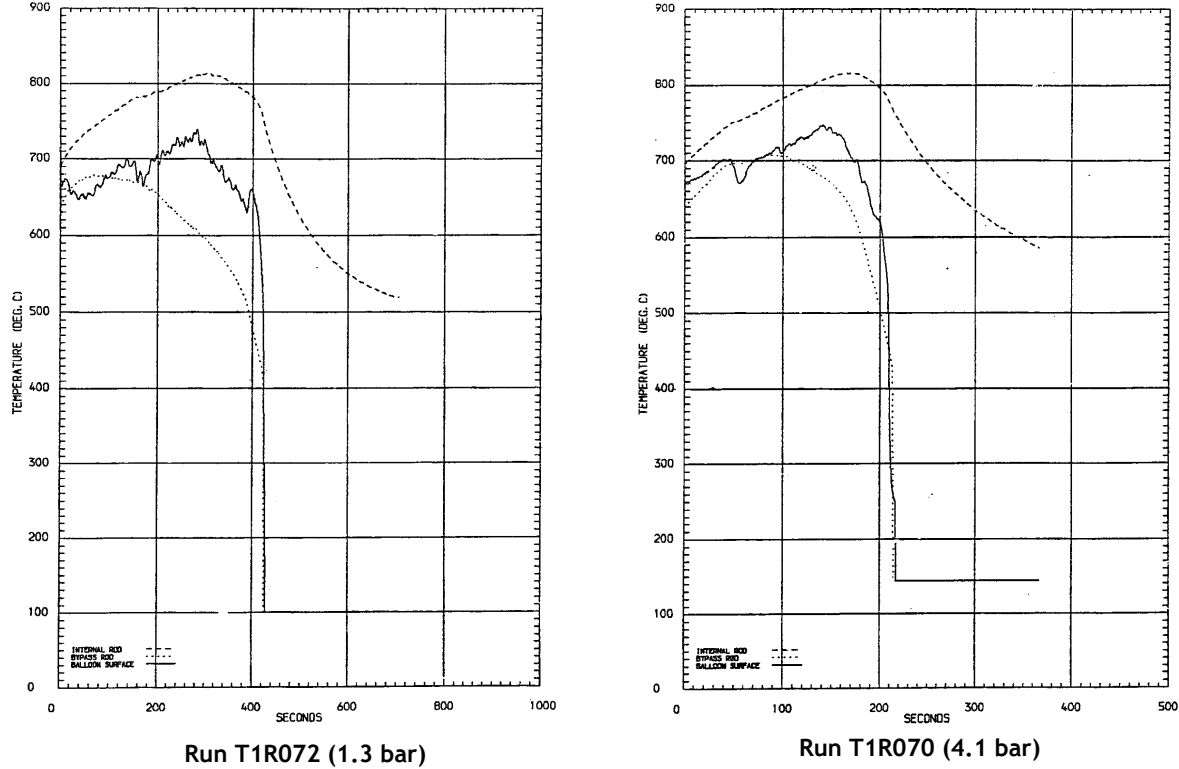


Figure 39: THETIS - Effect of pressure on blockage and by-pass temperatures.

In summary, the system pressure only affects rewetting times, without noticeably influencing temperatures in the blockage and by-pass.

### 3.2.3 Effect of input temperature

The input temperature seems to only moderately affect the quench front velocity (cf. Figure 40) by about +10% for a 40°C reduction in input temperature. The effect upon blockage and by-pass temperature variations is illustrated in Figure 41 (to be compared with Figure 36), where early rewetting at 260 s was observed (compared to 300 s for  $T_i = 88^\circ\text{C}$ ) nevertheless with similar behavior and maximum temperatures.

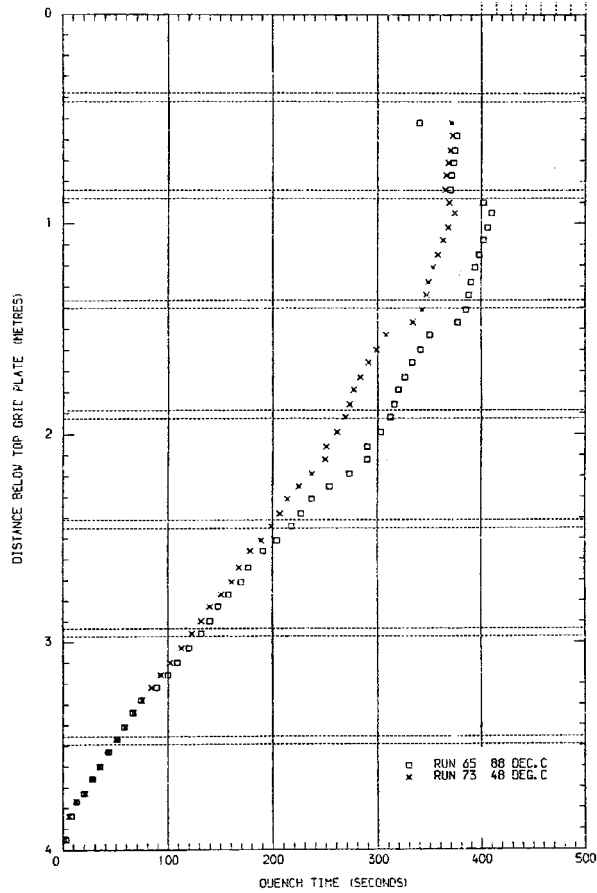


Figure 40: THETIS - Effect of inlet temperature on quench front progression.

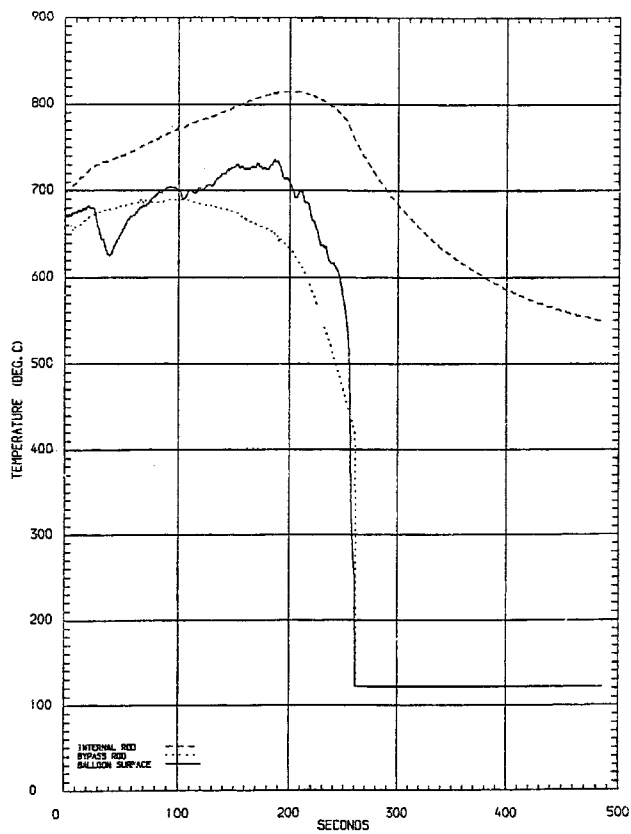


Figure 41: Run T1R073 (48 °C inlet) - Maximum blockage and by-pass temperatures.

### 3.2.4 Effect of reflood rate

The effect of the reflood rate was first examined in tests at different reflood rates, between 1 and 6 cm/s, for which the power -constant throughout the test- was chosen to ensure that the maximum balloon temperature did not exceed 800°C. This power depended on the reflood rate as follows:

Reflood rate (cm/s)	Power (kW)
1	75
2	100
4	150
6	200

Maximum temperature variations in the blockage and by-pass for reflood rates of 1, 2, 4 and 6 cm/s and their associated powers are provided in Figures 42 and 43. The comparison of these temperature variations does not make it possible to directly evaluate the effect of reflood rates, partially concealed by power differences. Therefore, it is not possible to conclude that a 90% blockage with an observed maximum temperature of 810°C for a reflood rate of 1 cm/s remains coolable, insofar as the power supply is significantly lower than the corresponding residual power in a PWR assembly under LOCA conditions.

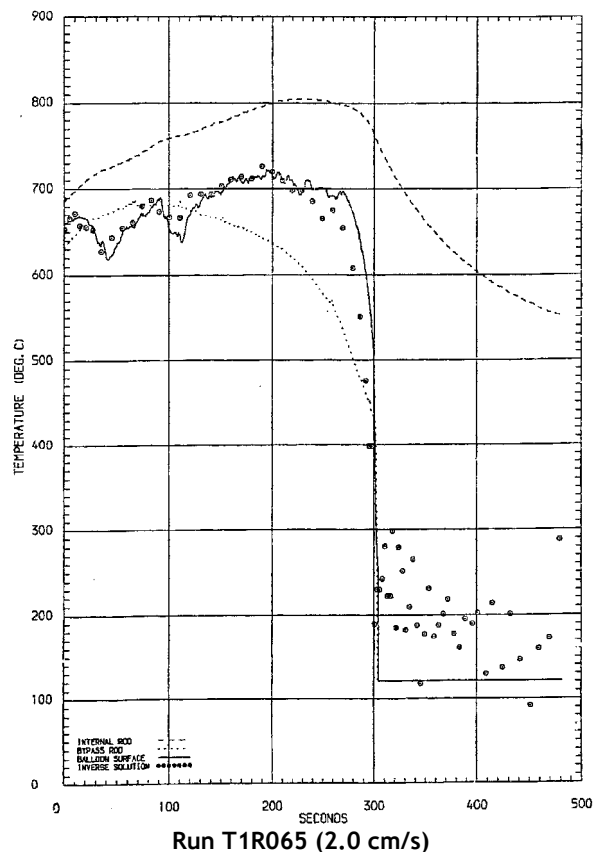
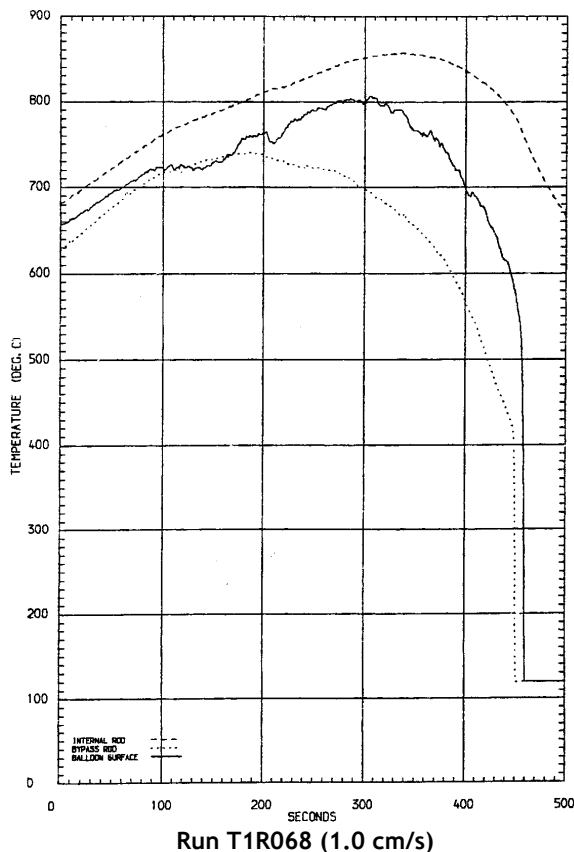


Figure 42: THETIS - Blockage and by-pass temperatures for 1 and 2 cm/s reflood rates.

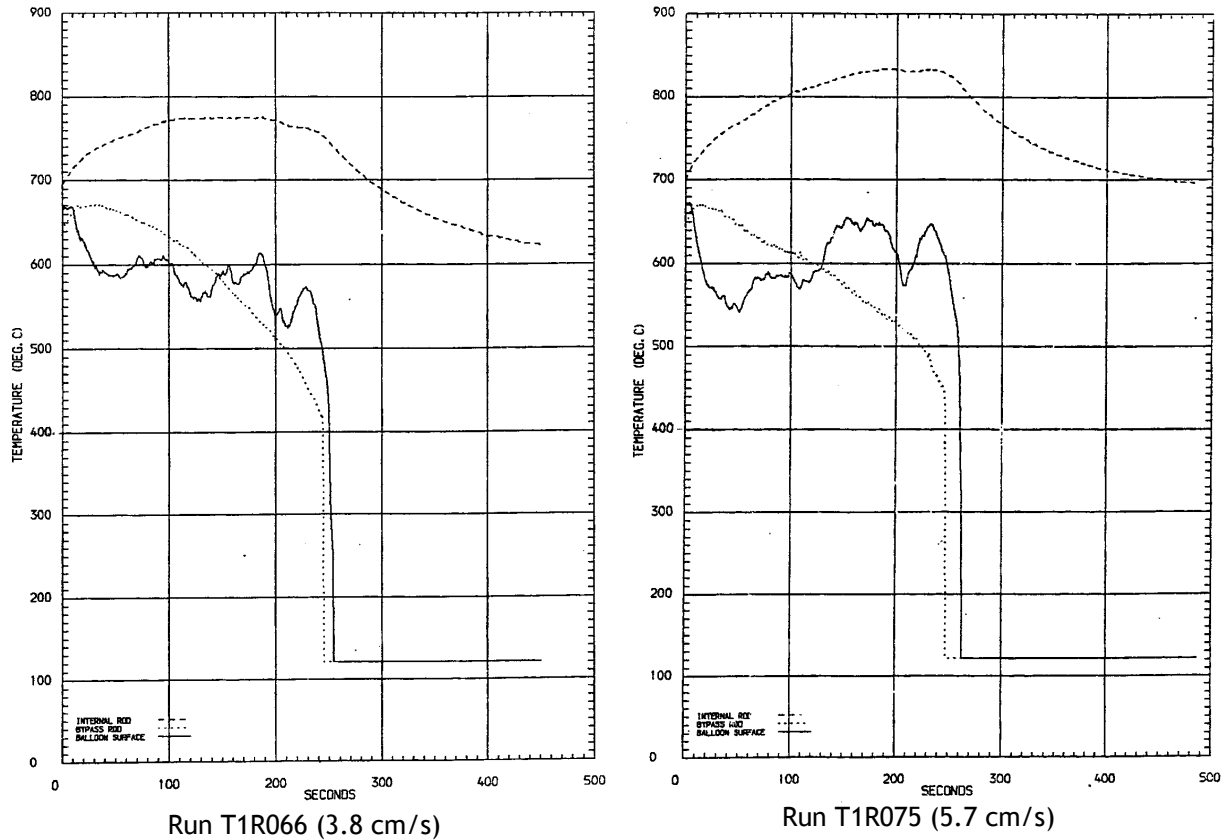


Figure 43: THETIS - Blockage and by-pass temperatures for 3.8 and 5.7 cm/s reflood rates.

### 3.2.5 Variable power tests

In order to provide more representative results than those obtained from tests performed at constant power, further tests were conducted in which the power rate was varied during the transient. The decay power curve represented in Figure 44 is based on a best-estimate residual power law (Gibson & Askew) applied to the power of a Sizewell B PWR hot rod (+34% in relation to the average rod) and transposed to a THETIS sub-channel flow passage (+65%) in order to obtain the same enthalpy increase in the coolant between inlet and rod to mid-plane level as in the reactor case. This scaling gives similar heat fluxes in the maximum heat flux region ( $1285 \text{ kW/m}^2$  for THETIS, in comparison to  $1389 \text{ kW/m}^2$  for Sizewell B with full power).

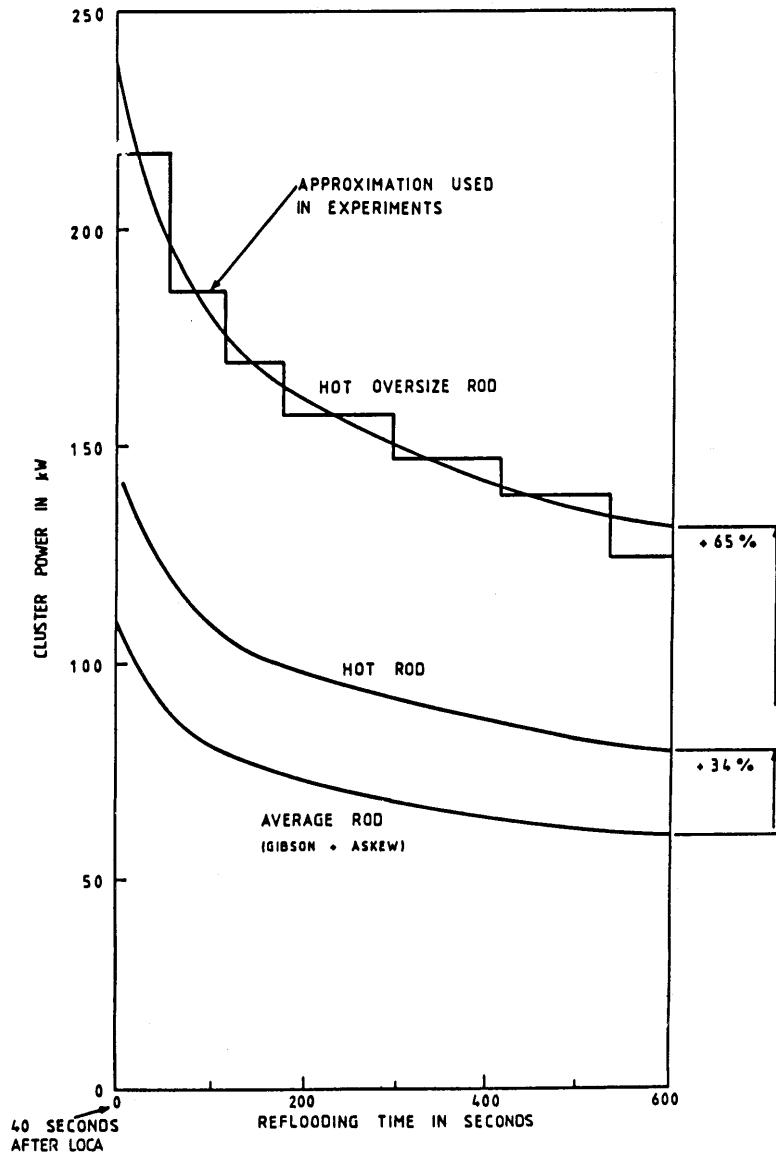


Figure 44: THETIS - Decay power curve for variable power tests.

Using this decay power curve, a series of 4 tests was performed with reflow rates of 6, 4, 3 and 2 cm/s while keeping the system pressure at 2 bar and the water inlet temperature at 90°C. However, for the two lowest reflow rates, initial bundle temperatures were reduced by approximately 100°C at mid-plane in order to avoid overheating the blockage.

Temperature variations in the upper part of the blockage and in the by-pass at the same level for reflow rates of 4 and 6 cm/s are provided in Figure 45. Comparison of these temperature variations with those illustrated in Figure 43 for constant power tests shows that:

- For a reflow rate of 6 cm/s, the two corresponding variations are similar with, as expected, slightly lower temperatures recorded during the second half of the transient for the variable power than for the constant power (200 kW); rewetting of the blockage also occurs 20 s earlier.
- For a reflow rate of 4 cm/s, balloon rewetting under variable power occurs later than under constant power (150 kW) due to the greater power rate during the first 300 s. The average balloon temperature level during the second half of the transient is greater by approximately 100°C than in the constant power test, despite a similar series of intermediary temperature drops and peaks.

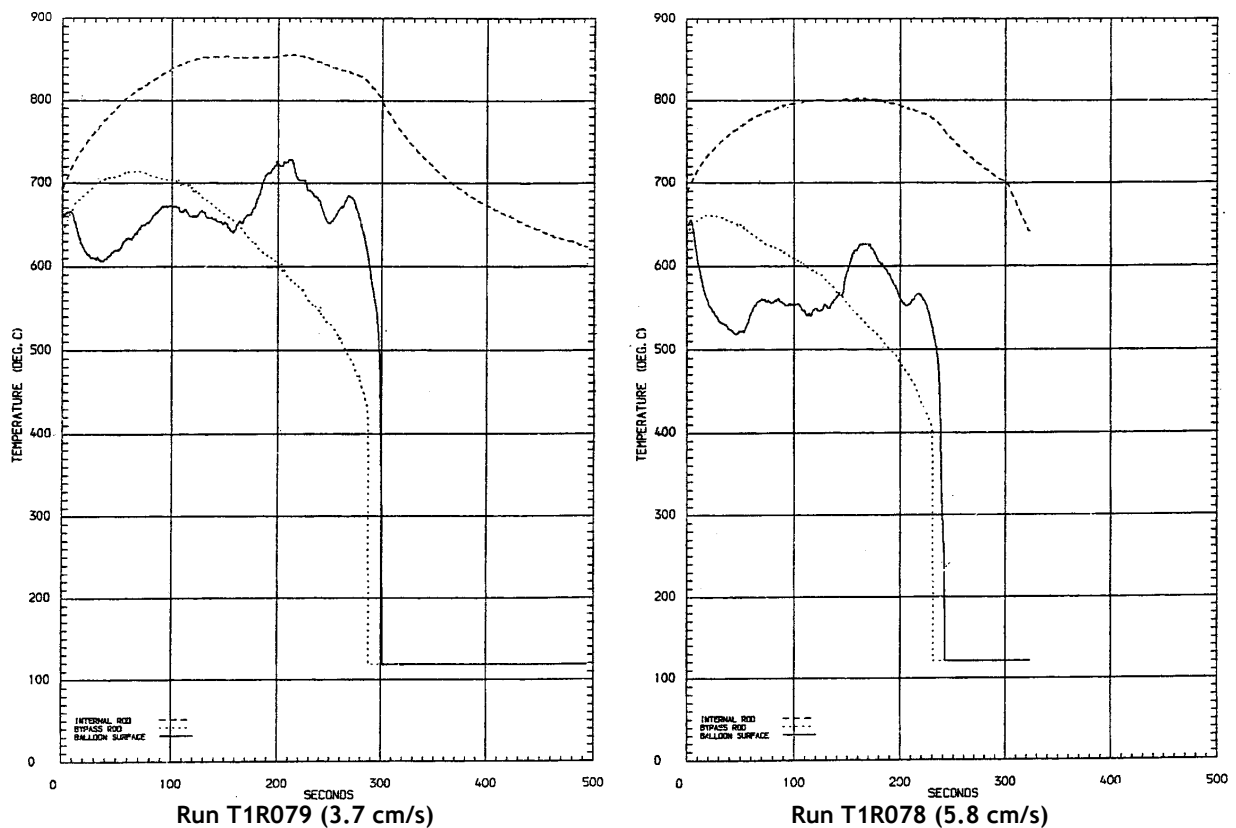


Figure 45: THETIS - Variable power. Blockage and by-pass temperatures for 3.7 and 5.8 cm/s reflood rates.

Temperature variations in the upper part of the blockage and in the by-pass at the same level for reflood rates of 3 and 2 cm/s are provided in Figure 46. Despite a reduction of 100°C in initial temperatures, an increase in the balloon temperature is observed at a much earlier stage for these reflood rates than for reflood rates of 3.7 cm/s or more.

- For a reflood rate of 2.9 cm/s, the maximum balloon temperature reaches 755°C, 60°C higher than the earlier temperature peak in the by-pass.
- For a reflood rate of 2 cm/s, the balloon temperature rises faster, reaching the limit of 800°C at about 190 s. At 220 s, when the temperature had reached 830°C, the cluster power was run down from 157 kW to 8 kW over a period of 60 s and kept at this value until the end of the test. Despite this reduction in power, the balloon temperature continued to rise for another 50 s, reaching a maximum of 850°C before rapid cooldown that precedes rewetting at 335 s. It is therefore difficult to predict the maximum balloon temperature that could have been reached if the programmed power decay had been maintained.

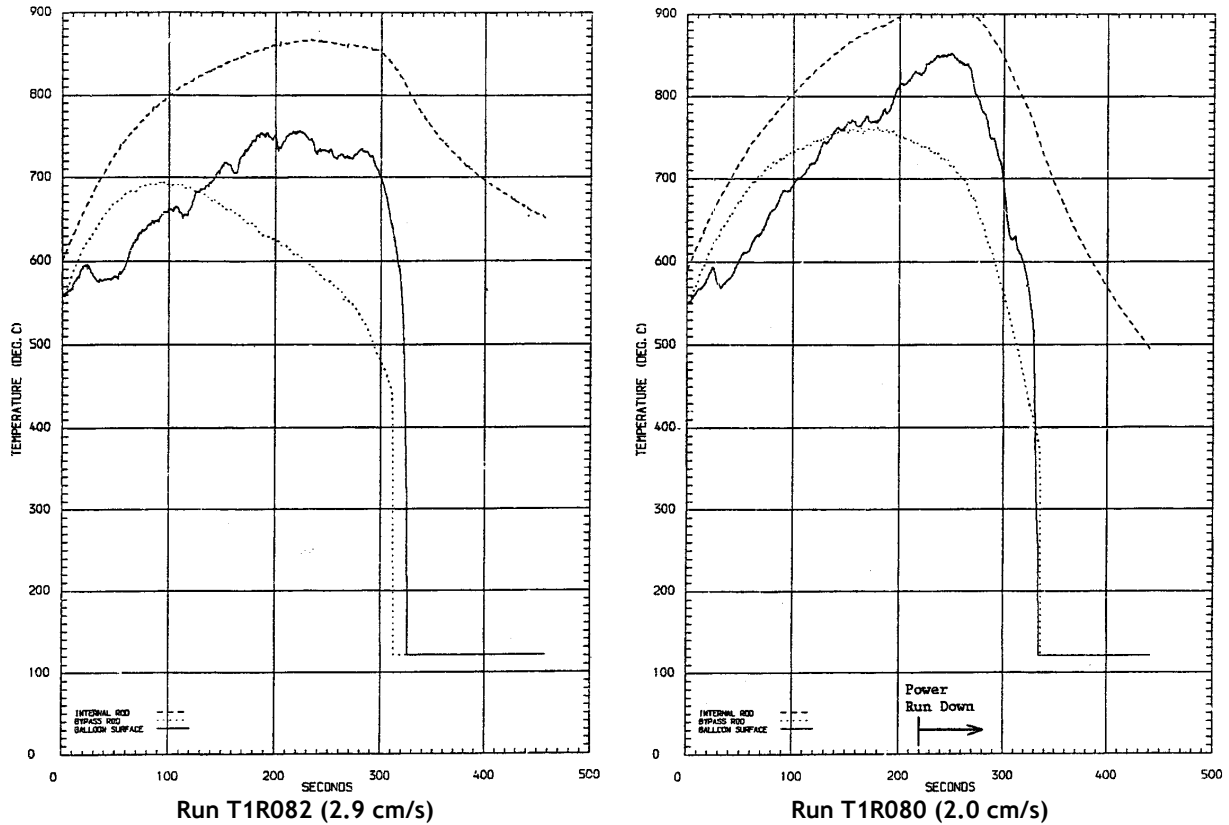


Figure 46: THETIS - Variable power. Blockage and by-pass temperatures for 3.7 and 5.8 cm/s reflood rates.

### 3.2.6 Tests with variable power and reflood rate

Finally, in order to evaluate the range of possible blockage temperatures during a more representative transient, a test was performed with varying both the power (as indicated in Figure 44) and reflood rate at values recommended by NNC and CEGB (on the basis of an evaluation calculation):

0 to 8 s	:	8 cm/s
8 to 58 s	:	3 cm/s
≥ 58 s	:	2 cm/s

This test (Run No.124) was conducted at the very end of the program, after the series of gravity reflood tests in which leaks occurred in the balloons and at the end of which rod distortion had appeared in the blockage region (mainly on the outer ballooned rods) most probably due to the large radial temperature gradients across these rods. Therefore, to evaluate the possible incidence of such events upon the facility, one of the preceding constant reflood rate tests (Run 82) was first repeated (Run 123). Table 2 shows how the conditions of these two tests are very similar. Further examination of the initial axial temperature profiles also illustrates great similarities. Temperature variations in the upper part of the blockage and in the by-pass at the same level for both tests are provided in Figure 47. Due to the failure of several TCs fitted inside the balloon, the balloon surface temperature was not measured in test Run 123 and was obtained using an inverse conduction calculation from the rod temperature. Compared on this basis, the blockage appears better cooled in Run 123 after 100 s, with a difference of ~ 60°C in the maximum temperature and with rewetting occurring 15 s earlier in comparison to Run 82.

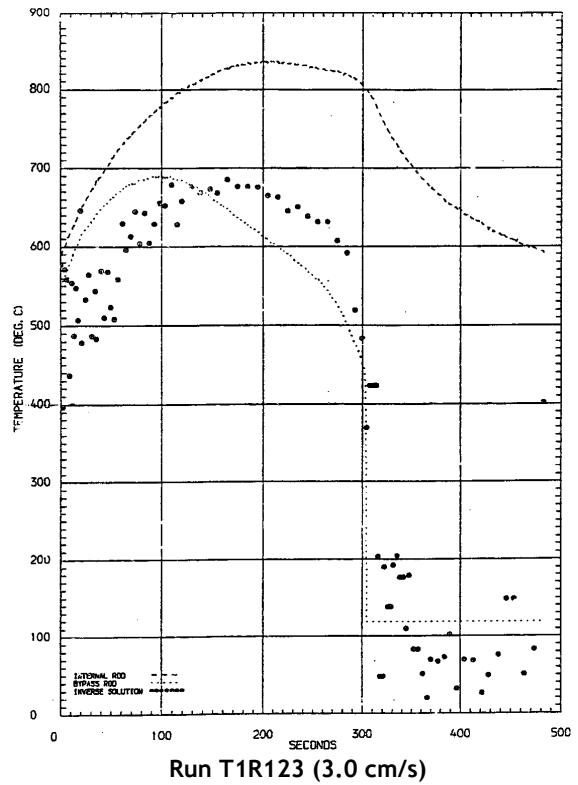
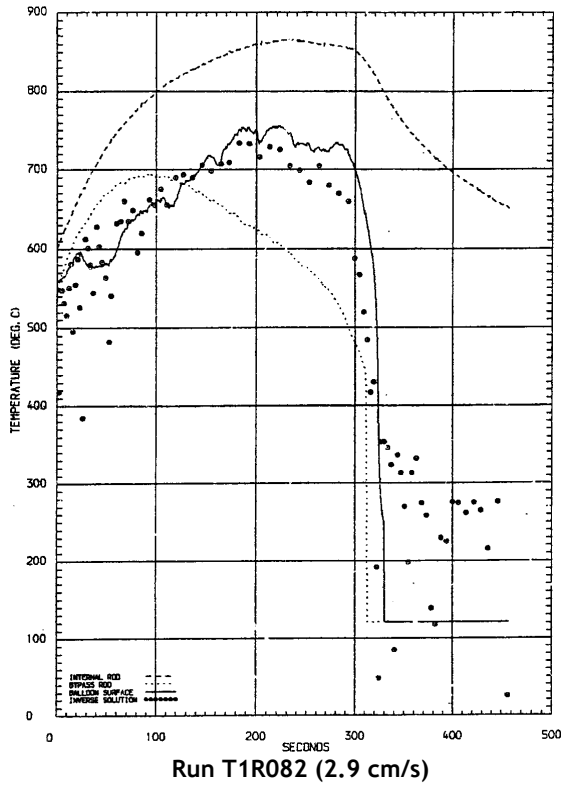


Figure 47: THETIS - Blockage and by-pass temperatures in tests T1R082 and T1R123.

Examination of steam temperatures at the exit of central blockage sub-channel in both tests (cf. Figure 48) indicates rewetting of the in-stream TC at ~ 130 s in Run 123, in comparison to ~ 200 s in Run 82. These various elements are consistent, which suggests that rod distortions improved heat transfer in the blockage region and - in the absence of these distortions - maximum temperatures could have increased by 60°C or more.

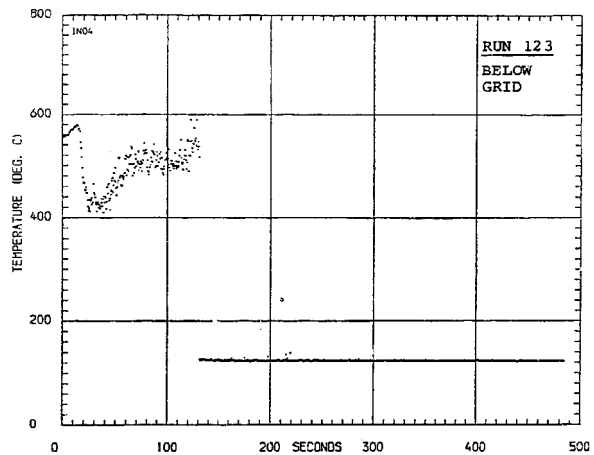
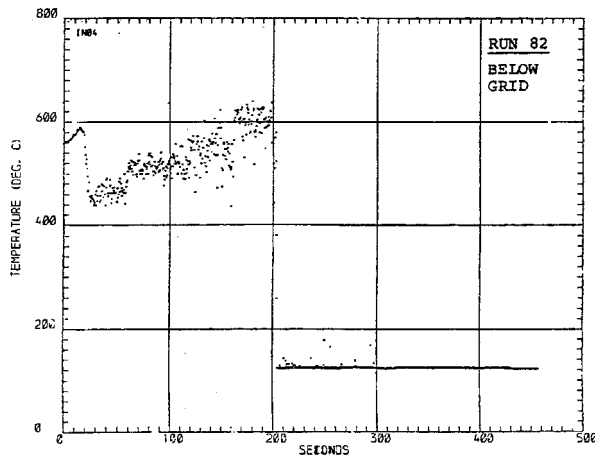


Figure 48: THETIS - Steam temperatures above blockage centre in tests T1R082 and T1R123.

The axial progress of the quench front in the by-pass for Run 124 is shown in Figure 49 in comparison with runs with 2 and 3 cm/s constant reflood rates. Quench front rises are almost identical up to 100 s for all runs, then this rise slows down after 200 s in Run 124, with rewetting at the bottom of the blockage close to that in the 2 cm/s reflood rate run. The quench front rise slows down further, with the blockage outlet undergoing rewetting at 375 s in Run 124, in comparison to about 310 s in Run 82 (3 cm/s) and 335 s in Run 80 (2 cm/s). However, it must be recalled that for the latter run, the power had been greatly reduced at 220 s due to the problematic rise in the blockage temperature at 180 s (cf. Figure 46), therefore explaining the increase in the quench front velocity.

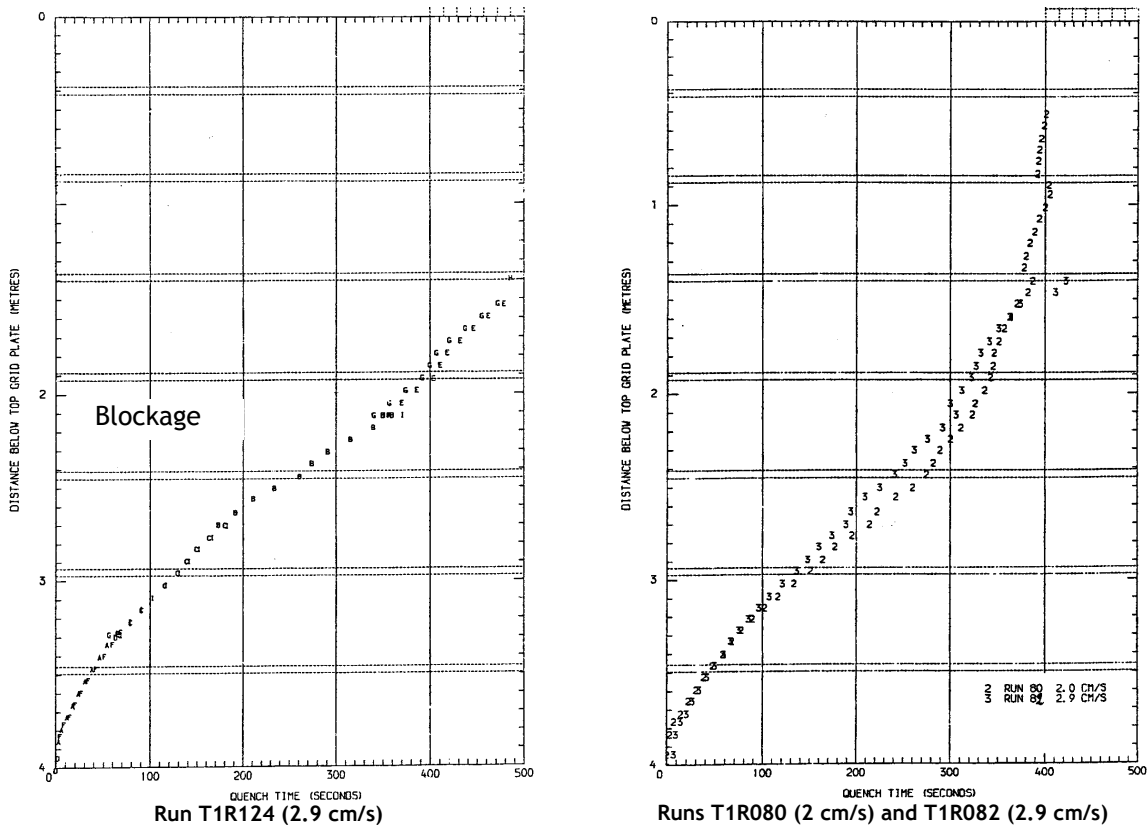


Figure 49: THETIS - By-pass quench times for test T1R124 and tests with 2 and 3 cm/s reflood rates.

Maximum temperature variations in the by-pass and blockage (using the inverse conduction calculation for the latter) are compared to Run 80 temperatures with a 2 cm/s constant reflood rate in Figure 50. The blockage temperature most probably takes advantage of the high reflood rate during the first 8 seconds, before rising to 600°C as early as 60 s. From this point, it remains comparable to that in Run 80 up until 160 s where it stabilises at ~ 760°C just before rewetting occurs, and without demonstrating the sudden increase observed in Run 80 after 180 s. However, taking into account the effect of assembly distortions existing in Run 124 and for which it was possible to evaluate the effect in the comparison of runs 123 and 82, it nevertheless remains difficult to predict how temperatures would have developed in an assembly identical to that used in Run 80.

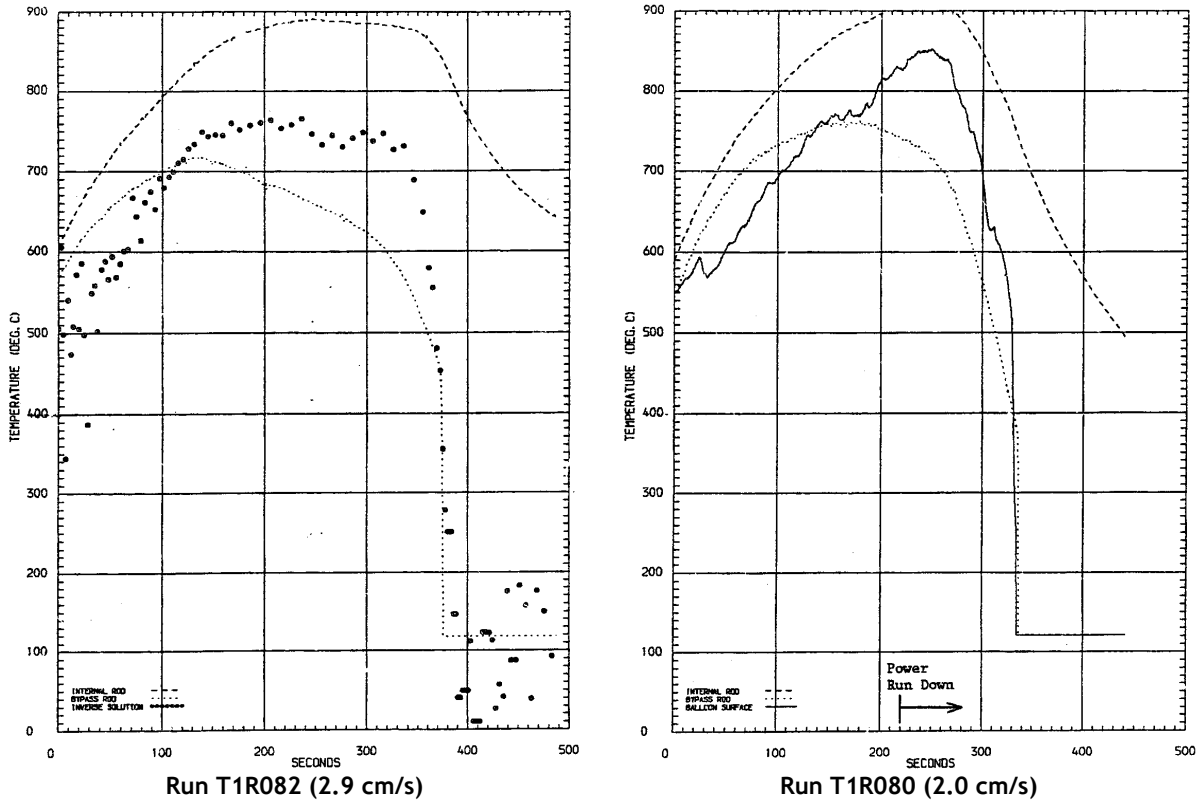


Figure 50: THETIS - Blockage and by-pass temperatures in tests T1R124 and T1R080.

### 3.3 Tests with an 80% blockage ratio

The 80% blockage geometry only differs from the 90% blockage geometry by the sleeve section in the most deformed region and the corresponding tapers (cf. Figure 51).

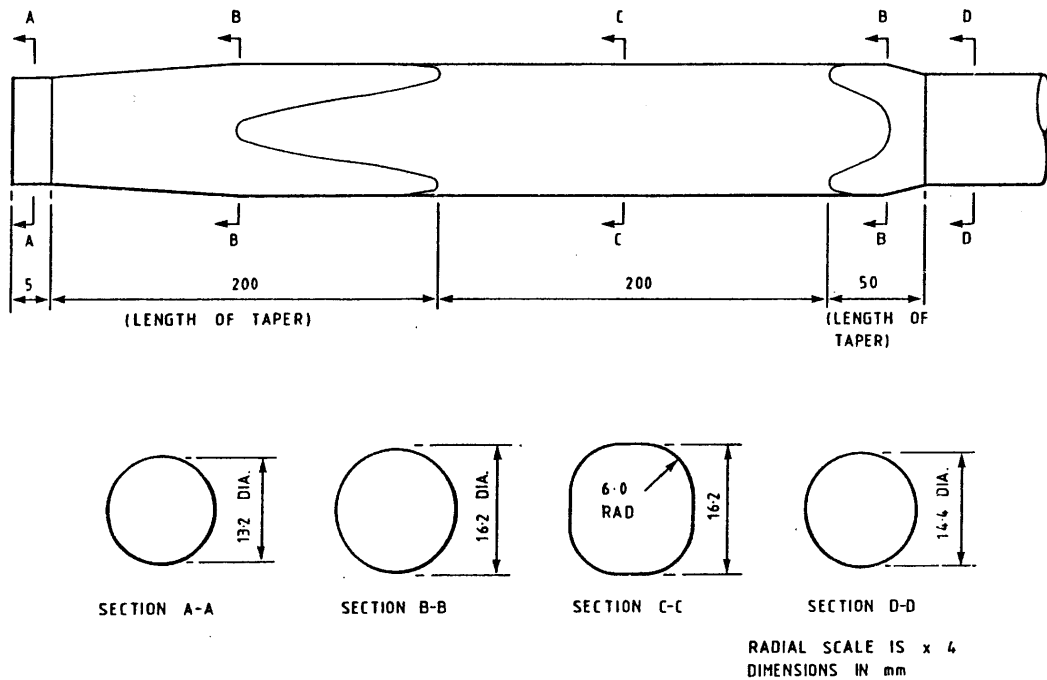


Figure 51: Shape of the cladding sleeve for the THETIS 80% blockage

A test matrix almost identical to that of the 90% blockage tests was produced for the 80% blockage. However, results of this 80% blockage tests will not be discussed in detail here, as focus was put on the 90% blockage in view of comparing results with other programs dealing with the same blockage ratio - 90% ratio being considered as the maximum blockage value for a fuel rod assembly in a LOCA ballooning phase. It is nevertheless interesting to compare selected results of the two test series performed under very similar conditions in order to obtain an indication of the impact of a variation in the blockage ratio, at these high values, upon the cooling of balloons in the blocked region. Comparisons will only concern temperature variations in the blockage and by-pass with decay power as shown in Figure 44 and defined in chapter 3.2.5, using several previously examined reflood rates.

Figure 52 compares temperature variations for a 4 cm/s reflood rate. After a cooling period of approximately 30 seconds, the temperature of the 80% blockage rises to 750°C at about 130 s, before a slow cooldown preceding rewetting that occurs at ~ 230 s. For the 90% blockage, temperature variations are more complex, with successive falls and rises and a maximum of 730°C. In the by-pass, temperatures vary in a very similar manner in both tests, with a slightly better cooldown as early as 70 s for the 90% blockage, with rewetting occurring 25 s earlier than in the 80% blockage test.

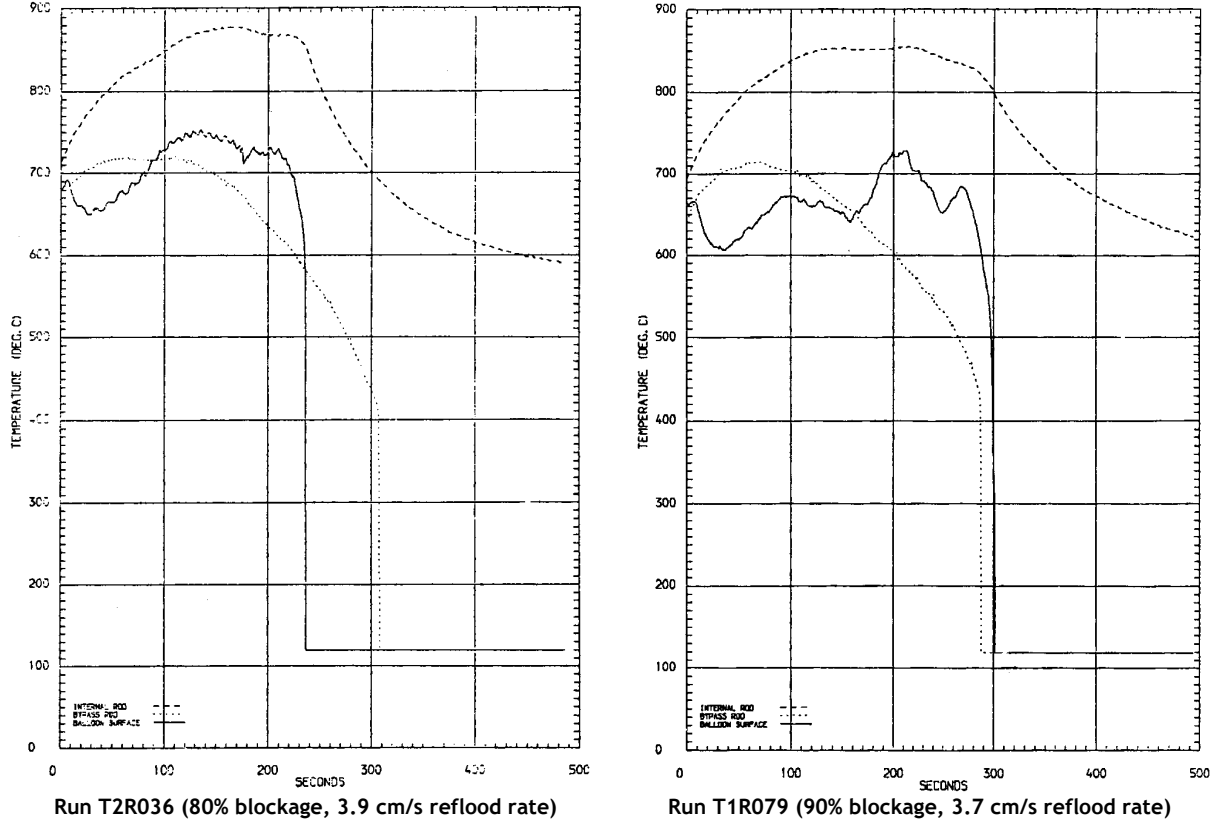
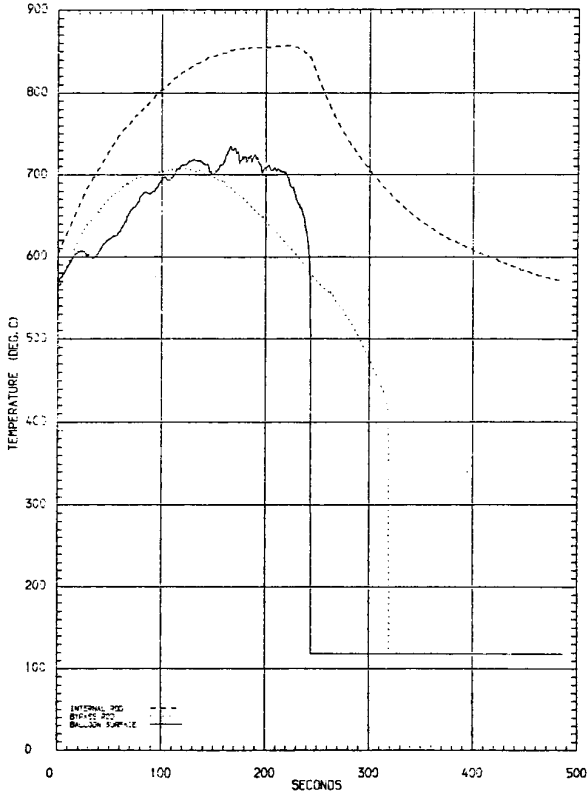
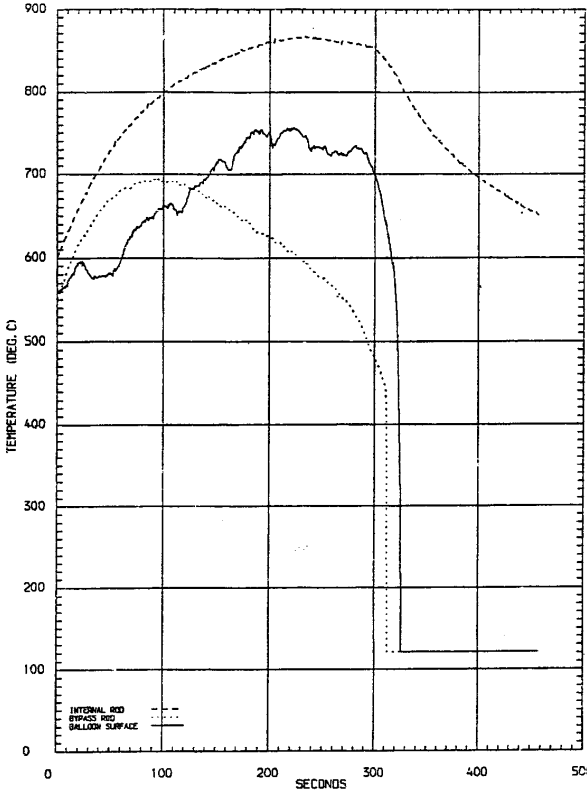


Figure 52: Blockage and by-pass temperatures for 80% and 90% blockages with about a 4cm/s reflood rate.

Figure 53 compares temperature variations for a 3 cm/s reflood rate. It is important to remember that the initial temperature of the rods was set at 550°C for reflood rates  $\leq 3$  cm/s instead of 650°C for higher reflood rates, to avoid excessive peak temperatures during the transient. Temperature variations in the blockage are similar even though several differences can be observed. The cooling enhancement following the onset of liquid entrainment ( $\sim 25$  s) is more efficient in the 90% blockage, so that the temperature at 130 s is 685°C - 35°C lower than the corresponding temperature in the 80% blockage. However, after this time, the 80% blockage temperature hardly increases, reaching its peak value of 735°C at 165 s, whereas the 90% blockage temperature continues to rise noticeably towards a maximum of 755°C at 190 s. Comparison of the by-pass temperatures again shows slightly better cooling in the 90% blockage test.



Run T2R037 (80% blockage, 2.9 cm/s reflood rate)



Run T1R082 (90% blockage, 2.9 cm/s reflood rate)

Figure 53: Blockage and by-pass temperatures for 80% and 90% blockages with a 2.9 cm/s reflood rate.

Figure 54 compares temperature variations for a 2 cm/s reflood rate. It is important to remember that the 90% blockage T1R080 test underwent a power run-down at 220 s in order to limit the maximum temperature that tended to rise in an unpredictable manner above the recommended value. Therefore, meaningful comparisons of temperature variations can only be made up to 220 s. As observed at higher reflood rates, blockage cooling improvement following the onset of liquid entrainment is accentuated for the 90% blockage, thus leading to a balloon temperature after 30 s that is approximately 50°C lower than the corresponding temperature for the 80% blockage. This temperature difference then reduces slightly to a difference of 30°C at 220 s, after which temperature variations can no longer be compared. The peak balloon temperature for the 80% blockage reaches 880°C at about 275 s, which suggests that the peak balloon temperature for the 90% blockage would have most probably surpassed this value if the power hadn't been run down. The rather surprising fact remains that, with a reflood rate of 2 cm/s, the 80% blockage is no better cooled than a 90% blockage for at least 220 s in the transient.

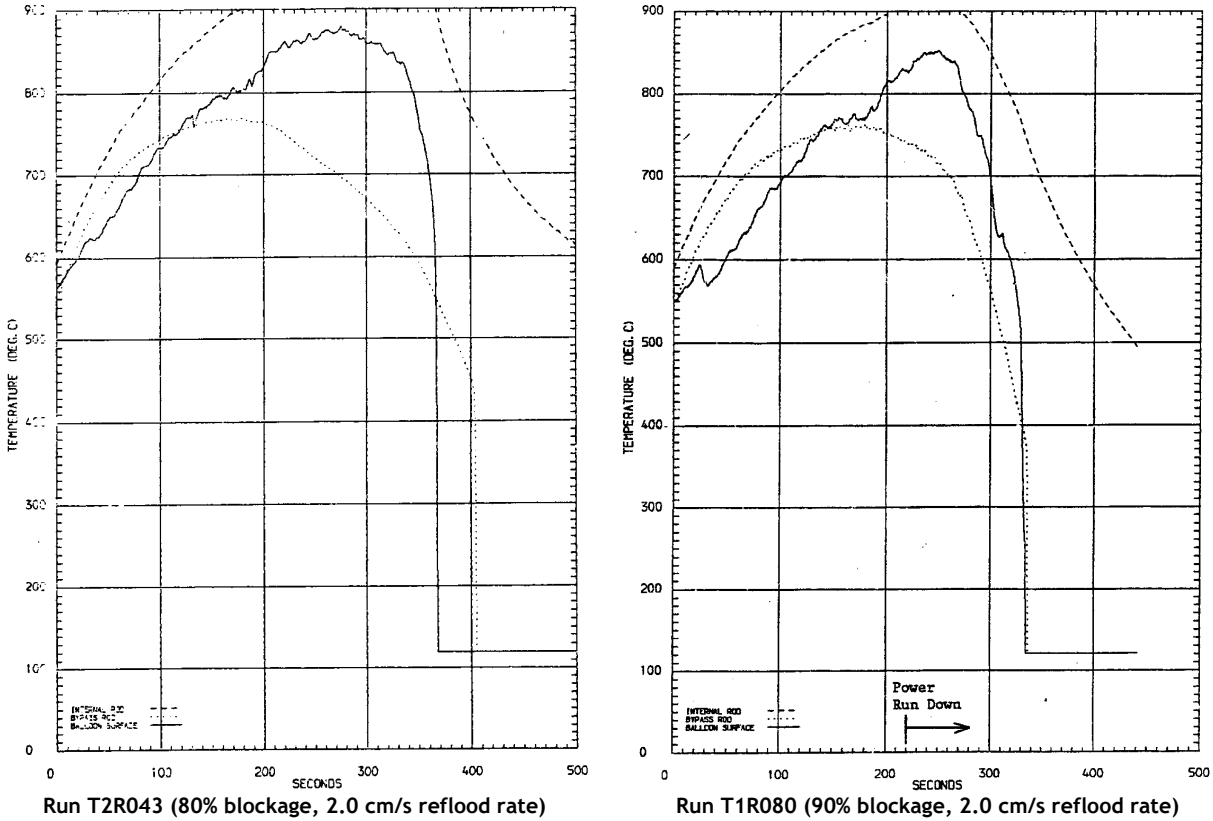
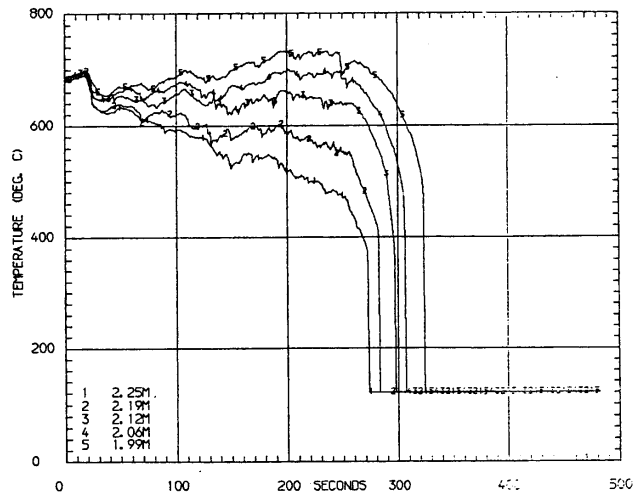
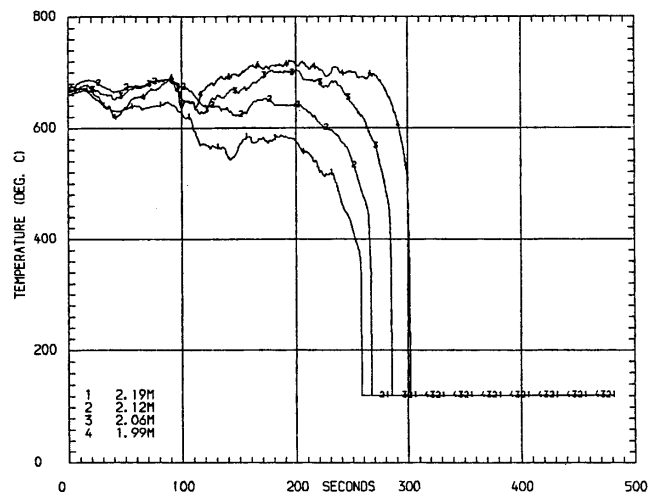


Figure 54: Blockage and by-pass temperatures for 80% and 90% blockages with a 2.0 cm/s reflood rate.

Another example of this unexpected behavior is provided in Figure 55 through the comparison of temperature variations recorded from the bottom (marker 1) to the top (marker 4 or 5) of a balloon bordering the central sub-channel of the blockage, in two reference tests with an 80% and a 90% blockage respectively (conducted under the same conditions: reflow rate = 2 cm/s; system pressure = 2 bar; inlet water temperature = 90 °C; cluster power = 100 kW).



Test T2R020 (80% blockage)



Test T1R065 (90% blockage)

**Figure 55: Distribution of balloon temperatures in comparative 80% and 90% blockage tests.**

- For the 90% blockage, the cooldown following the onset of liquid entrainment in the steam is particularly efficient at the top of the blockage (4), which tends to cool down much better than the mid-plane levels (2 and 3) at 40 s. Thereafter, cooling at the top of the blockage deteriorates until 90 s, before improving again until 115 s where the temperatures settle into the expected order with the hottest temperature at the top and a monotonous axial gradient along the throat. Rewetting occurs in a sequential manner from level 1 to 4.
- For the 80% blockage, temperature variations are generally similar to those observed in the 90% blockage, but less erratic at the top of the balloon (level 5) so that the temperature gradient from bottom to top is constantly positive. Overcooling periods are not observed in the top of the balloon and the maximum temperature appears to be slightly higher here than for the 90% blockage. The better cooling in the bottom part of the balloon during the second half of the transient is insufficient to compensate for the lack of overcooling periods in the top of the balloon at the beginning of the transient.

As part of the 80% blockage test series with a decay power curve as shown in Figure 44, a further test was performed in which the reflood rate was varied in a manner identical to that applied in run T1R124 with a 90% blockage (cf. § 3.2.6). Comparing the results of the latter test - conducted at the end of the series having undergone rod distortion - with results obtained from the corresponding 80% blockage test would have led to hazardous conclusions. It appeared wiser to compare results of the 80% blockage, variable power and reflood rate test (T2R039) with results of tests performed at the same power but with a constant reflood rate of 3 cm/s and 2 cm/s (runs T2R037 and T2R043 respectively). Figure 56 compares the temperature variations at the top of the blockage and in the by-pass at the same level for runs T2R043 and T2R039. Concerning the variable reflood rate test, the blockage temperature benefits temporarily from the high reflood rate in the first few seconds but by 60 s, when the flooding velocity is reduced from 3 cm/s to 2 cm/s, the temperature nevertheless reaches 635°C; about the same temperature as that observed in run T2R037 (with a constant reflood rate of 3 cm/s) at the same time. The peak blockage temperature observed in run T2R039 reaches 825°C at approximately 200 s, only 5°C lower than the temperature recorded at the same time in run T2R043 (2 cm/s), whose temperature continued to rise for another 75 s until reaching a maximum of 880°C. Blockage temperature variations in run T2R039 are closer to those of the constant 2 cm/s test, seeing that much of the temperature rise occurred during the period when the reflood rate was equal to 2 cm/s. The difference between maximum temperatures in the blockage and in the by-pass remains practically the same (~110°C) for both the variable reflood rate and the constant 2 cm/s reflood rate tests: the reduction in the peak by-pass temperature, which is due to a higher reflood rate in the first 60 s of run T2R039, is the same as the reduction in the peak blockage temperature due to an earlier rewetting.

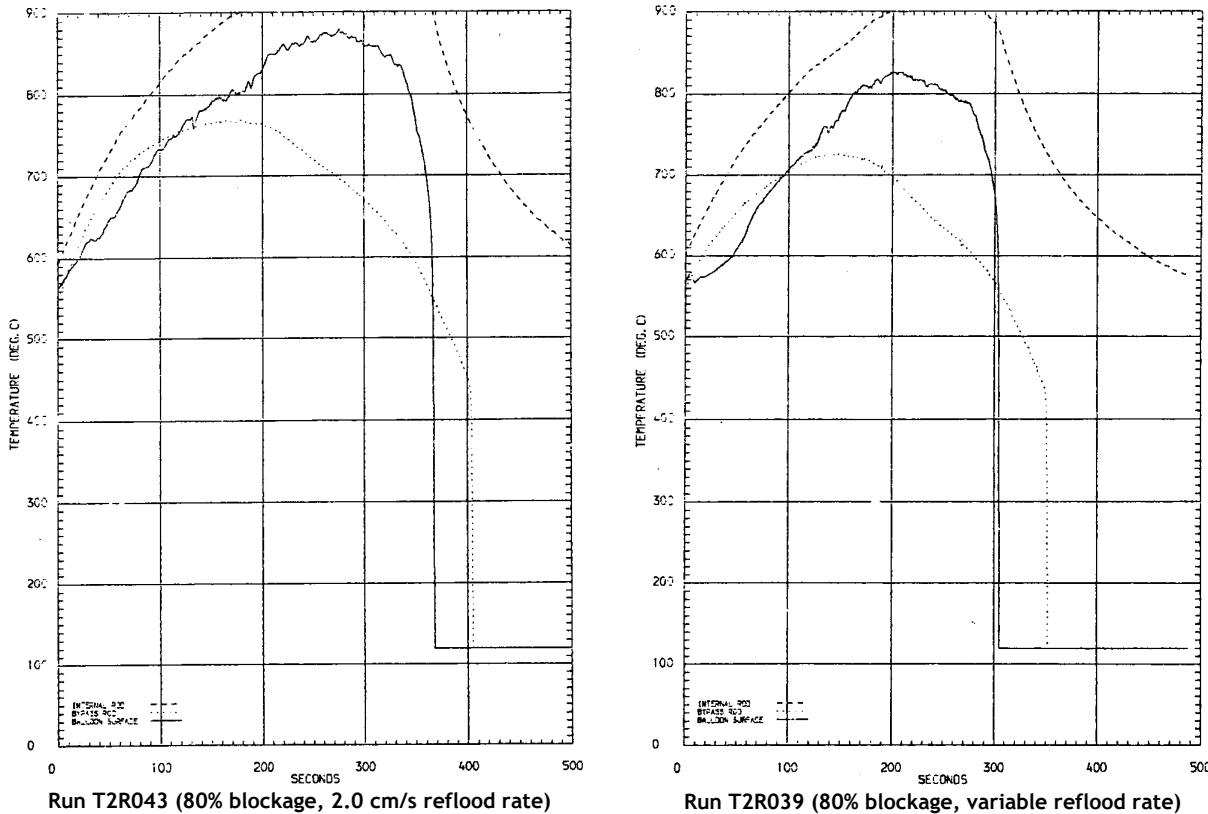


Figure 56: Blockage and by-pass temperatures for an 80% blockage with a 2.0 cm/s or variable reflood rate.

### 3.4 Discussion: qualitative analysis of phenomena

Balloon temperature variations in the upper part of the blockage result from the combination of blockage effects upon flow hydraulics and heat transfers.

In terms of hydraulics, a blockage introduces a major singularity, causing the coolant flow to divert into the by-pass. Straightforward methods for evaluating the flow rate in the blockage have been validated by air flow tests using a model of the THETIS 90% blockage geometry (cf. Figure 57). These models demonstrated that, for long blockages such as those used in the THETIS tests, the mass flow rate in the blockage sub-channels is reduced more or less in proportion to the flow area, or a little higher at low Reynolds numbers <2000. Consequently, the steam velocity in the maximum blocked section is comparable to that in the unblocked section.

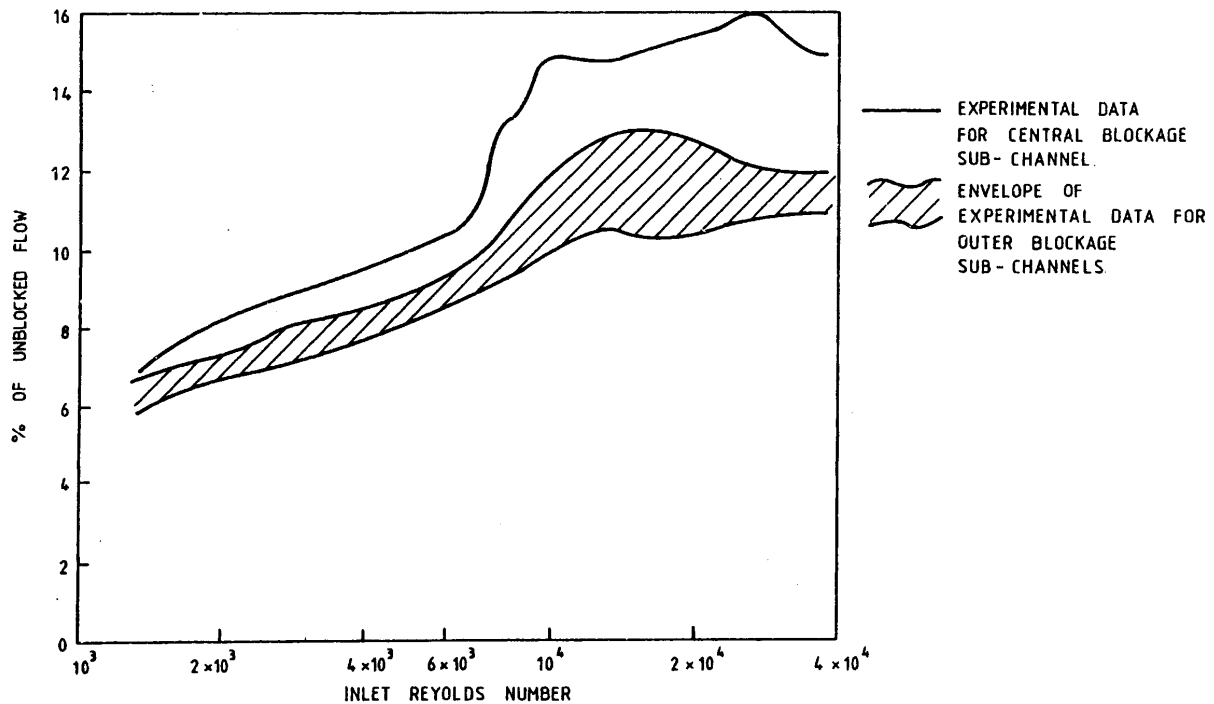


Figure 57: THETIS - Fraction of unblocked single phase flow through 90% blockage.

In terms of heat transfer, a significant change in heat fluxes per sub-channel unit of length could have been expected in the blockage in comparison to the by-pass. Once again, a straightforward evaluation of the different associated factors indicates that this is not the case, both for turbulent and laminar flow. This can be explained by the quasi-compensation of effects associated with the reduction in the hydraulic diameter: increase in the surface heat transfer coefficient and decrease in the effective transfer surface due to the geometry of the flow passage and extensive contact between rods. The heat transfer coefficient per unit length also remains practically the same for 80% and 90% blockages.

It could then be expected that the drastic reduction of steam flow in the blocked sub-channel (of a factor of 10 in relation to the by-pass for a 90% blockage), associated with the equivalent in energy deposition, lead to considerable superheating of steam in the blockage in comparison to the by-pass. It would also be expected that, as the heat transfer between the surface and the two-phase flow coolant occurs essentially by convection to steam, the balloon surface temperature should also follow the steam temperature.

However, the steam temperature - and therefore surface temperature - at the blockage outlet is also highly dependent on heat transfer between steam and the liquid droplets carried downstream from the quench front and which can more or less penetrate the blockage. Figures 58A and 58B illustrate steam and droplet speeds entering the blockage that condition droplet penetration in the maximum blocked region.

- As the flow rate in the maximum blocked region has been reduced in proportion to the flow area, steam speed is therefore the same both upstream from the blockage and in the maximum blockage region. In the 90% blockage (Figure 58A) for example, the steam flow in the tapered region - where the flow passage decreases from 100% to 10% over 200 mm - is progressively diverted towards the by-pass. This diversion can be considered complete about half way along this entry taper, where the balloons come into contact and isolate the sub-channels. At this level (60% blockage), the flow passage has been reduced to 40% of its nominal value, which means that the steam speed must be 4 times slower here than at the maximum blockage level where the flow passage represents only 10% of its nominal value. Along the tapered entry region therefore, the axial speed of steam falls by a factor of 4 over the first half before rising to its initial value over the second half.
- When the quench front is rather far upstream, the entrained droplets are accelerated by the steam flow due to the progressive acceleration of steam caused by the heating and evaporation of the liquid phase. These droplets will reach the blockage entry with sufficient enough speed to break through the deceleration region and enter the maximum blocked region; once in this smaller volume, the droplets can efficiently de-superheat the steam and limit heating of the reduced flow of steam. The greater the slowdown, the longer the transit time of the droplets in the blockage region and the greater the heat transfer from the steam to the liquid. This explains why the cooldown in the early stages of reflood is more efficient in the 90% blockage than in the 80% one, with the temporary development of a negative axial temperature gradient. The more erratic temperature variations in the 90% blockage also result from compensation between the surface-to-steam heat transfer and a varying equivalent or greater steam-to-liquid heat transfer. It is interesting to note that the "advantage" gained early in the reflood for the 90% blockage can possibly last long enough in the transient so that the peak blockage temperature remains lower than that observed for the 80% blockage test.
- Later on during reflooding, as the quench front approaches the bottom of the blockage, the droplets experience only slight acceleration and fall back towards the blockage entry where they are swept aside into the by-pass, unable to break through the deceleration region. Without cooling from the liquid droplets, steam will superheat significantly in the maximum blockage section, driving the corresponding surface temperatures at the throat outlet.

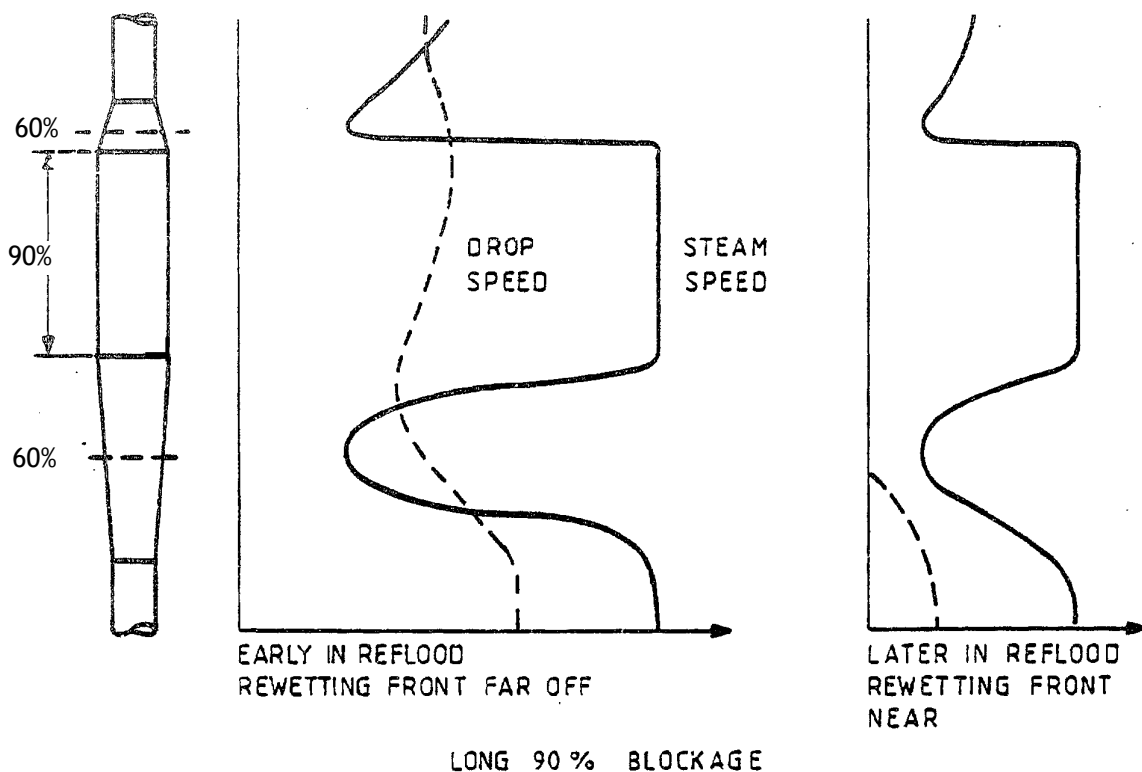


Figure 58A: Axial variation of steam and drop speed along the long 90% blockage.

Figure 58B illustrates the behavior induced by the reduction in the maximum blockage rate or in its axial extension.

- For an 80% long blockage, the minimum flow passage represents 20% of its nominal value, therefore half of the flow passage at mid-height of the entry taper where steam speed only falls by a factor of 2 in comparison to the speed upstream from the blockage. Due to this slight deceleration, penetration of droplets in the maximum blocked section is maintained over a longer period in comparison to the 90% blockage case, but this also reduces the transit time of droplets in the throat and therefore the efficiency of steam de-superheating. These two events have opposing effects and it is difficult to evaluate their relative importance, but results drawn from comparisons discussed in the previous paragraph seem to indicate that the effect of transit time is predominant.
- For a 90% short blockage, the steam speed in the maximum blocked section is greater than that measured upstream from the blockage as the steam flow here has been reduced into a smaller proportion than that of the flow passage. Therefore, even though the minimum steam speed (at approximately mid-height of the entry taper) is still 4 times slower than the steam speed in the maximum blocked region, deceleration in relation to the speed upstream from the blockage is less than for the long 90% blockage case. More importantly, the shorter connecting length favours the crossing of the deceleration region by droplets. Cooling of steam by liquid droplets will therefore occur over an extended time interval, which should limit the maximum temperature of the balloon surface.

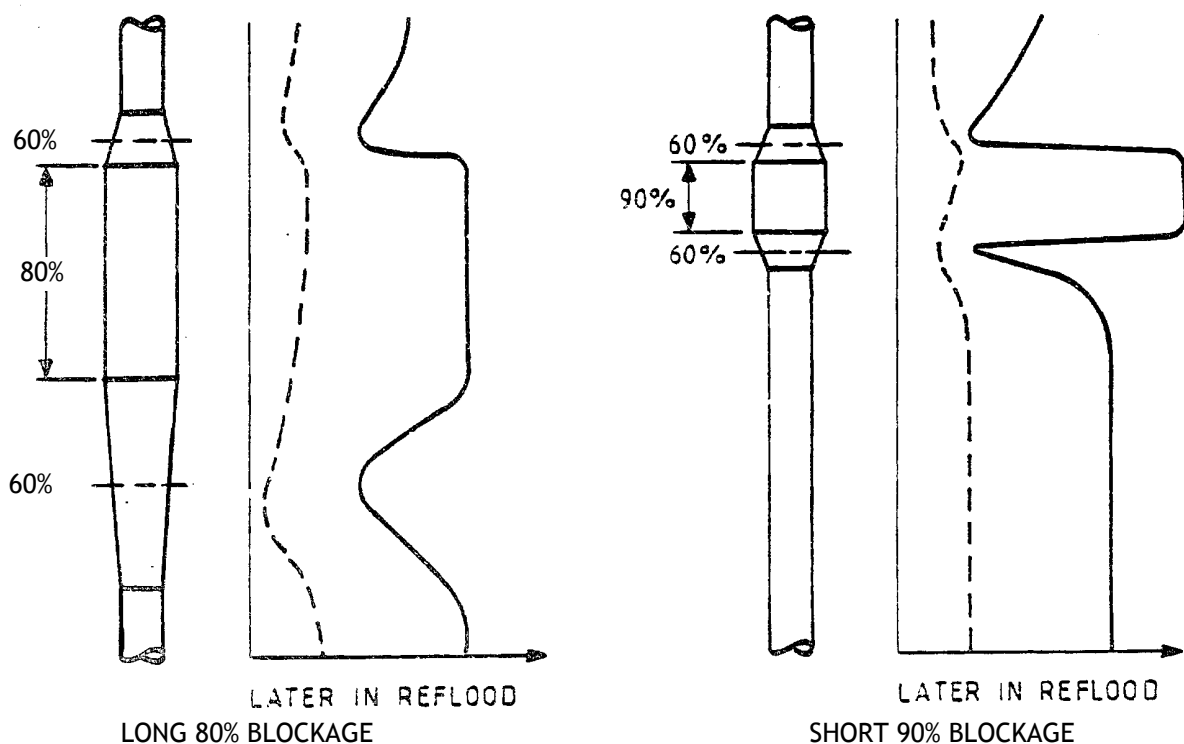


Figure 58B: Axial variation of steam and drop speed along the long 80% blockage and short 90% blockage.

### 3.5 Gravity reflood tests with an 80% blockage ratio

The gravity reflood tests were performed to briefly investigate the inlet flow oscillation and steam binding effects - which are predicted to occur in a reactor system during reflooding - upon the cooling of a fuel assembly containing significant blockage. For this purpose, a tubular downcomer was connected in parallel to the test section (cf. Figure 31) with scaled flow area and correct height with respect to the reactor situation. A restrictive orifice was fitted to the steam exit to roughly simulate the pressure drop in the hot leg mainly due to steam generators. A combination of valves made it possible to perform experiments with the downcomer initially empty, partially filled or completely filled.

Table 3 lists the conditions of the 16 gravity reflood tests performed with an 80% blocked cluster. The varied test parameters included pressure (2 or 4 bar), inlet temperature (50°C to 90°C), inlet flow rate (0.15 to 0.6 kg/s, corresponding to reflood rates of 2cm/s to 8 cm/s assuming the whole flow passed through the test section), downcomer initial level (full or empty) and steam outlet orifice (24 to 34 mm). A constant power fixed at 100 or 150 kW was chosen for 12 tests and a variable power for tests 116 to 119, according to Figure 44, in order to simulate a best-estimate decay power level representative of a PWR hot rod.

Test number	Pressure (bar)	Inlet flow rate (kg/s)	Power (kW)	Inlet temperature (°C)	Initial temperature (°C)	Orifice diameter (mm)	Initial downcomer water inventory
64	2.0	0.29	152	88	660	29	Full
66	3.9	0.29	152	91	659	29	Full
68	1.9	0.16	102	86	643	29	Full
69	3.9	0.15	101	90	650	29	Full
70	2.0	0.30	152	90	659	29	Empty
73	4.0	0.30	152	89	640	29	Empty
74	1.9	0.15	100	83	651	34	Full
75	3.9	0.15	101	90	646	34	Full
76	3.9	0.15	101	87	647	29	Empty
77	1.9	0.30	157	89	656	29	Full
116	2.0	0.57	Fig 44	92	563	34	Full
117	2.0	0.57	Fig 44	92	573	29	Full
118	2.0	0.58	Fig 44	85	566	24	Full
119	2.0	0.57	Fig 44	87	562	26	Full
120	2.1	0.15	101	68	650	29	Full
121	2.0	0.15	102	49	652	29	Full

#### NOTES

1. An inlet flow rate of 0.3 kg/s corresponds to a reflooding rate of 4 cm/s if all of the flow passes into the test section.
2. Initial temperatures quoted are at mid-height in the L-shaped by-pass region around the blockage.
3. The balloon filling gas was nitrogen for all gravity reflood tests.

**Table 3: Nominal conditions of the THETIS 80% blockage gravity reflood tests.**

### 3.5.1 Hydraulic behavior

The hydraulic behavior of a gravity reflood test with an initially full downcomer is summarised in Figure 59, showing the variations in time of the quench front on non-deformed rods, the collapsed liquid level in the test section and the downcomer water level. During the first few seconds, a fraction of the downcomer is dumped into the test section which immediately rewets the bottom 0.2 m of the bundle causing an abrupt rise in the collapsed liquid level of about 0.4 m. Thereafter this collapsed liquid level experiences violent oscillations of about 5 s in initial period, until about 90 s where they vanish within an irregular signal. As the test section level builds up, the downcomer level also rises after 100 s, to maintain a sufficient pressure difference in order to overcome the pressure drop through the steam orifice. After 180 s, the steam flow begins to decrease, thereby reducing the exit pressure drop, which leads to a fall in the downcomer level, although the test section level continues to rise.

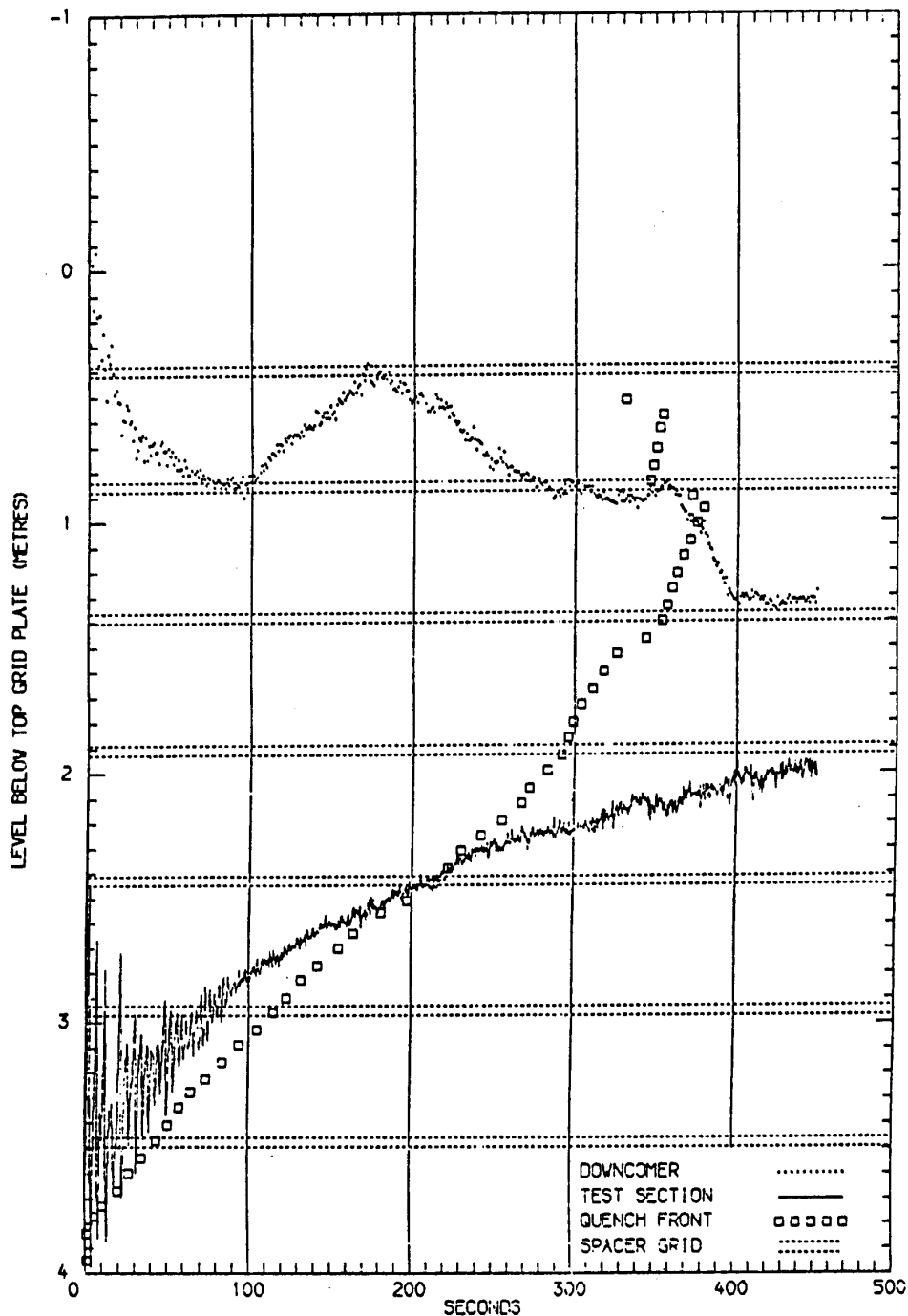


Figure 59: Gravity reflood test T2G068 - Downcomer, test section and quench front levels.

Apart from the almost instantaneous rewetting of the bottom 0.2 m of the assembly, quench front variations are on the whole rather similar to those observed during a forced reflood test under similar conditions, such as the run T2R020 illustrated in Figure 60.

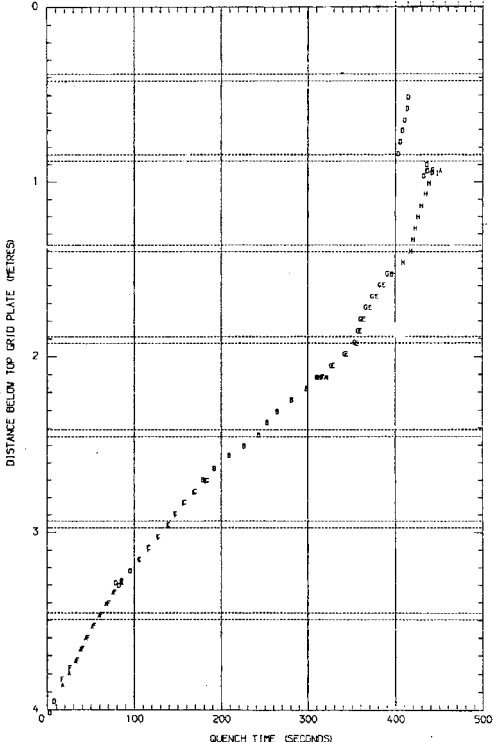


Figure 60: THETIS -Quench front level in forced reflood test T2R020.

Oscillations of the collapsed liquid level are accompanied by greater oscillations of the inlet flow rate in the test section (cf. Figure 61), with substantial reverse flows; these oscillations again die out rapidly after 90 s.

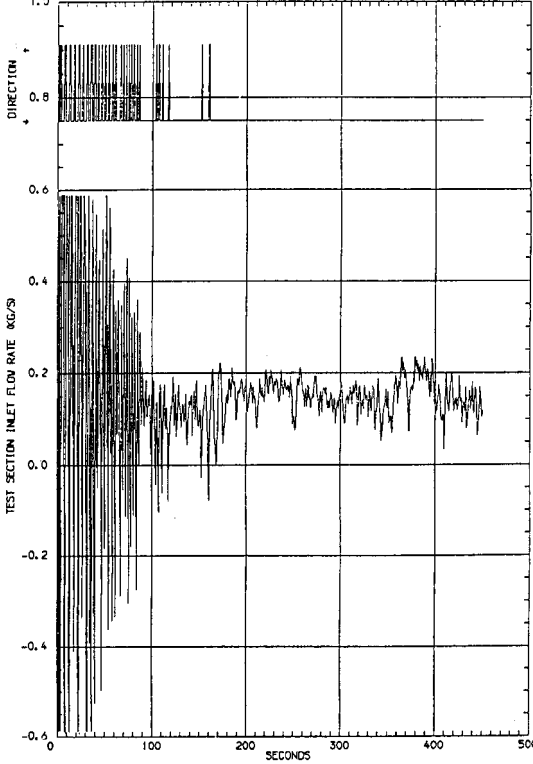


Figure 61: Gravity reflood test T2G068 - Test section inlet flow.

Reference [6] provides a detailed analysis of results obtained by successively varying the different test parameters: system pressure, inlet flow rate, inlet temperature, initial downcomer level and steam exit orifice diameter. Results from these investigations agree with the expected effect of variations applied to the different parameters. For illustrative purposes, only the impact of the initial downcomer level will be discussed here. Figure 62 compares variations in the different levels for the two tests performed under identical conditions, except for the initial water level in the downcomer, which is full for run T2G077 and empty for run T2G070. As far as the latter test is concerned, the downcomer level rises to its maximum value for 160 s before it stabilises (via overflow into the weir vessel) until about 230 s and then declines. The collapsed level in the test section shows no initial surge such as that occurring in the case with the downcomer initially full. However, oscillations in the collapsed level appear as early as 20 s and last up to 120 s. Furthermore, the quench front does not immediately cover the bottom of the assembly, but its progression remains similar to that observed during the full downcomer test with a delay of some 60 s.

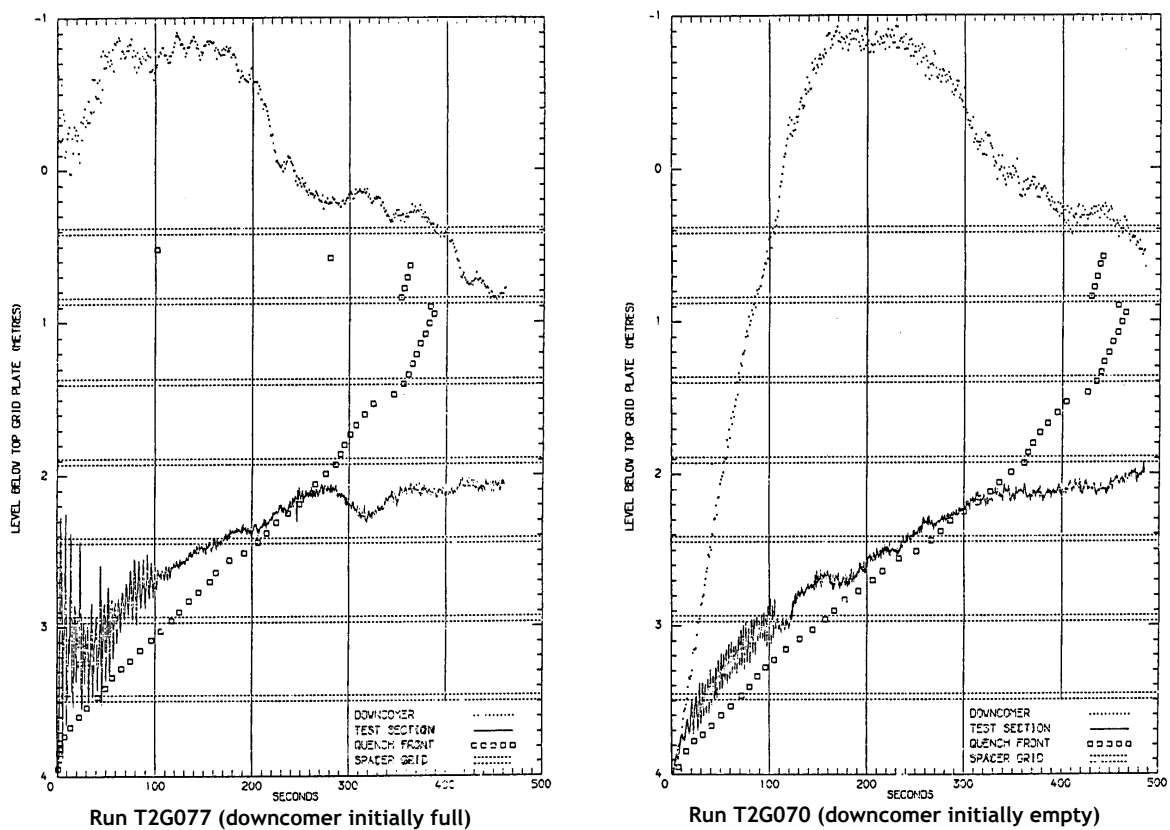


Figure 62: Downcomer, test section and quench front levels for gravity reflood tests with downcomer initially full or empty.

The occurrence and disappearance of oscillations in the test section collapsed level, as well as in the test section inlet flow, were observed in all the gravity reflood tests. The fact that oscillations cease rather abruptly, after a period of about 80 s, leads us to speculate that the driving mechanism for these oscillations may be related to a change in the flow regime, particularly at the level of the rewetting front. In this way, it is suggested in reference [6] that this mechanism might be associated with the existence of an inverted annular film boiling region above the quench front in the early stages of the transient when the liquid arriving at the quench front is subcooled. Later on, as the quench front progresses upwards, the subcooling is cancelled out and the inverted annular film regime disappears. In these tests, it was evaluated that the time needed to cancel out the liquid subcooling corresponded approximately to the time at which the level oscillations cease.

The 4 successive runs (116 to 119) listed in Table 3 - with a best-estimate decay power and different values of the restrictive orifice size - were designed to simulate the conditions of a more realistic test with variable reflood rate, such as those applied in run 124 with a 90% blockage and a forced reflood rate (cf. § 3.2.6). However, test results revealed that it was not possible to evaluate a progressive reduction in the flow rate during the test using this procedure, as the reduction in the orifice section merely affects the flow rate at the beginning of the reflood. Furthermore, the poor simulation of pressure drop in the reactor hot leg (including the SGs) using a simple orifice at the steam exit from the test section steam/water separator was also underlined, particularly as it does not take into account the  $\Delta P$  resulting from the evaporation of the liquid in the SG.

3.5.2 Thermal behavior

Figure 63 compares temperature variations downstream and upstream from the mid-plane spacer grid of a rod in the by-pass region for both forced and gravity reflood tests performed under similar conditions. The better cooling downstream of the spacer grid is obvious, but it is noticeably better in the gravity reflood test whose grid rewets within a few seconds after the start of reflood, whereas the grid in the forced reflood test only undergoes rewetting at about 150 s. Rod rewetting also occurs slightly earlier on in the gravity reflood test, about 60 s before that in the forced reflood test. The advantage of a gravity reflood rate with an initially full downcomer results from the high flow rate during the first few seconds owing to the surge of water from the downcomer, which leads in particular to almost instant rewetting of all the grids; the presence of wet grids will improve better cooling by steam over the whole transient.

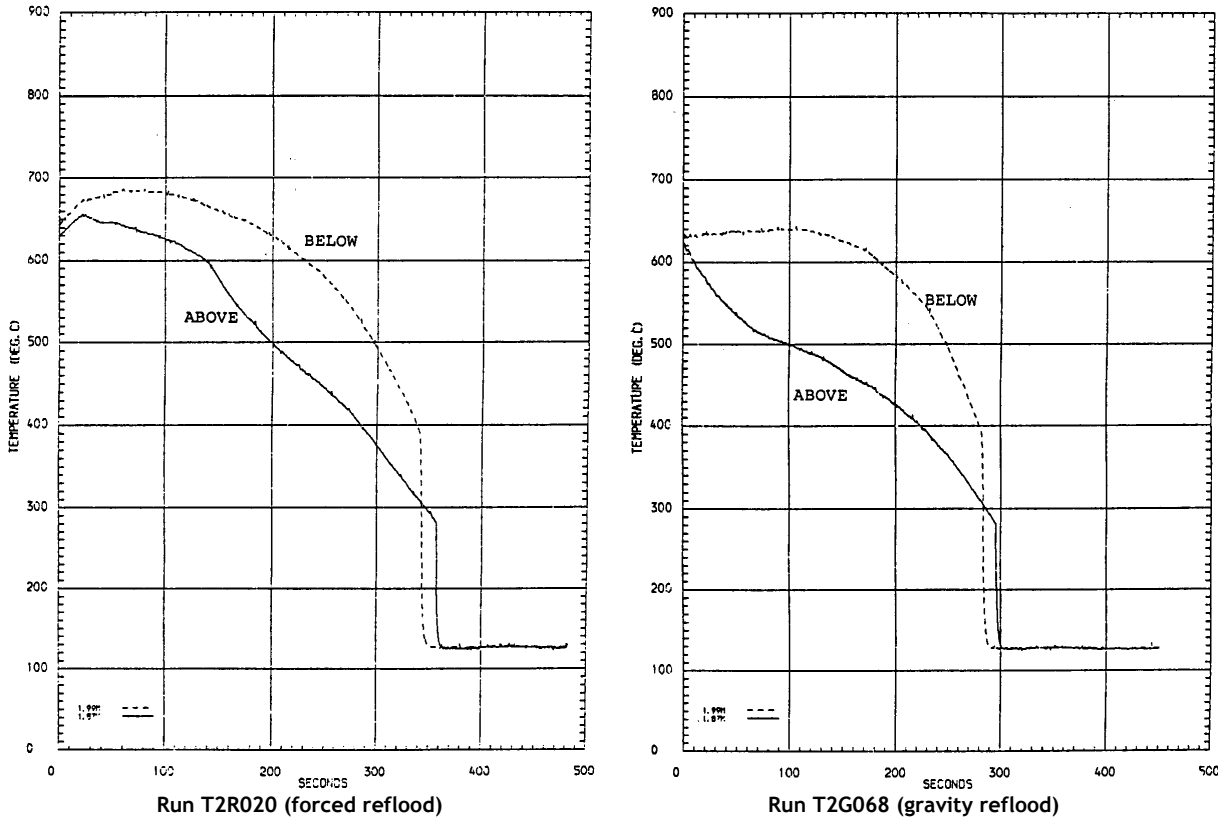


Figure 63: By-pass temperatures below and above the mid-plane spacer grid for comparative forced and gravity reflood tests.

Figure 64 compares temperature variations recorded at different elevations remote from grids of by-pass rods for the same two above-mentioned tests. This Figure shows that these temperatures hardly rise during the gravity reflow test, whereas they reach maximum levels during the forced reflow test. Rewetting also seems faster in the upper levels, due to the cumulative cooling effects when passing through the different spacer grids.

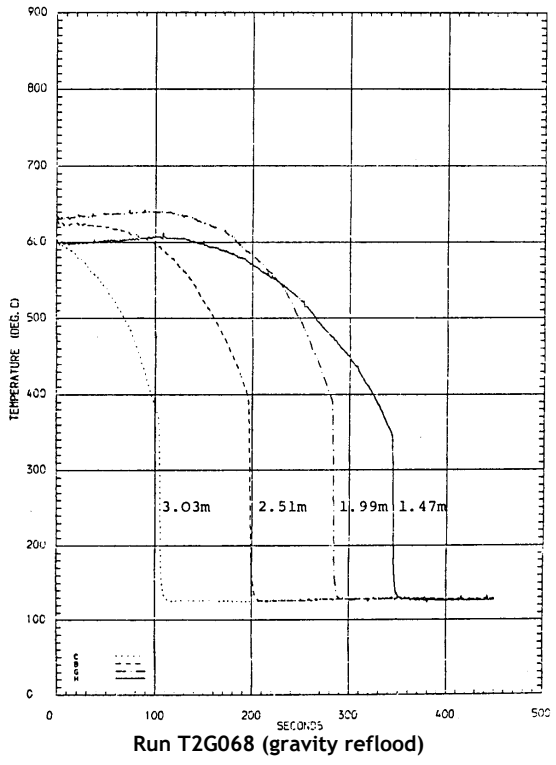
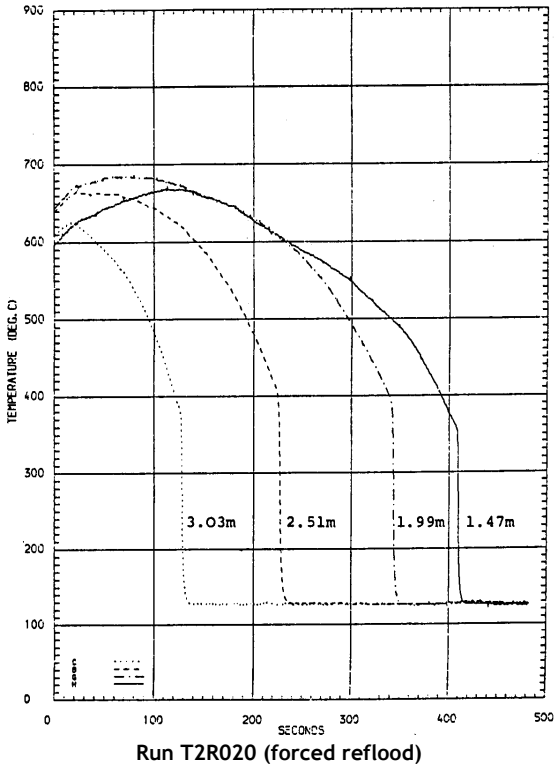


Figure 64: By-pass temperatures remote from successive spacer grids for comparative forced and gravity reflow tests.

Figure 65 compares temperature variations at 5 different levels for both a by-pass rod and a blockage rod in run T2G068 with gravity reflood. As expected, the temperature distribution for the unballoned rod shows a steady increase towards the downstream grid. Distribution within the blockage is more complicated, with a general cooldown during the first 10 seconds, followed by a temperature drop at the blockage entry and in the bottom part of the blockage, but with a temperature rise in the upper part of the blockage. This leads to the development of an axial gradient of approximately 250°C along the balloon. The marked cooldown that appears in the lower part of the blockage after 120 s was explained by the accumulation of a plug of water in the throat sub-channel, with this influencing the upper part of the blockage in various ways, such as early rewetting for the considered sub-channel. Similar behavior was also observed in the forced reflood test with an 80% blockage.

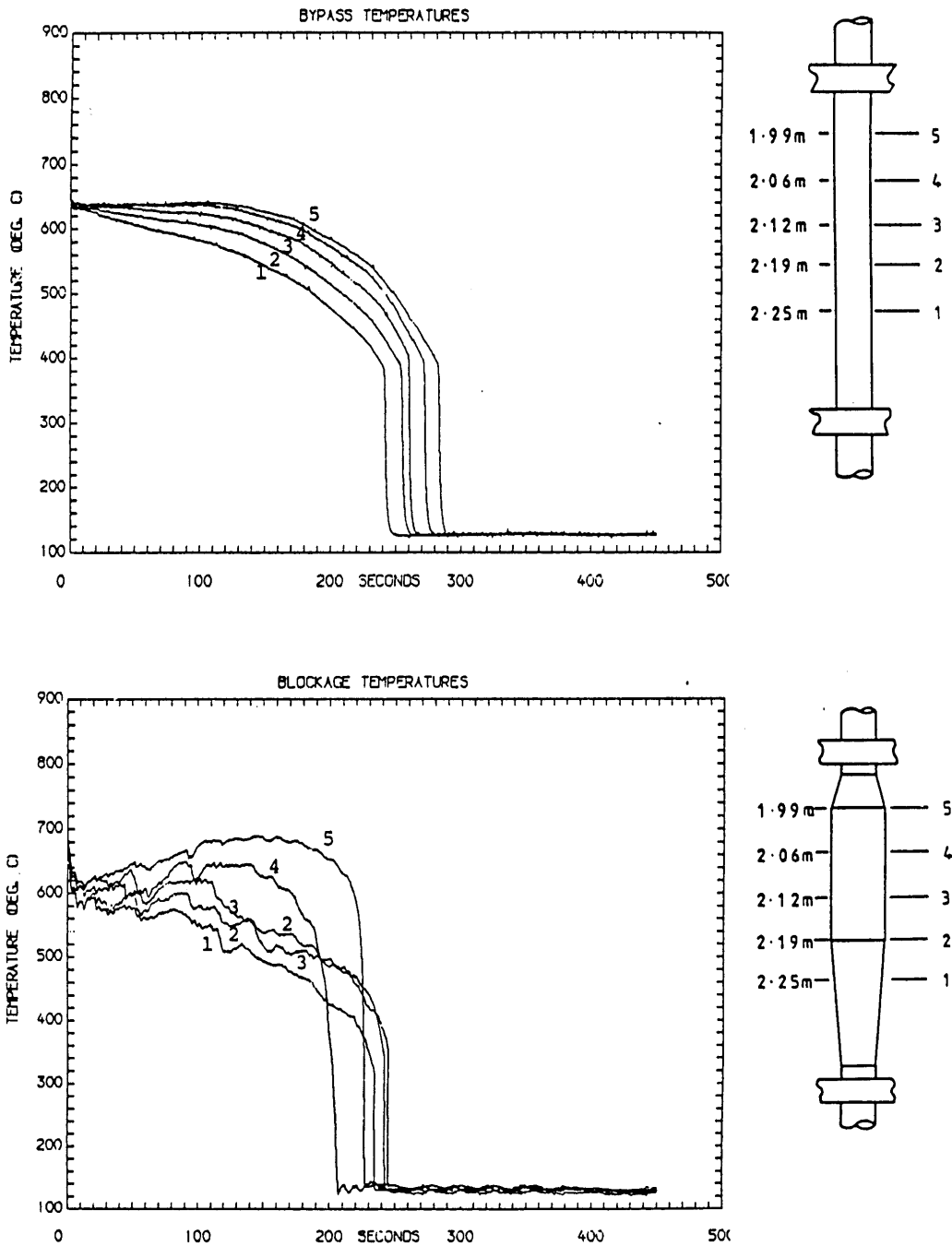


Figure 65: Axial distribution of by-pass and blockage temperatures in gravity reflood test T2G088.

Last of all, Figure 66 compares temperature variations at 5 different levels of a blockage rod in run T2G068 with gravity reflood and in run T2R020 with forced reflood, both under identical conditions. In a general way, variations are rather similar which seems to indicate that these variations are determined by the same fundamental processes in terms of heat transfer.

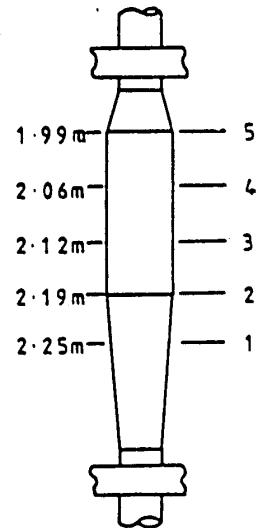
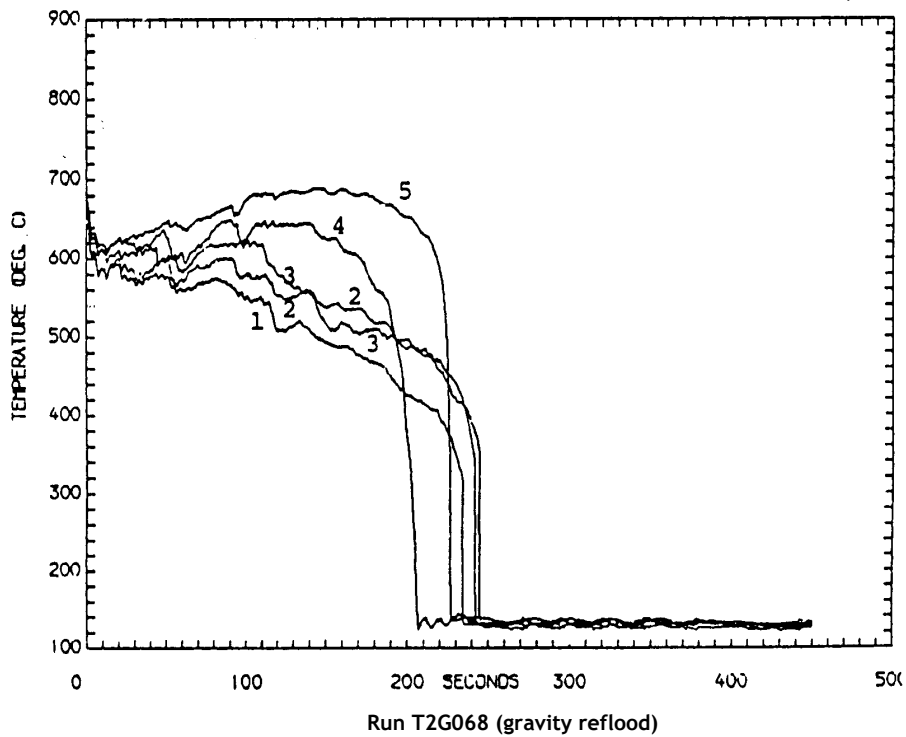
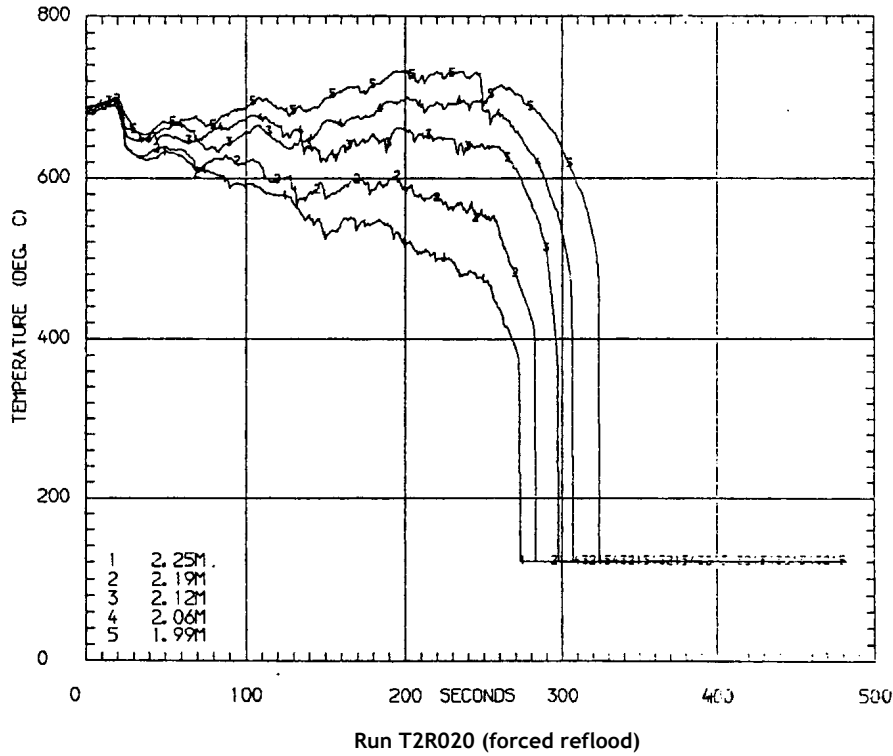


Figure 66: Axial distribution of by-pass and blockage temperatures in comparative forced and gravity reflood tests.

### 3.5.3 Impact of flow and level oscillations

In light of the comparisons previously discussed, it appears that the considerable flow oscillations observed in the test section inlet, such as indicated in § 3.5.1, do not introduce any major new effects.

In order to better evaluate any influence of such oscillations, two specific forced reflood tests were performed (T2R079 and T2R080) in which the reflood rate approximately reproduced the inlet flow rate in two gravity reflood tests (T2G077 and T2G070 respectively) but without the inlet flow oscillations. However, neither of these "mimics" were precise simulations of gravity reflood minus the flow oscillations only, due to the difficulty in evaluating the average inlet flow rate in gravity reflood, particularly for the test with an initially full downcomer (T2G077).

Only results concerning the initially full downcomer case will be discussed in this state-of-the art review. Figure 67 illustrates the inlet flow rate variations actually recorded during both the gravity reflood run T2G077 and the "mimic" forced reflood run T2R079.

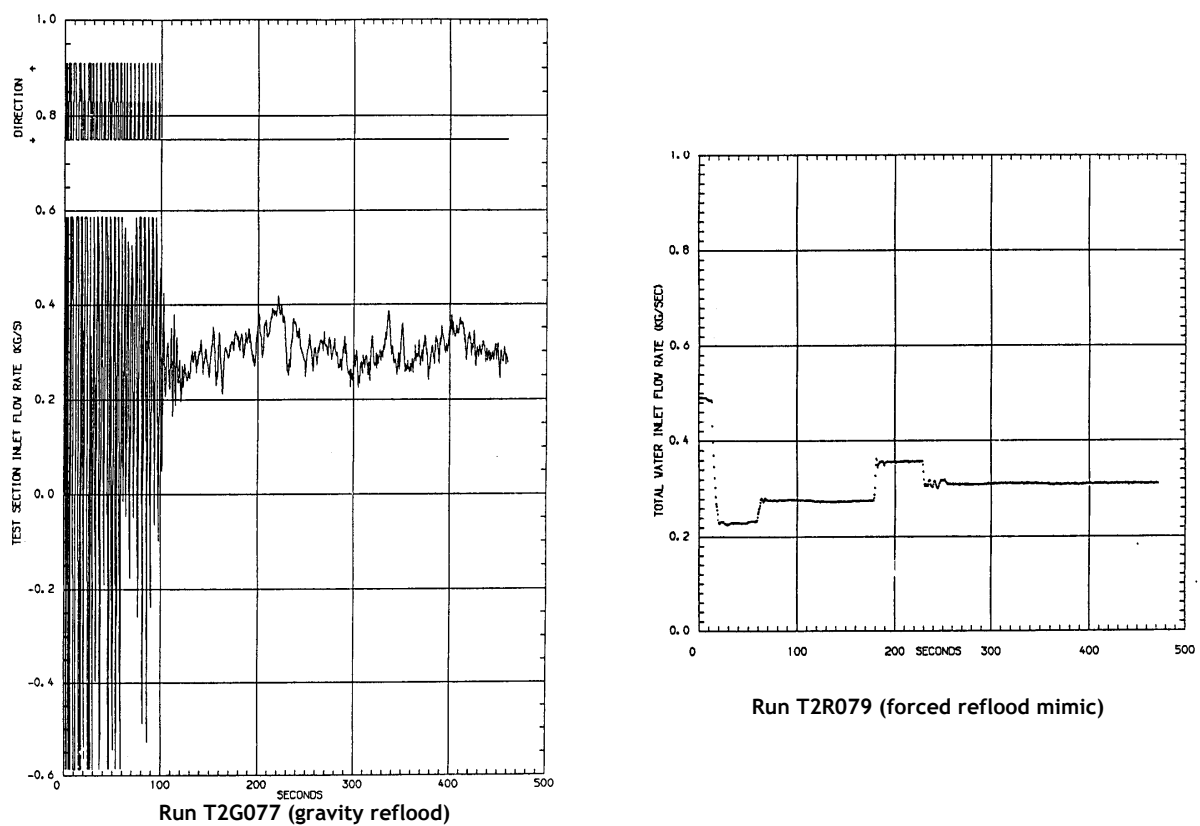


Figure 67: Test section inlet flow in gravity reflood test T2G077 and "mimic" forced reflood run T2R079.

Figure 68 compares variations in both the collapsed liquid level in the test section and the quench front on the non-deformed rods. These variations are very similar, apart from the non instant rewetting of the bottom 0.2 m in run T2R079 (in contrast to run T2G077) due to the impossibility of simulating the high flow rate of the first few seconds caused by the limitation of the injection pump. Variations in run T2R079 appear only slightly delayed by about 10 s.

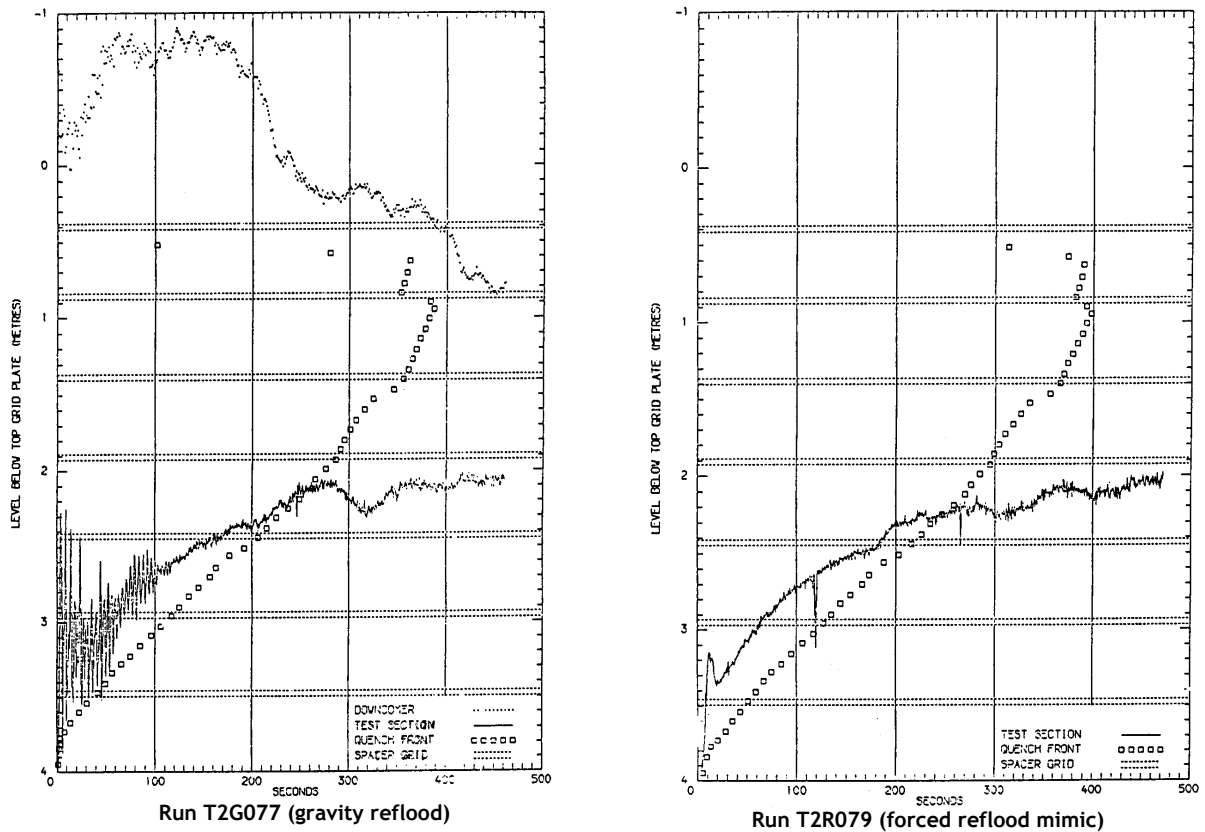


Figure 68: Test section and quench front levels in gravity reflood test T2G077 and "mimic" forced reflood run T2R079.

Last of all, Figure 69 compares the temperature variations at 5 levels on both a by-pass rod and blockage rod for the same two tests (T2G077 and T2R079). Once again, this comparison reveals very similar variations, with only marginal differences which can easily be attributed to the uncertainty concerning the forced flow rate in the mimic test.

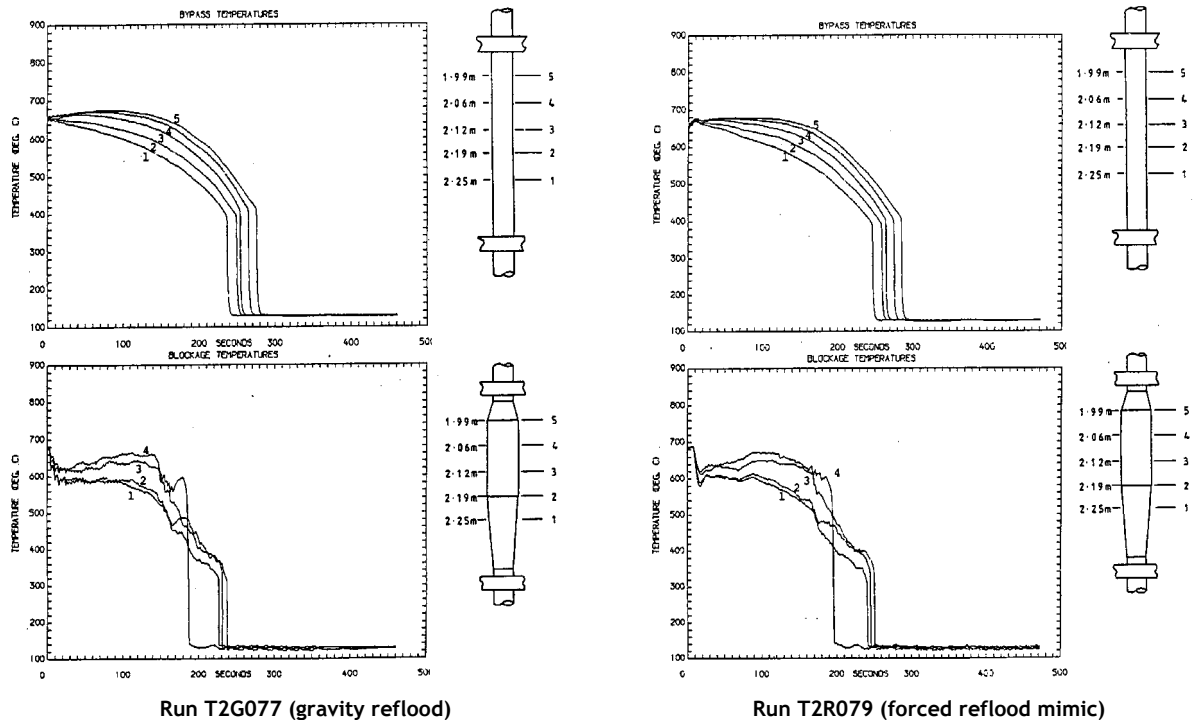


Figure 69: Axial distribution of by-pass and blockage temperatures in gravity reflood test T2G077 and "mimic" forced reflood run T2R079.

### 3.5.4 Conclusions

It therefore appears that the violent flow oscillations occurring in gravity reflood runs demonstrate no notable effect upon heat transfer processes governing temperature variations in both the blocked or unblocked part of the rod cluster during test assembly reflood. This result may seem surprising, but it should be associated with the fact that even with a forced constant reflood rate, cooling in the two-phase flow region located just above the quench front may be quite oscillatory.

Temperature variations in the by-pass and blocked rods during test assembly reflood seem to be mainly affected by the average flow rate at the test section inlet, which is concealed at the beginning of the transient by violent oscillations. Qualitatively, the trends are identical to those observed during forced reflood tests, particularly for the temperature distributions in the blockage, where competition between the superheating of the reduced steam flow and the cooling effect by liquid droplets entering the blockage remains the dominant process.

In conclusion, the coolability analysis of a blocked region under gravity reflood can be backed up by forced reflood tests, which represent a set conservative conditions in comparison to similar conditions applied during gravity reflood tests with the downcomer initially full.

### 3.6 Coolability of THETIS blockages

THETIS tests performed on an assembly containing a long severe blockage of 80% or 90% of the original unblocked area over a distance of 200 mm contributed to our understanding of the physical phenomena governing temperature variations in this blockage under LOCA reflood conditions. More particularly, 90% blockage test results can be compared with results of tests with the same blockage ratio conducted in other programs (FEBA, SEFLEX and CEGB).

As in other programs, THETIS tests were separate effects tests, where the effects of various parameters were studied separately and under constant conditions. Nevertheless, a certain number of tests were performed with variable decay power, simulating that from a group of the hottest fuel rods in a PWR reactor.

Straightforward qualitative analysis of the thermohydraulic processes occurring near and in the blockage explains temperature variations in the blockage in terms of the combination of heat transfers between the balloon surface and steam on the one hand, and between steam and liquid on the other hand. Such heat transfers are directly associated with the quantity of liquid penetrating the maximum blockage region and its transit time, which is dependant on the maximum blockage ratio, blockage length, reflood rate and quench front progression.

The series of forced reflood tests simulating a 90% blockage with a pressure of 2 bar and an inlet temperature of 90°C produced the following observations:

- With a 3 cm/s reflood rate, the blockage was found to be coolable, with the peak blockage temperature not exceeding the peak by-pass temperature by more than 60°C.
- With a 2 cm/s reflood rate, the maximum blockage temperature rose above the facility operating limit, which made it necessary to reduce power before the complete cooling of the blockage was achieved. It may therefore be believed that these test conditions do not permit suitable blockage cooling.
- The experiment in which the reflood rate was reduced from 3 to 2 cm/s showed adequate cooling. However, as this test was performed at the end of the program using an assembly with distortions that favour cooldown, the validity of these results cannot be guaranteed.

THETIS test results seem to imply that a long 90% blockage may no longer be coolable at a constant reflood rate below 2 to 3 cm/s.

When comparing results of tests performed with 90% and 80% blockages under similar conditions, it became apparent that an 80% blockage is more efficiently cooled at high reflood rates. However, differences tended to be minor, sometimes proving to be even better for the 90% blockage, with intermediate reflood rates that are most relevant to reactor safety analysis. These results therefore reveal that the blockage ratio of 90% - considered as an upper bound value of the blockage ratio possibly obtained under a LOCA with a fresh fuel assembly - does not necessarily represent the most penalizing case in terms of coolability for axially extended deformations such as those simulated in the THETIS experiments.

### **3.7 Interpretation of THETIS results**

The BERTHA (Blockage Experiments: Reflood Thermal Hdraulic Analysis) computer code was developed at AEE Winfrith to assist in interpretation of the results of the THETIS experiments (cf. [5] Appendix B).

The BERTHA code is based on the mechanistic modelling of the main thermohydraulic processes occurring downstream from the quench front. Taking into account the relatively short transit time of the coolant through this region, a quasi steady-state formulation is employed.

Heat transfers between the surface and coolant and between the liquid and steam are considered for three regions corresponding to flow rate conditions:

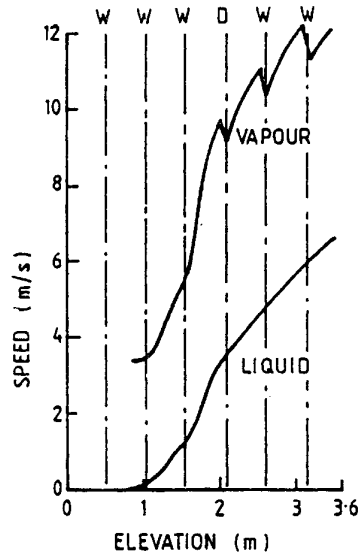
- 1) film boiling,
- 2) transition,
- 3) dispersed.

The effect of spacer grids upon heat transfer is taken into account through the increase in turbulent convective transfer to steam, as well as the absorption of radiation from the surface by the liquid film on the rewet spacer grids. Furthermore, concerning the rewet spacer grids, heat transfer between the liquid film and steam is taken into account using an effective heat transfer area that is significantly higher than the surface area of the grid (a factor of 4 is currently used to take into consideration the continuous perturbation of this interface owing to the impact of droplets).

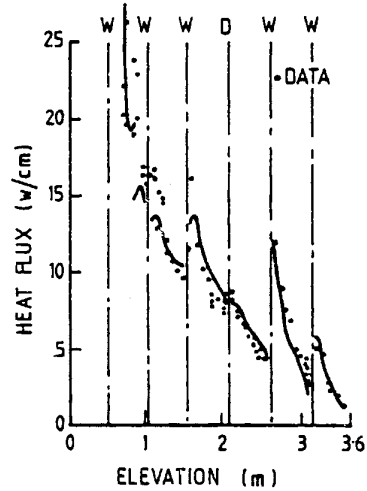
A description of the blockage is obtained by modelling two types of sub-channels; one for the blockage region and one for the by-pass region. The diversion of the vapour phase (cross-flow) appears upstream in the blocked sub-channel at the start of the clad swelling and ceases where the deformed cladding come into contact, isolating the blocked sub-channels from each other and from

the by-pass region. The cross-flow restarts further downstream where the transverse gaps open again. Steam cross-flow calculation is based on the balance in pressure upstream and downstream from the two groups of parallel sub-channels and takes into account the variation in the lateral passage width associated with the balloon geometry. The entrainment of liquid droplets in the steam cross-flow is explicitly calculated by integrating the transverse acceleration of these droplets while adjusting the entrainment coefficient to a more suitable value in order to correctly balance pressure drops between the sub-channels.

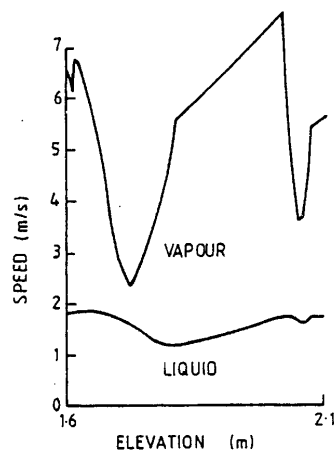
Figure 70 provides an example of calculation results obtained using the BERTHA code for an 80% blockage under reference conditions (2 cm/s reflood rate, pressure 2 bar, inlet temperature 90°C). The figures represent a point in transient for which the quench front position is rather low (0.73 m); the vertical lines give the position of the spacer grids, with the symbol W and D indicating whether they are wet or dry.



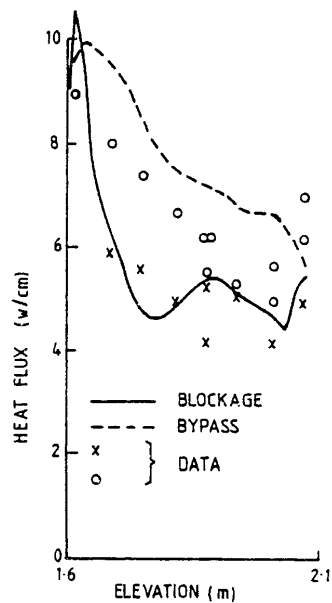
A. By-pass vapor and liquid speeds



B. By-pass heat flux  
(reflood rate = 2 cm/s ; p=2 bar)



C. Speeds in blockage



D. Heat fluxes in blockage and by-pass

Figure 70: Simulation of a THETIS 80% blockage test with the BERTHA model.

- Figure 70A shows the axial distribution of liquid and vapour speeds in the by-pass. A noticeable increase in the vapour speed alongside the blockage (between 1.6 and 2 m) was observed owing to the by-passing of the blockage, as well as sudden reductions in vapour speed at wet grids, owing to steam cooling.
- Figure 70B compares the measured and calculated heat fluxes in the by-pass, showing a fair agreement between experiment and calculations on an overall level. The abrupt increase in heat transfer when passing through wet spacer grids is also well reproduced by the model.
- Figure 70C shows the liquid and vapour speeds along the blockage. The vapour speed falls significantly in the upstream area up to the elevation where the lateral gaps between swellings close, before increasing again up to the entry to the maximum blocked section (80%). The vapour speed then increases more slowly in the parallel part of the blockage due to evaporation of the liquid before slowing down in the downstream widening section.
- Figure 70D compares the measured and calculated heat fluxes, over the blockage length, in the by-pass and blockage. Along the blockage, the heat flux undergoes a significant fall in the steam deceleration region, due to the rapid overheating of steam, before stabilising within the maximum blocked region.

It can be concluded that BERTHA heat flux calculations are in good agreement with measurements taken in the blockage and by-pass regions of the THETIS cluster. However, it must be underlined that this comparison has remained limited to a small number of the THETIS tests and has not been applied to other blockage experiments with different configurations.

## 4 ACHILLES program

Although very valuable, the THETIS experiments had some known limitations, notably the diameter of the rods (12.2 mm compared to 9.5 mm for most PWR rods) and the absence of mixing vane grids. Following the submission of the Sizewell B pre-construction report, the Nuclear Installations Inspectorate emitted reservations on the claims made about the limited extent of clad ballooning and its consequences. This finally led to the requirement for carrying complementary experiments, within the ACHILLES<sup>a</sup> program, which was performed in the late 80s at the Winfrith Atomic Energy Establishment (AEEW) under full funding by the CEGB. This program consisted of low flooding rate heat transfer experiments on an assembly comprising 69 full-length fuel rod simulators, in both unblocked and partially blocked configurations.

### 4.1 Experimental characteristics

A detailed description of the ACHILLES rig that was used for all series of experiments is provided in Reference [7]. The test section was housed in a shroud vessel that was connected to a tubular downcomer via a connecting line. Reflood water with a temperature up to 150°C could be injected into this line by a steady flow pump. Coolant leaving the top of the test section flowed into a steam separator where the liquid and vapour phases were separated.

The test section comprised a bundle of 69 fuel rod simulators in a square array, held by 8 prototypic spacer grids within a cylindrical shroud vessel of 128 mm in internal diameter. A partial blockage in a 4x4 rod group was simulated by fitting balloon sleeves to the rods in the positions shown in Figure 71.

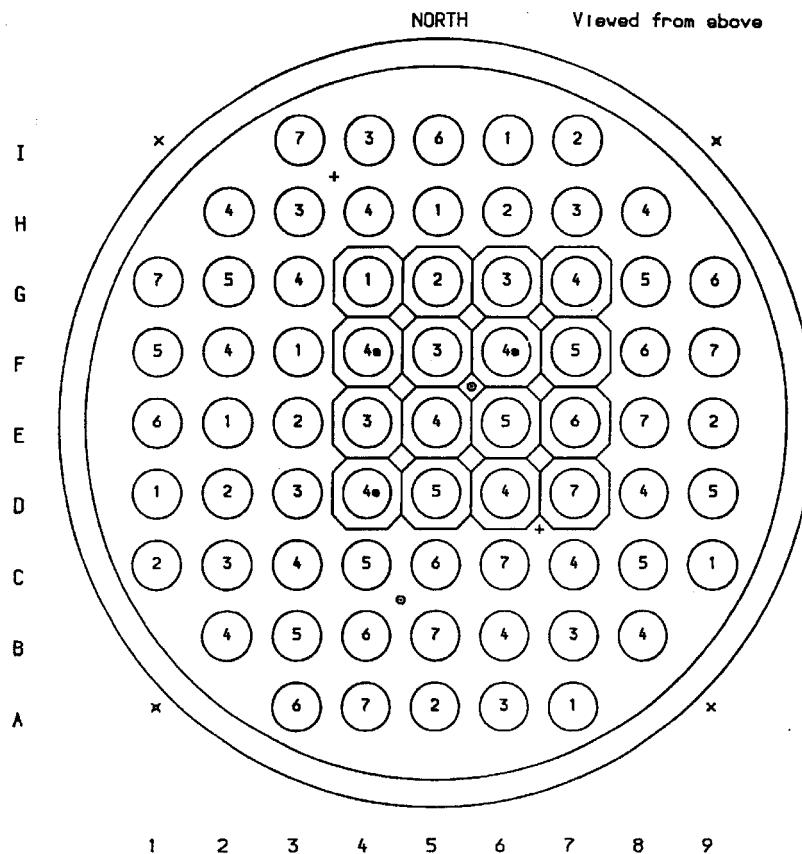


Figure 71: Cross-section of the ACHILLES test section.

<sup>a</sup> *Author's note:* In Greek mythology, ACHILLES was the son of the nymph THETIS. According to AEE/ Winfrith, THETIS is credited to have performed the earliest "quench experiment" on ACHILLES in the waters of Styx. It may be said that the post-quench behavior of the sample revealed a weakness in the non-rewet part during quenching. As everyone well knows this weakness led to the ruin of the test device.

The fuel rod simulators were solid-type electric simulators composed of a central heater coil encased in boron nitride insulation and enclosed in a 0.7 mm thick Inconel sheath. The rod outside diameter (9.5 mm), pitch (12.6 mm) and heated length (3.66 m) were typical of PWR dimensions.

The blockages were created using hollow pre-shaped Inconel sleeves that were fitted onto the rods between grids 4 and 5 to simulate deformed cladding. These sleeves were similar to THETIS sleeves, with a maximum blocked region extending over 100 mm, and entry and exit tapers, 200 mm and 50 mm respectively, connecting the regular section of the rod with the sleeve square section (cf. Figure 72).

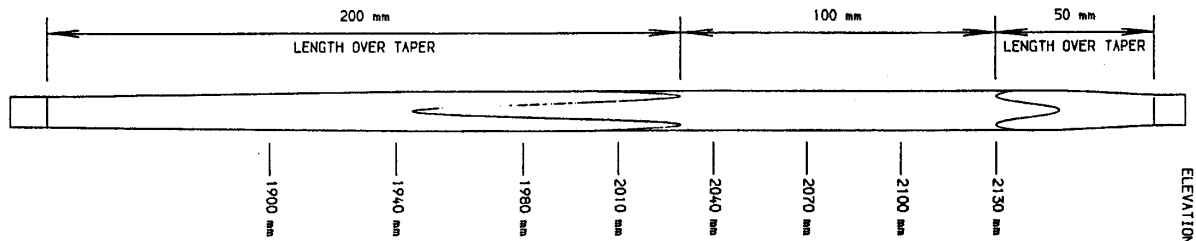


Figure 72: Shape of the cladding sleeve for the ACHILLES 80% blockage

Only a blockage ratio of 80% was used in the ACHILLES ballooned cluster experiments. As the blockage only covered a group of 4x4 rods in the 69 rod array, an ample region was available for flow by-pass in the unblocked sub-channels.

The axial power profile along the rods was approximated to a truncated cosine in 11 steps with a long flat region around mid-height. The specific peak form factor for the whole cluster was 1.4. The shroud vessel was equipped with external heater cables tightly wrapped around the vessel and providing a 46 kW heating over 5 axial zones whose power could be independently controlled.

Each rod contained 6 internal thermocouples (a total of 414 within the cluster), these being arranged in one of 8 groupings which concentrated the measurements in the 8 axial zones corresponding to the successive grid spans. A thermocouple in each group was at a common level of 2.13 m corresponding to the throat outlet of the blockage sleeve.

At the mid-elevation, four pairs of quartz windows were fitted to the shroud wall to enable the droplets in the field of view to be filmed during the course of an experiment.

#### 4.2 Experimental program

Only the blocked cluster experiments will be discussed hereafter, sometimes with reference to the comparable results of the unblocked cluster test series. Test results are reported in [8].

The reflood experiments were performed after an initial series of five single phase cooling experiments.

In all of the reflood experiments, the bundle power transient was based upon the American Standard usually referred to as ANS (1979) plus allowance of  $2\sigma$  for the uncertainty and actinides contribution to the decay power. The reference power level was the decay heat generated in the peak rated rod, assuming that reflood starts 40 s after reactor shutdown.

A base case experiment was chosen to serve as a comparator for the other experiments, with the nominal conditions as follows:

Pressure:	2 bar
Reflood rate:	2 cm/s (constant)
Inlet subcooling:	20°C
Initial cluster temperature:	650°C
Initial shroud temperature:	600°C
Power:	70% ANS(79)+ $2\sigma$

This base case run was repeated three times during the program in order to check the repeatability of the tests with respect to the expected distortion of the blockage (as experienced in the THETIS program) and provide updated reference runs taking account of the effects of such distortion.

The following parameters were varied around base case values, the effects of which are discussed in Section 4.3.2.

Pressure:	1.5 and 4 bar
Reflow rate:	1 cm/s and decreasing rate
Reflow flow oscillation	
Inlet subcooling:	50° C
Power:	42 to 90% ANS (79)+ 2σ
Unpowered rods:	4

The blocked bundle reflow test matrix is given in Table 4.

### 4.3 Main results

#### 4.3.1 Results of the base case test (Run A2R038)

This test was used to validate the Westinghouse licensing computer code BART.

The boundary conditions for this test were the same as for the unblocked bundle base case test (Run A1R030) so that the results of these two experiments may be directly compared.

Figure 73, which illustrates the axial variation of rewetting times on the blocked rods in A2R038, shows that the top of the blockage rewet from the top downwards in the same time as the bottom half rewet from the bottom upwards. The two rewetting fronts moved simultaneously and at the same speed, and thus met at mid-elevation of the blockage (located between grid 4 and 5).

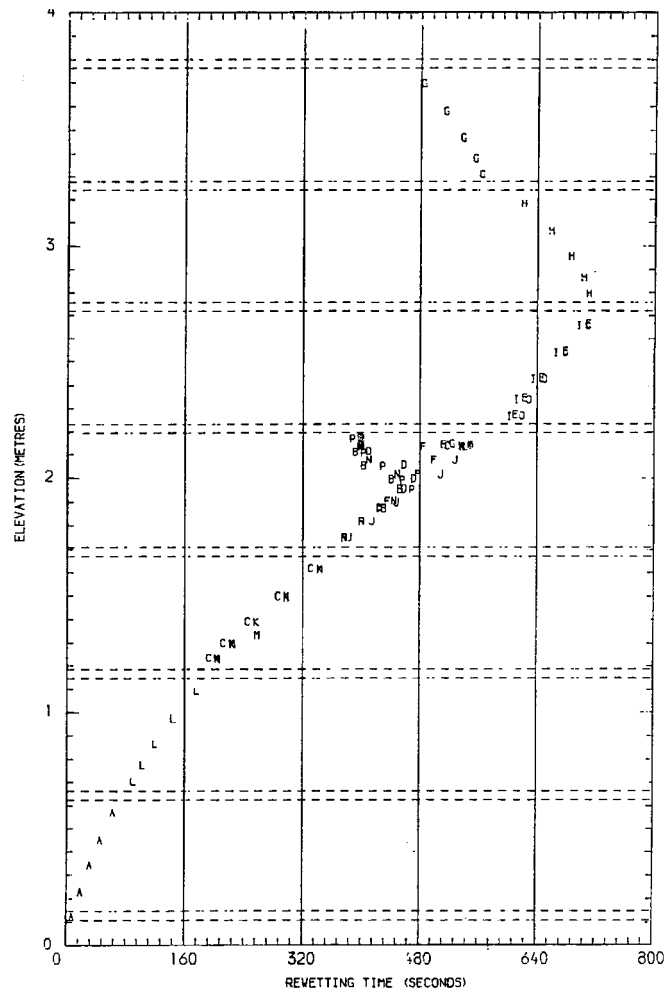


Figure 73: Run A2R038 - Axial variation of the rewetting time in the blocked region.

Run Number	Description	Nominal Test conditions					Max Balloon Temperature			Max By-pass Temperature		
		Rig Pressure (bar)	Reflood Rate (cm/s)	Subcooling (°C)	Initial Temp. (°C)	% power (ANS+2 $\sigma$ )	Temp. (°C)	Time @Tmax (s)	Time Quench (s)	Temp. (°C)	Time @Tmax (s)	Time Quench (s)
A2R036	Initial low power	2	2.0	21	643	52	900	235	323	861	162	462
A2R037	Initial surge 4 Unpowered rods Low shroud temp.	2	Var.	23	652	70	769	198	308	827	170	659
A2R038	Base case	2	2.0	21	638	70	1030	278	425	959	179	555
A2R039	4 Unpowered rods Low shroud temp.	2	Var.	21	666	70	853	181	421	870	182	727
A2R040	Low pressure	1.5	2.0	20	640	70	1033	340	679	993	220	749
A2R041	High pressure	4	2.0	22	641	70	955	191	269	940	171	356
A2R042	High subcooling	2	2.0	50	643	70	974	222	387	965	175	481
A2R043	Low flow Low power	2	1.0	20	640	42	1007	317	529	988	310	664
A2R044	Base case repeat 1	2	2.0	19	643	70	957	186	378	968	172	567
A2R045	Oscillating flow	2	2.0	18	641	70	992	300	629	976	265	751
A2R046	Initial surge 4 Unpowered rods Low shroud temp. High power	2	Var.	18	646	90	866	295	620	933	402	988
A2R047	Base case repeat 2	2	2.0	20	641	70	937	186	437	946	150	543
A2R048	Initial surge 4 Unpowered rods Low shroud temp. High initial rod temp.	2	Var.	20	772	70	822	100	392	878	107	506
A2R049	Initial surge 4 Unpowered rods Low shroud temp. High initial rod temp. High power	2	Var.	20	743	90	888	129	620	960	153	693
A2R050	4 Unpowered rods	2	2.0	19	665	70	883	119	366	916	140	464
A2R051	Base case repeat 3	2	2.0	19	643	70	914	146	443	954	158	533

Table 4: Summary of ACHILLES ballooned cluster reflood experiments

Figure 74 compares the temperature histories at the instrumented levels on rod E5 along the central sub-channel blockage for run A2R038 with those of the same rod for the unblocked run A1R030.

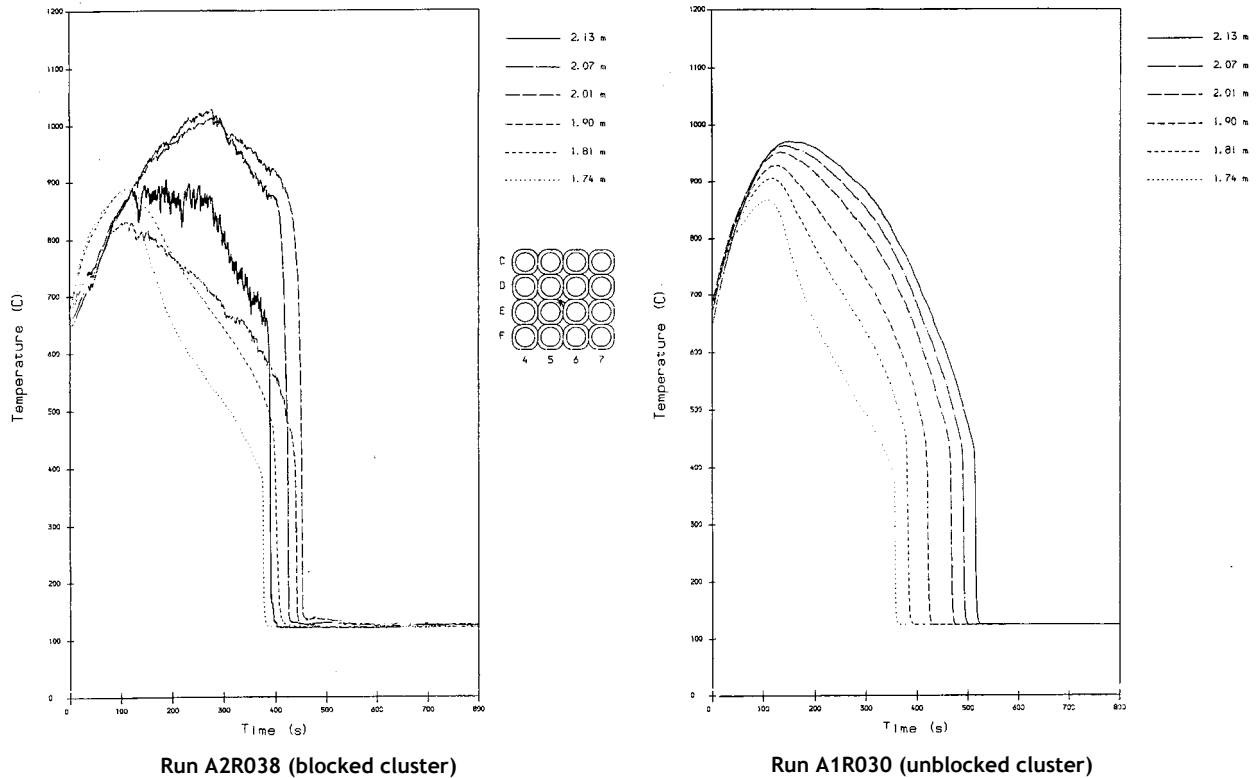


Figure 74: Axial distribution of temperature transient along the central sub-channel in run A2R038 (blocked) and A1R030 (unblocked).

Below the blockage in A2R038 (at levels 1.74 and 1.81 m), the temperature variations are very similar in both runs.

The balloon temperature behavior in the blockage region shows marked differences with that of the unblocked cluster. At 1.90 m, the temperature rises until about 110 s and falls steadily until rewetting occurs in sequence with the two levels below the balloon. At 2.13 m, the temperature rise is terminated abruptly at about 120 s after which the trace becomes very noisy, indicating a heterogeneous cooling medium in the region. Because of the improved cooling, the maximum temperature does not occur at this blockage outlet elevation as it does in the unblocked cluster case. At the two elevations below (2.01 and 2.07 m), the temperatures behave similarly, rising until 280 s then falling until rewetting, which occurs progressively from the top, in sequence with the 2.13 elevation but from a significantly higher temperature level. The reason for this is that falling films in upwards flow do not greatly influence the heat transfer in the region below them, in contrast with the rising quench fronts where the advancing front significantly increases the heat transfer ahead of it so that rewetting appears to occur from about the expected temperature. The peak temperature measured on the rod balloons in run A2R038 was 1030 °C at 2.01 m in the central sub-channel. In comparison with the peak temperature of 971 °C at 2.13 m in run A1R030 for the unblocked cluster, the temperature penalty due to the blockage is 59 °C.

Figure 75 compares the heat flux variations at 2.07 m (near mid-elevation of the blockage throat) in the central blocked sub-channel with that in the corresponding sub-channel in the unblocked cluster. After about 50 s the heat flux in the blockage remains below that in the unblocked cluster until about 290 s. Thereafter, the heat fluxes are comparable until rewetting, which occurs earlier in the blocked cluster. The fact that the balloon temperature at 2.07 was lower than the clad temperature at the same level in the unblocked cluster for the first 200 s of the transient (see Figure 74) is consistent with the lower heat flux in the blockage: because of a higher thermal decoupling from the heater, the balloon is easier to cool than the unballooned cladding for some time.

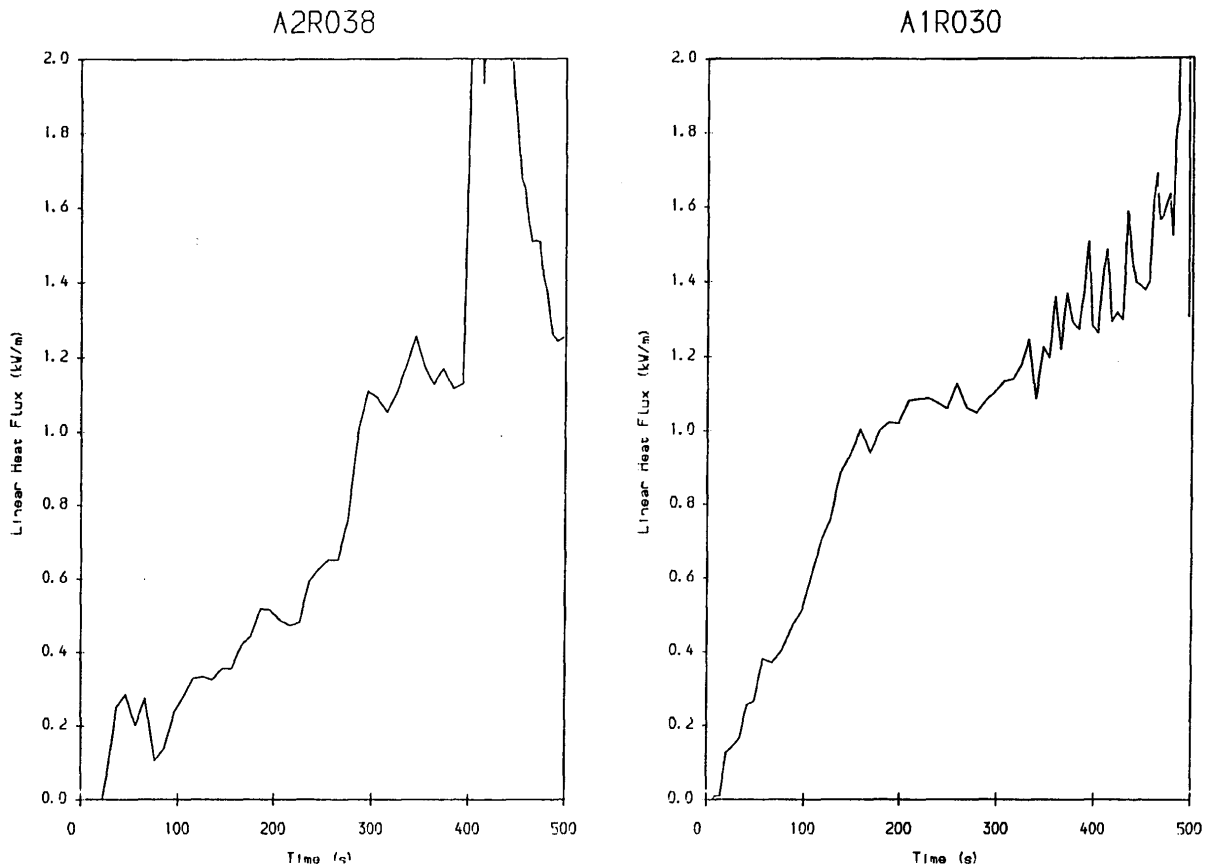


Figure 75: Linear heat flux in blockage at 2.07 m compared to unblocked cluster.

#### 4.3.2 Results of variations about the base case at constant reflood rate

##### 4.3.2.1 Repeatability

Because of the blockage distortion that was expected to occur in this test program as it did during the THETIS experiments discussed in the previous chapter, the base case run was repeated three times at different time intervals (see Table 4) and the effects of changing various system parameters should be compared with the most recent base case run.

In the by-pass region, repeatability was correct with the peak temperature of the four runs within a 22°C interval. In contrast, repeatability of the balloon temperatures was not good with the peak balloon temperature in the central sub-channel continuously decreasing in the successive repeat runs and moving down the blockage to 882°C at 2.01 m in the final run A2R051 (compared with 1030°C at 2.07 m in A2R038) while the location of the maximum temperature moved towards the periphery of the blockage. This behavior was attributed to the earlier accumulation of water just downstream from the blockage in relation to the distortion of the blockage, which improved the cooling of the blockage and resulted in its earlier rewetting by the falling film.

#### 4.3.2.2 Effect of pressure

The effect of pressure was observed in the results of two tests at 1.5 and 4.0 bar respectively, in comparison with the results of the base case run at 2 bar. Increasing the pressure resulted in a reduction in peak clad temperature, both in the by-pass and the blockage, as well as in the rewet time. Table 5 below summarises the results of these three runs.

Run	Pressure (bar)	Balloon			By-pass		
		Tmax (°C)	t(Tmax) (s)	t(quenched)* (s)	Tmax (°C)	t(Tmax) (s)	t(quenched)* (s)
A2R040	1.5	1033	340	679	993	220	749
A2R038	2	1030	278	425	959	179	555
A2R041	4	955	191	269	940	171	356

\* t(quenched) is the time at which the maximum temperature location rewets.

Table 5: Effect of pressure

#### 4.3.2.3 Effect of inlet subcooling

Run A2R042 was performed with an inlet subcooling of 50°C. In comparison with the base case run, increasing the subcooling from 20 to 50°C reduced the peak temperature by 77°C (from 1030 to 953°C) in the blockage central sub-channel, but had little effect on the peak temperature in the by-pass region.

#### 4.3.2.4 Effect of rod power

Run A2R036 was performed with a power of 52% of ANS (1979)+2σ. In comparison with the base case run, reducing the power from 70 to 52% reduced the peak temperature by 130°C in the blockage central sub-channel, and by 98°C in the by-pass region. Rewetting of the peak balloon temperature location occurred 102 s earlier with reduced power, again by a falling liquid film.

#### 4.3.2.5 Effect of unpowered rods

Run A2R050 was performed under base case conditions except that the four rods just outside the blockage (C3, C8, F3 and F8) were unpowered. This test was to be compared with the third repeat base case A2R051. In both these runs, the whole balloon and the region just below it were rewet by a falling film before the main quench front arrived from below, therefore indicating that both these runs had been affected by blockage distortion.

With four unpowered rods, the peak by-pass temperature was reduced by 38°C in comparison with the repeat base case. In the blockage, the behavior was similar in both runs with a maximum balloon temperature occurring at the edge of the blockage and with a reduction by 60°C of the peak balloon temperature in the central sub-channel for A2R050 in comparison with the repeat base case.

#### 4.3.2.6 Effect of imposed flow oscillations

Run A2R045 was performed under base case conditions except that the flow in the lower plenum was caused to oscillate with a period of 4 s, the reflood rate thus varying sinusoidally between +60 and -56 cm/s. This test was to be compared with the first repeat base case A2R044.

In the blockage, the peak balloon temperature in the central sub-channel was increased by 24°C in comparison to the repeat base case. However, the maximum balloon temperatures occurred in outer sub-channels in both runs, with an increase by 35°C for the oscillatory run. Rewetting of the blockage was delayed considerably, by 251 s at the maximum temperature location. It was suggested that the flow oscillations could have prevented the accumulation of liquid just above the blockage, which was thought to have caused earlier rewetting of the blockage in other runs; this may also explain why the maximum balloon temperature was much closer the top of the blockage in this run. However, rewetting of almost all the balloon height occurred from the top downwards.

### 4.3.3 Results of experiments with varying reflood rates

In order to provide more realistic simulations of reactor conditions than those selected in the base case and its variations, a limited series of five experiments was carried out in which the reflood rate was varied, starting from a high initial value and decreasing during the run. In four of these five experiments an additional initial surge of flow was activated by dumping water from the tubular downcomer; thereafter the flow was supplied from the steady flow pump using a programmed flow run down. Four rods just outside the blockage were unpowered as in run A2R050, and the initial shroud temperature was reduced to 400 °C.

#### 4.3.3.1 Reference case (A2R037)

The inlet flow rate variation with initial surge is shown in Figure 76.

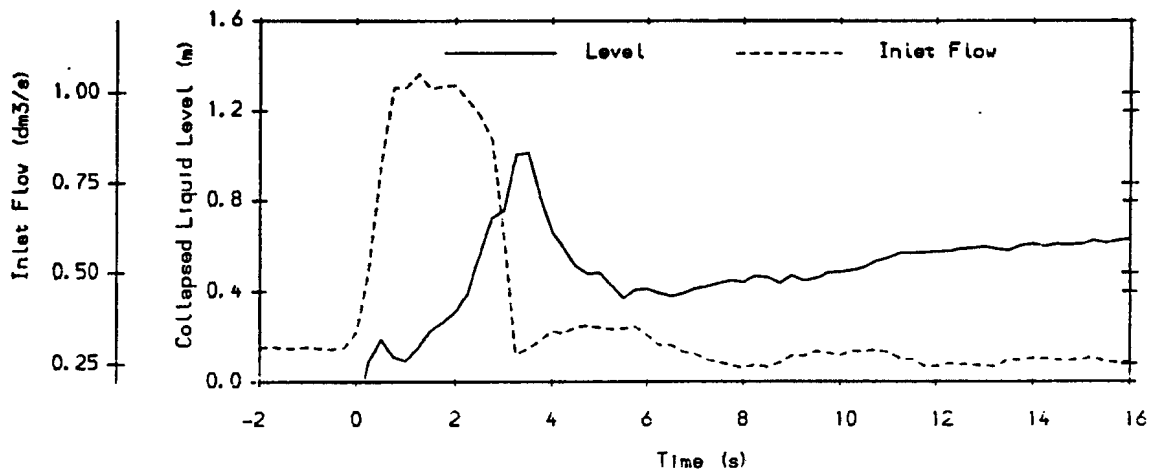


Figure 76: Inlet flow rate and collapsed liquid level in Run A2R037.

The combined effects of the high initial flow rate and the cooler structures reduced the peak balloon temperature from 1030 to 769 °C and the corresponding rewetting time from 425 to 308 s compared with the base case run A2R038 (see Table 4). The effects are greater in the central sub-channel of the blockage with a peak temperature not exceeding 711 °C, well below the peak by-pass temperature of 827 °C. Even when the reflood rate has fallen to a low value, the earlier gains are not offset. The large reduction in the balloon temperature again seems to have been caused by water accumulating just downstream from the blockage.

Run A2R039 was run with identical conditions to those of A2R037 excepting the absence of initial surge in the inlet flow rate. The cooling was still better than that in the base case, with a maximum balloon temperature of 853 °C, lower than the peak by-pass temperature of 870 °C.

#### 4.3.3.2 Effects of rod power and initial rod temperature

In run A2R046, the rod power was increased to 90% of ANS (1979)+2 $\sigma$  while maintaining the initial rod temperature at about 650 °C as in the reference run A2R037. In run A2R048, the rod power was maintained at 70% of ANS (1979)+2 $\sigma$  while increasing the initial rod temperature to 772 °C. In run A2R049, both parameters were increased to 90% of ANS (1979)+2 $\sigma$  and 743 °C respectively.

Table 6 below summarises the results of these three runs in comparison with the reference run A2R037.

Run	Rod		Balloon			By-pass		
	% power (ANS+2 $\sigma$ )	Initial temp. (°C)	Tmax (°C)	t(Tmax) (s)	t(quenches)* (s)	Tmax (°C)	t(Tmax) (s)	t(quenches)* (s)
A2R037	70	652	769	198	308	827	170	659
A2R046	90	646	866	295	620	933	402	988
A2R048	70	772	822	100	392	878	107	506
A2R049	90	743	888	129	620	960	153	693

\* t(quenches) is the time at which the maximum temperature location rewets.

Table 6: Effects of rod power and initial temperature

For run A2R046, the maximum temperatures in the blockage and the by-pass were higher than the corresponding values for run A2R037 with lower power. However, the peak balloon temperature in the central sub-channel was 685°C, lower than the value for run A2R037 (711°C), which indicates that the result must have been seriously affected by blockage distortion.

For run A2R049, the increase of about 100°C in the initial temperature with respect to run A2R046 increased the peak balloon temperature by only 22°C and did not affect the corresponding rewetting time. Therefore, much fewer effects were observed than those observed at 70% power between runs A2R037 and A2R048.

General trends observed in runs A2R046, A2R048 and A2R049 appear as expected, but the magnitude of the effects has most likely been influenced by blockage distortion, which occurred progressively during the performance of the test series.

#### **4.4 Discussion**

The cooling behavior observed in the ACHILLES blocked cluster experiments appears very consistent with the main observations obtained on the THETIS blocked cluster experiments discussed in the previous chapter.

During the early phases of the reflood transient, the liquid droplets that had been accelerated below the blockage penetrated the reduced section region due to their inertia. The local increase in the liquid fraction enhanced the cooling within the sub-channel, leading to balloon temperatures that were lower than by-pass temperatures. Later, as the quench front approached the blockage, the entrained liquid droplets just below the blockage were slower and so more easily diverted towards the by-pass. This reduced the liquid fraction within the blockage, leading to higher vapour temperatures and causing a late peak in the balloon temperatures. The axial position of the peak generally occurred near the top of the throat.

A particularly important mechanism in ACHILLES blocked cluster experiments was the mutual benefit resulting from the rewetting of the blockage and spacer grid just downstream from it (grid 5). From the beginning of the transient, water accumulated between the top of the blockage and the underside of grid 5, stopping the rise in temperature at the top of the blockage. Following the rewetting of the grid, liquid fell from its underside into the top of the blockage, enhancing its cooling and leading to its quench.

#### **4.5 Conclusions**

A program of low flooding rate heat transfer experiments was performed in the ACHILLES facility on an assembly comprising 69 full length rod electric simulators of PWR dimensions. Two principal series of tests were carried out; firstly on a normal assembly, and secondly on an assembly bearing a partial blockage at about mid-elevation on a 4x4 group of rods. The blockage was simulated by fitting thin sleeves onto the heater rods, with the flow area in the restricted region being reduced by 80% of the nominal flow passage.

For the base case transient, the effects of changing main system parameters one by one led to the following observations:

- Increasing the rod power from 52 to 90% of ANS+2<sup>2</sup> increased the peak clad temperature in the blocked region by 130°C.
- Increasing the pressure from 1.5 to 4 bar decreased it by 78°C.
- Increasing the inlet subcooling from 20 to 50°C decreased the temperature by 56°C.
- Superimposing very large flow oscillations on the steady reflood flow increased the peak balloon temperature by 35°C.

In some cases however, the magnitude of these effects was affected by the distortion of the blockage that developed during the experimental program.

The blockage penalty, defined as the difference between the peak temperature achieved anywhere in the blocked cluster and the peak temperature achieved in a comparable experiment on the unblocked cluster, is summarised in the following table for the various parameter changes that were investigated.

Experiment	Unblocked cluster test		Blocked cluster test		Blockage penalty (°C)
	Run number	Peak Temp. (°C)	Run number	Peak Temp. (°C)	
Base case	A1R030	971	A2R038	1030	59
Lower power	A1R032	879	A2R036	900	21
Low pressure	A1R044	987	A2R040	1033	46
High pressure	A1R045	947	A2R041	955	8
Subcooling	A1R047	984	A2R042	974	-10
Low flow & power	A1R037	960	A2R043	1007	47
Flow oscillation	A1R050	966	A2R045	992	26

**Table 7: Comparison of unblocked cluster and blocked cluster peak temperatures**

In the experiments with a more realistic decreasing flow rate, cooling was much better than in the experiments with a constant flow rate and the blockage rewet earlier. This was explained by the fact that the amount of water that accumulated above the blockage during the initial surge was greater than in the constant flow rate experiments. Furthermore, as this levitated liquid mass could not be supported after the surge end, it fell into the top of blockage causing it to rewet. No blockage penalty was observed for the combinations of rod power/ rod initial temperature that were selected for these experiments.

It was finally concluded that an 80% blockage remains coolable in the most penalizing conditions selected for the Westinghouse 'Evaluation Model' reflooding transient.

However, it should be pointed out that the length of maximum flow restriction was reduced by a factor of 2 in comparison to the THETIS experiments. Also, only one flow blockage ratio of 80% was used in the ACHILLES experiments, which prevents any comparisons with test results from experiments with higher flow blockage (FEBA, SEFLEX, CEGB). According to the trends indicated by the sensitivity study on flow blockage ratio and blockage length using the analytical model developed at the CEGB (see section 5.4.3), it may be considered that the conditions of the ACHILLES ballooned cluster experiments are just at the lower bounds of blockage lengths and flow blockage ratios that may threaten blockage coolability.

## 5 CEGB program

A very similar experimental program to that of the THETIS program was carried out by the Central Electricity Generating Board (CEGB) in the Berkeley Nuclear Laboratories (Great Britain).

The tests were carried out on a 44 rod bundle containing either a 61% or 90% blockage in a central 4x4 group of rods. The blockage was simulated using different sleeve configurations superimposed on the electrically heated rods. For 90% blockage tests, one short blockage of 51 mm and two long blockages of 196 mm were investigated (cf. Figure 77).

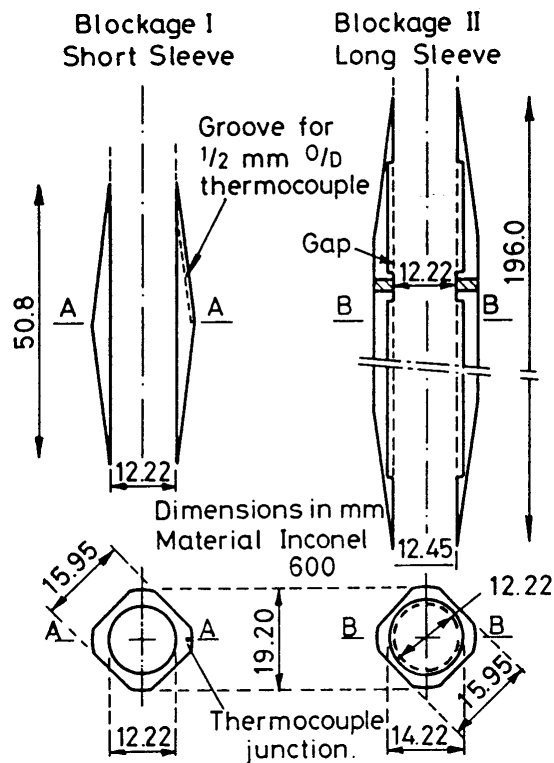


Figure 77: Shape of the cladding sleeves for the CEGB 90% blockage tests.

Only the main results concerning the 90% long blockage tests - identified as Blockage 2 and Blockage 3 for both configurations in the following figures - will be discussed here. Test results are reviewed in detail in [9].

### 5.1 Experimental characteristics

The test bundle contained 44 rods that were electrically heated over a length of 1 m and held together by a mid-plane spacer grid and two end grids. The bundle was enclosed in a cylindrical transparent silica shroud. The blockages were formed by metal sleeves attached to the central 4x4 group of rods.

The heater rods were of solid--type, composed of a Kanthal heating element embedded in boron nitride insulation and enclosed in a 0.9 mm thick Inconel cladding with an outside diameter of 12.2 mm.

The Blockage 2 Inconel sleeves were machined into size according to the dimensions provided in Figure 77 with thickness varying from 0.86 to 2.5 mm; they were attached to the rods by a single grub screw. Blockage 3 sleeves had the same external shape as Blockage 2 but were formed in the same manner as the SEFLEX balloons, using 0.9 mm thick Inconel tubes pressurised to fit the inside shape of a die and thereby reproducing the desired sleeve external shape; the average resulting thickness was 0.3 mm, which was representative of a ballooned PWR cladding thickness. The axial location of the sleeves for both types ranged between 540 and 736 mm from the bottom of the heated length.

Three sleeves were equipped with a total of 7 thermocouples for Blockage 2, whereas five sleeves were equipped with a total of 15 T thermocouples for Blockage 3.

As in the THETIS program, different series of tests of increasing complexity were performed:

- 1) isothermal air flow tests,
- 2) steady-state heat transfer tests in a steam environment,
- 3) steam and droplet tests,
- 4) forced reflood tests.

All tests were carried out under atmospheric pressure.

Isothermal air flow tests were conducted at room temperature and were designed to evaluate the velocity axial profile at the centre of the blockage sub-channels using a Pitot tube. The comparison of the axial profiles in the blockage with the corresponding data obtained in the blockage-free geometry helped infer the mass flow axial distribution in the blockage and by-pass. Figure 78 provides the axial distribution of the relative mass flow rate in the blockage and by-pass for Blockage 3; the reduction in the blockage flow rate to approximately 15% of the flow rate upstream from the blockage is comparable with results of air flow tests performed with the THETIS geometry (cf. Figure 57).

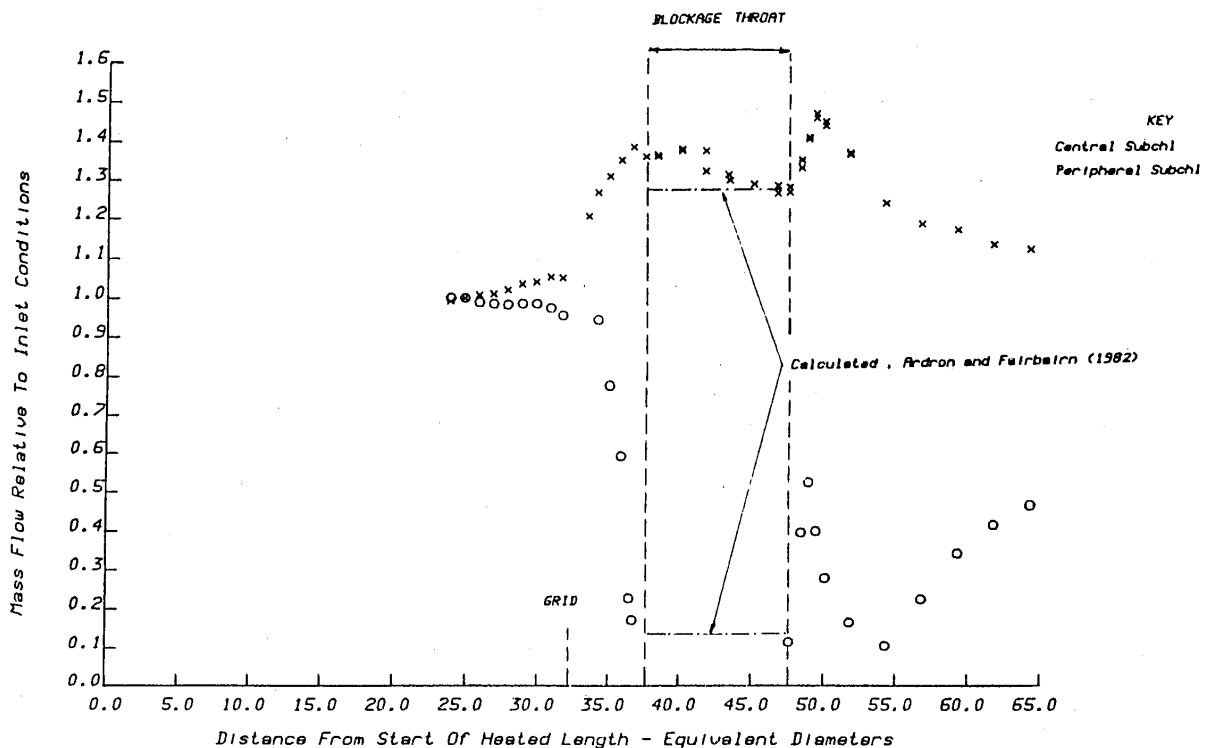


Figure 78: CEGB tests - Axial flow distribution in blockage and by-pass.

Steam heat transfer tests were mainly designed to determine flow and heat transfer regimes near and in the blockages, as well as determining the corresponding heat transfer coefficients.

The steam and droplet tests were designed to provide both flow visualisation and heat transfer data for dispersed two-phase flows with well defined inlet conditions. These inlet conditions were obtained by directly injecting liquid droplets into the centres of the sub-channels, after having established a steady-state steam flow with a temperature of 400°C or 800°C. High speed movies were taken with water injected into the central sub-channel only and were used to measure drop velocities and sizes.

## 5.2 Reflood tests

Reflood tests were performed on blockage-free or ballooned bundles whose initial temperatures were stabilised between 600°C and 800°C . The reflood water was injected at a constant flow rate and temperature of approximately 100°C into the lower plenum and passed over a calming length before entering the test section.

Tests on Blockage 1, which will not be discussed here, revealed a more efficient cooling and an earlier rewetting in the blockage than in the by-pass at the elevation of maximum blockage.

Tables 8A and 8B provide the matrices of reflood tests performed on Blockage 2 and 3 respectively. Two types of tests were performed, differing by the power fed into the rods during the test: steady power was maintained at its initial permanent state in the first case ("steady"); in the second case, the power in each fuel rod was increased by 1 kW just prior to reflood ("+1 kW").

Test run	Initial temperature (°C) (at control elevation)	Cold reflood rate (mm/s)	Power
Q6RA10	600	20.1	Steady
Q7RA10	700	19.9	Steady
Q8AU10	800	19.3	Steady
QC7S10	700	17.7	Steady
Q6KA09	600	20.2	Plus 1kW *
QF1A10	600	10.5	Plus 1kW *
QF2S14	600	24.7	Plus 1kW *
QF3S14	600	36.4	Plus 1kW *
QF4S15	600	51.2	Plus 1kW *

Table 8A: Blockage 2 reflood test matrix.

Test run	Initial temperature (°C) (at control elevation)	Cold reflood rate (mm/s)	Power
Q6JN23	600	20.6	Steady
Q7JN23	700	20.2	Steady
Q8JN23	800	20.3	Steady
QF1J24	600	11.0	Steady
QF2J27	600	25.3	Steady
QF3J27	600	35.8	Steady
QF4J27	600	38.4	Steady
Q6KJ24	600	20.2	Plus 1kW *
Q71KJ6	700	19.4	Plus 1kW *
Q81KJ7	800	19.2	Plus 1kW *

Table 8B: Blockage 3 reflood test matrix.

\* Pins steady at initial temperature, then 1 kW added to all pins just prior to reflood  
Nominal water temperature of 100°C, excepting run QC7S10 that used water at 20°C.

Rewetting times for Blockage 2 and 3 were compared with those obtained under identical conditions and at the same level for a non-deformed bundle.

The axial location of the blockage for both geometries was located between levels 36 and 49 in units of equivalent diameter.

### 5.2.1 Tests performed on Blockage 2

As all temperature variations were generally very similar, only one representative test will be discussed (Run Q8AU10: initial clad temperature = 800°C; reflood rate = 2 cm/s; inlet water temperature = 100°C; pressure = 1 bar).

Figure 79 illustrates temperature variations recorded upstream and downstream from the blockage for two rods located in the by-pass and blockage region respectively. Rewetting of the blockage rod occurs with a slight delay upstream from the blockage in comparison to the by-pass rod, while it occurs slightly earlier downstream from the blockage. The progression of a descending quench front from the top of the central rod is also observed.

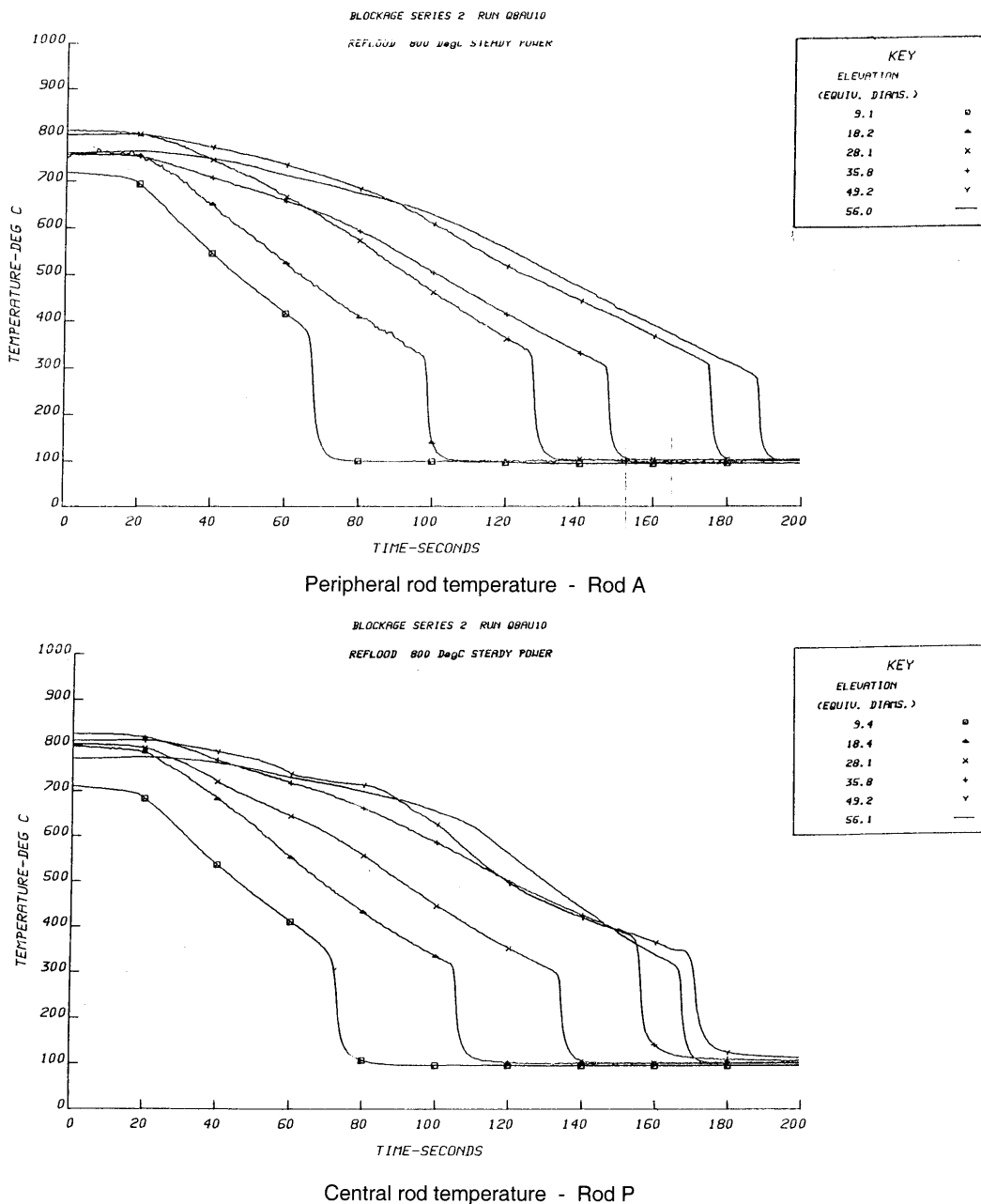


Figure 79: CEGB Blockage 2 - Peripheral and central rod temperatures.

Figure 80 compares temperature variations at the same level on 1) a blockage sleeve, 2) the rod surface under the sleeve and 3) a by-pass rod. Cooldown is significantly slower on the blockage sleeve in comparison to the by-pass rod up until rewetting, which takes place almost 60 s later than for the by-pass rod; the rod under the sleeve does not quench as it is decoupled from the wetted surface by the gas gap.

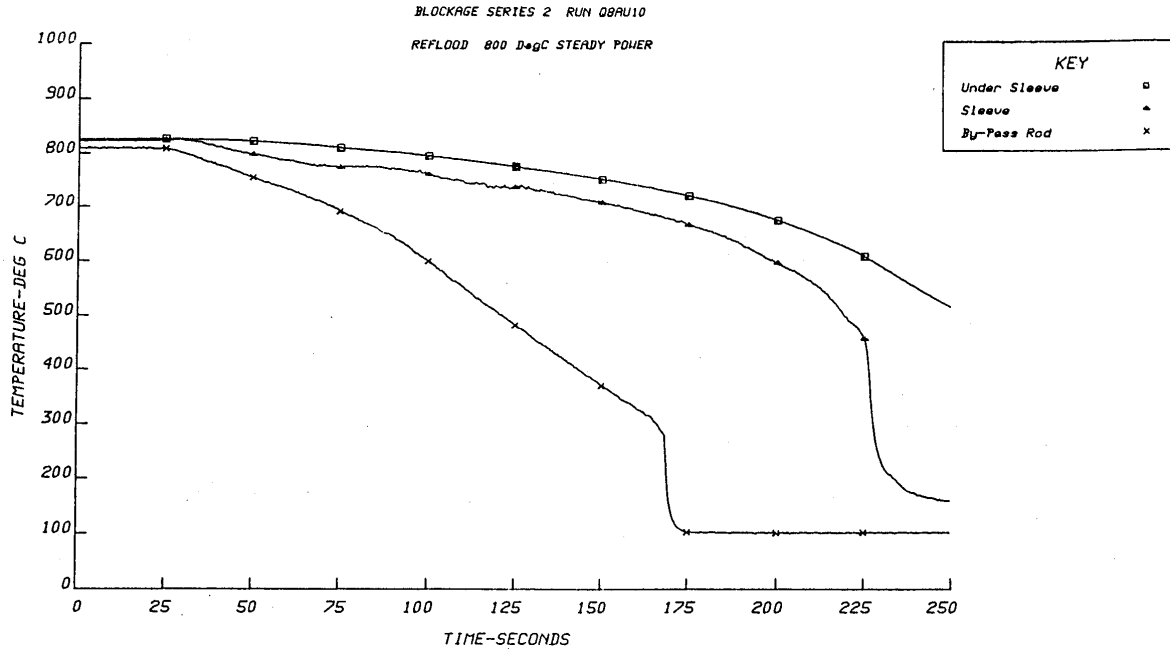


Figure 80: CEGB Blockage 2 - Blockage sleeve and by-pass rod temperatures.

Figure 81 provides rewetting times for all thermocouples in the bundle in relation to their axial elevation. The rewetting times for peripheral rods (by-pass) are in close agreement with those observed for the non-deformed bundle. Above the blockage, the central rods undergo early rewetting, due to the accumulation of liquid water in this region and the presence of a descending quench front. However, rewetting of the blockage sleeves is significantly delayed in comparison to the by-pass, from about 25% for outer sleeves to about 40% for inner sleeves.

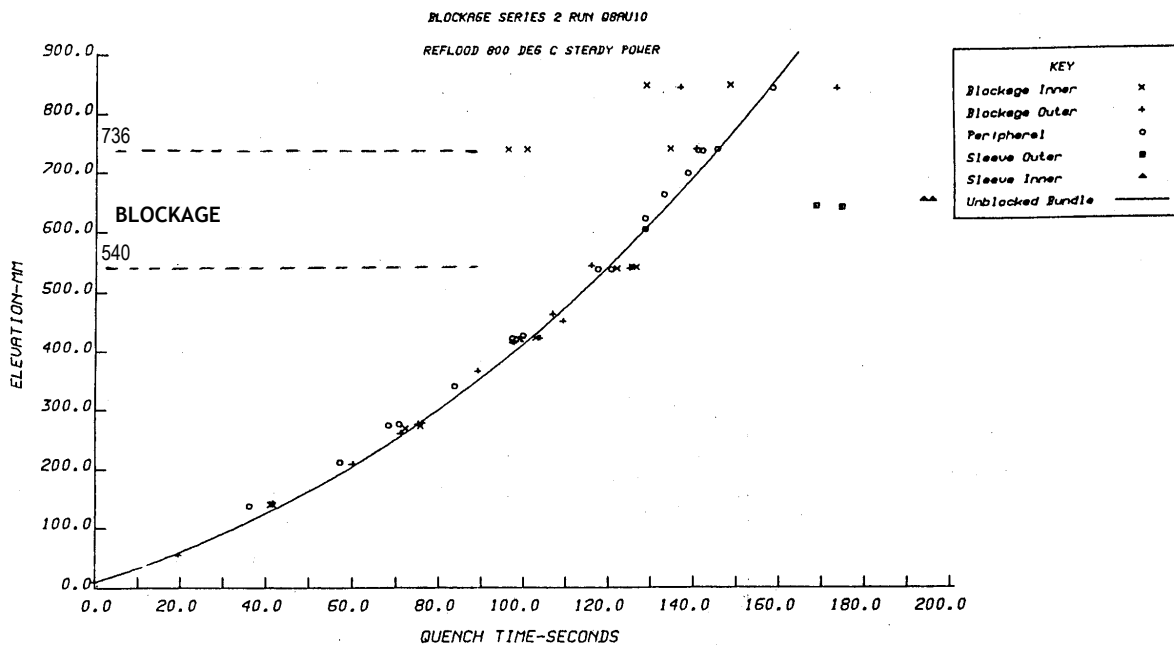
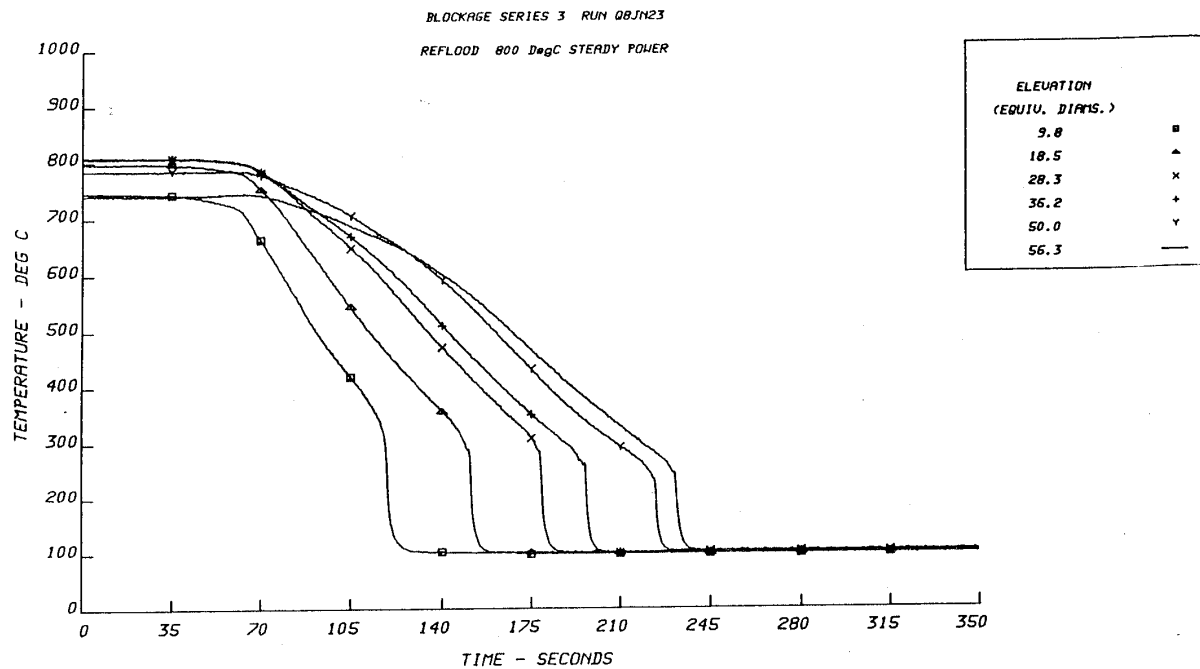


Figure 81: CEGB Blockage 2 - Bundle quench times versus elevation.

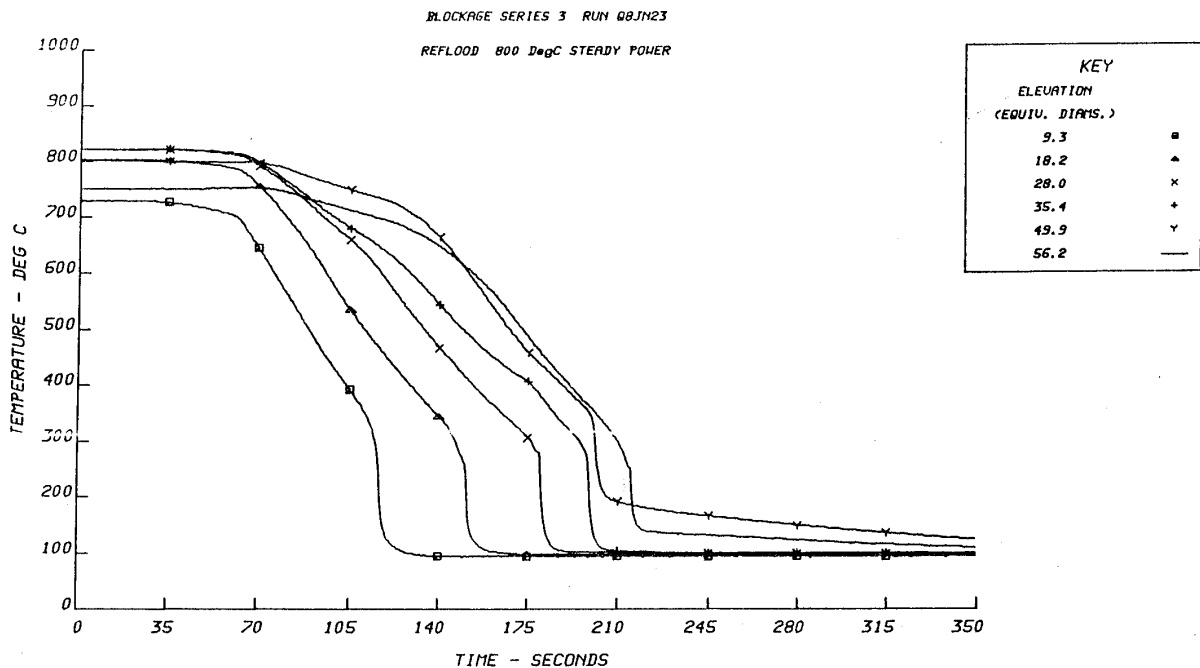
## 5.2.2 Tests performed on Blockage 3

### 5.2.2.1 Steady power tests

For a test with an initial temperature of 800°C, Figure 82 provides temperature variations upstream and downstream from the blockage for two rods located respectively in the by-pass region and the blockage region. An ascending rewetting is observed in both fuel rods, which takes place a little earlier downstream from the blockage for the blockage rod than for the by-pass rod.



Peripheral rod temperature - Rod I3



Central rod temperature - Rod I1

Figure 82: CEGB Blockage 3 - Peripheral and central rod temperatures.

Figure 83 compares temperature variations at the same level for 1) a blockage sleeve, 2) the rod surface under the sleeve and 3) a by-pass rod. In comparison with the equivalent Blockage 2 test (cf. Figure 80), sleeve cooling is now just slightly less efficient than by-pass rod cooling; however, sleeve rewetting occurs 40 s earlier than by-pass rod rewetting, due to the much lower thermal capacity of these blockage sleeves in comparison to those in Blockage 2 tests.

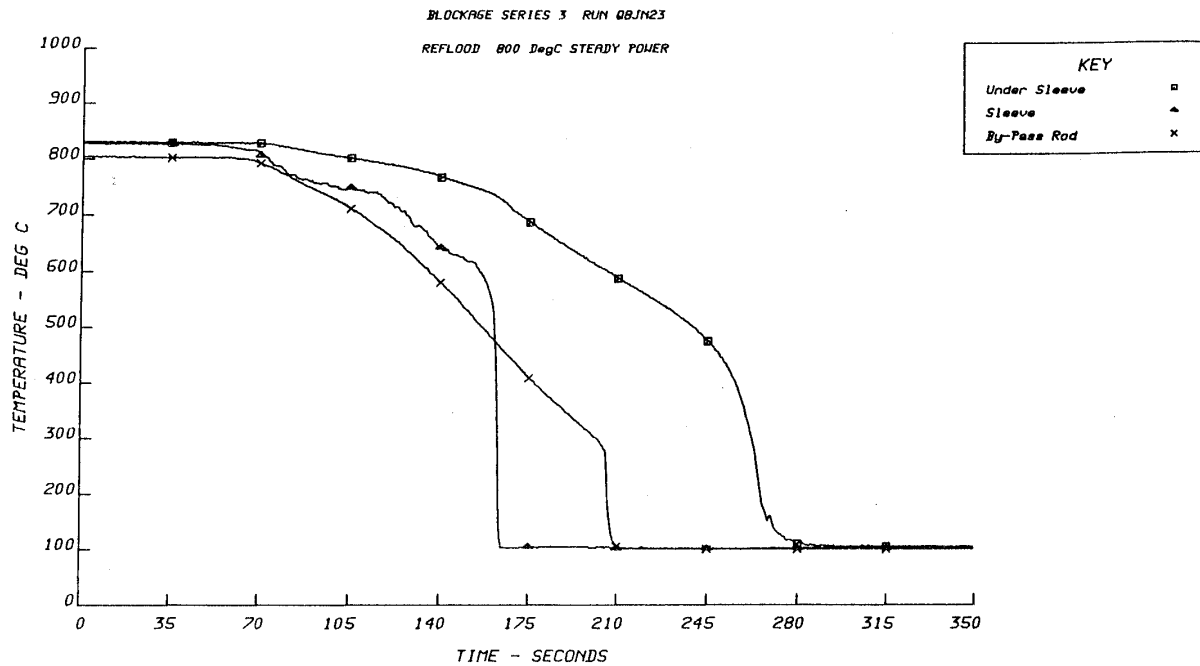


Figure 83: CEGB Blockage 3 - Blockage sleeve and by-pass rod temperatures.

Figure 84 provides temperature variations at different levels for a blockage sleeve measured by thermocouples facing into the central sub-channel. Better cooling is observed near the ends of the sleeve in comparison to the intermediary levels. The sleeve quenches from the top downwards, which corresponds to a reflux of liquid when the steam flow downstream from the blockage is cooled to saturation and consequently slows down.

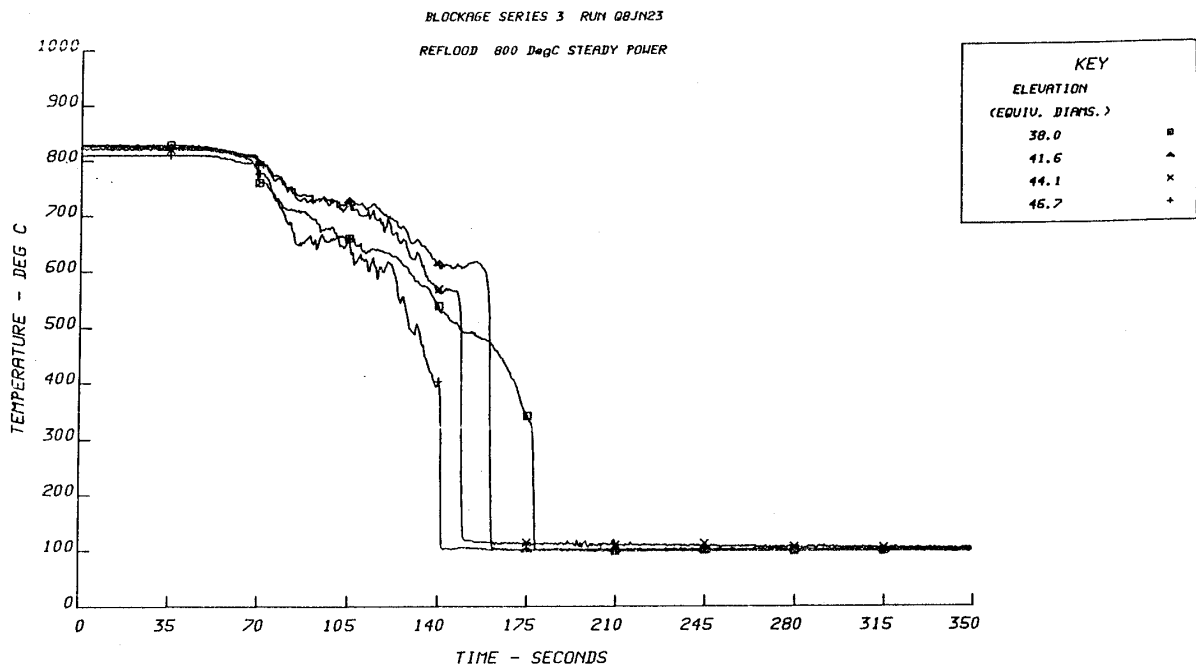


Figure 84: CEGB Blockage 3 - Sleeve temperatures at different levels.

Figure 85 provides rewetting times for all thermocouples in the bundle in relation to their axial elevation. Again, the rewetting times for by-pass rods are in close agreement with those observed for the non-deformed bundle. Blockage sleeves are rewet by a descending quench front, which occurs well before rewetting in the by-pass at the same levels. Above the blockage, blockage rods are also subjected to earlier rewetting compared to that in the by-pass, due to the combination of ascending and descending quench fronts that meet just downstream from the blockage.

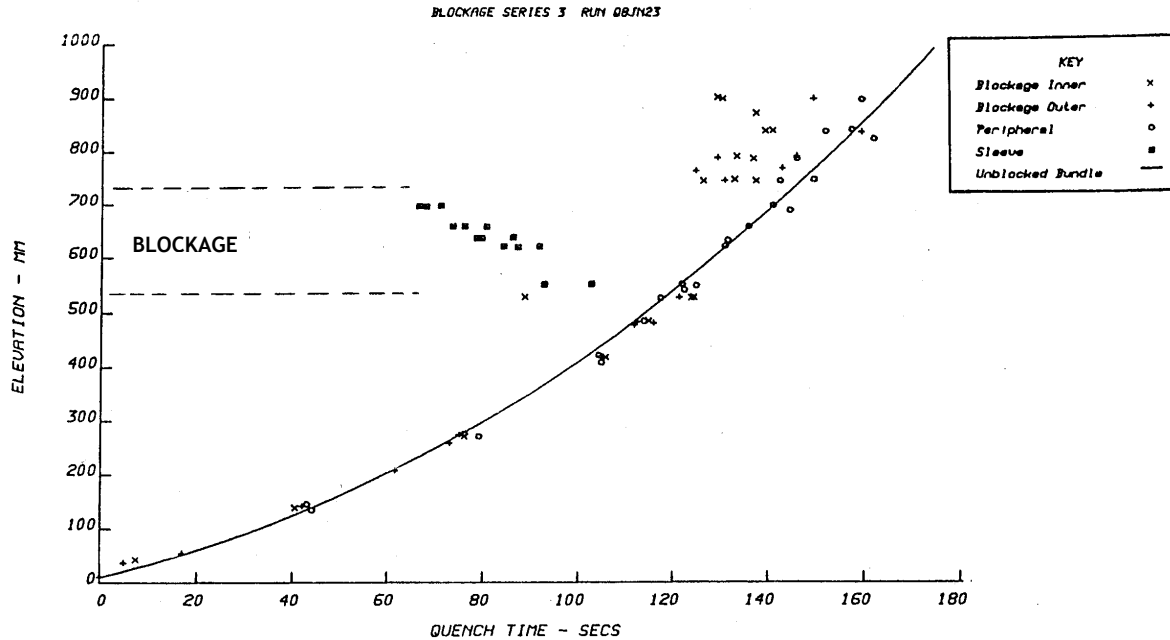


Figure 85: CEGB Blockage 3 - Bundle quench times versus elevation.

### 5.2.2.2 +1 kW power tests

Results of these tests were similar to the steady power tests results but with some noticeable differences. Figure 86 reveals an accentuation in temperature differences between the sleeve and the by-pass before rewetting, which still occurs earlier on the sleeves but much closer to the by-pass rods than in the steady power case (cf. Figure 83). The maximum temperature recorded in the throat of an inner sleeve is higher - surpassing 900°C - leading to temperature differences of more than 300°C with temperatures recorded at the sleeve ends (cf. Figure 87).

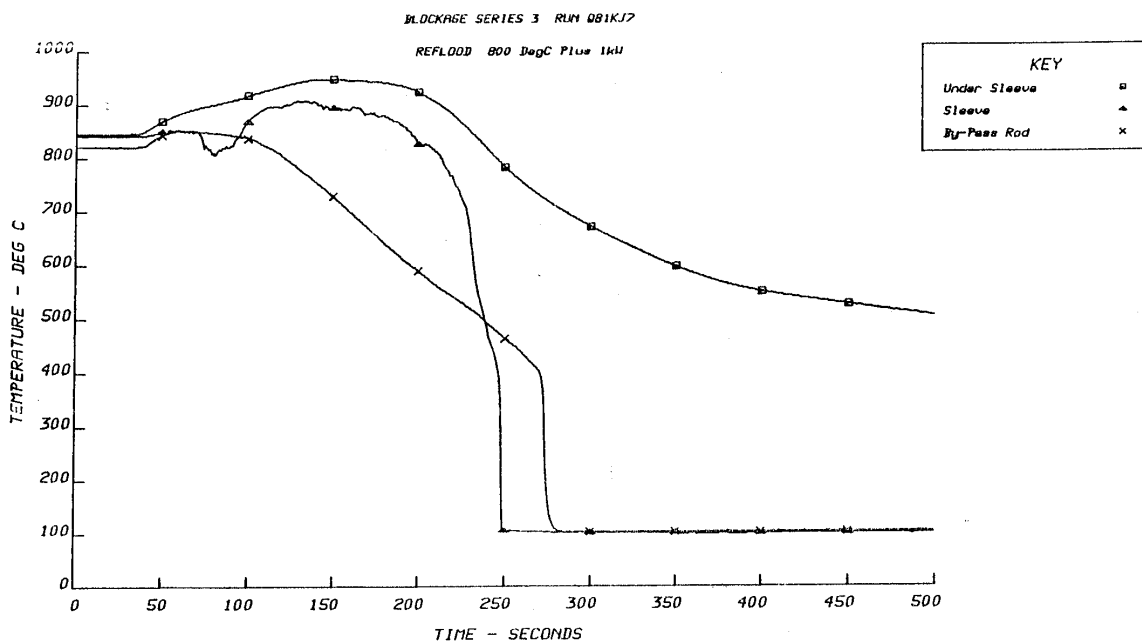


Figure 86: CEGB Blockage 3(+1kW test) - Blockage sleeve and by-pass rod temperatures.

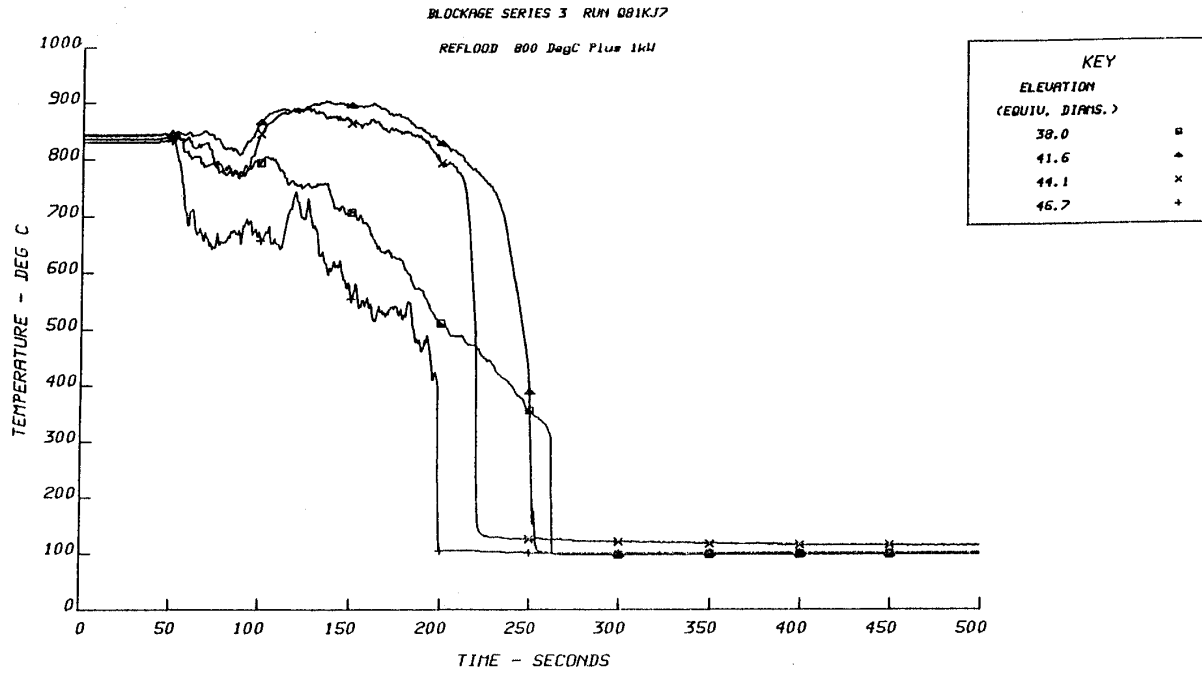


Figure 87: CEGB Blockage 3 (+1kW test) - Sleeve temperatures at different levels.

Figure 88 provides rewetting times for all thermocouples in the bundle in relation to their elevation. Blockage sleeves are still rewet from the top downwards, but at a time closer to the by-pass rods rewetting time. Above the blockage, the inner rods in the blockage region are subjected to quench by descending films, occurring almost simultaneously with the by-pass rewetting, whereas the outer rods of the blockage undergo rewetting approximately 50 s later.

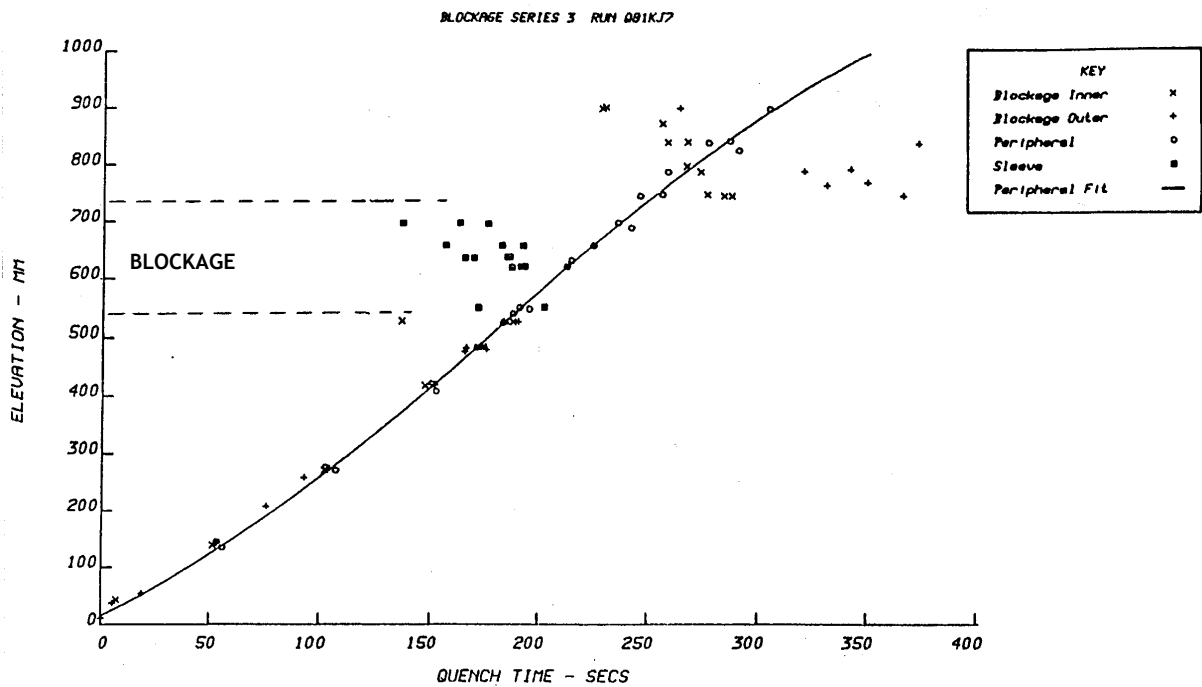


Figure 88: CEGB Blockage 3 (+1kW test) - Bundle quench times versus elevation.

### 5.3 Comparison of CEGB results with THETIS and FEBA/SEFLEX results

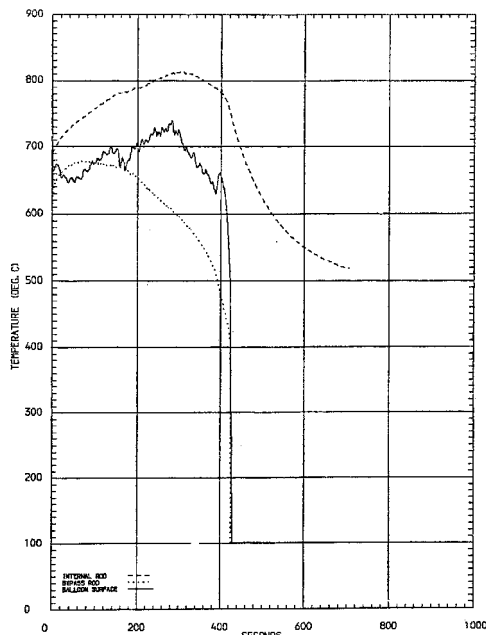
With the THETIS and FEBA/ SEFLEX tests with the same blockage ratio, the CEGB program reflood tests on an assembly with a 90% coplanar blockage represent a set of comprehensive results that are worth comparing. It is important however to point out the main geometrical differences between the blockage simulations used in the different tests, such as:

- the length of the 90% blocked section: 65 mm in FEBA and SEFLEX; 147 mm in CEGB; 200 mm in THETIS;
- the length of the entry taper linking the nominal section to the maximum blockage section: 25 mm in CEGB; 57.5 mm in FEBA and SEFLEX; 200 mm in THETIS;
- the thickness of the ballooned cladding (or sleeve) in the blockage section: 1 to 2.35 mm in FEBA; 0.48 mm in SEFLEX; 0.3 mm in THETIS; 0.865 to 2.5 mm in CEGB Blockage 2 and 0.3 mm in CEGB Blockage 3.

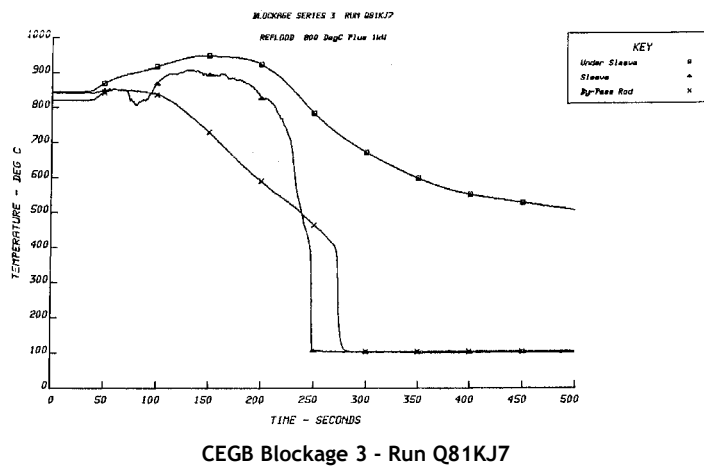
In addition to those in experimental conditions, these differences in geometries make it difficult to directly compare the results of the above-mentioned programs.

Comparison of FEBA and SEFLEX results, which was part of the SEFLEX program objectives, was discussed above in § 2.2.4.2.

In terms of maximum blockage lengths and corresponding balloon thicknesses, the similarity between THETIS sleeves and CEGB Blockage 3 sleeves makes it possible to directly compare results of tests run under similar conditions. With reflood conditions considered as the most severe (reflood rate = 2 cm/s, inlet temperature = 90°C, pressure = 1.3 bar), THETIS run T1R072 may be compared to CEGB run Q81KJ7. Temperature variations in the blockage and by-pass of these two tests are compared in Figure 89. A superheating of about 60°C in the blockage in comparison to the by-pass can be observed in both tests, which suggests that the balance between positive and negative factors is equivalent in both tests.



THETIS Run T1R072 (90% blockage; 1.3 bar)



CEGB Blockage 3 - Run Q81KJ7

Figure 89: Blockage and by-pass temperatures in comparative THETIS and CEGB tests.

Generally speaking, two quasi-systematic differences between THETIS and CEGB results of tests performed under similar conditions were observed:

- 1) In CEGB/Blockage 3 tests, the blockage sleeves rewet much earlier than the by-pass rods at the same elevation, whereas in THETIS tests the blockage sleeves rewet at roughly the same time as - or even slightly after - the by-pass rods (cf. Figures 36, 39, 43, 45).
- 2) Blockage rewetting takes place with an ascending quench front in THETIS tests and a descending quench front in most CEGB tests.

The first difference may be associated with the shorter heated length used in the CEGB tests, which results in lower steam and droplet velocities in the blockage, thereby favouring a more efficient cooling of the blockage surface. Rod to sleeve gap conductance - nitrogen-pressurised in THETIS tests - must also be considered. The second difference may result from the inlet taper length - markedly longer in THETIS tests - which creates a longer steam deceleration region upstream from the blockage, thus making subsequent droplet penetration more difficult. In CEGB tests, this deceleration occurs rather in the widening section at the throat outlet, leading to fall back of the droplets and a descending quench front. Furthermore, in the THETIS geometry, there is a residual blockage (~ 32%) at all elevations above the blockage itself due to the housing of thermocouple wires in an annular sleeve; this means increased steam and droplet velocities at the blockage outlet which therefore limits the possibility of a descending quench front.

#### 5.4 CEGB analytical model

An analytical model was developed by CEGB [10] to calculate cladding temperatures in a blockage formed by a group of ballooned rods in a larger assembly, under postulated LOCA reflood conditions. Though involving some of the same scientists, this model was not particularly developed in association with the above discussed experimental program whose results, seemingly, were not used to validate the model. Nevertheless, this model will be discussed here for its interesting use in parametric studies on the effect of maximum blockage rate and length.

##### 5.4.1 Model description

The model considers an idealised geometry in which a blockage is formed in a large rod array by axisymmetrical coplanar clad ballooning in a group of fuel rods (cf. Figure 90).

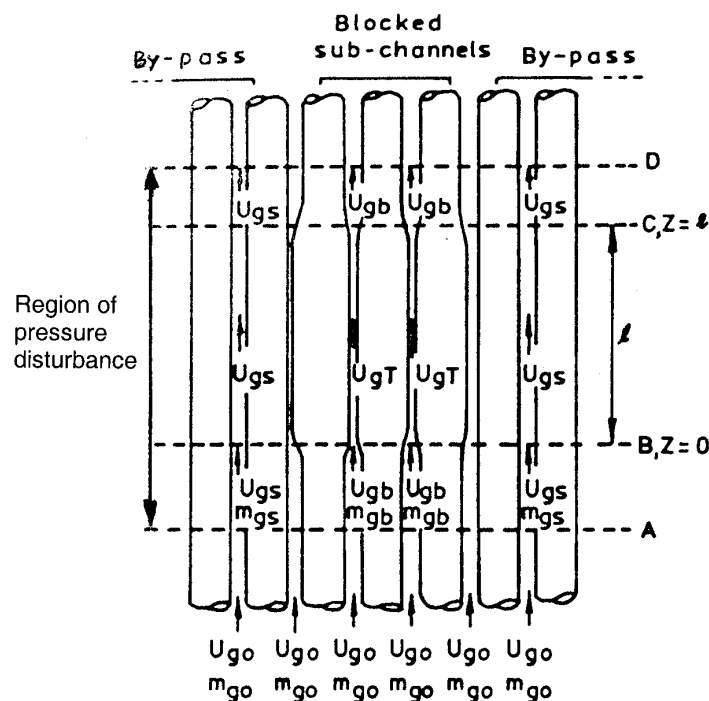


Figure 90: Blockage geometry and velocities used in the CEGB analytical model

For the coolant flow composed of a steam flux carrying droplets, only the behavior of the gaseous component is considered in the model.

The model mainly consists in calculating the:

- the steam velocity in the blockage sub-channels based on flow redistribution upstream from the blockage;
- the cladding temperature in the ballooned region, or the difference between cladding and by-pass temperatures at the same level.

a) Steam flow velocity in the blockage

This calculation is based on the balance of momentum between planes A and D (cf. Figure 90) for both blocked and unblocked sub-channels.

For a by-pass sub-channel (index bp), the pressure drops taken into account are:

- the friction losses, calculated in a standard manner:

$$\Delta P_{AD} = \frac{1}{2} K_{f_{bp}} U_{bp}^2 \quad \text{with } K_{f_{bp}} = 4f_{bp} L/d_0$$

with  $L$  = length of the friction region,  $d_0$  = hydraulic diameter

and with a friction coefficient that is function of Reynolds number as:  $f_{bp} = 0.085 Re_{bp}^{-0.25}$

- the singular pressure drop due to the presence of any spacer grids

$$\Delta P = \frac{1}{2} K_G U_{bp}^2 \quad \text{with } K_G \text{ based on the Aytekin correlation: } K_G = 6.95 Re_{bp}^{-0.21}$$

For a blocked sub-channel (index bl), the pressure drops taken into account are:

- the friction losses in the blocked region (BC):

$$\Delta P_{BC} = \frac{1}{2} K_{f_{bl}} U_{bl}^2 \quad \text{with } K_{f_{bl}} = 4f_{bl} l/d_b$$

with  $l$  = length and  $d_b$  = hydraulic diameter of the blocked region

with a friction coefficient that is function of Reynolds number as :

$$f_{bl} = \text{Max} (0.028 Re_{bl}^{-0.2}; 16/ Re_{bl})$$

- the pressure drop due to area change in the blocked region (BC) - mainly due to form losses at the blockage exit downstream from section  $A^*$  where fuel rods are no longer in contact; a tentative correlation for the form losses was proposed as:

$$K_{disbl} = 0.8 (1-A^*/A_0)^2 \text{ for a blockage with contact between fuel rods } (A_{bl} < A^*)$$

$$\text{or } K_{disbl} = 0.8 (1-A_{bl}/A_0)^2 \text{ for a blockage without contact between fuel rods } (A_{bl} > A^*)$$

- the friction losses in the non-deformed regions (AB, CD), calculated like in the by-pass using  $Re_{bl}$
- the grid losses, calculated like in the by-pass using  $Re_{bl}$ .

Figure 91 compares CEGB model predictions to experimental results of air flow tests done on a model of the THETIS 90% blockage geometry. The figure, which illustrates the relative fluid velocity in the blockage for Reynolds numbers between  $10^3$  and  $4 \times 10^4$ , shows good agreement for the central sub-channel of the  $4 \times 4$  blocked rod array, in which conditions corresponds most closely to the one-dimensional flow assumed in the CEGB model.

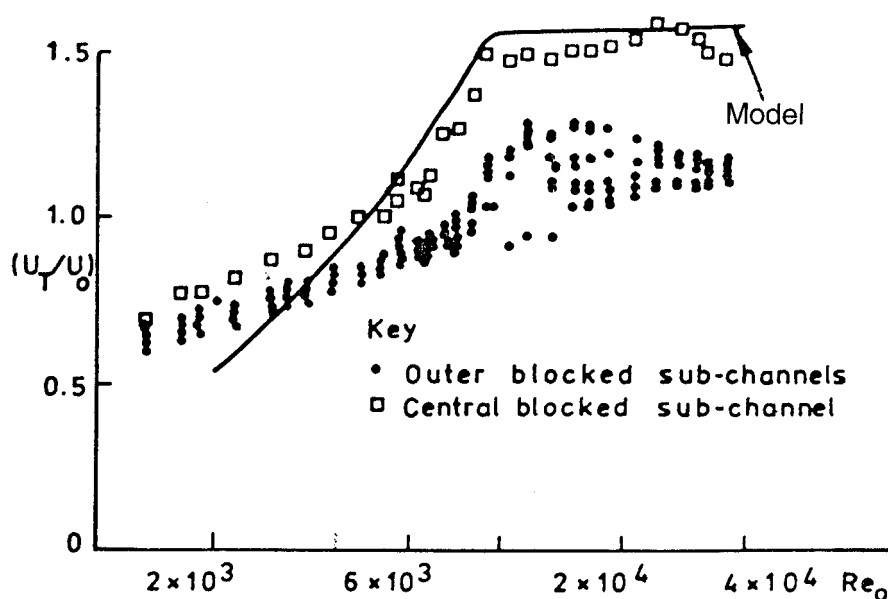


Figure 91: Comparison of THETIS experimental velocities to CEGB model predictions for a 90% blockage.

### b) Heat transfer in the blockage

The CEGB model only describes convection heat transfer between the rod surfaces and the fluid, which is considered as a superheated steam phase containing liquid droplets. Direct radiative transfers to droplets and pin-to-pin radiation are ignored. Heat transfer coefficients are obtained from single-phase flow correlations.

The temperature distribution is assumed to be a steady-state distribution corresponding to a stationary two-phase flow.

The steam flow rate in the blockage sub-channels is calculated using the flow diversion model described above where the effect of entrained droplets on flow diversion towards the by-pass and the contribution of droplet vaporisation to steam flow-rate are neglected. The liquid mass flow-rate is assumed to be same in both the blocked and unblocked sub-channels (i.e. no droplet diversion).

By applying an energy balance to the steam flowing between plane B ( $z=0$ ) and any level  $z$ , for a blockage sub-channel and a by-pass sub-channel, it is possible to establish a relationship relating the difference in local temperatures of blockage and by-pass surfaces  $\Delta T_w(z) = T_{wbl}(z) - T_{wbp}(z)$  to the clad-to-steam temperature difference in the by-pass and the flows and heat transfer characteristics in the blockage and by-pass:

$$\Delta T_w(z) = [T_w(z) - T_g(z)]_{bp} F(Q_{bl}, Q_{bp}, h_{bl}, h_{bp}, \chi_{bl}, \chi_{bp})$$

where  $h_{bl}$  and  $h_{bp}$  represent heat transfer coefficients in the blockage and by-pass,

$\chi_{bl}$  and  $\chi_{bp}$  represent - for the blockage and by-pass surfaces - the fraction of the heat flux which contributes to the steam phase enthalpy rise:  $\chi = 1$  corresponds to the extreme case with no steam de-superheating by droplets; CEGB calculations performed with a theoretical model showed that, under dispersed flow conditions, steam de-superheating increases with the surface temperature  $T_w$ , therefore with decreasing values of  $\chi$ :

$$T_w = 600^\circ\text{C} \quad \rightarrow \quad 0.84 < \chi < 0.92$$

$$T_w = 800^\circ\text{C} \quad \rightarrow \quad 0.42 < \chi < 0.78$$

$$T_w = 1100^\circ\text{C} \quad \rightarrow \quad 0.25 < \chi < 0.50$$

Assuming that both the size of the droplets and their velocity relative to steam are very similar in the by-pass and blockage, the following relationship can be established:

$$(1 - \chi_{bl}) / (1 - \chi_{bp}) = (T_{gbl} - T_{sat}) / (T_{gbp} - T_{sat})$$

with  $T_{gbl}$  and  $T_{gbp}$  representing the mean steam temperatures in the blockage and by-pass respectively.

In the by-pass, the heat transfer coefficient  $h_{bp}$  is obtained using the Dittus-Boelter correlation.

In the blockage, the heat transfer enhancement due to the flow development is taken into account by a multiplicative factor  $\Phi^*$ , derived from turbulent flow data as:

$$\Phi^* = \{0.184 \ln(z/d_{bl}) + 0.41\}^{-1} \quad \text{for } 1 < z/d_{bl} < 20$$

$$\Phi^* = 1 \quad \text{for } z/d_{bl} > 20$$

and the fully developed heat transfer coefficient is again obtained from the Dittus-Boelter correlation.

In the case of a laminar flow ( $Re_{bl} < 1000$ ) in the blocked sub-channels, the heat transfer coefficient  $h_{bl}$  is calculated from the Kays correlation:

$$h_{bl} = \frac{\lambda_{bl}}{d_{bl}} \left[ 4.4 + \frac{0.036 \xi}{1 + 0.0011 \xi} \right]$$

$$\text{where } \xi = (Re Pr)_{bl} d_{bl}/z$$

#### 5.4.2 Comparison of model predictions with experimental results

A brief comparison of model predictions with FEBA 62% and 90% blockage experimental results was carried out. Figure 92 compares model predictions with measured throat temperature variations for the two blockage ratios. Model predictions are in reasonable agreement for the 62% blockage where a cooling effect on the throat of 50°C to 100°C was observed in comparison to the by-pass. However, for the 90% blockage, the model predicts a 50 to 100°C temperature increase in comparison to the by-pass, whereas a reduction of about 150°C was observed. According to the authors [10], this inconsistency could be partially due to the fact that the FEBA blockage was located in a corner of the assembly with the possibility - particularly for the 90% blockage - of considerable thermal leakage by conduction with the cooler shroud.

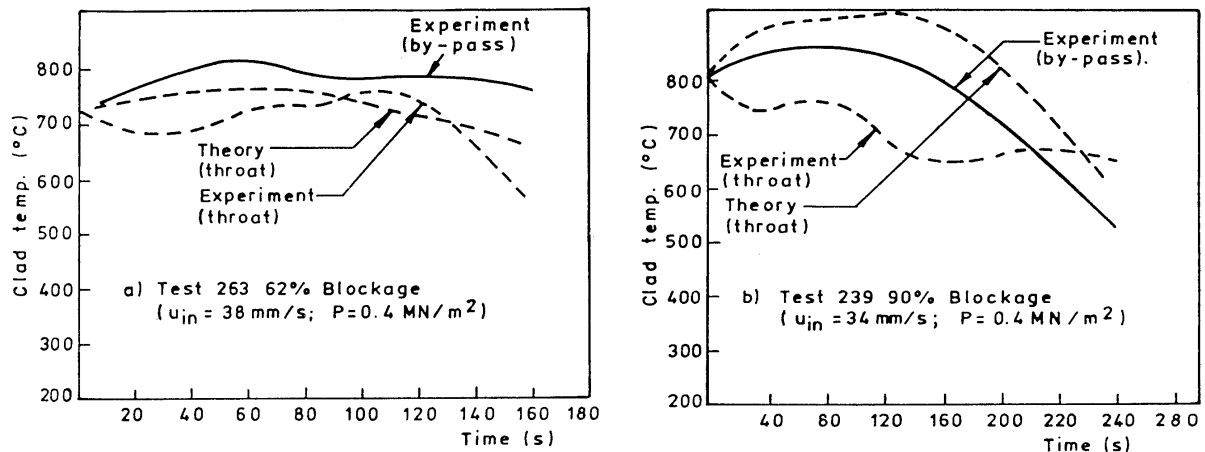


Figure 92: Comparison of pin surface temperature in blockage and by-pass regions measured in FEBA tests to CEGB model predictions.

#### 5.4.3 Parametric calculations under PWR reflood conditions

Using the previously described model, a set of calculations was carried out to evaluate maximum temperatures in the blockage under PWR reflood conditions, with the length of the maximum blocked section ( $l$ ) and its blockage ratio ( $\tau$ ) used as main parameters.

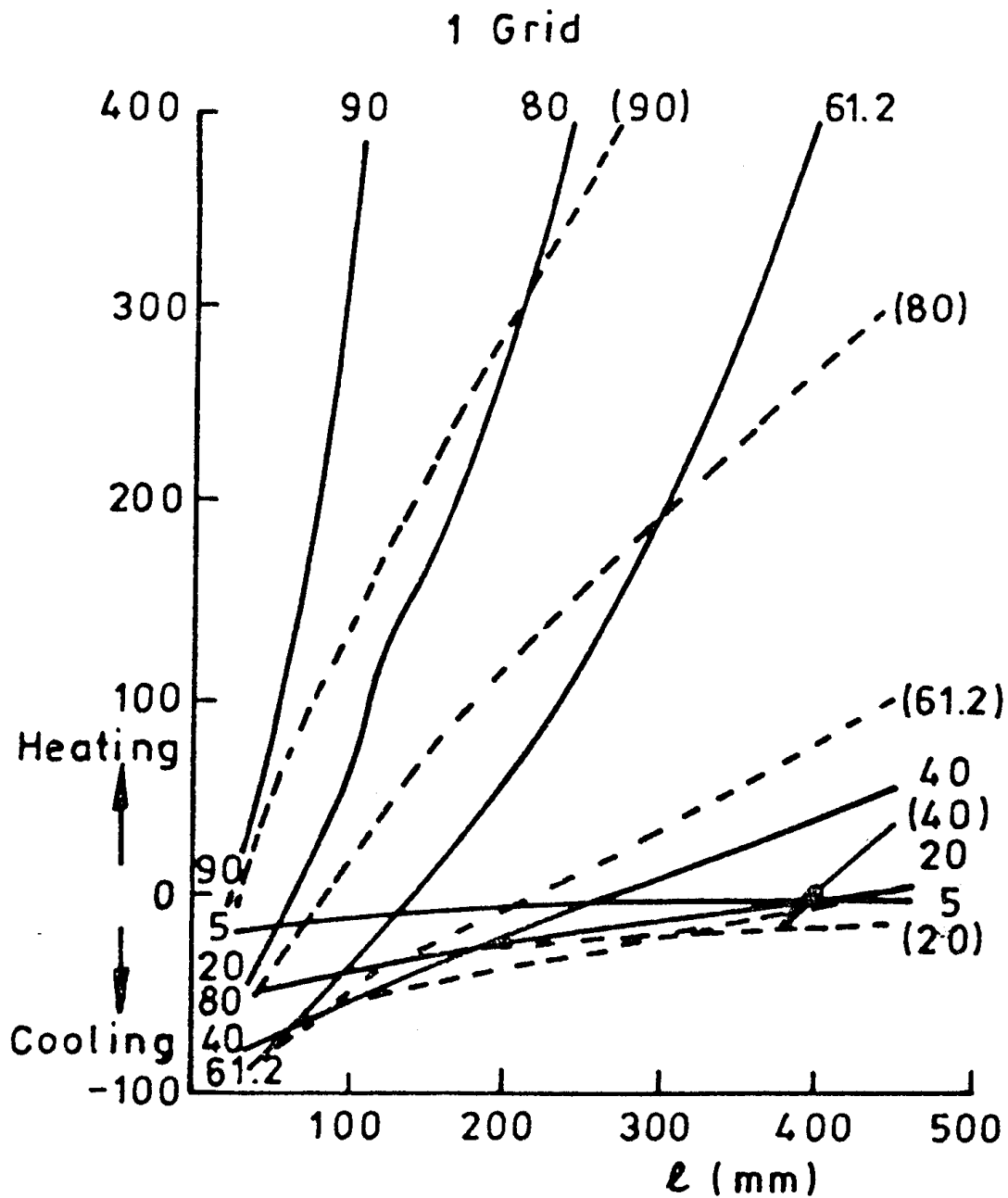
Conditions recorded during FLECHT SEASET Run 31805 were chosen to define the thermohydraulic conditions and temperature for the non-deformed rods:

- Reflood rate = 2 cm/s
- Pressure = 2.8 bar
- Power = typical reactor decay power for a highly rated rod
- $T_w = 1171^\circ\text{C}$  (= maximum temperature in the bundle centre)
- $T_w - T_g = 142^\circ\text{C}$
- Mass flow rate  $G_0 = 14.2 \text{ kg/m}^2/\text{s}$

Two series of calculations were performed:

- a) conservative calculations without steam de-superheating ( $\chi_{bl} = \chi_{bp} = 1$ );
- b) best-estimate calculations with steam de-superheating ( $\chi_{bp} = 0.4$ ).

Figure 93 illustrates the maximum temperature difference  $\Delta T_w$  between the blockage throat and the by-pass as a function of the blockage length  $l$  and with the blockage ratio  $\tau$  serving as parameter. The clad temperature increase refers to the peak value, obtained at the downstream end of the throat. The solid lines refer to the case  $\chi_{bp} = 1$ , whereas the dashed lines refer to the case  $\chi_{bp} = 0.4$ . This figure shows that negative  $\Delta T_w$  can be obtained for low blockage ratios ( $\tau < 40\%$ ) and short blockages ( $l < 100 \text{ mm}$ ). The figure also reveals a very rapid increase in  $\Delta T_w$  with a blockage length for high blockage ratios ( $\tau > 80\%$ ), due to steam superheating in the blocked passages. Consideration of steam de-superheating by liquid droplets lowers the temperature increase significantly, but still allows the possibility of high  $\Delta T_w$  for long severe blockages, such as those of THETIS 90% blockage tests.



**Key :**

———— :  $\chi = 1.0$  (upper bound calculation)      - - - :  $\chi = 0.4$  (best estimate calculation)

Figure 93: Maximum clad temperature increase in blockage throat calculated with the CEGB model as function of throat length and blockage ratio.

In conclusion, trends revealed by this parametric study appear to be consistent with previously discussed experimental program results, therefore confirming the absence of temperature penalties for short blockages or moderate blockage ratios (<60%). Furthermore, significant increases in blockage surface temperatures that may threaten blockage coolability require high blockage ratios (>80%) and long blockages (longer than 150 mm).

## 6 FLECHT SEASET program

The FLECHT SEASET<sup>[11]</sup> program (Full-Length Emergency Cooling Heat Transfer - Separate Effects And System Effects Tests) was an extensive program launched in 1977 by Westinghouse, EPRI and USNRC to provide data and analysis needed by the nuclear industry on large-break LOCA reflood heat transfer.

The program's main objective was to improve understanding of complex thermohydraulic phenomena occurring during a postulated LOCA scenario. In the short term, program results were to be used to identify excessive conservatism in the current licensing requirements so that realistic yet conservative requirements could be developed. In particular, a short-term goal was to provide reflood heat transfer data in unblocked and partially blocked assemblies and associated data analysis, which could be used to evaluate the relevance of the Appendix K rule relative to heat transfer under flow blockage conditions, which stipulates:

*"During refill and during reflood when reflood rates are less than one inch per second, heat transfer calculations shall be based on the assumption that cooling is only by steam, and shall take into account any flow blockage calculated to occur as a result of cladding swelling or rupture as such blockage might affect both local steam flow and heat transfer"*

This restrictive requirement stemmed from a lack of substantial databases available at the beginning of the 70s, which mainly dealt with forced reflood tests at reflood rates > 1 inch/s using partially blocked assemblies (whose results did reveal improvements in heat transfer at reflood rates above 1 inch/ sec).

Longer-term objectives of the FLECHT SEASET program involved 1) assessing the entire PWR cooling system behavior during gravity reflood scenarios and 2) understanding how the system behavior and the core heat release interact to yield the observed complex variations in flooding rate and associated heat transfer.

Following the occurrence of the TMI-2 accident in 1979, the FLECHT SEASET program content was redirected to include tests involving new thermohydraulic conditions such as those observed during the TMI accident. In particular, separate effects tests were performed to study low Reynolds number steam cooling. System effect tests were also revised to investigate the different natural convection cooling modes. All these complementary tests helped improve databases to address small-break LOCA transients.

The FLECHT SEASET program results were clearly expected to be used in the development of significantly improved analytical reflood models in computer codes such as RELAP-4 and 5, BART, TRAC and COBRA-TF. Conducted in parallel with tests, the analysis of results with COBRA-TF was expected to provide a sufficient physical basis to modify the Appendix K steam cooling rule. The outcome of such application should result in more realistic regulatory requirements, thereby providing the industry with more flexible operating margins.

Only the FLECHT SEASET program tests dealing with blocked assembly cooling will be discussed in this State-of-the-Art review. This part of the program involved performing three main tasks:

- Performing tests on a 21-rod array to determine the effects of different blockage configurations and geometries upon reflood heat transfer;
- Performing tests on a 163-rod array to evaluate the effect of a large flow by-pass under the most severe heat transfer conditions observed in the 21-rod bundle tests series;
- Analysing results and developing associated models with the COBRA-TF code.

Average blockage ratios tested in the FLECHT SEASET program remain rather moderate, no higher than 62% in the most detrimental coplanar configuration. Furthermore, the simulated balloons in this configuration were particularly short, 60 mm in total length for a cosine profile. Therefore, results of these tests cannot be compared to test results with high blockage ratios from previously discussed programs. It is nevertheless interesting to examine these test results owing to their particularities, i.e. several test series conducted with non-concentric and non-coplanar balloon configurations.

## 6.1 Tests performed on a 21 fuel rod array

### 6.1.1 Experimental characteristics

A review of the existing literature regarding ballooning and blockage results made it possible to choose six blockage configurations for the test series performed on a 21 rod array. Table 9 lists these different configurations.

Test Series	Configuration Description	Comments
A	No blockage on the rods	This configuration served as a reference.
B	Short concentric sleeve, coplanar blockage on 9 centre rods. Maximum strain = 32.6%	This series provided for both blockage effect and some by-pass effects.
C	Short concentric sleeve, coplanar blockage on all 21 rods. Maximum strain = 32.6%	This series was the easiest to analyse since it provided no flow by-pass effects with maximum flow blockage effect at one axial plane.
D	Short concentric sleeve, non-coplanar blockage on all 21 rods. Maximum strain = 32.6%	This test series examined a non-coplanar blockage distribution and was comparable to series C.
E	Long non-concentric sleeve, non-coplanar blockage on all 21 rods. Maximum strain = 36%	This test series permitted a one-to-one comparison with series D in which all rods were blocked. Comparison of series D and E with unblocked data indicated the worst shape.
F	Test series E with increased sleeve strain, non-coplanar blockage on all 21 rods. Maximum strain = 44%	This test series increased the blockage effect relative to series E.

#### Comments

- Configuration A served as reference and was blockage-free.
- Configurations B, C and D used concentric sleeves, representing Zircaloy clad swelling and burst in the  $\beta$  phase (isotropic strain), whereas configurations E and F used non-concentric sleeves representing swelling and burst in the  $\alpha$  phase (anisotropic strain).
- Sleeves were fixed to 9 central fuel rods in configuration B, creating a partial by-pass of the blockage, in comparison to configuration C with sleeves fixed to all 21 rods, thus without any by-pass.
- The comparison of results of tests in configurations D and E made it possible to evaluate the effect of the balloon geometry (short concentric sleeve in D and long non-concentric sleeve in E).
- Sleeves in configurations D, E and F were positioned in a non-coplanar manner designed to simulate the non-coplanar distribution observed in numerous out-of-pile rod swelling/burst tests

**Table 9: Blockage shapes and configurations tested in 21-Rod array.**

In non-coplanar configurations, the axial distribution of the blockage sleeves was based on the principle that the axial distribution of deformations coincides with the axial temperature distribution. It was assumed that all fuel rods shared a similar temperature distribution but that the maximum temperature values were statistically distributed after having taken into consideration local variations resulting from:

- (a) manufacturing parameters (pellet density, diameter, enrichment, etc.)
- (b) in-reactor operation (pellet densification, fragmentation, radial offset within clad, etc.)

Manufacturing tolerance upon parameters mentioned in (a) were input into Westinghouse standard design codes, which made it possible to evaluate their impact on local temperature variations. These variations were statistically combined to obtain the overall temperature uncertainty just

prior to the accident, the resulting standard deviation being found about 10°C. For variations mentioned in (b), only the effect of pellet offset was considered and evaluated by a series of finite-element calculations for various values of pellet eccentricity. The resulting temperature distribution was then convoluted with that resulting from variations mentioned in (a) and the convoluted sum corrected to account for the variability in burst temperature for a given temperature variability at power. Last of all, a standard deviation of 7°C, combined with the axial mean temperature distribution of Westinghouse using a standard statistical model for maximum temperature distribution, permitted the definition of an axial distribution of the blockage sleeves in a 21 rod array. This distribution was applied in all three non-coplanar configurations.

Based on ORNL and REBEKA burst tests, strain of 36% was chosen as the most representative value and applied to all non-concentric balloons in configuration E. A slightly greater deformation (44%) was applied in configuration F.

The choice of balloon lengths is not explained in reference [11]. Short concentric balloons in configurations B, C and D were 58 mm long and "long" non-concentric balloons in configurations E and F were 190 mm long, but with deformation essentially located over a length of 95 mm. Figure 94 provides a view of these balloons, simulated by hollow sleeves fitted to the rods. Both sleeves were obtained by hydro-forming, in which 0.76 mm thick stainless steel tubes were subjected to hydraulic deformation in a mould.

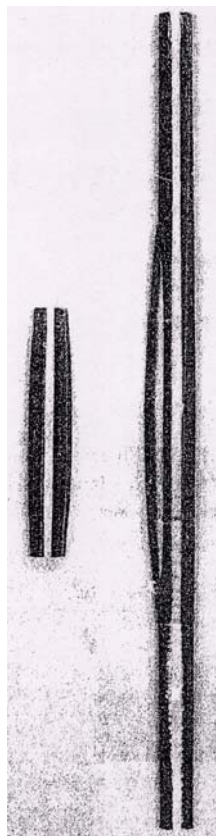


**Figure 94: View of short concentric and long non concentric blockage sleeves.**

Regarding non-concentric sleeves, the selection of bulge directions was based on the following principles:

- Orientation of maximum deformation towards the centre of a sub-channel rather than towards an adjacent rod (for practical reasons: fitting the sleeves onto the rods);
- Burst on the hot side, with bowing and ballooning towards the cold side;
- Comparison with the 163 rod configuration containing guide tubes that are a source of azimuthal heterogeneity orienting the balloons towards the cold spots (cf. Figure 95)

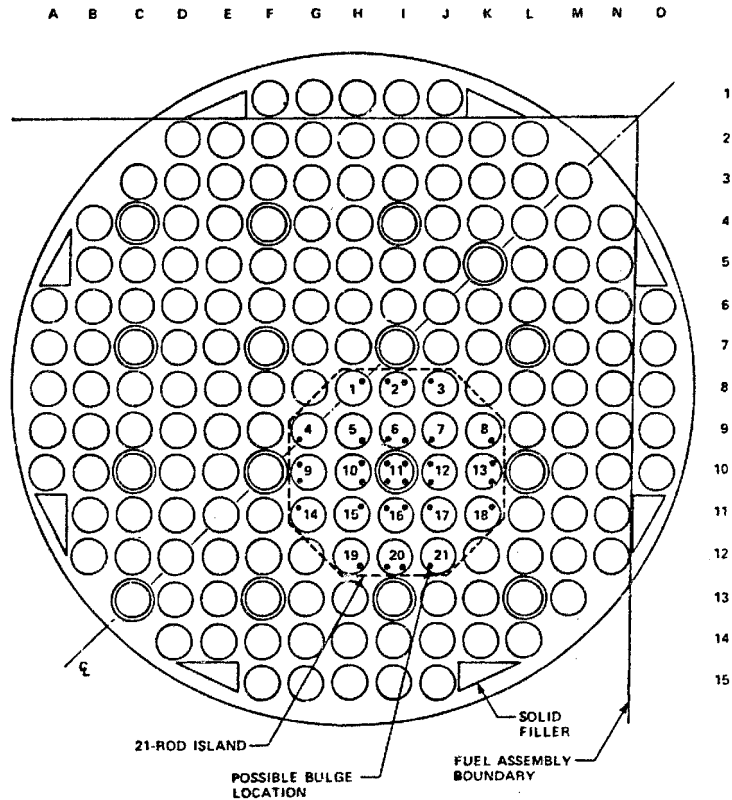


Figure 95: Potential bulge directions and comparison between 21 and 163 rod bundles.

A schematic representation of this configuration is provided in Figure 96, illustrating the bulge direction of maximum strains and their axial distribution.

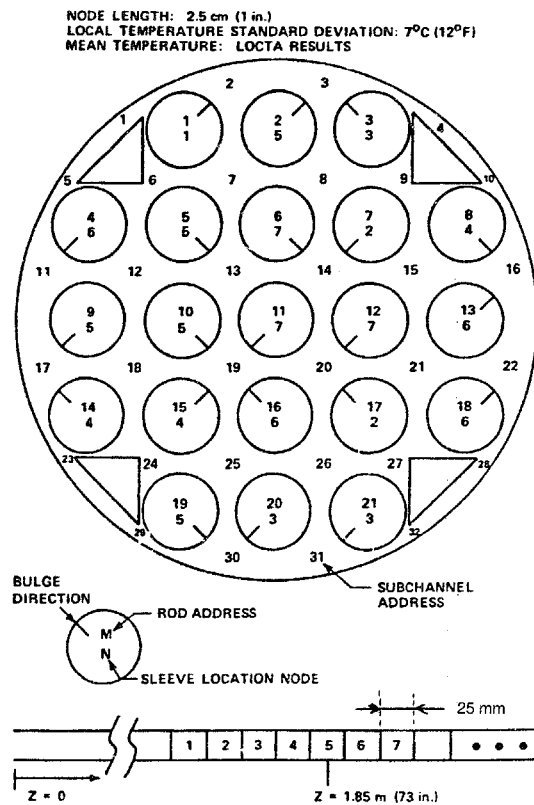


Figure 96: Non coplanar sleeve distribution and bulge direction for non concentric sleeves.

Figure 97 illustrates the axial distributions of bundle-wide blockage ratio for configurations C, D, E and F, all with a sleeve on all 21 fuel rods. As expected, configuration C (coplanar concentric) produces the highest blockage ratio (62%), whereas the non-coplanar configurations barely reach a maximum bundle blockage ratio of 30%, even if the local blockage in a specific sub-channel (as No. 19 in Figure 96) can reach much higher values (90%).

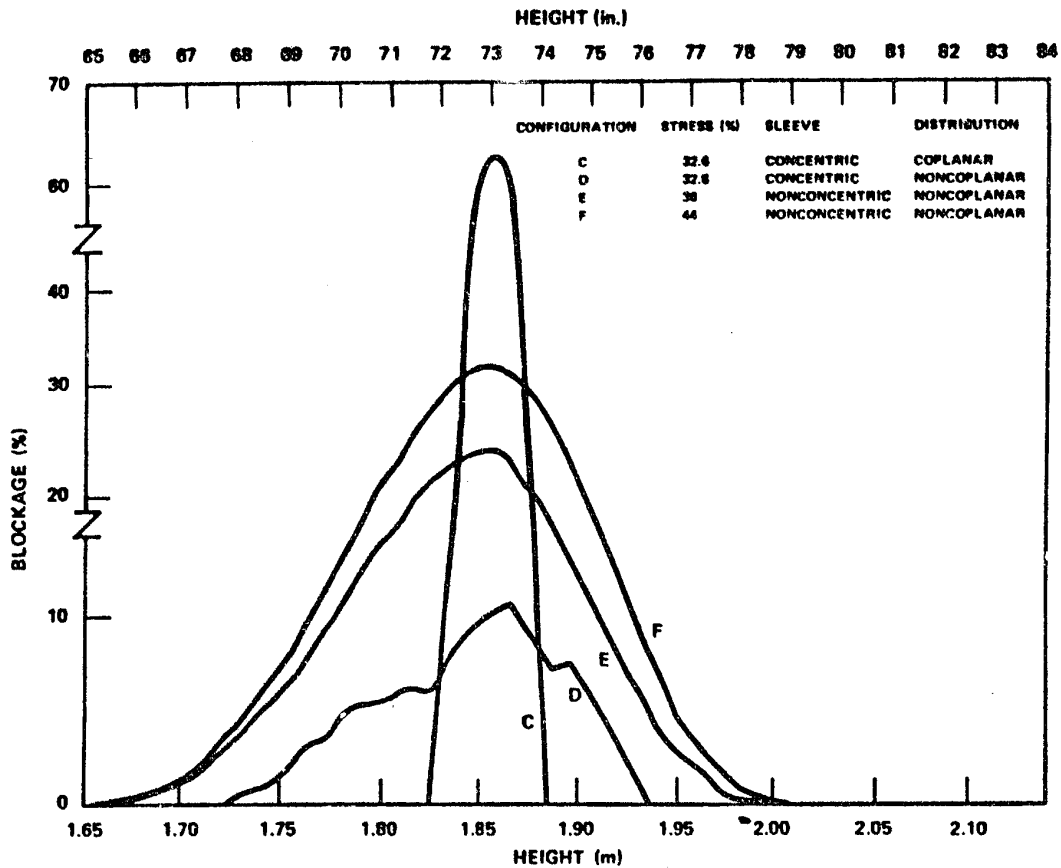


Figure 97: Bundle-wide blockage axial distributions for test configurations C, D, E and F.

The test assembly was composed of 21 full-length instrumented heater rods, with a diameter of 9.5 mm and a heated length of 3.05 m, held in 8 spacer grids and including 4 triangular solid fillers. The assembly was housed in a stainless steel cylindrical shroud, with an inside diameter of 6.82 mm and a thickness of 4 mm.

### 6.1.2 Test matrix

All configurations were subjected to hydraulic characterisation tests, steam cooling tests, and forced and gravity reflood tests (excepting configuration F without gravity reflood tests).

Hydraulic tests were performed to determine, under steady-state liquid flow, the pressure losses associated with rod friction, spacer grids and blockage sleeves.

Steam cooling tests were performed to evaluate the effects of the blockage upon single-phase steady flow heat transfer. The COBRA-IV-I code was used to analyse these tests with the hydraulic data for pressure loss coefficients obtained from the previous series of tests.

Forced reflood tests, which represented the main part of the different series, were performed to evaluate the effects of a blockage upon two-phase flow heat transfers. Gravity reflood tests were performed as scoping tests to ensure that no unexpected effects under gravity reflood could cause a more detrimental situation in terms of heat transfer in comparison to a forced reflood. In total, 87 forced reflood tests and 10 gravity reflood tests were conducted.

Forced reflood tests were useful to study the separate effects of variations upon the different test parameters:

- flooding rate: from 1.27 cm/s (0.5 in./s) to 15.2 cm/s (6 in./s);
- pressure: from 1.4 bar to 2.8 bar;
- inlet fluid temperature subcooling: 22°C (40°F) and 78°C (140°F)
- initial peak linear power: from 0.89 kW/m to 2.57 kW/m.

The same set of test conditions was used for each configuration. Only results of tests with the following peak power-to-flow ratio conditions will be discussed in this review:

- flooding rate: 2.29 cm/s (0.9 in./s);
- pressure: 2.8 bar;
- fluid inlet temperature: 53°C (127°F);
- peak linear power: 2.56 kW/m;
- initial cladding temperature: 871°C (1600°F).

### 6.1.3 Results

#### 6.1.3.1 Coplanar blockage

Figures 98 and 99 illustrate temperature variations on the central rod and a peripheral rod respectively, in the three configurations: A (blockage-free reference configuration), B (coplanar blockage with by-pass) and C (coplanar blockage without by-pass). Temperatures were measured at 1.93 m or 1.91 m respectively, approximately 3 cm to 5 cm downstream from the trailing edge of the blockage, centred at 1.85 m.

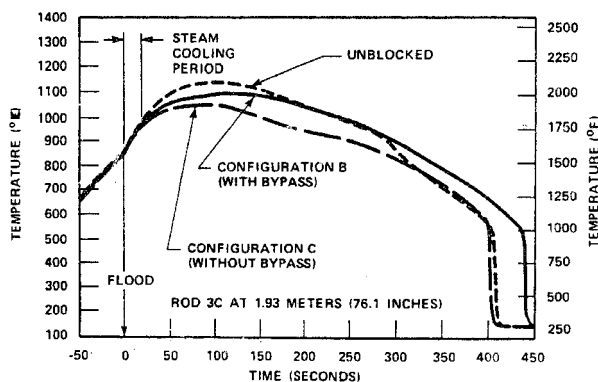


Figure 98: Central rod temperature for unblocked and coplanar blockage configurations.

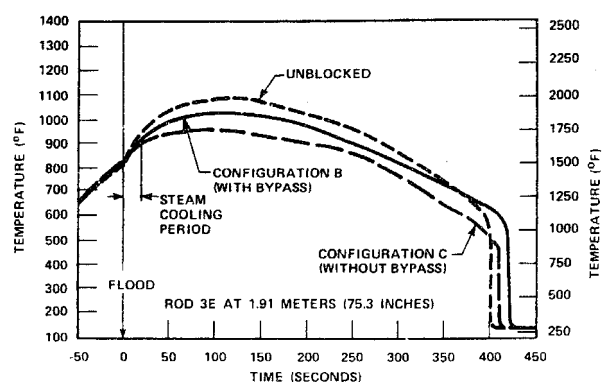


Figure 99: Peripheral rod temperature for unblocked and coplanar blockage configurations.

Following a short period of about 15 s after flood during which temperature variations appear undistinguishable (corresponding to the start of boiling at the assembly bottom), the temperature rise slows down in blockage configurations, particularly in the configuration without by-pass. This temperature reduction results from cooling generated by liquid droplets carried in the steam flow, which is even more pronounced when this flow is deprived of a by-pass. For the central rod, the difference in maximum temperatures approaches 100°C between the blockage-free configuration and the blockage configuration without by-pass, and about half that value between the blockage-free configuration and the blockage configuration with by-pass. However, for the latter configuration, the temperature after turnaround finally exceeds the temperature in the blockage-free configuration.

For the peripheral rod, temperature variations in the three configurations occur much in the same manner as for the central rod until in the vicinity of quenching. The temperature difference between the rods in both blocked configuration and the corresponding rods in the unblocked configuration is slightly greater than for the central rod, about 130°C at maximum value. In configuration B, the peripheral rod is located in the by-pass region and is thus subjected to a higher flow rate than the corresponding flow rate in the blockage-free test. Therefore, this peripheral rod

has a lower temperature than the corresponding rod in configuration A. In configuration C without by-pass, the peripheral rod does not benefit from this additional flow and its temperature would be expected to be higher than the corresponding rod in configuration B; the observation of an opposing result indicates that the cooling effect of the liquid droplets upon the balloon dominates the cooling effect of the by-pass flow.

The normalized heat transfer coefficient for the central rod in the coplanar blockage configurations (with and without a by-pass) as a function of the axial elevation in the blockage is shown in Figure 100 for various times after flood. The increase in heat transfer gradually subsides both as the distance increases downstream from the blockage and as the transient progresses. This last effect corresponds to a progressive slowing of the steam flow at the blockage inlet as the quench front rises, leading to a poorer entrainment of droplets and more importantly, a reduction in their fragmentation, which decreases heat transfers.

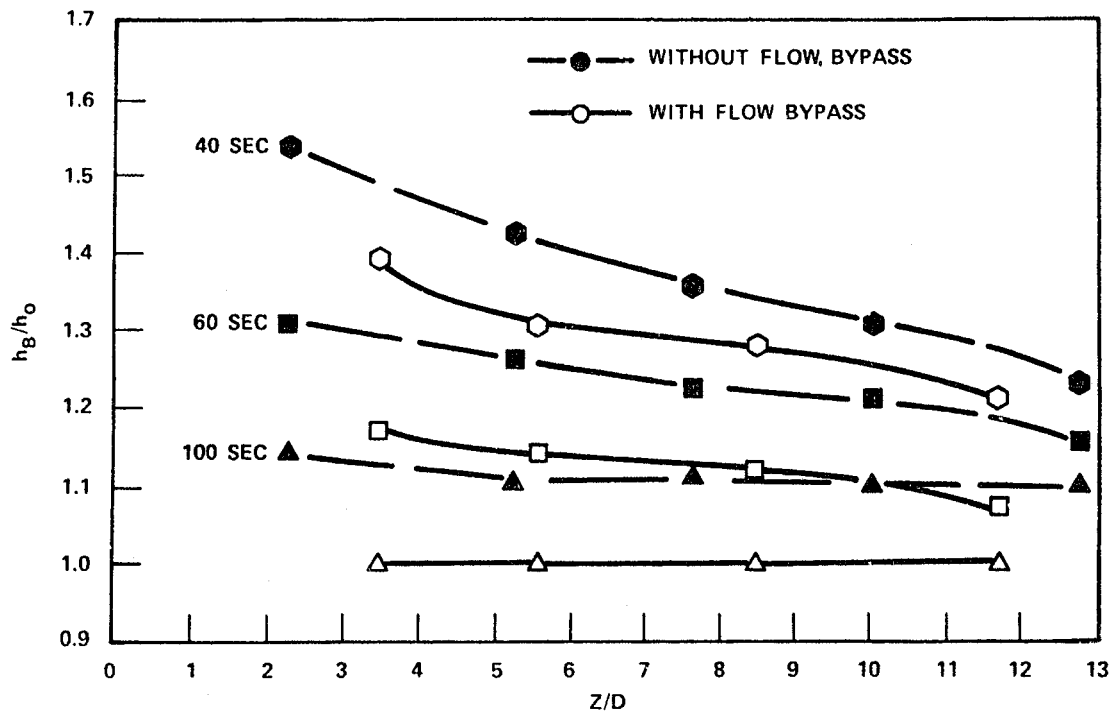


Figure 100: Normalized heat transfer coefficient for both coplanar blockage configurations.

### 6.1.3.2 Non-coplanar blockage

As mentioned above, balloons in non-coplanar configurations D, E and F were simulated with the same axial distribution.

In configuration D with short concentric sleeves, axial overlapping between sleeves of adjacent rods does not generally occur and the blockage ratio is rather low (< 13%). This blockage configuration is thus expected to have little effect upon heat transfers. It is nevertheless interesting to compare the temperature differences, illustrated in Figure 101, between the blockage-free configuration A and this configuration D on two adjacent rods (2D and 3C) with sleeves centred respectively at levels 1.78 m and 1.91 m. At the level 1.84 m - upstream from the sleeve on rod 3C and just downstream from the sleeve on rod 2D - the temperature on 3C can be as much as 43°C lower than the unblocked rod temperature, whereas for rod 2D, the temperature is only 13°C lower than the unblocked rod temperature (equivalent to 8°C after adjusting for initial temperature differences). This means that the flow redistribution around the 2D balloon improves heat transfer mainly on adjacent rods and to a slighter degree downstream from this rod. In the same way, temperature differences of as much as 56°C on rod 2D at higher levels of 1.88 m and 1.96 m are related to the effect of the 3C rod balloon.

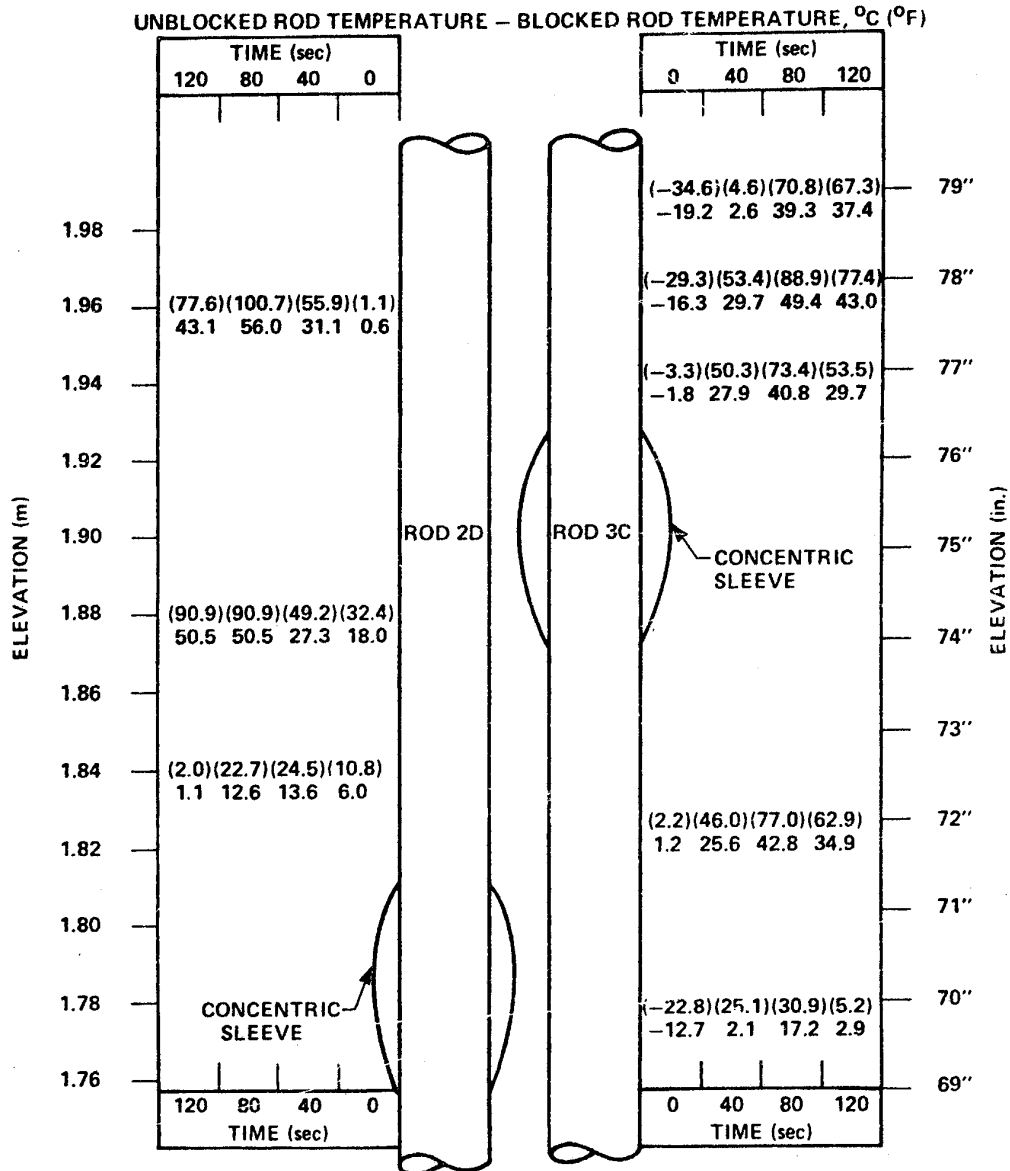


Figure 101: Rod temperature differences between non coplanar blockage and unblocked configuration for two rods.

It can also be expected that a short balloon in a non-coplanar blockage has a much less significant isolated effect upon the fragmentation of droplets in the adjacent sub-channel than for a coplanar blockage where this effect is reinforced by the neighbouring rod balloons. This is illustrated in Figure 102, which provides steam temperature variations at the blockage outlet level of 1.96 m and shows that the temperature is similar to that in the unblocked configuration. This indicates a poor steam de-superheating by the liquid droplets downstream from the blockage.

In configurations E and F with long non-concentric sleeves, there was considerable axial overlapping between balloons on adjacent rods and it was not possible to measure the temperatures within the blockage zone as it had been possible for configuration D. Only temperatures downstream from the blockage were measured. Figure 103, which compares steam temperature variations at the blockage outlet for configurations A, E and F, reveals considerable vapour de-superheating in blockage F in which the balloons have the greatest circumferential strain (44%). This de-superheating is a result of greater droplet break-up and evaporation when passing through the blockage.

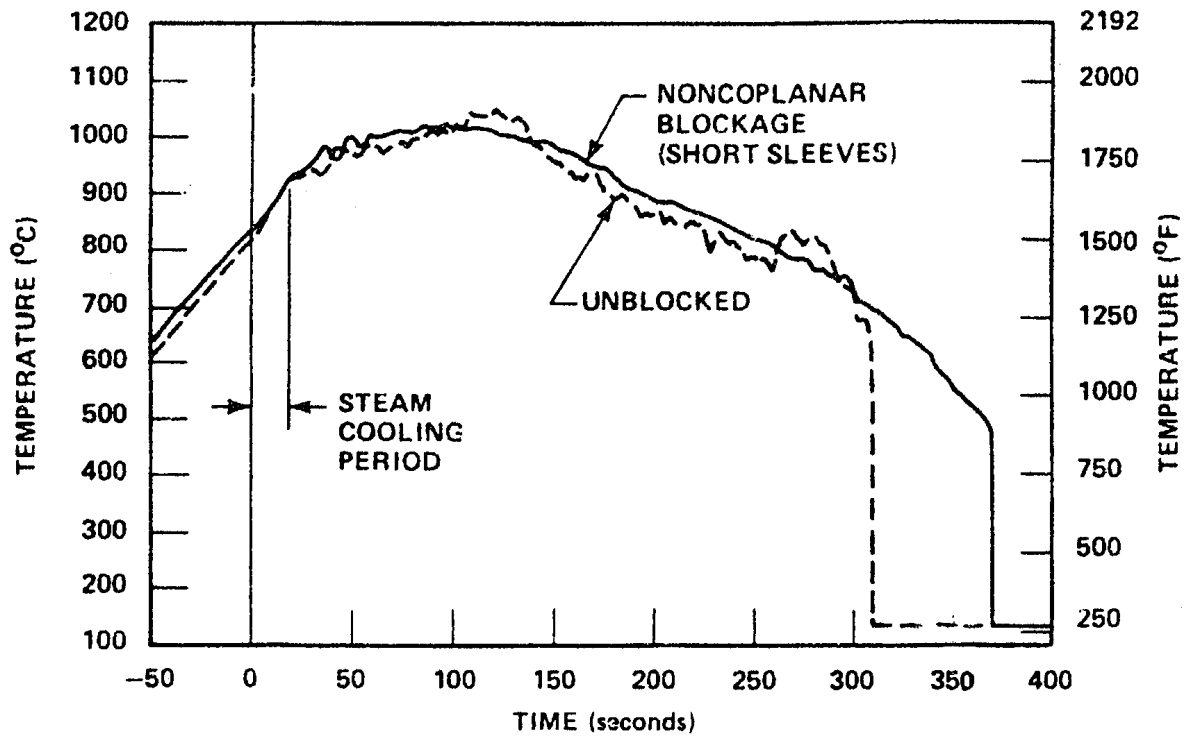


Figure 102: Vapour temperatures for unblocked and non coplanar blockage (short sleeve) configurations.

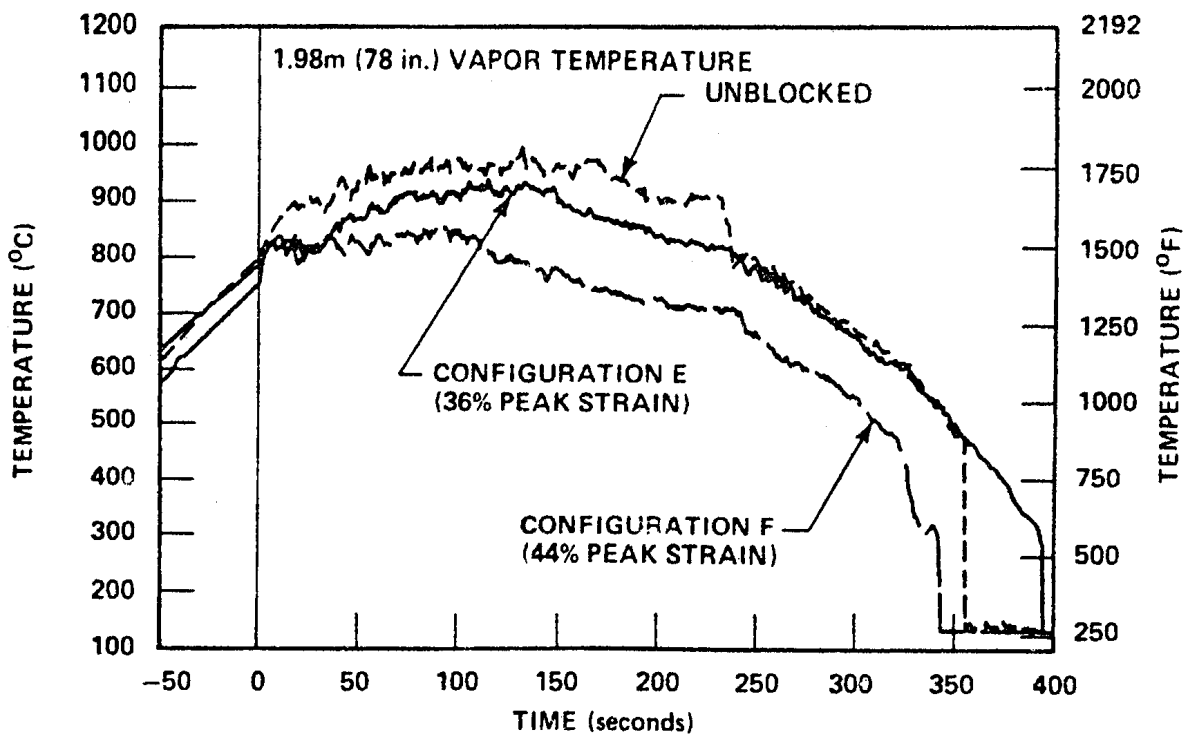


Figure 103: Vapour temperatures for unblocked and non coplanar blockage (long sleeve) configurations.

Figure 104 shows the heat transfer coefficient at the blockage outlet in the sub-channel with the maximum local blockage ratio (93% in configuration F) and reveals an increase in heat transfers during the entire transient in configuration F ( $\epsilon_{\max} = 44\%$ ), whereas the heat transfer increase only lasts the first 120 s in configuration E ( $\epsilon_{\max} = 36\%$ ). Therefore, it appears that configuration E would be more detrimental than configuration F in terms of heat transfer.

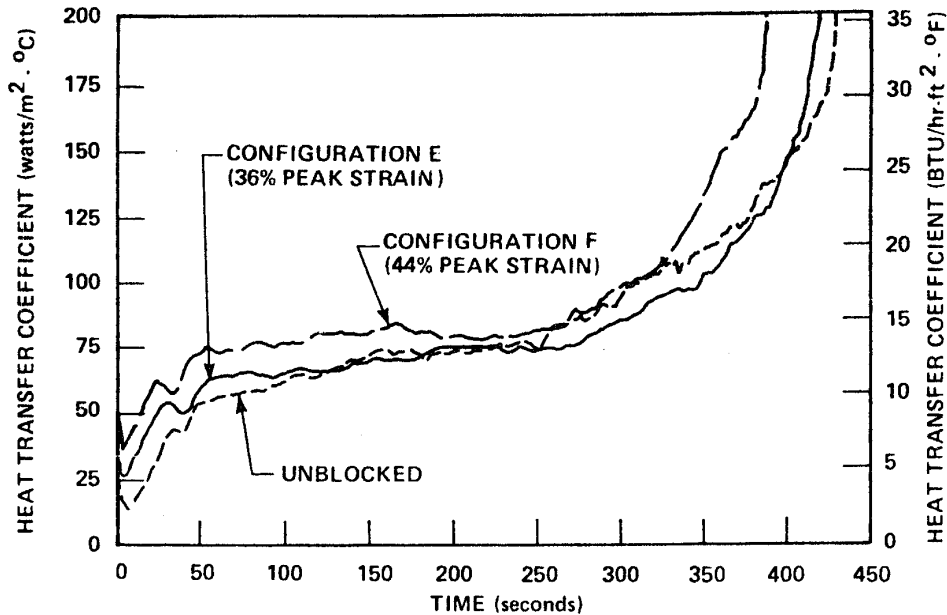


Figure 104: Heat transfer coefficient for unblocked and non coplanar blockage (long sleeve) configurations.

Figure 105 illustrates the heat transfer coefficient variations obtained under similar conditions for coplanar configurations B and C, and does not reveal any significant differences between coplanar and non-coplanar configurations for at least the first 250 s of the transient.

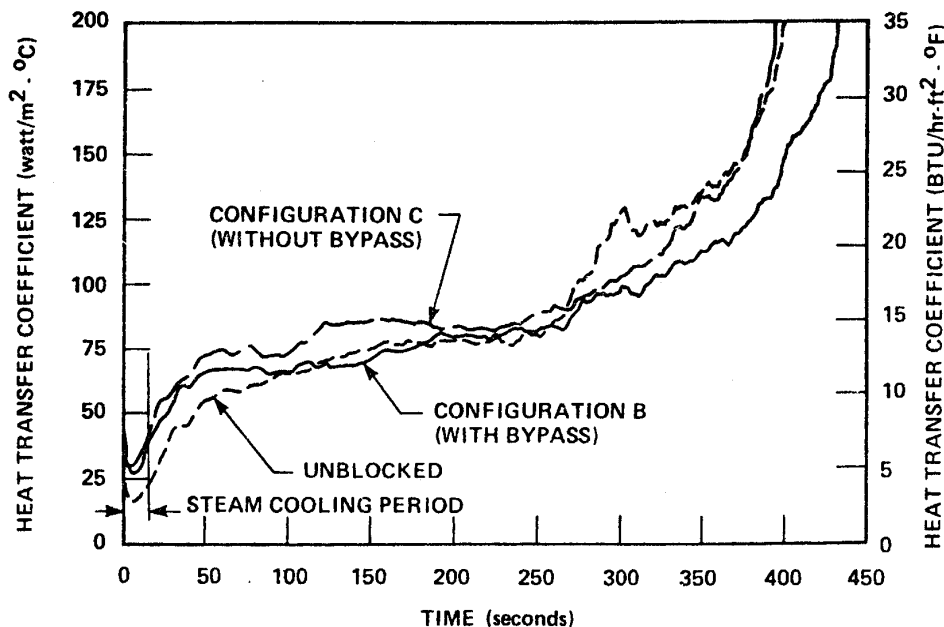


Figure 105: Heat transfer coefficient for unblocked and coplanar blockage configurations.

Tests results of the 21-rod bundle with flow blockage were used to develop a blockage heat transfer model. This model was then assessed through comparison and analysis of the 163-rod blocked bundle test results.

## 6.2 Tests performed on a 163 fuel rod array

Using a single-phase flow redistribution and heat transfer data from the least favourable 21-rod bundle blockage configuration, preliminary calculations performed with the COBRA-IV-I code for the 163 rod array revealed that the detrimental effect of the flow by-pass could possibly overrule the beneficial effect of the heat transfer improvement in the blockage, such that a net penalty could occur. In the continuation of the 21-rod array tests, a series of forced and gravity reflood tests were thus conducted on a 163-rod array, whose dimensions were typical of a PWR fuel assembly. The purpose of these tests was to evaluate the possible additional effects of an ample flow by-pass based on the most detrimental 21-rod bundle blockage configuration in terms of heat transfer.

### 6.2.1 Experimental characteristics

The 163-rod array test facility was very similar to that used in the 161-rod array (blockage-free) test program, in which two guide tubes were replaced with two heater rods.

Figure 106 provides a schematic cross-section of the test section with the blockage located in two 21-rod islands (two rods shared by both islands). Long non-concentric sleeves were placed on the heater rods of these two islands in the non-coplanar configuration of 21-rod bundle tests. Configuration F was chosen, which corresponds to the maximum blockage ratio (an average of 30% in the islands at level 1.85 m), even though it had been previously shown that this configuration was not the most detrimental in terms of heat transfer.

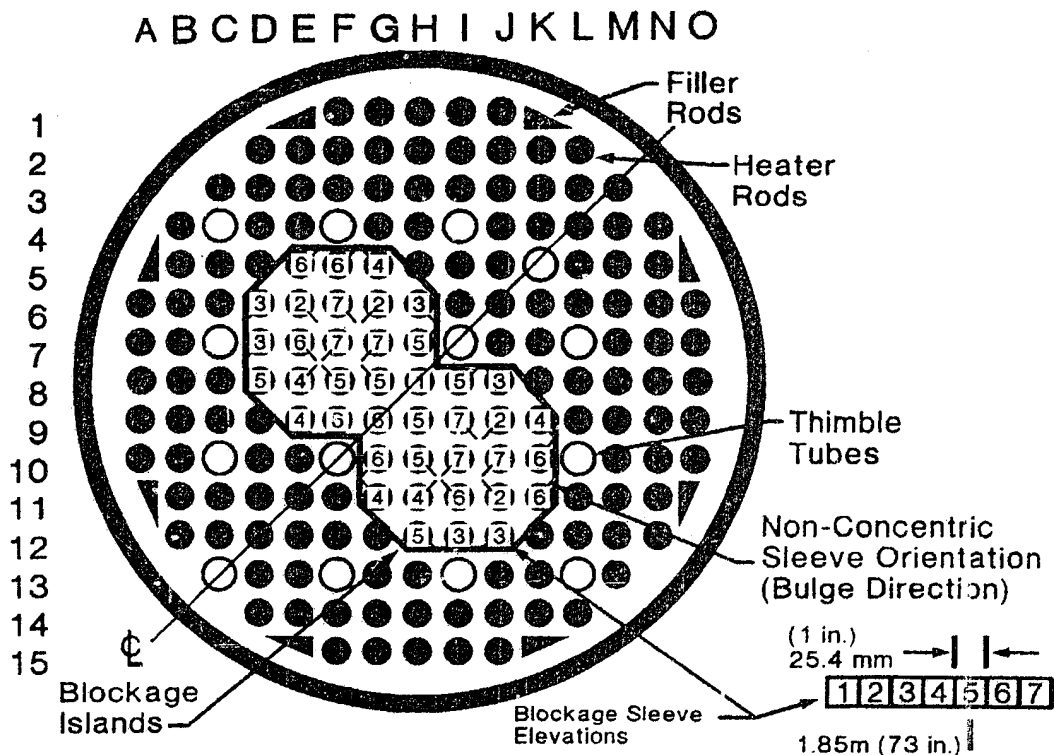


Figure 106: 163-rod bundle cross section.

In the 163-rod blocked bundle test program, 17 forced reflood tests and 2 gravity reflood tests were performed with the following range of parameters:

- flooding rate: from 1.52 cm/s (0.6 in./s) to 15.2 cm/s (6 in./s);
- pressure: from 1.4 bar to 4.2 bar;
- fluid inlet temperature: from 53°C (127°F) to 122°C (252°F);
- initial linear power: from 1.3 kW/m to 3.3 kW/m;
- initial cladding temperature : from 260°C to 871°C.

The 163-rod blocked bundle test conditions were chosen identical to the 161-rod unblocked bundle test conditions in order to allow comparisons of test results on a one-to-one basis.

## 6.2.2 Results

Figures 107 and 108 provide two examples of variations in cladding temperatures and blockage heat transfer coefficients, in comparison with unblocked bundle tests for reflood rates of 3.8 and 2 cm/s. A slight improvement in heat transfer is observed during the first 120 seconds of the transient, which is sufficient to reduce the maximum temperature in comparison to the blockage-free configuration. However, rewetting in the blocked configuration occurs later, or at best at the same time, in comparison to the blockage-free configuration.

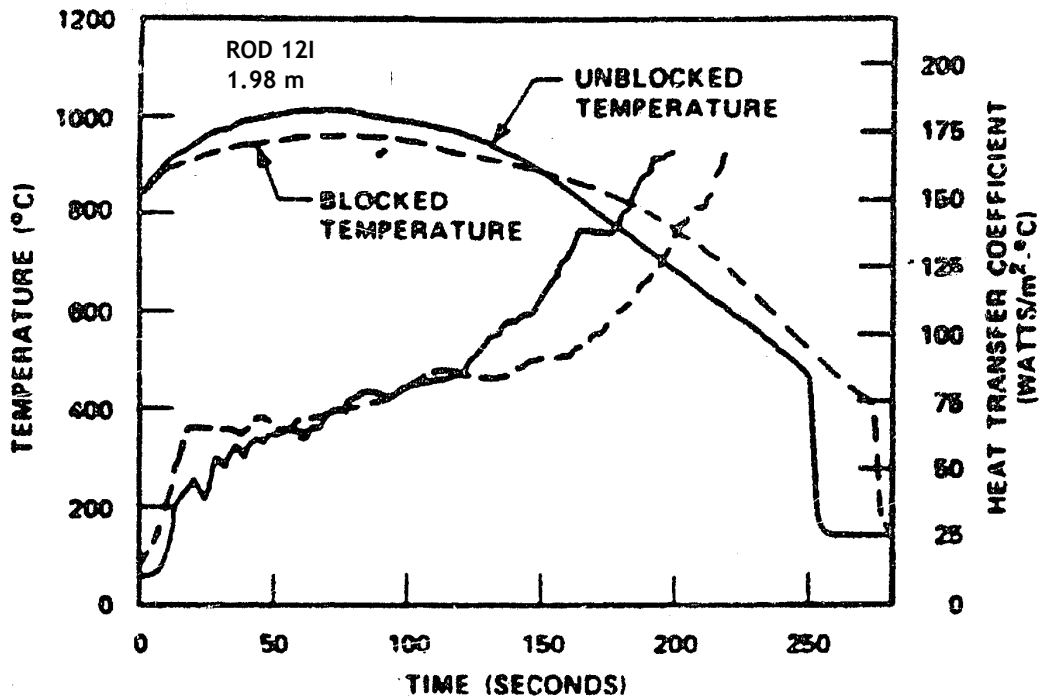


Figure 107: 163-Rod Bundle - Rod temperature and heat transfer coefficient for blocked and unblocked bundles at 38.1 mm/s flooding rate and 1.98 m elevation.

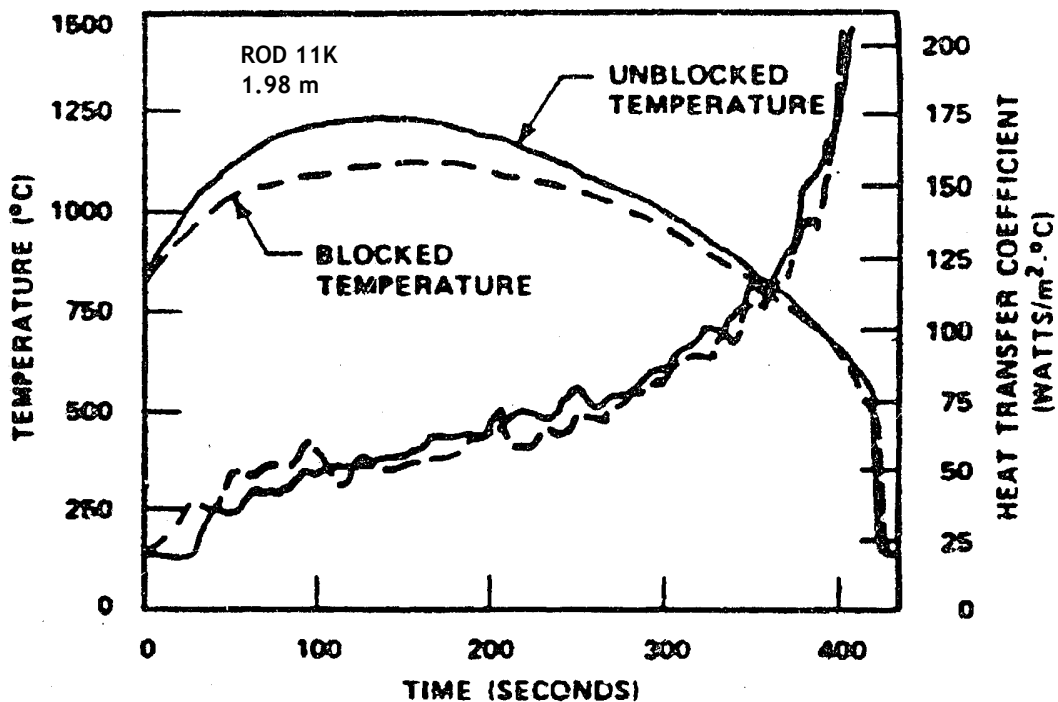


Figure 108: 163-rod Bundle - Rod temperature and heat transfer coefficient for blocked and unblocked bundles at 20.3 mm/s flooding rate and 1.98 m elevation.

Figure 109 provides vapour temperature variations at the blockage outlet level ( $z=1.98$  m) for two sub-channels located in the blockage and two located in the by-pass. Temperatures in the blockage (1,2) are lower than those in the by-pass (3,4) during the first 100 seconds, but this situation reverses after turnaround at about 150 s: early in the transient the effect of steam desuperheating due to liquid droplets is dominant, whereas late in the transient the effect of the flow by-pass becomes dominant, with a reduced steam velocity and poorer droplet break-up.

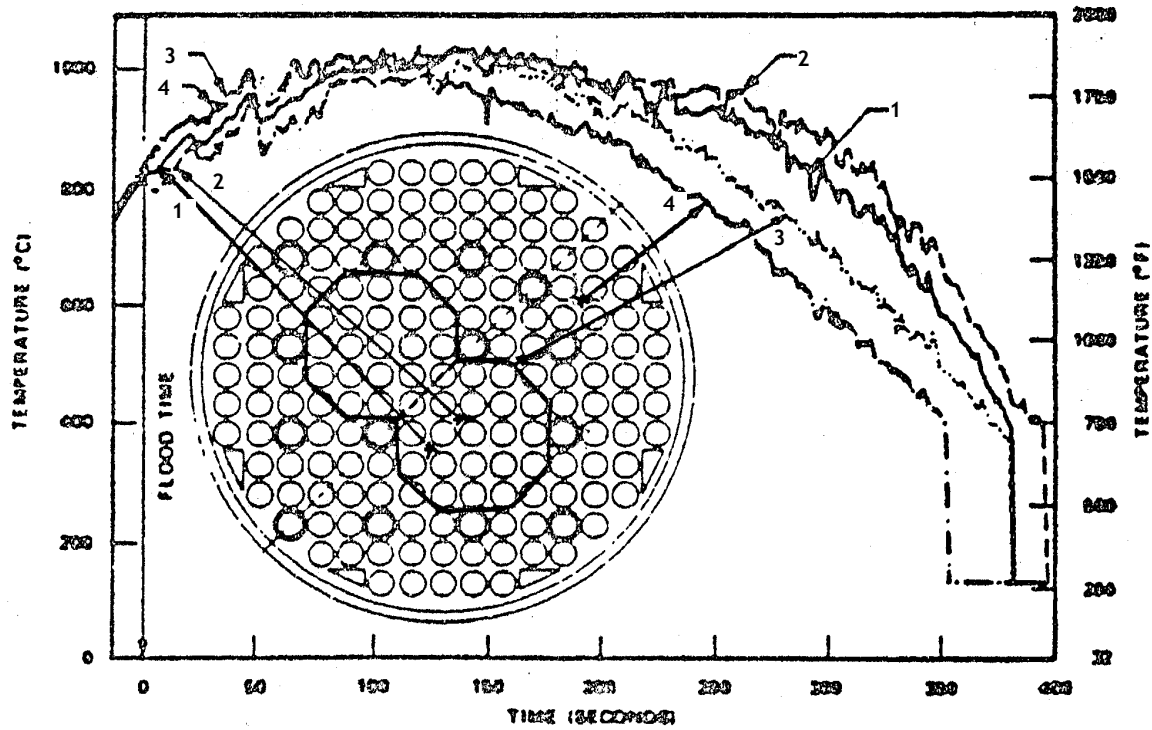


Figure 109: Vapour radial temperature distribution as a function of time.

Figure 110 illustrates the differences in maximum temperature rises between unblocked and blocked bundles, defined by:

$$\text{Maximum Temperature Rise Difference} = (T_{\max} - T_{\text{init}})_{\text{unblocked}} - (T_{\max} - T_{\text{init}})_{\text{blocked}}$$

as a function of the power-to-flow ratio and at different axial levels downstream from the blockage (immediately downstream from the blockage and in the next two grid spans), for 21 and 163-rod bundle tests.

The following phenomena were observed:

- The temperature rise difference, which is always positive, is greater in the 21-rod array than in the 163-rod array. The favourable effect of the blockage is therefore poorer in the 163-rod bundle, owing to the detrimental effect of the flow by-pass, which is not present in the 21-rod configuration F.
- The temperature rise difference tends to increase as the flooding rate decreases, indicating that the cooling effect induced by the blockage is as good as the reflood rate is low. This is in fact a relative effect: as the flooding rate decreases, the overall heat transfer level decreases and any improvement in heat transfer via droplet entrainment and fragmentation tends to have more effect.
- The temperature rise difference decreases as the distance downstream from the blockage increases, therefore the difference between blocked and non-blocked configurations decreases downstream, as is generally observed for a grid or other singularities.

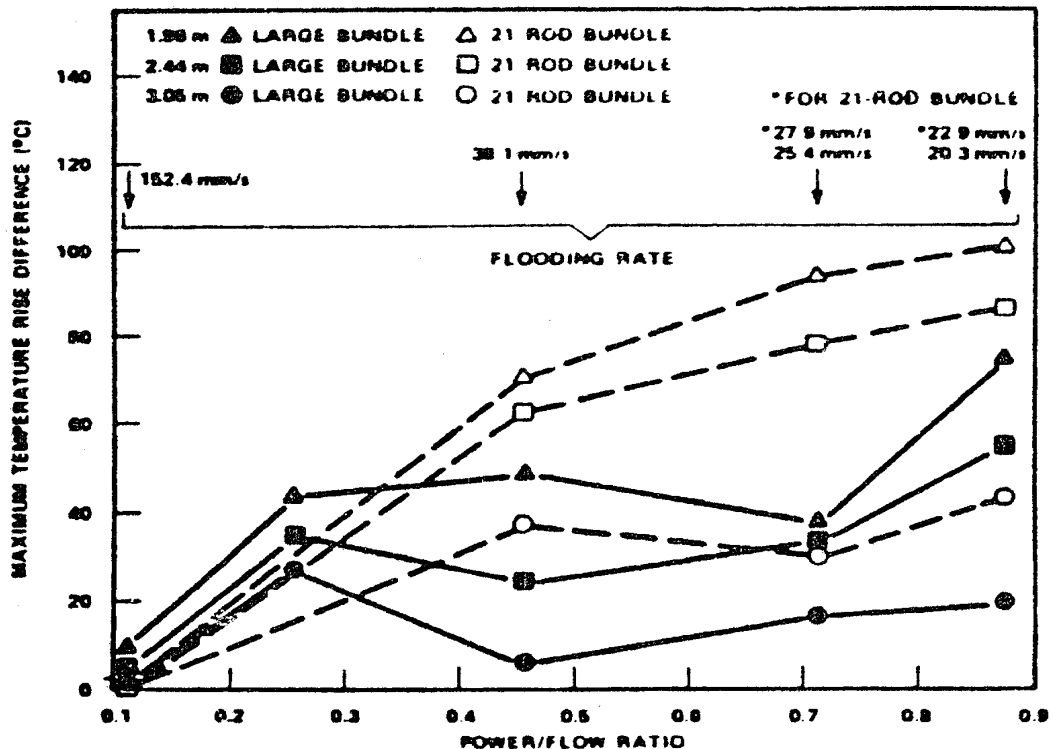


Figure 110: Maximum temperature rise difference between blocked and unblocked bundles as a function of flooding rate and elevation.

From 163-rod array test results, it was concluded that the beneficial effect of the blockage upon the increase in heat transfer remains sufficiently dominant, at least at the beginning of the transient, to compensate the detrimental effect of the flow by-pass, and produces lower maximum temperatures in comparison to those obtained in a blockage-free configuration.

### 6.3 Analysis of results using the COBRA-TF code

As previously pointed out, an important objective of the FLECHT SEASET program was to develop analytical models that could be used to evaluate the effect of a blockage in reactor calculations. A mechanistic approach combining a physically-based model for blockage heat transfers with an advanced two-phase flow computer code was chosen for evaluation purposes.

The COBRA-TF code was selected, which was briefly described in § 2.4.1 concerning the analytical simulation of FEBA and SEFLEX tests. It should be pointed out that data from FEBA tests were used in combination with data from FLECHT-SEASET tests to develop and validate COBRA-TF blockage models.

The hydrodynamic effects of the blockage, i.e. the flow diversion around the partially blocked region, can be directly handled by the momentum balance equations already in COBRA-TF, with only the input of the blockage hydraulic characteristics. This information was available from the FLECHT SEASET hydraulic tests for example.

Models were specifically developed to deal with heat transfer enhancement phenomena in the blockage, such as:

- The single-phase convective enhancement under dispersed flow film boiling or inverted annular film boiling;
- Heat transfer via the impact of droplets on the blockage walls;
- Droplet break-up in the blockage; the droplet fragmentation model, based on a coplanar blockage, was extended to the non-coplanar blockage configuration.

A key feature of blockage heat transfer modelling in the COBRA-TF computer code was the integration of an additional field to account for the fine liquid droplets shattered by impact with the blockage walls, in order to handle the increased evaporation of these droplets.

### 6.3.1 Comparison with 21 rod array test results

Figure 111 compares experimental values with cladding axial temperature distributions calculated by COBRA-TF at 60 seconds for a coplanar blockage test with short concentric balloons (configuration C). Experimental and calculated values correspond very well. Figure 112 provides a similar comparison of axial distributions of steam temperatures, showing satisfactory agreement between experimental and calculated values (low experimental values indicate early rewetting of the steam thermocouple).

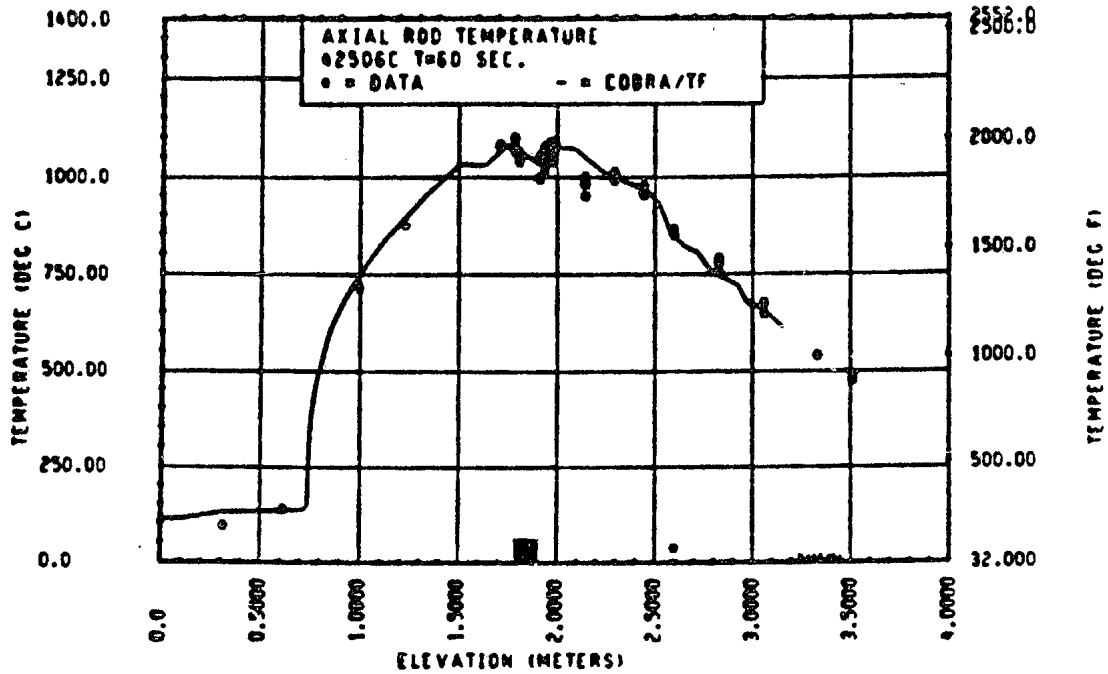


Figure 111: Comparison of COBRA-TF calculated axial rod temperature versus elevation with FLECHT-SEASET 21-rod data, Run 42506C, t=60 s.

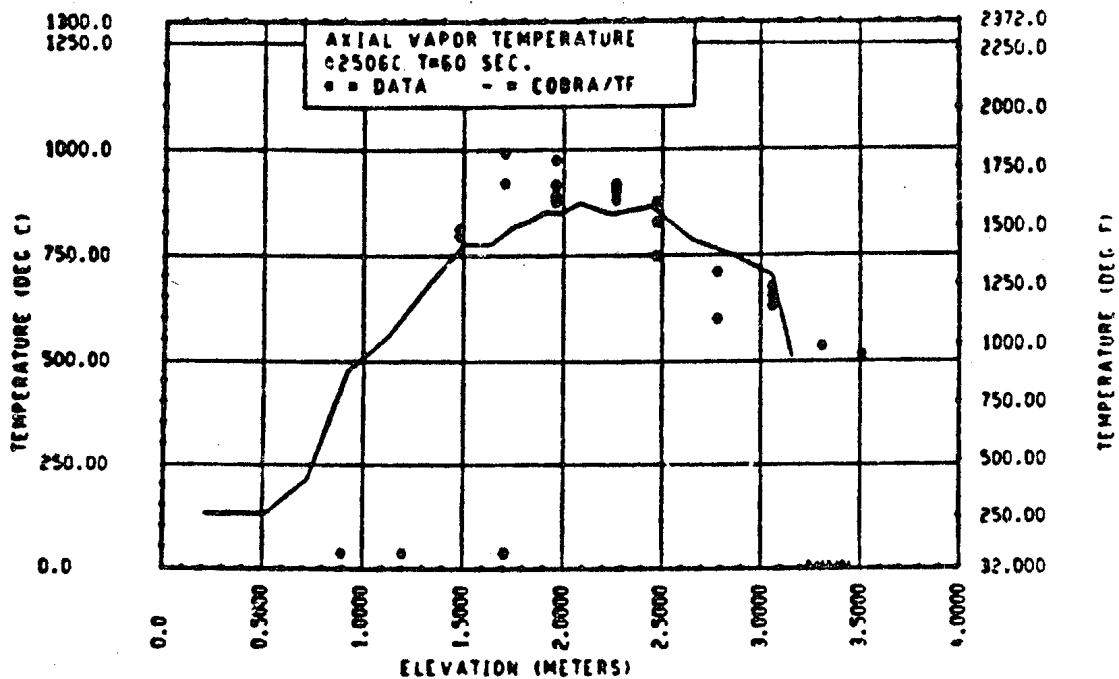


Figure 112: Comparison of COBRA-TF calculated axial vapour temperature versus elevation with FLECHT-SEASET 21-rod data, Run 42506C, t=60 s.

Similar comparisons are illustrated in Figures 113 and 114 for a non-coplanar blockage test with long non-concentric balloons (configuration F), once again showing satisfactory agreement between experimental and calculated values, which justifies applying the coplanar blockage models to non-coplanar blockages.

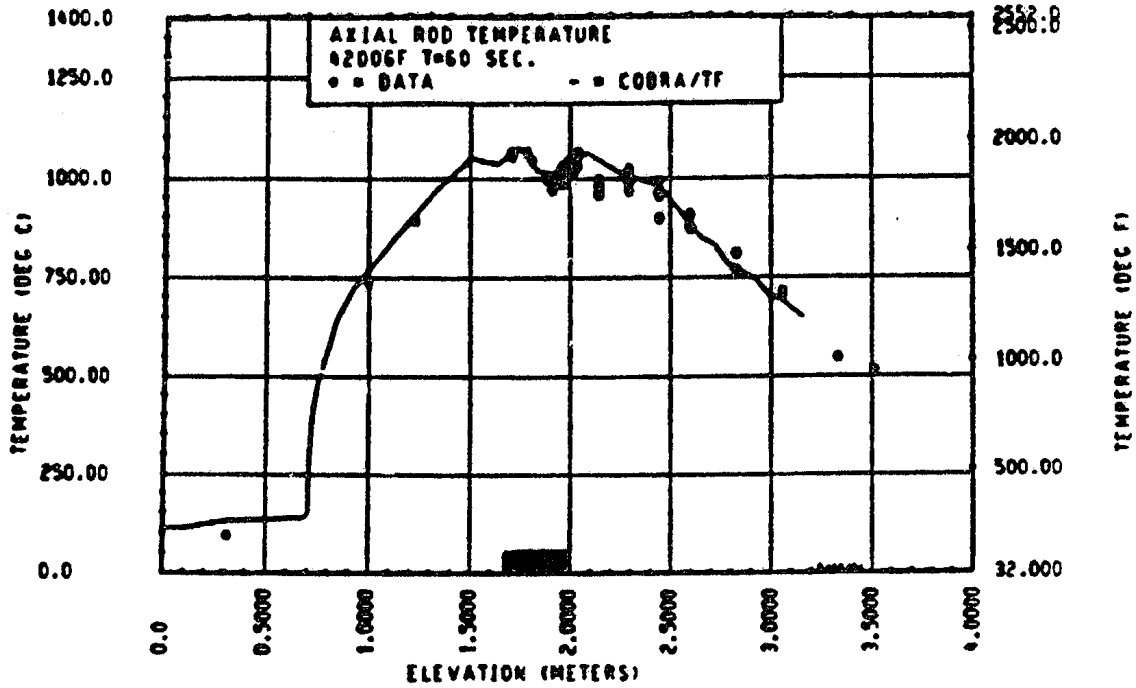


Figure 113: Comparison of COBRA-TF calculated axial rod temperature versus elevation with FLECHT-SEASET 21-rod data, Run 42006F, t=60 s.

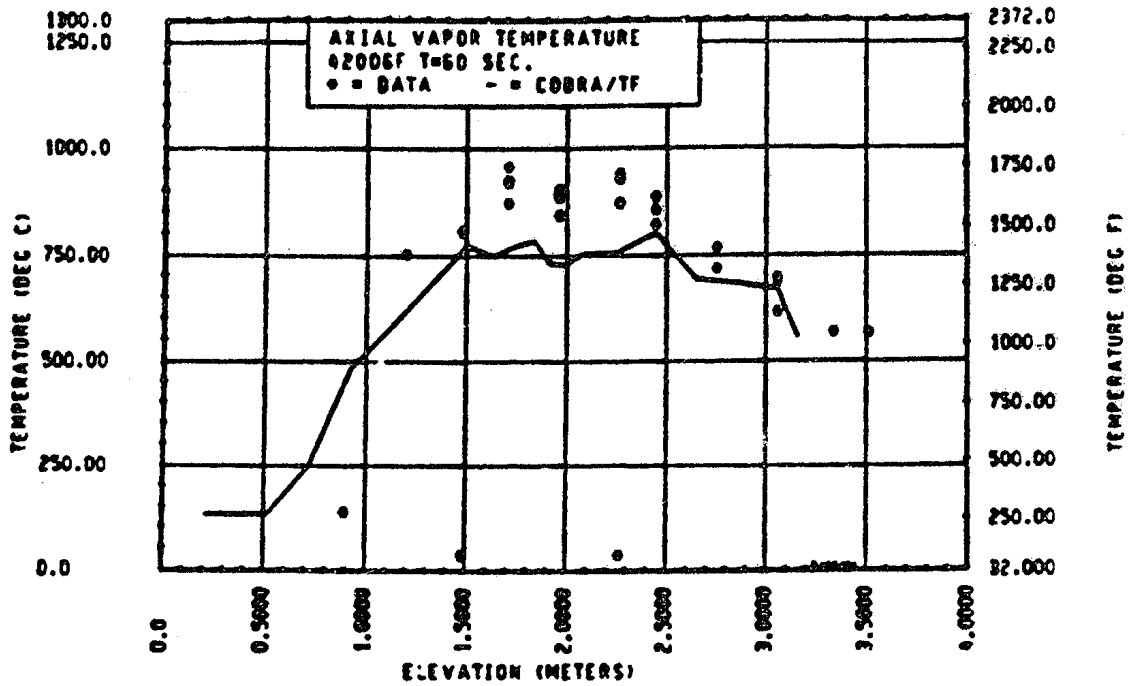


Figure 114: Comparison of COBRA-TF calculated axial vapour temperature versus elevation with FLECHT-SEASET 21-rod data, Run 425006F, t=60 s.

### 6.3.2 Comparison with 163 rod array test results

COBRA-TF predictions were then compared with 163-rod blocked bundle test results, without any change in the blockage models used in 21-rod calculations; thus the 163-rod data provide a true verification of the blockage models.

By way of example, Figures 115 and 116 provide a comparison of model predictions with corresponding experimental values of cladding and steam axial temperature distributions in a blocked island at 100 seconds. Calculations and experimental results correspond as well as they did for the 21-rod array configuration.

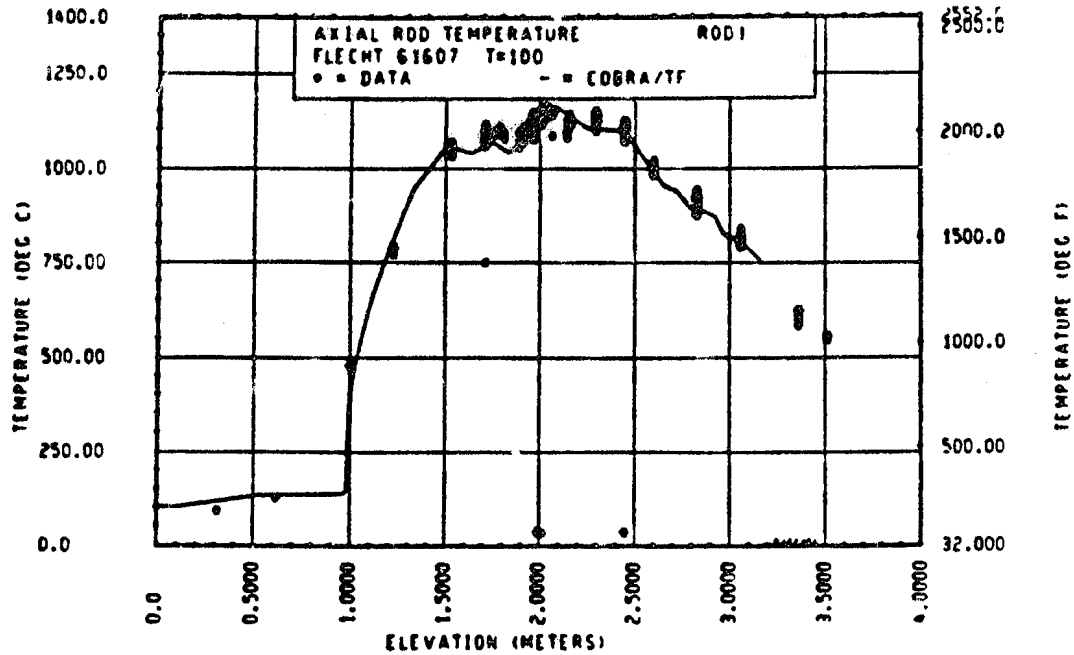


Figure 115: Comparison of COBRA-TF calculated axial rod temperature versus elevation with FLECHT-SEASET 163-rod data, Run 61607, t=100 s, Rod 1.

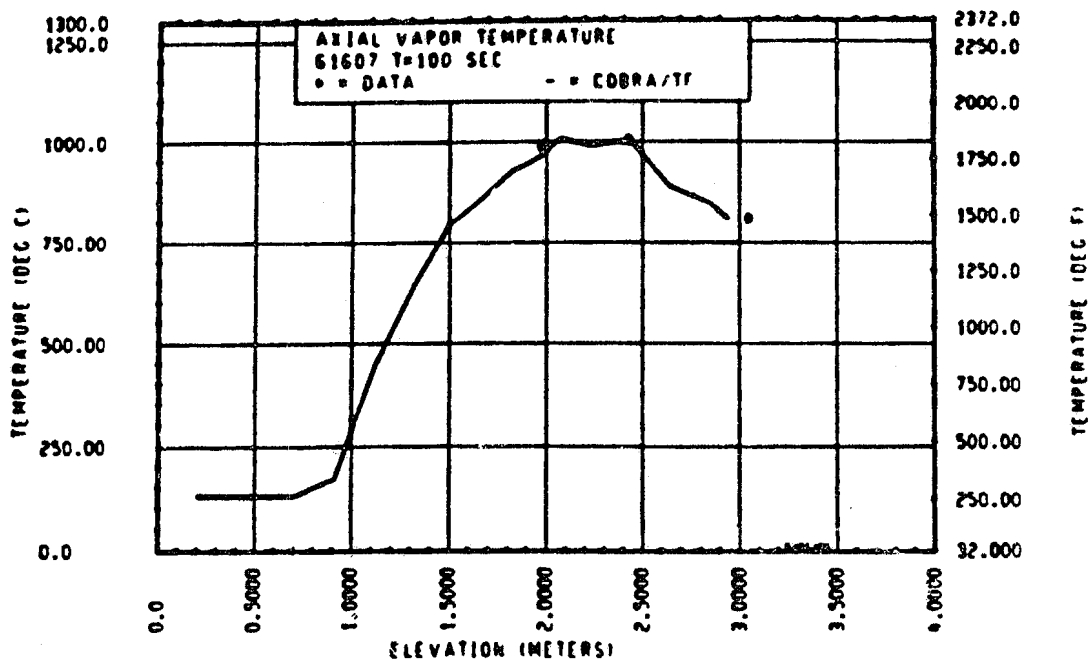


Figure 116: Comparison of COBRA-TF calculated axial vapour temperature versus elevation with FLECHT-SEASET 163-rod data, Run 61607, t=100 s, Rod 1.

These blockage models - developed from tests performed with regular balloon geometries - are believed to produce conservative predictions in comparison to a real reactor situation where irregular balloon geometries resulting from cladding burst with torn edges will increase heat transfers compared to smooth sleeves used in experimental simulations.

#### **6.4 FLECHT SEASET flow blockage program conclusions**

Blockage tests carried out in the FLECHT SEASET program mainly focused on assessing the conservative aspect of the Appendix K rule with regard to the evaluation of heat transfers during reflood of a partially blocked assembly. In this respect, FLECHT SEASET 21-rod array test results - backed up by FEBA 25-rod array test results - highlighted the importance of considering the two-phase nature of the flow and the considerable influence of the liquid droplets field via:

- The entrainment of droplets in the steam flux, even at low reflood rates (2.5 cm/s), which are swept into the blockage region when they have sufficient inertia;
- The shattering of these droplets on balloon surfaces, creating finer droplets, more easily evaporated, hence increasing steam de-superheating and surface heat transfer both in and downstream from the blockage.

The FLECHT SEASET 163-rod blocked array tests (with a significant flow by-pass) confirmed the 21-rod array test results, illustrating that the beneficial effects resulting from the increase in blockage heat transfer override the penalty of flow diversion in the by-pass, which produced maximum temperatures below those obtained in blockage-free tests under comparable conditions.

Identification of the dominating physical process related to the influence of droplets was corroborated through 1) the development of blockage models based on 21-rod test results, 2) integration of such models into the COBRA-TF code and 3) analysis of 21- and 163-rod tests showing satisfactory agreement between model calculations and experimental values. The physical modelling of the blockage in the COBRA-TF code was thus believed to provide a correct representation of actual flow blockage behavior.

It was therefore concluded in the final report [11] that the 1) blockage test results, 2) mechanistic models developed for COBRA-TF and 3) analysis conducted with this code, formed a solid basis for the revision of Appendix K requirements concerning flow blockage heat transfer, clearly in view of cancelling the steam cooling rule.

From a R&D point of view, it would have been very valuable if the FLECHT-SEASET flow blockage program, besides demonstrating the conservatism of Appendix K rule, had more thoroughly investigated the differences between test results with unique particularities (concentric/ non-concentric balloons, coplanar/ non-coplanar configurations).

Furthermore, the rather low blockage ratios and balloon lengths pointed to - in the light of previously discussed program test results - the expected result concerning the reduction in maximum rod temperatures in the blockage region.

## 7 CONCLUSION

A State-Of-the-Art review focusing on the question of the coolability under accidental LOCA conditions of a rod assembly containing a partial blockage in a group of ballooned fuel rods has now been compiled.

Vast experimental programs have been devoted to answering this question, all of which have focused on large-break LOCA scenarios and more particularly on blockage cooling under reflood conditions.

Examination of the main programs discussed in this document has helped establish a more global understanding of the physical processes involved in such a situation, which have been summarised below.

### 7.1 *Data obtained from experimental programs*

Temperature variations in and downstream from a blockage region in a fuel rod assembly due to cladding deformation during a LOCA transient are generally conditioned by heat transfers taking place at the beginning of the reflood phase with two-phase mist flow conditions. A blockage induces antagonistic effects whose relative significance depends on the geometrical conditions of the blockage and its by-pass, as well as the thermohydraulic conditions of the reflood. These effects result from the following physical phenomena:

- Reduction of the flow passage in the blockage leads to flow redistribution towards the by-pass, therefore reducing the mass flow in blockage sub-channels. For sufficiently long blockages ( $\geq 200$  mm), the reduction in the steam flow is approximately proportional to the reduction in the cross-sectional area. This reduction in the coolant flow therefore tends to restrict blockage coolability.
- However, in a two-phase flow, the inertia of droplets favours blockage penetration, particularly if the quench front is sufficiently far off, enabling the acceleration of these droplets in steam. Inside the blockage, the liquid droplets are dispersed due to their impact on the blockage surfaces, fragmented and re-entrained in the form of finer droplets, which significantly increases heat transfer with steam. This desuperheating of steam, associated with the increase in turbulence, improves the coolability of the blockage surfaces.
- At the blockage outlet, the deceleration of the steam flow in the widening section can cause bigger droplets to fall under gravity onto the hot blockage surfaces, thereby leading to dispersion and evaporation in steam jets, which once again leads to an accentuated cooling in the region.

In the programs discussed in this state-of-the-art review, the experimental characteristics - particularly blockage dimensions (blockage ratio, length of maximum blockage region and tapered regions, cladding balloon thickness, configuration, etc.) - and initial test conditions reveal the relative importance of each beneficial or detrimental phenomenon indicated above and consequently, their influence upon test results. This review has attempted to compile the most relevant information from these different programs, which has been classified by phenomenological features below.

#### 7.1.1 Blockage representativity

FEBA blockage tests and CEGB blockage 2 tests were simulated using thick sleeves ( $> 2$  mm), whereas balloons in all other blockage tests had a reduced thickness that was more representative of the rod cladding thickness after the swelling phase of an hypothetical LOCA transient.

Comparison of balloon temperature variations between FEBA and SEFLEX tests with 90% blockage clearly revealed early rewetting of SEFLEX balloons in comparison to FEBA balloons. This is a result of a much lower thermal capacity of the balloon cladding and its much greater thermal decoupling with the heater rod. Rewetting is then propagated via secondary quench fronts upstream and downstream from the blockage, leading to the early rewetting of the portions of the rods close to the balloon in comparison to an unblocked bundle. A similar trend was also observed in the comparison between CEGB Blockage 3 and Blockage 2 tests, though not as spectacular in terms of balloon rewetting owing to the more "severe" reflood conditions.

These observations highlight the substantial conservatism of FEBA test results, whose main interest lies in the comparative results with different blockage ratios and blockage configurations (blockage with or without by-pass, successive blockages).

### 7.1.2 Effect of blockage ratio

The effect of blockage ratio can be evaluated using both FEBA and THETIS test results.

For FEBA 62% blockage tests, blockage surface temperatures in and downstream from the blockage are always noticeably lower than cladding temperatures in the by-pass at the same level. For FEBA 90% blockages, sleeve temperatures in the blockage are lower than those of the claddings in the by-pass, except during the 30 seconds preceding rewetting for the test with a reflood rate of 3.8 cm/s, where sleeve rewetting is slightly delayed. Downstream from the blockage, the peak cladding temperature on the blocked rods appears to be slightly higher (~40 °C) than on the by-pass rods, with this difference accentuating up to about 100 °C during the cooldown preceding rewetting. However, compared to a blockage-free test under the same conditions, the maximum temperature at turnaround is no higher. Comparing rewetting times of blockage balloons with those of by-pass rods is irrelevant due to the non-representative thermal capacity of the balloons used in these tests; the same applies just downstream from the blockage due to the effect of axial conduction in the cladding under the blockage sleeves.

FEBA test results therefore indicate that a 62% blockage is better cooled than a blockage-free assembly. For a 90% blockage, results showed that the temperature penalty is moderate and, in the light of results from the more representative SEFLEX tests, it seems that a 90% blockage remains fully coolable. This widely admitted conclusion must nevertheless be put into perspective in consideration of FEBA and SEFLEX blockage lengths (65 mm) and test conditions (particularly the reflood rates  $\geq 3.8$  cm/s), which do not combine the most severe conditions.

THETIS tests, performed with markedly longer blockages (maximum blockage length of 200 mm) using an analytical separate-effects approach with a wide variation range of the main parameters, help clarify the coolability limits of severe blockages (80% and 90%) under penalizing reflood conditions. In this respect, the series of forced reflood tests simulating a 90% blockage with a pressure of 2 bar and an inlet temperature of 90 °C provided the following observations:

- With a 3 cm/s reflood rate, the blockage was found to be coolable, with the maximum blockage temperature not exceeding the by-pass temperature by more than 60 °C.
- With a 2 cm/s reflood rate, the maximum blockage temperature rose above the facility operating limit, which made it necessary to run down the power before the complete cooling of the blockage was achieved. It may therefore be thought that these test conditions do not permit suitable blockage cooling.

THETIS test results therefore seem to imply that a long 90% blockage may no longer be coolable at a constant reflood rate below 2 to 3 cm/s.

When comparing results of tests performed with 90% and 80% blockages under similar conditions, it became apparent that an 80% blockage is more efficiently cooled at high reflood rates. However, differences tended to be minor, sometimes proving to be even better for the 90% blockage with intermediate reflood rates that are most relevant to reactor safety analysis. These results therefore reveal that the blockage ratio of 90% - considered as an upper bound value of the flow blockage ratio possibly obtained under a LOCA with a fresh fuel assembly - does not necessarily represent the most penalising case in terms of coolability for extended axial deformations such as those simulated in the THETIS experiments.

### 7.1.3 Effect of the blockage length

Only CEGB program results in which both short and long blockages tests were performed can be used to directly evaluate the effect of the blockage length. From these results, it was asserted that short blockages are always better cooled in the middle of the blockage sleeve in comparison to the by-pass. This was not the case for long blockage sleeves, except during the first few seconds preceding rewetting in Blockage 3, owing to the propagation of secondary quench fronts.

Indication of the effect of the blockage length can be indirectly induced from FEBA tests containing two successive blockages (90% followed by 62%). A noticeable reduction in cladding temperatures just at the outlet of the 62% blockage was observed in comparison to temperatures in the by-pass at the same level. However, this trend reverses towards the bottom of the blockage where cladding

temperatures of the blockage rod array once again rise above those in the by-pass 200 mm downstream from the second blockage, which highlights behavior that may be penalizing in the event of long balloons.

The effect of the blockage length largely depends on the penetration and length of influence of the droplets in the maximum blocked region. In a short blockage, the droplet penetration is easy and the cooling effect up to the blockage outlet lasts throughout the entire transient. In a long blockage, the droplet penetration is more difficult, particularly when droplets slow down with the quench front rise, which can lead to the dry-out of the coolant flow in the blockage and result in a rapid rise in both steam and balloon cladding temperatures. This process involving droplet penetration and coolant dry-out greatly depends on the blockage ratio and test conditions, such as reflood rates and linear power.

#### 7.1.4 Effect of blockage configurations: coplanar or non-coplanar

The effect of a non-coplanar configuration in comparison to a coplanar configuration was explored only in the FLECHT SEASET program where a non-coplanar configuration was tested.

For a non-coplanar blockage containing short balloons with little axial overlapping, flow redistribution around a balloon increases local turbulence and therefore improves the coolability of neighbouring rods. However, it seems that the isolated effect of a short balloon in a non-coplanar blockage upon droplet fragmentation in the adjacent sub-channel is much poorer than for a coplanar blockage where this effect is reinforced by the neighbouring rod balloons, which leads to a poorer de-superheating of steam.

For a non-coplanar blockage with long balloons, implying considerable axial overlapping, the effect is more difficult to evaluate and comparison with coplanar configurations becomes problematic, these coplanar configurations being with short balloons only. However, the physical processes seem to be relatively unaffected in a non-coplanar configuration and heat transfer coefficients in both configurations are very similar.

#### 7.1.5 By-pass effects

The effect of a by-pass was explored through the comparison of both FEBA 9 and 25-rod blockage tests and FLECHT SEASET 21-rod (comparison of series B and C) and 163-rod tests.

The comparison of FEBA 90% blockage tests with and without by-passes showed an accentuated cooling of blockage sleeves with an earlier rewetting for the test without by-pass than for the by-pass test. More specifically, there was a very noticeable cooling downstream from the blockage occurring almost at the beginning of the transient. This is clearly related to the significant increase in the mass flux in the blockage sub-channels caused by the absence of a by-pass.

The comparison of FLECHT SEASET 21-rod test series B (with by-pass) with test series C (without by-pass) illustrated similar trends. Comparison of temperature variations on a peripheral rod also revealed that the cooling effect of liquid droplets upon the balloon dominates the cooling effect of the by-pass flow.

Examination of FLECHT SEASET 163-rod tests with a blockage located in two 21-rod islands illustrated the fact that blockage temperatures are lower than by-pass temperatures during the first 100 seconds, with this situation reversing beyond 150 s after turnaround. Early in the transient, the effect of steam de-superheating caused by liquid droplets is dominant, whereas during the second half of the transient, the effect of the by-pass becomes dominant as the steam flow slows down and droplet break-up reduces. Therefore, the main conclusion drawn from 163-rod test results was that the beneficial effect of the blockage upon the increase in the heat transfer remains sufficiently dominant, at least at the beginning of the transient, in order to compensate for the detrimental effect of the by-pass, thus producing lower maximum temperatures than temperatures obtained in a blockage-free configuration.

#### 7.1.6 Effect of reflood characteristics: forced or gravity

The effect of reflood characteristics was thoroughly explored during the THETIS gravity reflood tests performed under similar conditions to those used in forced reflood tests.

The distinctive feature of these gravity reflood tests is the appearance of violent oscillations at the beginning of the transient affecting the inlet flow rate and collapsed liquid level in the test section. These oscillations rapidly die down and disappear after approximately 90 seconds.

Comparison of temperature variations in the blockage and in the by-pass, between forced reflood and gravity reflood tests run under comparable conditions, revealed very similar behavioral patterns, which implies that these variations are governed by the same fundamental processes in terms of heat transfer and are barely affected by flow and level oscillations. This conclusion has been validated by the results of specific forced reflood tests reproducing the average flow rate (without oscillations) observed in gravity reflood tests and illustrating the absence of specific differences due to flow oscillations.

Temperature variations on by-pass and blockage rods during a gravity reflood test therefore appear to be mainly affected by the average flow rate at the test section inlet, concealed at the beginning of the transient by violent oscillations superimposed on it.

It can be concluded that the coolability analysis of a blocked region under gravity reflood can be supported by forced reflood tests, which represent a set of conservative conditions in comparison to similar conditions applied during gravity reflood tests with an initially full downcomer.

*In conclusion, pooling the various different test results helps improve our understanding of the physical phenomena governing the behavior of a partially blocked assembly during a LOCA reflood scenario. This also helps clarify the coolability limits of a blockage under the most penalizing geometrical (blockage ratio and length) and thermohydraulic conditions. Thus, though it seems that blockages - even of significant ratios (90%) but of moderate lengths (<10 cm) - do not create any particular problems in terms of coolability, it should not be assumed, as one might be tempted to do considering FEBA and SEFLEX test results, that a 90% blockage is always coolable. It has also been demonstrated that the maximum blockage ratio of 90% does not necessarily represent the most penalising case in terms of coolability for axially extended deformations.*

## **7.2 Analytical developments**

Key efforts in terms of model development were made in association with the FEBA and FLECHT SEASET tests. This model development was based on the COBRA-TF computer code, which is a best-estimate code developed to simulate the thermohydraulic behavior of a water reactor assembly during a LOCA reflood scenario.

The hydrodynamic effects of the blockage, i.e. the flow diversion around the partially blocked region, are directly handled by the momentum balance equations already integrated into COBRA-TF, with only the input of the blockage hydraulic characteristics. Specific models were developed to deal with heat transfer enhancement phenomena in the blockage vicinity, such as steam convective enhancement, heat transfer via the droplet impact on blockage surfaces and droplet break-up within the blockage.

It was possible to confirm the dominant physical process related to droplet effects through 1) the development of blockage models based on 21-rod tests, 2) the integration of such models into the COBRA-TF code and 3) the analysis of 21 and 163-rod tests showing satisfactory agreement between model calculations and experimental values. The physical modelling of blockages using the COBRA-TF code therefore seems to correctly represent actual blockage behavior.

Simplified models were also developed in order to analyse THETIS tests and calculate cladding temperatures in a blockage under LOCA reflood conditions. A set of calculations were performed to evaluate maximum blockage temperatures under PWR reflood conditions using this type of model, with the maximum blockage length and blockage ratio serving as main parameters. Trends highlighted by this parametric study correspond well with experimental program test results, which 1) confirms the absence of penalising temperatures for short blockages and moderate blockage ratios (<60%) and 2) corroborates the fact that significant increases in blockage surface temperatures, which may threaten blockage coolability, require high blockage ratios (above 80%) and long blockages (longer than 150 mm).

## **7.3 Pending questions**

In conclusion, it is important to underline the fact that the results and trends discussed in this review were drawn from out-of-pile tests performed on assemblies containing electric fuel rod simulators. The fixed heated elements in these simulators cannot be used to simulate a possible

accumulation of fuel in the balloons (fuel relocation) as was demonstrated in in-pile tests performed on irradiated fuel rods. Furthermore, the significant difference between comparable FEBA and SEFLEX program test results seems to indicate that significant thermal coupling between the heat source and the ballooned cladding - as may exist in a clad balloon full of relocated fuel fragments - is susceptible of significantly hindering the coolability of a blockage with such balloons, in comparison to a case where fuel relocation does not occur. This question cannot be correctly investigated by extrapolating FEBA or SEFLEX test results. The effect of fuel relocation (leading to a local accumulation of power and quasi-closure of the gap in the blockage) upon blockage coolability was not explored in any of the existing tests and therefore remains to be investigated in specific tests.

It is also important to point out that the thermohydraulic conditions of all program tests were mainly reflood conditions typical of a large-break LOCA scenario. In an intermediate-break scenario, a blockage is cooled by steam convection and the redistribution of the coolant flow around the blockage is susceptible to lead to considerable overheating of the reduced flow passing through the maximum blocked region. Yet, the question of blockage coolability during an intermediate-break scenario has not been investigated in tests with representative thermohydraulic conditions and was not discussed in this review. Therefore, this question also remains to be explored.

## REFERENCES

- 1 C. GRANDJEAN,  
A State-of-the-Art Review of Past Programs Devoted to Fuel Behavior Under LOCA Conditions.  
Part One: Clad Swelling and Rupture. Assembly Flow Blockage.  
IRSN Technical Report SEMCA-2005-313, December 2005.
- 2 P. IHLE, K. RUST,  
FEBA. Flooding Experiments with Blocked Arrays. Evaluation Report.  
KfK 3657, March 1984.
- 3 P. IHLE, K. RUST,  
SEFLEX. Fuel Rod Simulator Effects in Flooding Experiments. Part 1: Evaluation Report.  
KfK 4024, March 1986.
- 4 K.G. PEARSON, C.A. COOPER, D. JOWITT, J.H. KINNEIR,  
Reflooding Experiments on a 49-Rod Cluster Containing a Long 90% Blockage.  
AEEW - R 1591, January 1983.
- 5 C.A. COOPER, K.G. PEARSON, D. JOWITT,  
The THETIS 80% Blocked Cluster Experiment. Part 3: Forced Reflood Experiments.  
AEEW - R 1765, September 1984.
- 6 K.G. PEARSON, C.A. COOPER, D. JOWITT,  
The THETIS 80% Blocked Cluster Experiment. Part 4: Gravity Reflood Experiments.  
AEEW - R 1766, September 1984.
- 7 M.K. DENHAM, D. JOWITT, K.G. PEARSON,  
ACHILLES Unballoned Cluster Experiments. Part 1: Description of the ACHILLES Rig, Test Section  
and Experimental Procedures.  
AEEW-R2336, November 1989.
- 8 P. DORE, K.G. PEARSON,  
ACHILLES Balloned Cluster Experiments.  
AEA-TRS-1060 / AEEW-R2590, July 1991.
- 9 S.A. FAIRBAIRN, B.D.G. PIGGOTT  
Flow and Heat Transfer in PWR Rod Bundles in the Presence of Flow Blockage Due to Clad  
Ballooning. Experimental Data Report - Part 2.  
CEGB-TPRD/B/0511/N84, November 1984.
- 10 K.H. ADRON, S.A. FAIRBAIRN,  
A Method of Predicting the Temperature Response of Ballooning Fuel Cladding for PWR LOCA  
Conditions.  
Int. Meeting on Thermal Nuclear Safety, Chicago, Aug. 28 - Sept. 2, 1982.
- 11 L.E. HOCHREITER,  
FLECHT SEASET Program Final Report  
NUREG/CR-4167; EPRI NP-4112; WCAP-10926, November 1985.

## Abbreviations

AEE	Atomic Energy Establishment
ANS	American Nuclear Society
BERTHA	Blockage Experiments: Reflood Thermal Hydraulic Analysis
CEGB	Central Electricity Generating Board - Great Britain
COBRA-TF	Coolant Boiling in Rod Arrays - Two Fluid
EDF	Electricité de France
EPRI	Electric Power Research Institute
FEBA	Flooding Experiments with Blocked Arrays
FLECHT SEASET	Full Length Emergency Cooling Heat Transfer - Separate Effects and System Effects Test
HBWR	Halden Boiling Water Reactor
HETRAP	Heat Transfer Analysis Program
KfK	Kern Forschungszentrum Karlsruhe (Karlsruhe Nuclear Research Centre), now called the Forschungszentrum Karlsruhe (FZK).
LOCA	Loss of Coolant Accident
LWR	Light Water Reactor
NNC	National Nuclear Corporation
ORNL	Oak Ridge National Laboratory
PNL	Pacific Northwest Laboratory
PWR	Pressurised Water Reactor
SEFLEX	(Fuel Rod) Simulator Effects in Flooding Experiments
SG	Steam Generator
SGHWR	Steam Generating Heavy-Water Reactor
TC	Thermocouple
UKAEA	United Kingdom Atomic Energy Authority
USNRC	United States Nuclear Regulatory Commission